NOVEL SOLVENTS AND REACTION CONDITIONS FOR THE OXIDATION OF 5-HYDROXYMETHYLFURFURAL TO 2,5-FURANDICARBOXYLIC ACID

by

Jacob Magowan Molinaro

A dissertation submitted in partial fulfillment
of the requirements for the degree

of

Doctor of Philosophy

in

Chemical Engineering

MONTANA STATE UNIVERSITY
Bozeman, Montana

May 2025

©COPYRIGHT

by

Jacob Magowan Molinaro

2025

All Rights Reserved

DEDICATION

The completion of a PhD is a transformative experience, and one that cannot be finished alone. To my loving wife Kaitlin, for your support and help not only through graduate school, but in life. You are a constant source of motivation and stability that I value beyond words. To my parents, for instilling in me a love of science and a curious mindset. And to my sister, Elise, for being an example of hard work and perseverance.

ACKNOWLEDGEMENTS

I would like to express my appreciation to several people and organizations who were instrumental to the completion of the research contained herein:

To Dr. Stephanie Wettstein, my PhD advisor. Thank you for the mentorship these last four years; without you, I wouldn't be the researcher I am today. To Dr. David Hodge, Dr. Ryan Anderson, and Dr. Paul Gannon, my PhD committee, for their support and guidance. To Dr. Karlene Hoo and Dr. David Martin Alonso, my collaborators and co-authors. To Joel Swartzentruber, Gabriel Griffin, Rio Moore, and Campbell Putnam, my fellow graduate students and peer support network. To Van Ledger, for being a phenomenal undergraduate researcher and for his help collecting experimental data. To Dr. Joe Seymour, for being an excellent mentor and instructor. To Zachary Fredericks, Annabelle Young, Matthew Carroll, and Nathaniel Cayen, for their work as undergraduate researchers. And to the National Science Foundation CBET, Grant No. 2230355 for funding my research.

I would like to express thanks to those who helped balance my life outside of the lab as well. To Dr. Brendan Christensen, for being a caring friend and running partner, and for sharing the Ranch with me and Kaitlin. To Kyla, for telling me that a 100-mile race wasn't that far… and to Kaitlin, Val, and Savannah for keeping me upright when I learned it was, in fact, rather far. To Dezzie, for being a listening ear while out on the trails. To the "Vert Bois" for being a source of balance and community. To the Bozeman Christadelphians, for being spiritual support and a community to call home. To my brother-in-law, Adam, for being a reliable hiking buddy and friend. To Richie, for great album recommendations. And to Dylan, Logan, Dan, Gabe, Ari, Josh, and Shay, for phone calls and being support from afar on long evenings in the lab.

TABLE OF CONTENTS

1. INTRODUCTION 1

1.1 Introduction and Motivation 1
1.2 Background 5
1.3 Hansen Solubility Parameter Theory 8
1.4 Artificial Neural Network Models 12
1.5 Catalysis Background 15
1.6 Organization of this Document 18

2. RECENT DEVELOPMENTS IN SOLVENT AND CATALYST SELECTION FOR 5-HYDROXYMETHYLFURFURAL OXIDATION TO 2,5-FURANDICARBOXYLIC ACID 20

2.1 Contributions of Authors and Co-Authors 20
2.2 Manuscript Information 21
2.3 Abstract 22
2.4 Introduction 22
2.5 Mechanistic Insights 26
Initial 5-Hydroxymethylfurfural Reaction 28
Intermediates to 2,5-Furandicarboxylic Acid 31
2.6 Aqueous Reactions 33
Noble Metal Catalysts 34
Platinum 35
Gold and Palladium 41
Ruthenium 50
Non-noble Metal Catalysts 58
Single Metal Non-Noble Catalyst 59
Bimetallic Non-Noble Catalysts 62
2.7 Organic Solvent Reactions 66
Noble Metal Catalysts 70
Non-Noble Metal Catalysts 75
2.8 Conclusions and Future Outlook 87

3. SOLUBILITY OF 2,5-FURANDICARBOXYLIC ACID IN PURE AND MIXED ORGANIC SOLVENT SYSTEMS AT 293 K PREDICTED USING HANSEN SOLUBILITY PARAMETERS 92

3.1 Contributions of Authors and Co-Authors 92
3.2 Manuscript Information 93
3.3 Abstract 94
3.4 Introduction 95

TABLE OF CONTENTS CONTINUED

3.5 Theory 97
3.6 Experimental Methods 100
Solubility Determination 100
HSP Calculations 103
MATLAB Modeling Methods 103
3.7 Results and Discussion 105
Binary Aqueous/Organic Solvent Systems 105
Ternary Aqueous/Organic/Organic Solvent Systems 113
Solvent Selection Optimization Using MATLAB 115
3.8 Conclusions 117

4. USING ARTIFICIAL NEURAL NETWORKS TO PREDICT 2,5-FURANDICARBOXYLIC ACID SOLUBILITY FOR SOLVENT SELECTION 119

4.1 Contributions of Authors and Co-Authors 119
4.2 Manuscript Information 120
4.3 Abstract 121
4.4 Introduction 121
4.5 Methods 126
Chemicals 126
Solubility Assessment 126
Artificial Neural Network 127
COSMO-RS 129
4.6 Results and Discussion 130
Solubility Data 130
ANN Models Using Hansen Solubility Parameters 132
COSMO-RS Data 140
4.7 Conclusions 147

5. NOVEL SOLVENT SYSTEMS FOR THE BASE-FREE OXIDATION OF 5-HYDROXYMETHYLFURFURAL TO 2,5-FURANDICARBOXYLIC ACID 149

5.1 Contributions of Authors and Co-Authors 149
5.2 Manuscript Information 150
5.3 Abstract 151
5.4 Introduction 152
5.5 Materials and Methods 155
Chemicals 155
Catalysts 155
HMF Oxidation Procedure 155

TABLE OF CONTENTS CONTINUED

Solvent Degradation Assessment 156
5.6 Results and Discussion 157
Solvent Effects 157
Effect of HMF Concentration 162
Effect of Reaction Temperature 166
5.7 Conclusions 167

6. CONCLUSIONS AND FUTURE OUTLOOK 170

REFERENCES CITED 176

APPENDICES 193

APPENDIX A: SUPPLEMENTAL MATERIALS FOR SOLUBILITY OF 2,5-FURANDICARBOXYLIC ACID IN PURE AND MIXED ORGANIC SOLVENT SYSTEMS AT 293 K PREDICTED USING HANSEN SOLUBILITY PARAMETERS 194
Error Assessment 195
MATLAB Code 196
Code 1 196
Additional Tables and Data 199
HSP Values at 303 K 209
Organic/Organic Binary Mixtures 212

APPENDIX B: HMF OXIDATION AND REACTION ANALYSIS PROCEDURE 217
Parr Reactor Reaction Procedure 218
Reactor Effluent Analysis 222
HPLC Sample Prep and Chromeleon 7 Setup 226
Data Collection Using Chromeleon 7 Software 228

APPENDIX C: SUPPLEMENTAL MATERIALS FOR 'USING ARTIFICIAL NEURAL NETWORKS TO PREDICT 2,5-FURANDICARBOXYLIC ACID SOLUBILITY FOR SOLVENT SELECTION' 230
Additional Figures, Tables, and Equations 231
Derivation 1: HSPs to Excess Enthalpy 236
Background 236
Formal Derivation 238
Test Case Demonstrating Eqn. 50 240

TABLE OF CONTENTS CONTINUED

APPENDIX D: SUPPLEMENTAL MATERIALS FOR 'NOVEL SOLVENT SYSTEMS FOR THE BASE-FREE OXIDATION OF 5-HYDROXYMETHYLFURFURAL TO 2,5-FURANDICARBOXYLIC ACID' 242
Additional Figures 243
Solvent Degradation..... 243

LIST OF TABLES

Table Page

1. Table 1. Oxidation states and electron orbital configuration of different noble metals. 35

2. Table 2. Platinum catalysts that have been studied for aqueous based HMF oxidation. 36

3. Table 3. Effects of different catalyst synthesis techniques for aqueous HMF oxidation using ZrO2 supports[118] and CaZSM-5 supports (marked with *).[82] For synthesis methods: IW = incipient wetness impregnation; DP = deposition-precipitation; IRB = impregnation-reduction under basic conditions; IRA = impregnation-reduction under acidic conditions. 42

4. Table 4. Gold and palladium catalysts studied for aqueous HMF oxidation. 43

5. Table 5. Ruthenium catalysts studied for aqueous HMF oxidation using 1 MPa O2 at 100% HMF conversion. 51

6. Table 6. Non-noble single metal catalysts studied for aqueous HMF oxidation. 59

7. Table 7. Non-noble bimetallic catalysts that have been studied for aqueous-based HMF oxidation with NaOH base additive. 64

8. Table 8. Overview of properties and FDCA solubility at 303 K[a] or 293 K for various solvents. [a]Xu et al.,[158] [b]Ryu et al.,[36] [c]Molinaro et al.,[34] [d]R. Stenutz,[159] [e]HSPiP Software Package.[56] 68

9. Table 9. Noble metal catalysts on carbon supports studied in organic solvent systems for HMF oxidation. 71

10. Table 10. Oxidation and electron orbital configurations of different non-noble metals. 75

11. Table 11. Non-noble metal catalysts studied in organic solvent systems for HMF oxidation at 353 K. 83

12. Table 12. Solvents and solute used in experiments. [a]AK = AK Scientific, SA = Sigma-Aldrich, FS = Fisher Scientific, AO = Acros Organics 102

LIST OF TABLESCONTINUED

13. Table 13. HSP Parameter Data (MPa$1/2$) for Pure Compounds at $T = 293$ K as Determined Using the HSPiP Software Where Δ Calculates the Difference Between the Pure Component and FDCA. 104

14. Table 14. The Amount of FDCA Solubilized in Each Pure Solvent Ranked from Highest to Lowest FDCA Solubility at 293 K and the Ranking Predicted by $\Delta\delta T$ and Ri,j with 1 Being the Highest Expected Solubility and 8 the Lowest.[a] [a]Standard uncertainties were $u(T)$ = 0.3 K, $u(P)$ = 0.1 kPa and relative uncertainties were $ur(wFDCA)$ = 0.061 (for $102wFDCA$ < 5), 0.128 (for $102wFDCA$ > 5).....112

15. Table 15. Comparison of Experimental Maximum Solubility to MATLAB Predicted Maximum Solubility in Binary and Ternary Mixtures at $T = 293$ K and $P = 0.1$ MPa.[a] [a]Standard uncertainties were $u(w1, w2, ww)$ = 0.002, $u(T)$ = 0.3 K, $u(P)$ = 0.1 kPa and relative uncertainties were $ur(wFDCA)$ = 0.061 (for $102wFDCA$ < 5), 0.128 (for $102wFDCA$ > 5). [b]The $102wFDCA$ "predicted" values represent the experimentally determined solubility at the predicted solvent composition. 116

16. Table 16. Ranges of values for ANN model training inputs. 128

17. Table 17. Ranking of differing solvents by maximum system FDCA solubility and minimum system excess enthalpy. 144

18. Table 18. Experimental Mass Fraction Solubilities of FDCA ($wFDCA$), HSP Values, and Values of $\Delta\delta T$ and Ri,j in Binary Mixtures of Water and ACN at Varying Organic Mass Fractions ($wOrg$) at $T = 293$ K and $P = 0.1$ MPa.[a] [a]Standard uncertainties were $u(wOrg)$ = 0.002, $u(T)$ = 0.3 K, $u(P)$ = 0.1 kPa and relative uncertainties were $ur(wFDCA)$ = 0.061 (for $102wFDCA$ < 5), 0.128 (for $102wFDCA$ > 5)..... 199

19. Table 19. Experimental Mass Fraction Solubilities of FDCA ($wFDCA$), HSP Values, and Values of $\Delta\delta T$ and Ri,j in Binary Mixtures of Water and GVL at Varying Organic Mass Fractions ($wOrg$) at $T = 293$ K and $P = 0.1$ MPa.[a] [a]Standard uncertainties were $u(wOrg)$ = 0.002, $u(T)$ = 0.3 K, $u(P)$ = 0.1 kPa and relative uncertainties were $ur(wFDCA)$ = 0.061 (for $102wFDCA$ < 5), 0.128 (for $102wFDCA$ > 5)..... 200

LIST OF TABLES CONTINUED

20. Table 20. Experimental Mass Fraction Solubilities of FDCA ($wFDCA$), HSP Values, and Values of $\Delta\delta T$ and Ri,j in Binary Mixtures of Water and EtOH at Varying Organic Mass Fractions ($wOrg$) at $T = 293$ K and $P = 0.1$ MPa.[a] [a]Standard uncertainties were $u(wOrg) = 0.002$, $u(T) = 0.3$ K, $u(P) = 0.1$ kPa and relative uncertainties were $ur(wFDCA) = 0.061$ (for $102wFDCA < 5$), 0.128 (for $102wFDCA > 5$)..... 201

21. Table 21. Experimental Mass Fraction Solubilities of FDCA ($wFDCA$), HSP Values, and Values of $\Delta\delta T$ and Ri,j in Binary Mixtures of Water and GBL at Varying Organic Mass Fractions ($wOrg$) at $T = 293$ K and $P = 0.1$ MPa.[a] [a]Standard uncertainties were $u(wOrg) = 0.002$, $u(T) = 0.3$ K, $u(P) = 0.1$ kPa and relative uncertainties were $ur(wFDCA) = 0.061$ (for $102wFDCA < 5$), 0.128 (for $102wFDCA > 5$)..... 202

22. Table 22. Experimental Mass Fraction Solubilities of FDCA ($wFDCA$), HSP Values, and Values of $\Delta\delta T$ and Ri,j in Binary Mixtures of Water and THF at Varying Organic Mass Fractions ($wOrg$) at $T = 293$ K and $P = 0.1$ MPa.[a] [a]Standard uncertainties were $u(wOrg) = 0.002$, $u(T) = 0.3$ K, $u(P) = 0.1$ kPa and relative uncertainties were $ur(wFDCA) = 0.061$ (for $102wFDCA < 5$), 0.128 (for $102wFDCA > 5$)..... 203

23. Table 23. Experimental Mass Fraction Solubilities of FDCA ($wFDCA$), HSP Values, and Values of $\Delta\delta T$ and Ri,j in Binary Mixtures of Water and MeOH at Varying Organic Mass Fractions ($wOrg$) at $T = 293$ K and $P = 0.1$ MPa.[a] [a]Standard uncertainties were $u(wOrg) = 0.002$, $u(T) = 0.3$ K, $u(P) = 0.1$ kPa and relative uncertainties were $ur(wFDCA) = 0.061$ (for $102wFDCA < 5$), 0.128 (for $102wFDCA > 5$)..... 204

24. Table 24. Experimental Mass Fraction Solubilities of FDCA ($wFDCA$), HSP Values, and Values of $\Delta\delta T$ and Ri,j in Binary Mixtures of Water and SULF at Varying Organic Mass Fractions ($wOrg$) at $T = 293$ K and $P = 0.1$ MPa.[a] [a]Standard uncertainties were $u(wOrg) = 0.002$, $u(T) = 0.3$ K, $u(P) = 0.1$ kPa and relative uncertainties were $ur(wFDCA) = 0.061$ (for $102wFDCA < 5$), 0.128 (for $102wFDCA > 5$)..... 205

25. Table 25. Experimental Mass Fraction Solubilities of FDCA ($wFDCA$), HSP Values, and Values of $\Delta\delta T$ and Ri,j in Binary Mixtures of Water and DMSO at Varying Organic Mass Fractions ($wOrg$) at $T = 293$ K and $P = 0.1$ MPa.[a] [a]Standard uncertainties were $u(wOrg) = 0.002$, $u(T) = 0.3$ K, $u(P) = 0.1$ kPa and relative uncertainties were $ur(wFDCA) = 0.061$ (for $102wFDCA < 5$), 0.128 (for $102wFDCA > 5$)..... 206

LIST OF TABLES CONTINUED

26. Table 26. HSP Values for Chemicals Studied by Zhuang et al. at $T = 303$ K and $P = 0.1$ MPa, as Retrieved from the HPSiP Software.[a] [a]Standard uncertainties were $u(T)$ = 0.05 K and $u(P)$ = 5 kPa. 209

27. Table 27. Solubility ($102wFDCA$) Data Calculated from Zhuang et al. for H_2O/Organic ($wOrg$) Mixtures at 303 K.[29] Temperature Corrected $\Delta\delta T$ and Ri,j Values Calculated from HSP Values Determined Using the HSPiP Software (Table S1).[a] [a]Standard uncertainties were $u(T)$ = 0.05 K, $u(P)$ = 5 kPa 210

28. Table 28. Solubility ($102wFDCA$) Data Calculated from Ban et al. for H_2O/Organic ($wOrg$) Mixtures at 303 K. [31] Temperature Corrected $\Delta\delta T$ and Ri,j Values Calculated from HSP Values Determined Using the HSPiP Software.[a] [a]Standard uncertainties were $u(T)$ = 0.02 K, $u(P)$ = 5 kPa. 211

29. Table 29. Values of Ri,j and $\Delta\delta T$ for Organic-Organic Mixtures at Varying Mass Fractions of Organic 1 ($wOrg$). Data collected at $T = 293$ K and $P = 0.1$ MPa.[a] [a]Standard uncertainties were $u(wOrg)$ = 0.002, $u(T)$ = 0.3 K, $u(P)$ = 0.1 kPa and relative uncertainties were $ur(wFDCA)$ = 0.061 (for $102wFDCA < 5$), 0.128 (for $102wFDCA > 5$). 215

30. Table 30. Values of Ri,j and FDCA Solubilized ($102wFDCA$) for Ternary H_2O, DMSO ($wDMSO$), and Secondary Organic ($wOrg$) Mixtures at $T = 293$ K and $P = 0.1$ MPa.[a] [a]Standard uncertainties were $u(wDMSO, wOrg) = 0.002$, $u(T)$ = 0.3 K, $u(P)$ = 0.1 kPa and relative uncertainties were $ur(wFDCA)$ = 0.061 (for $102wFDCA < 5$), 0.128 (for $102wFDCA > 5$). 216

31. Table 31. HSP data ($MPa^{1/2}$) for pure compounds at T = 293 K as determined using the HSPiP software.[56] 232

32. Table 32. Statistical metrics for ANN models for alcohol and non-alcohol datasets. 234

LIST OF FIGURES

Figure Page

1. Figure 1. A simplified scheme showing the conversion of biomass to PEF, with fructose, HMF, and FDCA shown as intermediates. 3

2. Figure 2. The oxidation reactions and intermediates for the upgrading of HMF to FDCA through two separate pathways. The top (HMFCA) oxidizes the aldehyde functional group of HMF first, while the bottom (DFF) pathway first oxidizes the alcohol functional group. 6

3. Figure 3. A structural comparison between terephthalic acid (left) and FDCA (right). 7

4. Figure 4. Generalized architecture of an artificial neural network, showing the inputs (I), hidden nodes (H), targets (T), and weights (w, W). 14

5. Figure 5. The 30 mL Parr reactor vessel used for oxidation reactions presented in this dissertation (left) and the overall reaction setup (right). 16

6. Figure 6. Simplified scheme to produce PEF starting from biomass to produce fructose, then dehydration to HMF, oxidation to FDCA, and the final polymerization. 24

7. Figure 7. Number of journal articles and reviews in the last 15 years (obtained via Web of Science using: 2,5-Furandicarboxylic acid (Topic) AND cat* (Topic) and Article or Review Article (Document Types) and English (Languages).[89] 25

8. Figure 8. HMF to FDCA reaction pathway, adapted from Chen et al. [REF: 35] The kinetic parameters presented are for a semi batch reaction in acetic acid over a Co/Mn/Br catalyst at 413 K. (Scheme 1 in Manuscript) 28

9. Figure 9. Reaction mechanism for the oxidation of HMF to DFF. A hydroxy radical attacks the carbinol carbon of the alcohol before a secondary oxidant facilitates the formation of a π-bond. (Scheme 2 in Manuscript) 29

LIST OF FIGURES CONTINUED

10. Figure 10. Reaction mechanism for the oxidation of HMF to HMFCA. The conversion of the aldehyde to a carboxylic acid is facilitated through a geminal diol intermediate followed by a β-hydride elimination. 31

11. Figure 11. Reaction mechanism for oxidation of DFF to FFCA. The conversion of an aldehyde to a carboxylic acid progresses through the geminal diol intermediate before a β-hydride elimination allows the formation of a new C=O bond. 32

12. Figure 12. Reaction mechanism for the oxidation of HMFCA to FFCA. A hydroxy radical attack first targets the carbinol carbon of the alcohol group before a second oxidant results in the formation of a π-bond. 32

13. Figure 13. Reaction mechanism for the oxidation of FFCA to FDCA. The remaining aldehyde of FFCA is converted to a carboxylic acid via a geminal diol intermediate a β-hydride elimination. 33

14. Figure 14. Impact of P dopant amount on the surface of the catalyst (determined by XPS) on FDCA (■) and FFCA (●) yields for the MnP_yO_x catalyst (100% HMF conversion for all). Reaction conditions: 100: 1 HMF: Pt molar ratio, 1.25 wt% HMF, T = 383 K, P_{O2} = 1 MPa, 24 h.[108] 38

15. Figure 15. Effect of reaction temperature on FDCA yield with a Pt/UiO-66 catalyst (□)[123] and a Pt/MnP0.50Ox catalyst (■).[108] [43] Reaction conditions for Pt/UiO-66 catalyst: HMF: Pt 200: 1 molar ratio, PO2 = 0.5 MPa, t = 14 h[123] and for $Pt/MnP_{0.50}O_x$ catalyst: HMF: Pt 100: 1 molar ratio, P_{O2} = 1 MPa, t = 24 h.[108] 40

16. Figure 16. Product yields for reactions using impregnation-reduction under acidic conditions synthesized catalysts using Au (■), Pd (■), and Au-Pd (■) on ZrO_2[118] and deposition-precipitation method on Au/C (■), Pd/C (■), and Au-Pd/C (■) catalysts.[78] Reaction conditions for impregnation-reduction catalyst: 100:1 HMF:catalyst molar ratio, 0.2 mol $NaHCO_3$, 0.63 wt% HMF, T = 353 K, P_{O2} = 0.5 MPa, and t = 24 h.[132] For deposition-precipitation catalyst: 110:0.93:0.07 HMF:Pd:Au molar ratio, 20 mmol $NaHCO_3$, 5 mmol HMF, T = 363 K, P_{O2} = 0.3 MPa, and t = 6 h.[78] 44

LIST OF FIGURES CONTINUED

17. Figure 17. Yields and conversion of adding metals to an Au/$MgAlO_x$ catalyst. Reaction conditions: 70:1 HMF:metal molar ratio, 0.25 wt% initial HMF, T = 363 K, P_{O2} = 0.5 MPa, and t = 2 h.[122] 47

18. Figure 18. Effect of silver loading on a bimetallic a) Au/Ag SiO_2 catalyst (conditions: 79:1 HMF:Au molar ratio, 0.4 mmol $NaHCO_3$, T = 353 K, P_{O2} = 1 MPa, and t = 6 h)[118] and b) Pt/Ag catalyst where the x-axis represents the mass fraction of Ag of the total mass of the metals. Reaction conditions: 50:1 HMF:Pt molar ratio, 0.8 mmol $NaHCO_3$, T = 373 K, O_2 bubbling at 75 mL/min, and t = 1 h.[110] 48

19. Figure 19. Remaining HMF (♦) and product yields of FDCA (■), HMFCA (●), and FFCA (▲) for a 5.6 wt% Au catalyst on MnO_2. Reaction conditions: 9.3:1 HMF:catalyst molar ratio, and t = 12 h.[115] 49

20. Figure 20. Support and metal effects on FDCA (■) and FFCA (■) yields for HMF oxidation using 4 wt% Ru (when noted) on various Cu, Co, and Mg oxides supports. Reaction conditions: 0.5 wt% HMF, T = 383 K, P_{O2} = 1 MPa, t = 12 h.[116] 52

21. Figure 21. The effect of Ru loading on FDCA (■) and FFCA (■) yields on a Cu1-Co1-O·MgO,[116] Cr2-Fe1-O,[124] and NC support.[21] Reaction conditions for Ru/Cu1-Co1-O catalyst: 0.5 wt% HMF, T =383 K, P_{O2} = 1 MPa O_2, t = 12 h,[116] for Ru/Cr2-Fe1-O catalyst: 6 mmol $KHCO_3$ additive, 0.5 wt% HMF, T = 373 K, P_{O2} = 1 MPa, t = 16 h,[124] and for Ru/NC catalyst: 0.6 wt% HMF, 0.25 mmol $CaCO_3$ additive, T = 413 K, P_{O2} = 1 MPa, t = 2 h.[21] 53

22. Figure 22. Impact of dopant amount on FDCA (■), FFCA (■), and HMFCA (■) yields for a MgO dopant loaded on a 4% Ru/ Cu1-Co1-O·MgO catalyst (100% HMF conversion for all)[116] and Nb loading on a Ru/SBA-15 catalyst.[135] Reaction conditions: P_{O2}= 1 MPa, t = 12 h and for Cu1-Co1-O·MgO catalyst: 0.5 wt% HMF, T= 383 K,[116] and for Nb-SBA-15 catalyst: 1.25 wt% HMF, T = 393 K.[135] 55

23. Figure 23. Effect of initial HMF concentration on final FDCA yields observed in an aqueous system using a Ru/MnO_2 catalyst without the addition of base. Reaction conditions: 2:1 HMF:catalyst weight ratio, T = 373 K, P_{O2} = 3 MPa, t = 24 h.[25] 57

24. Figure 24. The effect of graphitization on FDCA yields. Reaction conditions: 0.024 HMF:catalyst molar ratio, T = 338 K, P_{O2} = 0.5 MPa, t = 12 h.[141] 61

LIST OF FIGURES CONTINUED

25. Figure 25. FDCA yields of various Cu- and Co-based catalysts where G represents graphite deposited catalysts and GP represents the PVP-organized catalyst on graphite. All HMF conversions were greater than 95%. Reaction conditions: 0.525:1 HMF:catalyst by weight, 3.2 mmol NaClO, 0.5 mmol HMF, T = 303 K, P = atm, t =1 h.[142] 63

26. Figure 26. The effect of NaOH on HMF conversion (♦) and FDCA yield (■) using a Co-Bi oxide catalyst. Reaction conditions: 0.056 HMF:catalyst molar ratio, 0.8 mmol of NaOH, T = 380 K, P_{O2} = 0.6 MPa, t = 3 h.[144] 65

27. Figure 27. Relationship between the Ri,j parameter and FDCA solubility in a) pure solvents and b) binary aqueous/organic mixtures, and ternary aqueous/organic/organic mixtures from (●),[32] (■),[29] and (♦).[31] 69

28. Figure 28. Effect of lattice oxygen content of Ru catalysts supported by a range of Ni-Mn supports on FDCA yield at an HMF conversion of 100% (excluding Ru/NiO where the HMF conversion was 63%). Reaction conditions: 1.43:1 catalyst:HMF by weight; 70/30 H_2O/ACE w/w; 5 wt% initial HMF; T = 383 K; P_{O2} = 1 MPa; t = 12 h.[104] 73

29. Figure 29. Comparison of the effect of catalyst a) metal surface area and b) Ru particle size on an HMF oxidation reaction. Reaction conditions: 1:1.43 HMF:catalyst by weight, 70/30 w/w water/ACE, 5 wt% initial HMF, T = 383 K, P_{O2} = 1 MPa, t = 12 h.[104] 74

30. Figure 30. Comparison of FDCA yields on single metal and bimetallic catalysts containing Mn-Cu (♦), Fe-Co (■),[42] and Cu^{2+}-VO^{2+} over a PVDTA support (●).[157] Reaction conditions for the Mn-Cu and Fe-Co catalysts: 1:4 HMF:catalyst by weight, pure ACN, 13:1 TBHP:HMF molar ratio, 3.5 wt% initial HMF, T = 333 K, P = atm, t = 3 h,[42] and for the Cu-VO/PVDTA catalyst: 32/68 w/w DMSO/TBA, 0.37 wt% initial HMF, T = 363 K, P = atm, t = 5 h.[157] 77

31. Figure 31. The relationship between FDCA yield and a) surface area and b) pore volume for NNM catalysts on α-MoO_3 supports (□) and different MoO_3 phases without additional metal (■) (Reaction conditions: 4 mL TBA solvent, 4 mmol TBHP, 0.4 wt% HMF, T = 353 K, P = atm, t = 12 h).[102] 78

LIST OF FIGURES CONTINUED

32. Figure 32. Relationship between catalyst surface acidity and FDCA yield. Reaction conditions: 30:1 HMF:Catalyst molar ratio, 50/50 w/w DMSO/water, 0.95 wt% HMF, T = 383 K, P = atm, t = 15 h.[85] 79

33. Figure 33. Impact of graphitic N content on FDCA yield (■) and total catalyst basicity (●). Reaction conditions: MeOH solvent, 0.1 M K_2CO_3 weak base additive, 0.89 wt% HMF, T = 433 K, P_{O2} = 2 MPa, t = 6 h.[81] 81

34. Figure 34. Temperature effect on FDCA yield of doped Co-Fe catalysts on a layered double hydroxide hydrotalcite support. Reaction conditions: 1:1 HMF:catalyst by weight, ACN solvent, 0.61 wt% initial HMF, P = atm, t = 6 h.[84] 82

35. Figure 35. Effect of solvent a) hydrogen bond acceptance capacity and b) polarity on HMF conversion (♦) and FDCA (■), DFF (∗), and FFCA (●) yields for ACN, DMF, and DMSO solvents. Reaction conditions: CoFeP-400/LDH catalyst, 0.36 mL TBHP oxidant additive, 0.44-0.61 wt% HMF, T = 353 K, P_{O2} = 1 MPa, t = 6 h.[84] 84

36. Figure 36. Trends of HMF conversion (◊), DFF (∗), and FDCA (□) yields for toluene, ACN, DMF, and DMSO pure solvents compared to a) the KT β parameter and b) the HSP polarity parameter and the same trends for MeOH, EtOH, n-PrOH,, and i-PrOH in figure c) and d), respectively. Reaction conditions: Co/MnO_2 catalyst, 0.57-0.80 wt% HMF, T = 413 K, P_{O2} = 0.3 MPa, t = 4 h.[154] 86

37. Figure 37. Plot of the mass fraction of FDCA solubilized ($wFDCA$) in varying binary mixtures of H_2O and organic solvent (THF (▲), SULF (■), MeOH (□), EtOH (♦), ACN (◊), GVL (●), or GBL (○)) with the organic mass fraction ($wOrg$) on the horizontal axis. Solubility data for DMSO is shown on the secondary axis (△). Lines are provided to guide the eye. Raw data is provided in the Supplemental Materials (Appendix A, Tables 16 to 23). 105

38. Figure 38. Mass fraction of FDCA solubilized ($wFDCA$) in aqueous/organic binary solvent systems plotted versus a) δH, b) δD, and c) δP. Markers represent H_2O/DMSO (■), H_2O/THF (▲), and all other components (●) with the dashed lines (---) representing the respective HSP value of FDCA. 107

LIST OF FIGURES CONTINUED

39. Figure 39. The Ri,j (▲), $\Delta\delta T$ (□), and the mass fraction of FDCA solubilized ($wFDCA$; ●, secondary axis) versus the mass fraction of organic ($wOrg$) in binary mixtures of H_2O and (a) DMSO, (b) THF, (c) GVL, (d) GBL, (e) MeOH, (f) EtOH, (g) ACN, or (h) SULF where the dashed line indicates the minima of Ri,j (---). Data collected at $T = 293$ K and $P = 0.1$ MPa. 109

40. Figure 40. The Ri,j for H_2O/DMSO (♦), H_2O/THF (▲), all other H_2O/organic (●) mixtures plotted against mass fraction of FDCA solubilized ($wFDCA$). 111

41. Figure 41. Mass fraction of FDCA solubilized ($wFDCA$) in ternary mixtures of H_2O/DMSO/organic, where the second organic was either GVL (●), THF (X), or SULF (■), plotted against Ri,j 114

42. Figure 42. Solubility data for mixtures of water and (a) DMAc, (b) acetone, and (c) 2-PrOH presented on the left (black) axis (♦). The Ri,j of the solvent blend at that composition is shown on the right (blue) axis (●). 131

43. Figure 43. Comparison of the experimental and predicted FDCA solubilities for the training set (●) and independent test sets of acetone (◊), 2-PrOH (◊), and DMAc (Δ) for the non-alcohol (a) and alcohol (b) ANN models. Also shown are the 95% confidence intervals (---) on either side of the parity line (···). 134

44. Figure 44. Median R values from two-layer feed forward ANNs trained with different combinations of HSPs as input variables for alcohol (blue) and non-alcohol (gold) models. Each value represents the median R from five training runs using the final model design and the complete dataset with the shading within a color representing one, two, and three inputs (from light to dark). 136

45. Figure 45. Plots of individual HSPs versus FDCA solubility for non-alcohol (●) and alcohol (×) datasets. A line denoting the HSP value for FDCA is shown in red (---); the value for δD occurs at at 19.4. 137

46. Figure 46. Relationship between the minimum excess enthalpy value for aqueous/organic blends of non-alcohol solvents (●; DMSO, THF, acetone, GBL, GVL, sulfolane, acetonitrile) and alcohol solvents (◊; MeOH, EtOH, 2-PrOH, 1-BuOH) at a consistent FDCA concentration (1 wt%). Trendline added to guide the eye. 141

LIST OF FIGURES CONTINUED

47. Figure 47. Excess enthalpy values for ternary mixtures of constant FDCA (1 wt%) and variable aqueous/organic solvent ratios of water and (●) DMSO, (●) THF, (●) acetone, (●) GVL, (●) GBL, (●) sulfolane, (●) acetonitrile, and (●) cyclohexane. 142

48. Figure 48. Relationship between the minimum excess enthalpy value for blends of alcohol solvents (2-PrOH, EtOH, MeOH), water, and 1 wt% FDCA and the maximum FDCA system solubility. 146

49. Figure 49. Reaction schematic for the oxidative upgrading of HMF to FDCA. 152

50. Figure 50. Final compositions of HMF oxidation reactions in DMSO (a), acetonitrile (b), sulfolane (c), GBL (d), GVL (e), and THF (f). Product yields are represented as FDCA (■), FFCA (■), DFF (■), and remaining HMF (■). Total bar height indicates final mass balance value. Reaction conditions: 363 K, 4 h, 40 bar O_2, 1000 rpm stirring, 1 wt% HMF concentration, 7.5:1 HMF:Pt. 158

51. Figure 51. Maximum FDCA yields from HMF oxidation reactions in water (●), DMSO (♦), acetonitrile (■), sulfolane (□), GBL (○), GVL (▲), and THF (+). Lines were added to guide the eye. Reaction conditions: 363 K, 4 h, 40 bar O_2, 1000 rpm stirring, 1 wt% HMF concentration, 7.5:1 HMF:Pt. 160

52. Figure 52. The effect of initial HMF concentration on yields of FDCA in pure water (■) and 50/50 sulfolane/water (■) sampled immediately after the reaction (a) and after catalyst and reactor rinsing (b). Reaction conditions: 363 K, 4 h, 40 bar O_2, 1000 rpm stirring, 0.437 g of 5% Pt/C catalyst, varying HMF concentration. A * indicates that a 10% Pt/C catalyst was substituted at the same catalyst weight. 163

53. Figure 53. Product yields for different initial HMF concentration for FDCA (■), FFCA (■), DFF (■), and remaining HMF (■) in water (a) and 50/50 sulfolane/water (b). Reaction conditions: 363 K, 4 h, 40 bar O_2, 1000 rpm stirring, 0.437 g of 5% Pt/C catalyst, varying HMF concentration and the catalyst was rinsed after reaction. A * indicates that a 10% Pt/C catalyst was substituted at the same catalyst weight. 165

LIST OF FIGURES CONTINUED

54. Figure 54. Impact of temperature on product distribution of FDCA (■), FFCA (■), DFF (■), and remaining HMF (■). Reaction conditions: 7.5 wt% HMF concentration, 50/50 SULF/water solvent, 4 h, 40 bar O_2, 1000 rpm stirring, 0.437 g of 5% Pt/C catalyst..... 166

55. Figure 55. The Ri,j (▲), $\Delta\delta T$ (□), and the mass fraction of FDCA solubilized ($wFDCA$; ●, secondary axis) collected at 303 K by Zhuang, et al.[29] versus mass fraction organic ($wOrg$) present in binary mixtures of H_2O and (a) THF, (b) 1,4-dioxane, (c) 1,2-dimethoxyethane, and (d) diethylene glycol dimethyl ether. The dashed red line indicates the minima of the Ri,j curve (---)..... 207

56. Figure 56. The Ri,j (▲), $\Delta\delta T$ (□), and the mass fraction of FDCA solubilized ($wFDCA$; ●, secondary axis) collected at (a) 297 K and (b) 299 K by Ban, et al.[31] versus mass fraction organic ($wOrg$) present in binary mixtures of H_2O and (a) MeOH and (b) EtOH. The dashed red line indicates the minima of the Ri,j curve (---)..... 208

57. Figure 57. Comparison of solubility, Ri,j, and $\Delta\delta T$ in Organic/Organic binary systems. (a) DMSO/MeOH (b) DMSO/THF (c) EtOH /GVL (d) GVL/DMSO (e) GVL/MeOH (f) GVL/THF (g) THF/MeOH. A dashed red line (---) indicates the minimum Ri,j to help guide the eye..... 214

58. Figure 58. HPLC standard line and equation for FDCA analysis..... 231

59. Figure 59. MATLAB generated plots for the assessment of error distribution across training data (blue), validation data (green), and test data (red) for the non-alcohol model (left) and the alcohol model (right). 233

60. Figure 60. Experimental (○) and non-alcohol ANN predicted (◊) values of FDCA solubility in blends of water and DMSO, from pure water on the far left to pure DMSO on the far right. 235

61. Figure 61. Visualization of the non-linear relationship between the Hansen Ri,j parameter and FDCA solubility. Data represented with blue circles (●) has solubility below 2 wt% and is fairly linear, while data represented with black circles (●) has solubility above 2 wt% and is quite nonlinear..... 236

LIST OF FIGURES CONTINUED

62. Figure 62. Comparison of degradation products visually apparent in a pure water system (left) and a 50/50 sulfolane/water system (right). Reaction conditions: 90°C, 4h, 40 bar O_2, 1000 rpm stirring, 0.43698 g of 5% Pt/C catalyst, 10 wt% HMF concentration. 243

63. Figure 63. Synopsis of solvent degradation for DMSO (-), ACN (-), SULF (-), GBL (-), GVL (-), and THF (-). Treated solvent samples are designated with dashed lines. Reaction conditions for treated solvent samples: 90°C, 4h, 40 bar O_2, 1000 rpm stirring, 0.43698 g 5% Pt/C catalyst. 244

64. Figure 64. Degradation study on sulfolane at 403 K. The standard injection is shown as a solid black line (−) while the treated sample is shown as a dashed blue line (---). 246

ABSTRACT

2,5-Furandicarboxylic acid (FDCA) is an important biomass-derived monomer for the production of sustainable materials and bioplastics. Upgrading FDCA to polymers could effectively replace petroleum-derived plastics, reducing carbon emissions and reliance on fossil fuels while also improving the material properties of the final products. However, FDCA production is not economically viable in its current form. In this dissertation, two critical challenges to FDCA production are addressed: (1) its poor solubility in most solvents, which complicates separations and purification processes and (2) the limited understanding of how solvent selection influences the oxidation reaction to produce FDCA. To do so, FDCA solubility was systematically assessed in a range of organic solvents and aqueous/organic solvent blends. Solubility data was correlated first to the Hansen Radius of Interaction ($R_{i,j}$) parameter, allowing for optimization of blend ratios, and then more deeply to fundamental molecular properties, structures, and thermodynamic behaviors. Solubility behavior was found to be correlated with the type of solvent, specifically alcohol or non-alcohol, with the impact of factors like capacity for hydrogen bond formation, strength of London dispersion forces, and molecular polarity differing based on solvent type. These findings were used to develop artificial neural network models for solubility prediction. Solubility rankings were also correlated to excess enthalpy values for mixed solvent systems, where more negative excess enthalpies correlated to higher solubility. A select group of solvent blends were assessed for FDCA production in batch reactors using a commercial 5% Pt/C catalyst. The effects of solvent choice, initial reactant concentration, and temperature on reaction yields were examined in detail. Solvent degradation at reaction conditions was also investigated. Mixtures of sulfolane and water were found to balance FDCA yields, initial reactant concentration, and solvent robustness most effectively out of the solvents studied. Connections to prior upstream work in the conversion of biomass to FDCA precursor 5-hydroxymethylfurfural also suggest potential for a combined biomass-to-FDCA system. Finally, a comprehensive review of recent literature highlights paths forward for future research.

CHAPTER ONE

INTRODUCTION

1.1 Introduction and Motivation

The biomass-derived platform chemical,[1, 2] 2,5-furandicarboxylic acid (FDCA), has diverse applications that could help build a sustainable future. With the diminishing availability of nonrenewable resources, there is a growing emphasis on sustainable materials and production methods for consumer goods. One area affected by this is the petrochemical and plastics industry, as everyday products like food containers, shipping packaging, and water bottles are made from polyethylene terephthalate (PET).[3] Historically, over 1.4 trillion kilograms of PET have been produced[4] and an estimated 4% of fossil fuels extracted each year go to plastics manufacturing.[5] Using FDCA as a precursor to polyethylene furanoate (PEF), a bioplastic with structural similarities to PET, is a promising avenue for reducing fossil-based plastics consumption. Derived from C_6 sugars that are found in lignocellulosic biomass sources including corn stover, sugarcane bagasse, or wood pulp,[6] PEF is a fully biobased plastic. A recent estimate values the future commercial PEF industry at over $200 billion USD,[7] making PEF of both environmental and economic interest.

PEF has several advantages over PET, including an environmental one since PET is a leading contributor to plastic waste and environmental impact.[3, 8-10] Previous studies have explored emissions reductions through use of recycled PET and material reductions, but these strategies only achieve 24-28% reduction of CO_2.[11] By contrast, a transition to PEF could reduce non-renewable energy usage by an estimated 40-50% and greenhouse gas emissions by an

estimated 45-55%.[12] Additionally, the material properties of PEF are equivalent to or better than those of PET. Initial studies have shown that PEF has superior gas barrier properties than PET, with at least twice the resistance to O_2 and CO_2 permeation.[8, 13] This advantage is particularly valuable in applications like soft drink or beer bottling, where improved barrier properties can increase shelf life through the prevention of carbonation loss or product oxidation. PEF also has a higher glass transition temperature and thus a higher resistance to heat before deformation,[14] a valuable difference when working in high-temperature environments. At the same time, PEF's slightly lower melting temperature makes it less energy-intensive to process, improving manufacturing efficiency.[15] Mechanical testing via stress-strain studies demonstrate that PEF is stiffer than PET, with a more pronounced yield after a delayed onset of strain hardening.[16] This makes PEF an excellent choice for applications where material strength is critical, and allows for a reduction in material thickness compared to PET. These prior studies show the opportunity of bio-derived compounds like PEF to replace petroleum-based plastics such as PET. However, for PEF to be viable, manufacturing issues must first be addressed.

To produce PEF from biomass, several reactions need to take place (Figure 1). First, 5-hydroxymethylfurfural (HMF) must be produced through the dehydration of C_6 sugars extracted from biomass,[13] followed by the well-studied oxidation of HMF to FDCA.[17-21] The final reaction, upgrading FDCA to PEF, has been the subject of significant scientific study since the mid-twentieth century[22] with several major reviews published in recent years.[23-26] Despite this significant progress made to improve the HMF to FDCA process, the low solubility of FDCA in reaction solvents and the cost of noble metal catalysts still pose significant barriers to the production of FDCA. Since FDCA is the monomeric precursor to PEF, these challenges directly

affect the economic feasibility of PEF, currently preventing it from being a replacement for PET on the industrial scale.

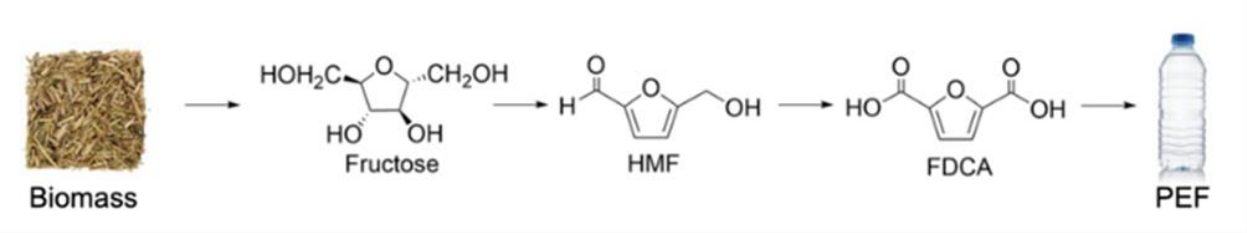

Figure 1. A simplified scheme showing the conversion of biomass to PEF, with fructose, HMF, and FDCA shown as intermediates.

The first challenge, FDCA solubility, has been studied previously in a limited range of solvents.[27-32] For example, Payne and Kerton found that in pure water, FDCA solubility was only 0.10 wt% at room temperature.[33] Later researchers found it to be slightly higher (~0.2 wt%) at 303 K.[27] Low solubility was also observed in organic solvents like acetonitrile (ACN, 0.02 wt% FDCA solubility)[32] and ethanol (EtOH, 0.92 wt% FDCA solubility).[32] Such low product solvation necessitates large reactors and volumes of solvent to yield small amounts of product or the use of costly additives to improve solubility, both of which increase the financial barrier to production.[34, 35] While other organic solvents and solvent blends have been found to increase FDCA solubility, including γ-valerolactone (GVL, 1.3 wt% FDCA solubility in a 50/50 w/w aqueous/organic blend),[27] dimethyl sulfoxide (DMSO, 30.7 wt% FDCA solubility in pure solvent),[32] and 1,4-dioxane (DX, ~3.1 wt% FDCA solubility in a 20/80 aqueous/organic blend),[36] minimal work has been done to understand the reasoning behind FDCA's solvation behavior in

these solvents. Elucidating the key factors that impact FDCA solubilization could lead to improved solvent selection for upgrading HMF to FDCA, and ultimately, more efficient production of PEF. On this front, only a narrow range of solvents have been applied in the HMF to FDCA oxidation reaction.[37-41] Though results in these solvents have been summarized in reviews,[26] these publications typically focus on catalyst effects or reactions conditions, rather than the impact of the solvent on reaction progress. Further study of solvent effects is necessary. Understanding solubilization behavior and solvent impact on reaction progress in a greater variety of solvents holds the promise of higher FDCA yields at a lower price point in the future.

The second challenge for FDCA commercialization is catalyst cost and activity, which have also been studied extensively in the literature.[25] The most reported catalysts use noble metals like platinum, gold, ruthenium, or palladium.[42] However, these noble metal catalysts are increasingly scarce[43] and lead to environmental and economic concerns with their use. Alternative catalysts using non-noble metals such as copper and iron have been previously investigated and shown promise, but the range of catalysts studied remains quite narrow.[42] Non-noble metal catalysts also tend to suffer from lower catalytic activity and reduced selectivity towards FDCA compared to noble metal catalysts. Development of a better understanding of these non-noble catalysts and how they impact the HMF to FDCA oxidation process could lead to improved conversion and yields, especially when combined with better solvents, and lower overall process costs.

This dissertation addresses these two challenges, aiming to advance the understanding of FDCA solubility and catalyst performance. This is done through synthesis of previous literature, experimentation, and modeling of both experimental and literature data using Artificial Neural

Networks. In addition to its direct relevance to FDCA production, this work provides insights into solubility, solvent behavior, and catalytic oxidation that may be valuable for research into other biomass-derived compounds and oxidation reactions. Ultimately, by addressing the two main challenges present in FDCA production, this work provides a foundation for future industry-scale production, contributing towards long-term reduction of carbon emissions.

1.2 Background

FDCA was first synthesized in 1876 by the German chemists Fittig and Heinzelmann.[44] Though initially regarding the compound as interesting, Fittig commented that "investigation [of FDCA] is not yet complete." Over the course of the 20th century other furan compounds, such as furfural,[45] were isolated and studied, with suggested applications as fungicides, additives or feedstocks in resin production, or as paint removers.[46] It was not until the early 2000s when the U.S. Department of Energy identified FDCA as a platform chemical for building a green future that the investigation of FDCA usage began to focus on producing sustainable polymers.[1]

Currently, the most effective process for making FDCA begins with the hydrolysis of lignocellulosic biomass to access the sugars, which are primarily fructose, glucose, and xylose, but can vary depending on the biomass type. These sugars, the most effective of which for furan production is fructose,[7] are then dehydrated to form compounds such as 5-hydroxymethylfurfural (HMF; Figure 2). Though there are other compounds that can be used as a starting point for FDCA synthesis, the most efficient pathway begins with HMF.[10] This is because HMF upgrading is relatively free of side reactions, as can be visualized in Figure 2.

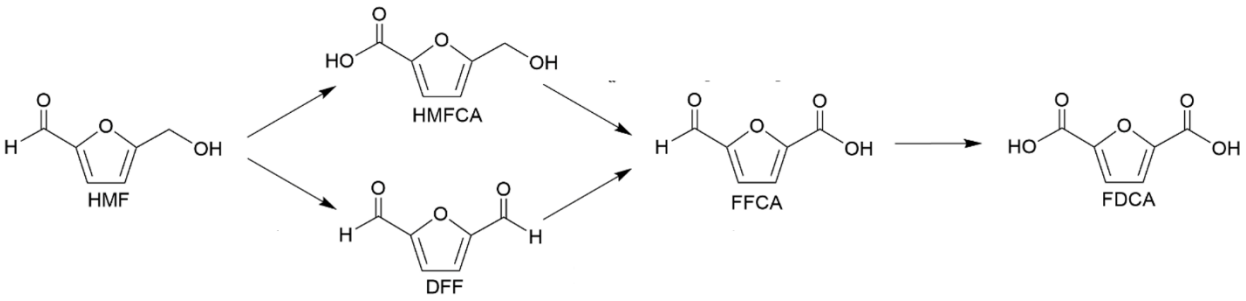

Figure 2. The oxidation reactions and intermediates for the upgrading of HMF to FDCA through two separate pathways. The top (HMFCA) oxidizes the aldehyde functional group of HMF first, while the bottom (DFF) pathway first oxidizes the alcohol functional group.

Of particular interest to researchers were the structural similarities of FDCA to terephthalic acid, the petroleum-derived monomeric precursor to PET (Figure 3). This observation led to the investigation and development of processes to convert FDCA into PEF, a bioplastic with excellent material properties and improved environmental impact compared to fossil-based PET. Though several companies, including Coca-Cola[47] and Carlsberg Brewing,[48] have announced intentions to begin implementing PEF in their product packaging, only one corporation has taken the leap to begin commercial production of PEF.

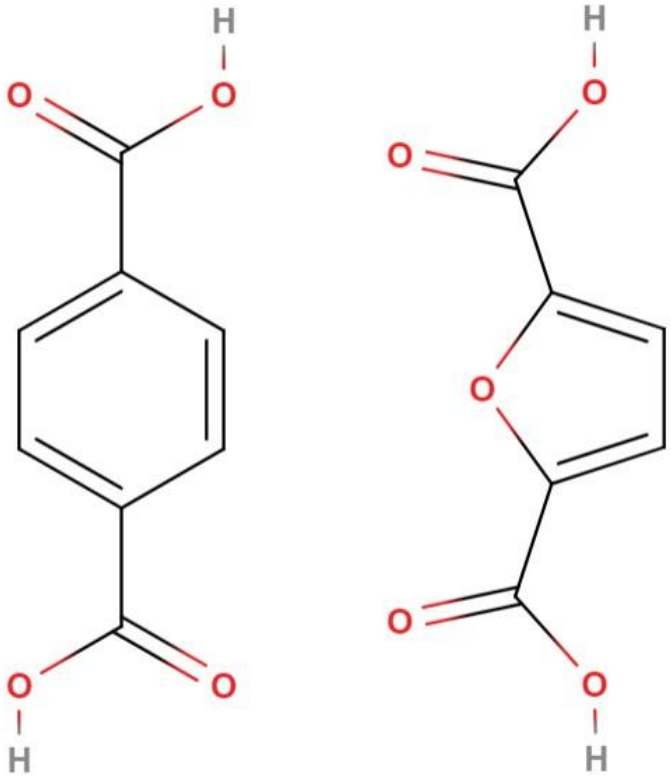

Figure 3. A structural comparison between terephthalic acid (left) and FDCA (right).

In 2021, the research and development sector of Avantium Technologies BV announced their commitment to producing PEF from FDCA as a primary research endeavor. In 2022, Avantium broke ground on a flagship plant in Delfzijl, Netherlands with plans to start full time production of PEF products in the near future. Current projections from within the company anticipate that PEF will sell at prices ranging from $4.73 to $5.92 (USD) per kilogram, while the necessary price range to be truly competitive with PET is between $1.78 and $2.96 (USD) per kilogram.[6] Such real-world progress and proof-of-concept are encouraging for the further study of FDCA production for PEF, while the economics affirm the need for improvements to the

efficiency of this promising process. Due to the economics, as of 2025, Avantium intends to sell PEF as an additive to PET.

As summarized in Section 1.1, improving FDCA production economics requires advances in reaction solvents to improve FDCA solubility and catalyst activity for improved HMF oxidation. An extensive, comprehensive literature review focusing on recent developments on these topics can be found in Chapter 2. This review provides an in-depth background on prior work in the field of HMF oxidation with a specific focus on catalyst and solvent effects and therefore, these topics will not be mentioned here. The review also laid the groundwork for work conducted in Chapters 3 – 5, highlighting knowledge gaps pertaining to key solvents and the application of key catalysts.

1.3 Hansen Solubility Parameter Theory

A range of thermodynamic models have been applied to the study and improvement of FDCA solubility, and more in-depth discussion of these models is presented in Chapters 2 and 3. Of specific applicability to the research presented in this dissertation are the Hansen Solubility Parameters, which are valued for their simplicity, applicability to large organic molecules like FDCA,[49, 50] and prior correlation to FDCA solubility.[29]

The conceptual basis for HSPs is that "like dissolves like", indicating that solutes are likely to dissolve in solvents sharing similar intermolecular properties.[29, 51-53] These properties are generalized to London dispersion forces (δ_D), molecular polarity (δ_P), and the capacity of the compound to form hydrogen bonds (δ_H). The HSP dispersion component, δ_D, is rooted in nonpolar atomic interactions relating to fluctuations in the electric field of molecules resulting from interactions with neighboring molecules. The dipole-dipole polarization value, δ_P,

addresses varying charge densities within a molecule, that then influence intermolecular organization. The hydrogen bonding value, δ_H, represents the electrostatic forces between a hydrogen atom and the dipole of another molecule. Both the polarity and hydrogen bonding parameters share a strict molecular nature, while the dispersion parameter relies on induced dipole interactions with other molecules.[51]

Solvation behavior is fundamentally governed by the Gibbs equation:

$$\Delta G_{mix} = \Delta H_{mix} - T\Delta S_{mix} \qquad (Eqn. 1)$$

where ΔG_{mix} is the change in the Gibbs free energy of mixing, ΔH_{mix} is the change in the enthalpy of mixing, T is temperature, and ΔS_{mix} is the change in the entropy of mixing for the system. A more negative change in Gibbs free energy of mixing is typically indicative of greater miscibility (or mixing) within the system. Relating to this, the HSP model focuses on the change in the enthalpy of mixing within a solvent-solute system by dividing ΔH_{mix} into its contributions from δ_D, δ_P, and δ_H. The individual HSPs are mathematically described by the following equations, which first combined the base HSPs into a "Total" HSP, δ_T:

$$\delta_T = \sqrt{\delta_D^2 + \delta_P^2 + \delta_H^2} \qquad (Eqn. 2)$$

and then relate this to ΔH_{mix}:[52]

$$\Delta H_{mix} = \varphi_1 \varphi_2 V_m \left(\delta_{T,1} - \delta_{T,2}\right)^2 \qquad (Eqn. 3)$$

where φ_i is the volume fraction of component i, V_m is the molar volume of the mixture, and components 1 and 2 are the solvent and solute, respectively. The volume fraction of a mixture, in the case of a multi-component solvent system, can be calculated as a mole-fraction weighted summation of each component using:

$$V_m = \sum_i x_i V_{m,i} \qquad (Eqn.\,4)$$

where x_i is the mole fraction of component i. From the forms of Eqns. 1-3, it follows that a solvent and a solute with similar contributions from δ_D, δ_P, and δ_H ("like dissolves like") would have a smaller ΔH_{mix} and thus a more negative change in Gibbs free energy of mixing, leading to greater miscibility between components.

Individual HSPs can be calculated for a system based on the prior work of Scott and Hildebrand.[54, 55] Scott and Hildebrand defined a general solubility parameter, δ, as the square root of cohesive energy density (CED) using:

$$\delta = \left(\frac{CED}{V_m}\right)^{\frac{1}{2}} \qquad (Eqn.\,5)$$

where E is the total cohesion energy of the compound. Hansen then divided this cohesive energy density into its intermolecular contributions, E_i, where:

$$CED = E_D + E_P + E_H \qquad (Eqn.\,6)$$

Using the intermolecular contributions from Equation 6, HSP parameters can be determined using:

$$\delta_i = \left(\frac{E_i}{V_m}\right)^{\frac{1}{2}} \qquad (Eqn.\,7)$$

for polarity (δ_P), dispersion (δ_D), and hydrogen bonding (δ_H).

Each chemical has specific, temperature-dependent values for these HSPs, which can be found tabulated in the literature or can be calculated using HSPiP software.[56] Pure component HSP values can be used to determine the HSPs of solvent mixtures via volume weighted averages of the individual components:

$$\delta_{mix} = \sum_i \varphi_i \delta_i \qquad (Eqn. 8)$$

which lays the foundation for further applications in solubility estimation.

Various approaches have been used to estimate solute solubility with HSPs. One of these methods, which was used by Zhuang et al.,[29] correlated a holistic comparison of total solubility parameters (δ_T):

$$\Delta\delta_T = \delta_{T,i} - \delta_{T,j} \qquad (Eqn. 9)$$

where i and j represent the solvent and solute, respectively, to FDCA solubility. By HSP theory, substances with lower $\Delta\delta_T$, and thus, more similar values of δ_T (Eqn. 2), are more likely to solubilize each other.[52]

A second holistic method to determine the likelihood of solubilization between a solvent and solute is the radius of interaction ($R_{i,j}$), which is defined by:[52]

$$R_{i,j} = \sqrt{4 * \left(\delta_{D,i} - \delta_{D,j}\right)^2 + \left(\delta_{P,i} - \delta_{P,j}\right)^2 + \left(\delta_{H,i} - \delta_{H,j}\right)^2} \qquad (Eqn. 10)$$

Similar to $\Delta\delta_T$, the lower the value of $R_{i,j}$, the more likely that the solute is soluble in the solvent.[57] A key difference between $\Delta\delta_T$ and $R_{i,j}$ is observed in their mathematical structures. While $\Delta\delta_T$ takes the difference between two unweighted solubility vectors, $R_{i,j}$ incorporates a weighting factor of 2 on δ_D. This coefficient has been experimentally determined and found necessary to create a spherical shape to an interaction plot.[51, 58] This is due to δ_D arising from atomic induced dipole interactions rather than as a function of molecular structure like for δ_H and δ_P, and thus being a weaker intermolecular force. Further, $R_{i,j}$ makes an explicit comparison between individual HSP values rather than the overall solubility vectors (δ_T) of the two compounds. Using $\Delta\delta_T$ it is possible for a pairing of solvent and solute to have significant

differences in values of δ_D, δ_P, and δ_H, but have similar values of δ_T. This is because δ_T is calculated for an individual component rather than a solvent-solute pairing, and a range of different inputs could equal the same δ_T value (Eqn 2). However, for $R_{i,j}$ (Eqn 10), since each HSP is compared individually and the parameter is calculated for a solvent-solute system rather than individual components, any discrepancies between the values of δ_D, δ_P, and δ_H will necessarily be captured.

For both holistic variables, solvents can be chosen to minimize the difference between them and the solute. Additionally, since the HSP values of a mixture are weighted by volume fractions of the individual components, mixing two individual solvents in different proportions can further minimize $R_{i,j}$ and $\Delta\delta_T$.

1.4 Artificial Neural Network Models

Non-linear systems, such as the solvent-solute interactions present in FDCA solubilization, require advanced models in order to be able to use inputs to predict outputs. One such methodology that has previously been used to characterize solvent-solute systems is the application of Artificial Neural Networks (ANN).[59, 60] In prior work, ANNs were used to correlate input data, such as physiochemical or thermodynamic properties, to output data like experimental solubility values. In this manner, the solubility of pharmaceutical compounds[61, 62] and proteins[63] were effectively estimated in a range of solvents. However, the application of ANNs as a modeling tool in the field of biomass engineering is less widespread. In 2021, Job et al. used a two-layer feed-forward ANN to estimate the yield of furfural from biomass-derived

sugars based on solvent polarity (δ_P) and severity,[64] but to the best of our knowledge, the solubility of FDCA has never been studied with ANN models.

A two-layer feed forward artificial neural network (ANN) is illustrated in Figure 4 where I_q^j represents input values with q indicating a different input type (from q to Q), and j indicating the experiment that the value comes from (j to J). An ANN model is designated to have Q input variables and J number of datapoints. Weights that connect input values I to hidden nodes H_k ($k = 1, \dots, K$) are designated with the following nomenclature: $w_{i,k}$ where i designates the affiliated input variable and k designates the affiliated hidden node. Weights that connect hidden nodes to the output (target) variables, T_n ($n = 1, \dots, N$), use the following nomenclature: $W_{k,n}$ where k designates the affiliated hidden node and n designates the affiliated target variable.

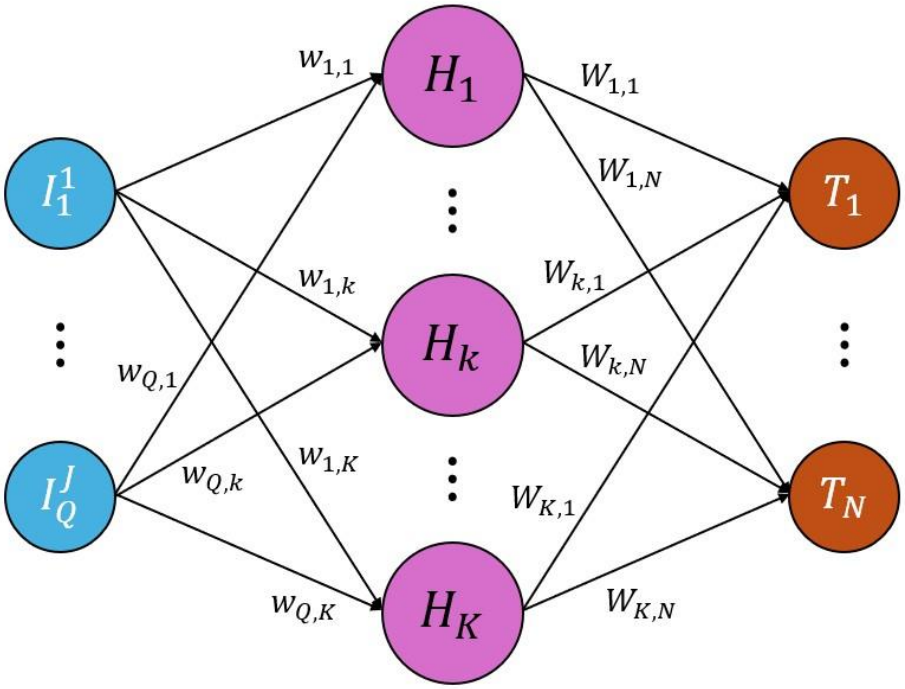

Figure 4. Generalized architecture of an artificial neural network, showing the inputs (I), hidden nodes (H), targets (T), and weights (w, W).

In this work, the number of hidden nodes was manually determined by minimization of a function, known as the corrected Akaike Information Criterion (AICc),[65] using the uncorrected form:

$$AIC = J * \log\left(\frac{SSE}{J}\right) + 2p \qquad (Eqn.\,11)$$

to calculate the corrected form:

$$AICc = AIC + \left(\frac{2p^2 + 2p}{J - p - 1}\right) \qquad (Eqn.\,12)$$

where J is the number of datapoints, SSE is the standard square error, and p is the number of parameters present in the ANN. Undefined parameters are calculated using:

$$p = H * (Q + 1) + T * (H + 1) \qquad (Eqn. 13)$$

where H is the number of hidden nodes, Q is the number of input variables, and T is the number of target variables. The sum of square errors (SSE) is defined as follows:

$$SSE = \sum_i (t_i - y_i)^2 \qquad (Eqn. 14)$$

where t is the experimentally determined (training) output data and y is the predicted target values.

Weighting parameters are adjusted to final values using a training algorithm performed by the ANN. Additionally, a transfer function is implemented between inputs I and hidden nodes H to transform weights before they are passed to the hidden node and then from the hidden nodes to the output. For all ANN models presented in this dissertation, the Levenberg-Marquardt gradient descent algorithm was used, and the transfer function was the hyperbolic tangent function:[64]

$$g(h) = \tanh(h) = \frac{e^h - e^{-h}}{e^h + e^{-h}} - 1 < g(h) < 1 \qquad (Eqn. 15)$$

for the inputs to the hidden nodes, and the transfer function was a linear function from the hidden nodes to the output.

1.5 Catalysis Background

Although the ANN model can predict the FDCA solubility of a solvent mixture using HSPs as inputs, the solvent needs to be able to convert HMF to high yields of FDCA.

Accordingly, reactions were run to assess a range of solvents for HMF oxidation. The work conducted in this dissertation used a Parr brand batch reactor for all catalyzed HMF oxidation reactions. (Figure 5) The experimental set-up consisted of an external heating jacket controlled by an Omega CN7500 temperature controller, a magnetic stir bar controlled by Fisher Scientific Isotemp stir plate, and the ability to be pressurized with 99.0% pure oxygen.

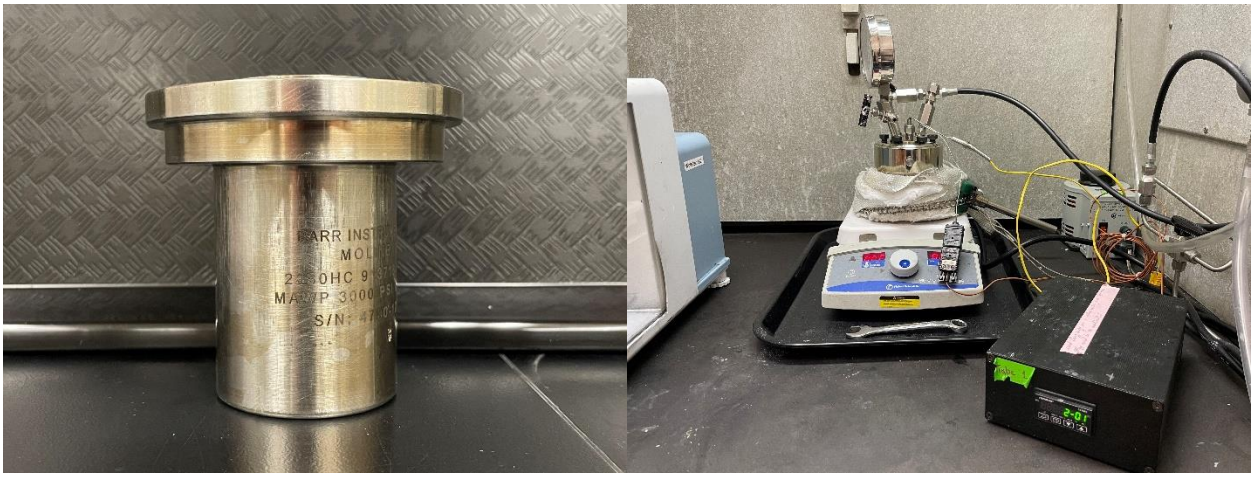

Figure 5. The 30 mL Parr reactor vessel used for oxidation reactions presented in this dissertation (left) and the overall reaction setup (right).

After the reaction, the effectiveness of a catalyst was assessed by determining the reactant conversion and product yield with higher values typically being desired. To calculate the conversion (X_{HMF}) of the initial reactant the equation would be:

$$X_{HMF} = \frac{N_{HMF_0} - N_{HMF_f}}{N_{HMF_0}} \qquad (Eqn. 16)$$

where N_{HMF_0} is the number of moles of HMF initially present in the reactor, and N_{HMF_f} is the number of moles of HMF present in the reactor at the end of the reaction period was used.[66] High

conversion is desirable, however, the distribution of products must be considered as side products can form. This can be done through the calculation of product yields (Y_i) using:

$$Y_i = \frac{N_i}{N_{HMF_0}} \qquad (Eqn. 17)$$

where N_i is the number of moles of product *i* obtained. *i*, In the case of the HMF to FDCA oxidation reaction, FDCA is the desired product and as such, high yields of FDCA indicate better catalysts and solvent systems. However, intermediates like DFF, HMFCA, and FFCA (Figure 2) are undesired but can be produced so selectivity (S_i) calculated using:

$$S_i = \frac{Y_i}{X_{HMF}} \qquad (Eqn. 18)$$

also needs to be considered.

A final metric used to assess batch reactions is a total mole balance on the system. Since the batch reactor is charged with a certain number of moles of HMF at the beginning of a reaction and mass is conserved in chemical reactions, the number of moles of final product plus the number of moles of unconverted HMF should be equal to the initial HMF moles (N_{HMF_0}). The total balance can be calculated using:

$$Total\ Balance = \frac{\sum_i N_{i_f}}{N_{HMF_0}} \times 100\% \qquad (Eqn. 19)$$

where N_{i_f} is the moles of each compound present at the end of the reaction. A mole balance of 100% means that there were no unidentified side products and that reactant or product were not lost to degradation, adsorption on the catalyst surface, or inefficient product separation / recovery during analysis.

1.6 Organization of this Document

Chapter 1 of this dissertation presents an introduction to the problems being addressed, a brief background on previous work, and relevant theory that the reader may find useful before continuing. Chapters 2, 3, 4, and 5 are inserted manuscripts that have been prepared for journal publication. Chapter 2 has been submitted for publication with *EES Catalysis* and has undergone peer-revision. It has been resubmitted for publication as of March 2025. Chapter 3 has been published in *ACS Omega*. Chapter 4 is still undergoing final preparations and will soon be submitted for publication with *Chemical Engineering Journal Advances*. Chapter 5 is undergoing final formatting and will be submitted to *Applied Catalysis A: General* for publication shortly. Chapter 6 summarizes the work conducted and presents an outlook on future work.

Chapter 2 is a comprehensive literature review on publications discussing 5-hydroxymethylfurfural (HMF) oxidation to 2,5-furandicarboxylic acid (FDCA) over heterogeneous catalysts in recent years. Interest in this topic has grown exponentially recently, and this substantial review covers noble and non-noble metal catalytic systems in both aqueous and organic solvent systems. Throughout the review, trends are discussed that were found when looking at the data from multiple papers collectively, and guidelines are provided to improve the catalytic activity and solvent selection for FDCA production. This literature review was published in *EES Catalysis*.

Chapter 3 presents FDCA solubility data in pure organic solvents, binary aqueous/organic solvent blends, and ternary blends containing water and two organics. Trends in the solubility data are correlated to the HSP thermodynamic model. The results presented have been

disseminated via publication in *ACS Omega* and as a part of conference proceedings at the American Institute of Chemical Engineers (AIChE) Annual Conference.

Chapter 4 describes the development and implementation of Principle Component Analysis (PCA), Artificial Neural Networks (ANNs), and the Amsterdam Modeling Suite COSMO-RS software to draw out the primary physiochemical properties of solvents that influence their capacity to solubilize FDCA. The ANN is trained using the data collected and presented in Chapter 3, and builds upon the trends found therein.

Chapter 5 presents a series of HMF upgrading reactions conducted in the solvents discussed and analyzed in Chapters 3-4. Additional analysis of solvent degradation is also presented to make recommendations about solvent selection for FDCA production. Trends observed in the literature (Chapter 2) are affirmed through novel experimental data.

Chapter 6 presents a summary of major findings across Chapters 2 through 5 and ties these findings back to the initial problems presented in Section 1.1. Then, recommendations are made for continuing the research conducted herein in both a specific sense (next steps for a future Montana State University graduate student in the Wettstein Laboratory) and a broad sense across the whole of academia.

CHAPTER TWO

RECENT DEVELOPMENTS IN SOLVENT AND CATALYST SELECTION FOR 5-HYDROXYMETHYLFURFURAL OXIDATION TO 2,5-FURANDICARBOXYLIC ACID

2.1 Contributions of Authors and Co-Authors

Author: Jacob M. Molinaro

Contributions: Conceptualization, Data curation, Analysis, Undergraduate supervision, Visualization, Writing – original manuscript preparation, revision, and formatting

Co-Author: Joel Swartzentruber

Contributions: Conceptualization, Data curation, Analysis, Undergraduate supervision, Visualization, Writing – original manuscript preparation, revision, and formatting

Co-Author: Van W. Ledger

Contributions: Data curation, Visualization, Writing – review and editing

Co-Author: Zachary T. Fredericks

Contributions: Data curation, Writing – review and editing

Co-Author: David Martin Alonso

Contributions: Data curation, Analysis, Writing – review and editing

Co-Author: Stephanie G. Wettstein

Contributions: Conceptualization, Analysis, Funding acquisition, Supervision, Visualization, Writing – original manuscript preparation, revision, and formatting

Manuscript in Chapter 2.

2.2 Manuscript Information

Jacob M. Molinaro, Joel Swartzentruber, Van W. Ledger, Zachary T. Fredericks, David Martin Alonso, and Stephanie G. Wettstein

EES Catalysis

Status of Manuscript:

_____ Prepared for submission to a peer-reviewed journal

_____ Officially submitted to a peer-reviewed journal

_____ Accepted by a peer-reviewed journal

__X__ Published in a peer-reviewed journal

Royal Society of Chemistry

31 January 2025

2.3 Abstract

The sustainable and economic production of bio-monomer 2,5-furandicarboxylic acid (FDCA) remains a major hurdle on the path to widescale adoption of biomaterials like polyethylene furanoate (PEF). PEF offers several advantages over conventional petroleum-derived plastics, including enhanced material properties and reduced environmental impact, making its economic feasibility a significant topic of study in recent years. Overcoming the challenges of high catalyst costs, low product solubility, and reactant degradation are key to improving the viability of the process. In recent years, significant research has been reported using both noble and non-noble metal catalysts over a variety of supports including activated carbons, transition metal oxides, and other polymer- or ceramic-based materials. Additionally, heterogeneous catalysts have been investigated in aqueous, organic, and binary aqueous/organic solvent systems to address solubility concerns. In parallel, a better understanding of the reaction mechanism and impact of reaction conditions such as temperature, time, and additives have provided insight into the factors that influence FDCA production. In this review, we report the impact these factors have on 5-hydroxymethylfurfural (HMF) oxidation, with key focus on noble and non-noble catalysts in both aqueous and organic solutions. Additionally, we present mechanistic insights as related to catalyst and solvent choice.

2.4 Introduction

Biomass is one of the most promising alternatives to replace petroleum as a source of carbon to produce chemicals. In 2004, the United States Department of Energy (DOE) identified the most promising chemical precursors that can be obtained from biomass[1] and in 2010, the list

was revisited by Bozell.[2] Among these building blocks, 2,5-furandicarboxylic acid (FDCA) has become one of the most relevant, with widespread interest in increasing yields to improve the economics of the process. If economic viability is achieved, there could be further commercialization of biomass-derived plastics, an industry that holds an estimated value of several billion dollars.[1, 7] Bio-based plastics have the potential to replace one of the most widely used materials for consumer goods like beverage bottles, food packaging, and textiles, polyethylene terephthalate (PET), which is derived from petroleum.[67] The process to create bioplastics starts from biomass to produce fructose, which is dehydrated to 5-hydroxymethylfurfural (HMF) then oxidized to form FDCA (Figure 6). The final step is polymerization of FDCA to the bioplastic polyethylene furanoate (PEF). This is a similar process to petroleum plastics with prior studies indicating that it would be feasible for existing PET production lines to transition to bioplastics production with minimal changes required.[68] PEF is the primary bioplastic made from FDCA and is fully recyclable using the same sorting technologies that are used for PET recycling.[69] Furthermore, PEF offers significant material advantages over PET including a higher glass transition temperature, improved O2 and CO2 barrier properties,[70] and being completely compostable under select conditions.[71] Although processes exist to efficiently polymerize FDCA to PEF, a bottleneck for PEF production persists in the economical production of FDCA.[13]

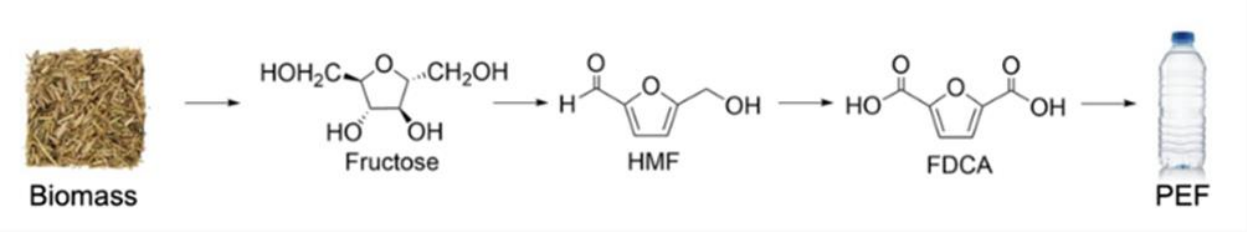

Figure 6. Simplified scheme to produce PEF starting from biomass to produce fructose, then dehydration to HMF, oxidation to FDCA, and the final polymerization.

Increasing interest in producing FDCA can be seen in research publications throughout the last 15 years (Figure 7), including several reviews of the subject,[23, 24] with the majority of the publications focused on catalytic HMF oxidation. Today, the most effective process to oxidize HMF uses a homogeneous Mn/Co/Br catalyst and acetic acid as the solvent (AMOCO process).[72, 73] A pilot-scale production plant using the AMOCO process is currently being operated in the Netherlands, but the total cost to synthesize PEF is currently estimated at twice that of PET.[5, 6] Recent projections suggest that PEF will sell at $4.73 - $5.92 USD per kilogram, while prices between $1.78 and $2.96 USD are necessary to be competitive.[6] Several research groups have conducted techno-economic analyses (TEAs) of FDCA production, consistently coming to similar conclusions.[7, 74-76] FDCA production using the AMOCO process in its current state is not economically feasible without subsidization, and limits the sustainability and environmental benefits of the process that heterogeneous catalysts could improve. However, to drive the reaction to FDCA there is a high cost affiliated with elevated reaction temperatures and pressures[77] and in many cases, the need for additives.[75] Thus, there has been a slow adoption of FDCA for plastics manufacturing. Recent research has focused on both noble and non-noble metal catalysts using a variety of catalyst supports including activated carbons,[78-82] mixed metal

oxides,[42, 83-85] and non-oxide ceramics.[20, 86] Research has also focused on a reduction in fouling[87] and sintering,[20] and an increase in catalyst recyclability,[88] to reduce economic considerations, particularly for more active noble metal catalysts.

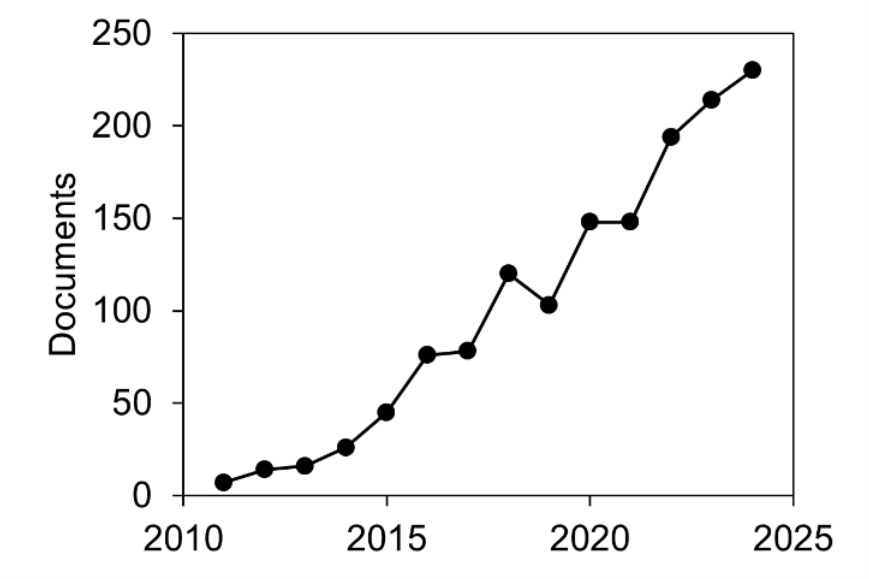

Figure 7. Number of journal articles and reviews in the last 15 years (obtained via Web of Science using: 2,5-Furandicarboxylic acid (Topic) AND cat* (Topic) and Article or Review Article (Document Types) and English (Languages).[89]

In addition to catalyst considerations, solvent stability and product solubility impose additional barriers to the HMF oxidation process. Solubility is of particular importance when dealing with diacids, such as FDCA, that have limited solubility in most common commercial solvents. For example, FDCA has a solubility of 0.2 wt% in water[32] and 1 wt% in ethanol[31] at STP, necessitating large solvent volumes and increased expenses with reactor sizing, material costs, and potential environmental impact. Low FDCA solubility has also been reported to result in separations and recovery challenges since FDCA can crystallize on the catalyst surface.[27, 76]

Though solubility can be partially mitigated by working at elevated temperatures,[27] this increases utilities costs and can lead to the degradation of sensitive furan compounds.[90] Thus, many studies have focused on reducing the expense of FDCA manufacturing by improving reaction conditions[91] and minimizing material costs using novel catalysts[70, 92] and solvents.[93] While the focus of this review is on heterogeneous metal-based catalysis, other oxidative approaches have demonstrated success in HMF upgrading. Electrocatalysis, particularly using bimetallic oxides[94-96] and layered double-hydroxide catalysts,[97] has achieved high selectivity towards FDCA under mild conditions. Similarly, photocatalysis has enabled HMF oxidation using visible-light-driven materials, achieving promising results at ambient conditions.[98-100]

In 2023, a comprehensive overview of catalyst selection was published by Prasad et al.[25] that described the state of the field and promising directions for further catalysis research. In recent years, significant progress has been made in improving FDCA solubility and in catalyst development. This present review furthers previous work by discussing insights to the mechanism of the HMF to FDCA reaction and highlighting recent advancements in the application of heterogeneous metal catalysts to production of FDCA, with a focus on the impacts that solvent, catalyst, and catalyst support selection can have on reaction efficiency and yield.

2.5 Mechanistic Insights

The oxidation of HMF to FDCA proceeds through a series of intermediates, shown broadly in Figure 8, with the specific reaction pathway being influenced by catalyst type, solvent choice, and reaction conditions. While the process involves several oxidation steps, the overarching theme is one of the stepwise conversions of functional groups attached to a central furan ring. This begins with an alcohol and aldehyde group on HMF and progresses to two

carboxylic acid groups on FDCA. Understanding the mechanism of this transformation allows for improved understanding of solvent and catalyst behaviors, potentially leading to more targeted development of reaction systems. The following section outlines the primary reaction pathways for the conversion of HMF to FDCA, discusses key intermediates, and provides insight to factors that influence selectivity.

In the initial steps of HMF oxidation, reaction conditions dictate whether the reaction proceeds through 5-hydroxymethyl-2-furancarboxylic acid (HMFCA) via initial oxidation of the aldehyde group or 2,5-diformylfuran (DFF) via initial oxidation of the alcohol group (Figure 8). The overall oxidation process starts with HMF, a furan ring with an alcohol group attached in the 2 position and an aldehyde group attached at the 5 position. The reaction then proceeds via one of the intermediates depending on which functional group is oxidized first with one path proceeding through DFF and the less common one through HMFCA.[101] The pathway followed is affected by the catalyst, solvent, and reaction conditions chosen, which will be discussed in more detail later in the review. From either the DFF or HMFCA intermediate, additional oxidation results in the formation of 5-formyl-2-furancarboxylic acid (FFCA), which contains an aldehyde at the 2 position and a carboxylic acid at the 5 position. The final oxidation step takes place at the aldehyde of FFCA, resulting in two carboxylic acid groups in the 2 and 5 positions and the formation of FDCA.

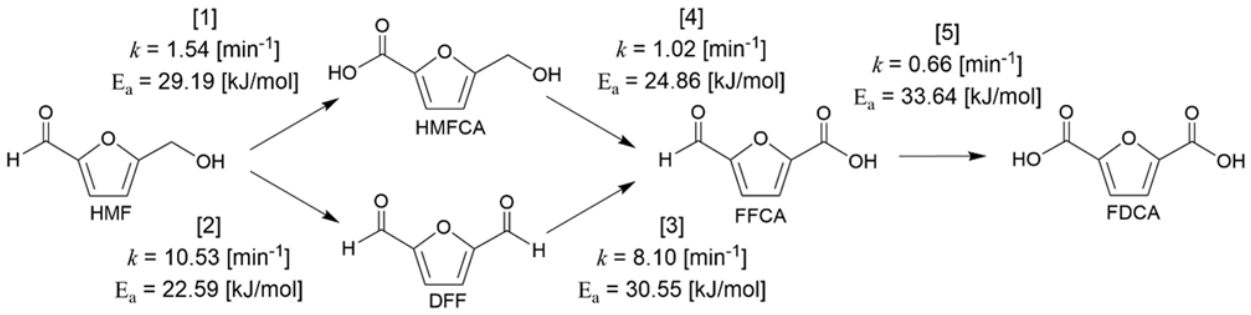

Figure 8. HMF to FDCA reaction pathway, adapted from Chen et al. [REF: 35] The kinetic parameters presented are for a semi batch reaction in acetic acid over a Co/Mn/Br catalyst at 413 K. (Scheme 1 in Manuscript)

These oxidations are facilitated by the breaking and reforming of bonds through interactions with oxidants, such as tert-butyl hydroperoxide (TBHP),[102, 103] O_2,[36, 79] or by interactions with alternate oxygen sources like water,[104, 105] and over a wide variety of catalysts including both noble and non-noble metals. It is advantageous to tailor the oxidant to the specific system being studied for the minimization of side products, particularly when using organic solvents or solvent blends. However, it has been shown that oxygen pressure has minimal impact on the conversion of HMF to FDCA above 2 MPa[106] and that a homogeneous oxygen source, such as water or TBHP, is more effective.[18] In some specific cases, an excess of oxygen has been observed to lead to catalyst poisoning,[107] suggesting that moderate pressures and concentrations may be optimal for HMF oxidation.

Initial 5-Hydroxymethylfurfural Reaction

For the first, more common pathway, the alcohol group of HMF is oxidized to an aldehyde, forming DFF (Figure 9), which according to Chen, G. et al.,[105] had a 29% lower activation energy than forming HMFCA using a Co-Mn-Br catalyst. This may be due to steric

hindrance on the bulkier aldehyde group, making it more energetically favorable for the alcohol to coordinate with a catalyst. This alcohol coordination can also be facilitated through Lewis acid-base chemistries present. Lewis-base sites on the metal catalyst surface interact with the mildly acidic hydroxyl hydrogen and weaken the carbinol C-H bonds, preparing the site for attack by a hydroxy radical. This radical can be sourced from either a peroxide, such as TBHP or hydrogen peroxide (H_2O_2), from water, or a homogeneous base such as sodium hydroxide (NaOH).[108] The hydroxy radical reacts with a scavenged hydrogen from HMF and forms water, while the carbinol carbon is left with an unbonded electron pair (Figure 9, top). This remaining lone pair facilitates the formation of a pi-bond with the oxygen in the alcohol, weakening the O-H bond and allowing for an oxidant radical, such as (·OH), to accept the hydrogen, resulting in a side product and the formation of DFF (Figure 9, bottom). Considering TBHP as an example oxidant and tert-butyl alcohol (TBA) as a solvent,[102] TBHP decomposes to form two radicals: tert-butoxy (t-BuO·) and hydroxy (·OH). The hydroxy oxidizes the -OH group of HMF, forming DFF, while the tert-butoxy radical reforms as TBA via the addition of hydrogen ions.

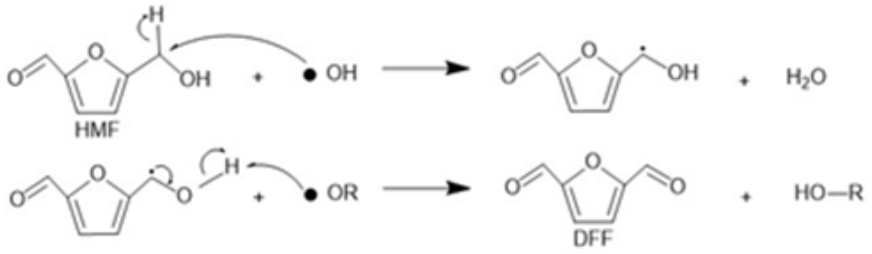

Figure 9. Reaction mechanism for the oxidation of HMF to DFF. A hydroxy radical attacks the carbinol carbon of the alcohol before a secondary oxidant facilitates the formation of a π-bond. (Scheme 2 in Manuscript)

An alternative reaction pathway to FDCA is to first oxidize the aldehyde group on the HMF molecule (Figure 8). Some selectivity to HMFCA is observed even under reaction conditions that favor the DFF pathway; however, researchers have reported that the addition of peroxide[109] or use of specific catalysts can increase selectivity towards the HMFCA pathway.[110, 111] It has been found that silver (Ag) catalysts are of particular use for selectivity towards HMFCA, with the most common choice being in the form of AgO_2 or $AgNO_3$.[110, 112] In aqueous media, the alkaline nature of the Ag(I) catalyst can prime the acidic carbonyl carbon of the aldehyde for conversion towards the diol intermediate (Figure 10), as has also been reported in other aldehyde oxidation reactions.[110, 113] Additionally, other novel catalysts have recently been found that are selective to HMFCA including those incorporating Mn in the 4+ valence state[109] and Mo in the 6+ valence state.[114]

The formation of a geminal diol intermediate state, which is not observed as a side product due to its instability, is critical to the transition from an aldehyde to a carboxylic acid (Figure 10). Following its formation, the geminal diol acts as a Brønsted-Lowry acid and gives up a hydrogen ion from its β-carbon. This elimination forms water or another side product and allows for the formation of a π-bond between the β-carbon and one of the alcohol groups. This alcohol group releases a hydrogen ion as well, completing the transition to HMFCA. As observed for the formation of DFF, a range of different oxidants can be used for the conversion to HMFCA, though the most common include water and peroxides like H_2O_2.[109, 112]

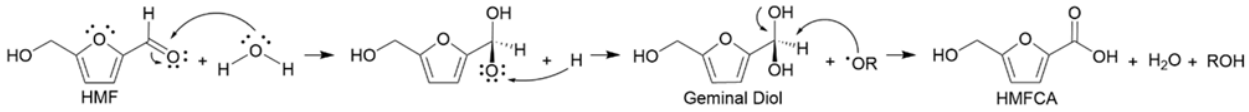

Figure 10. Reaction mechanism for the oxidation of HMF to HMFCA. The conversion of the aldehyde to a carboxylic acid is facilitated through a geminal diol intermediate followed by a β-hydride elimination.

Intermediates to 2,5-Furandicarboxylic Acid

The reaction mechanisms progressing from DFF or HMFCA to FFCA and FDCA follow similar chemistries to those presented for the conversion of HMF to DFF (an alcohol oxidation) and HMF to HMFCA (an aldehyde oxidation). DFF has two aldehyde groups, one at the 2 position and one at the 5 position, and both of these aldehydes must be converted to carboxylic acids for the formation of FDCA (Figure 11). For HMFCA, the alcohol group and the carboxylic acid group need to be oxidized (Figure 12). For DFF, the first oxidation targets one of the aldehydes and proceeds through the previously presented geminal diol intermediate (Figure 11). The second oxidation targets the unconverted aldehyde group, ultimately forming FDCA (Figure 13). The alcohol group will first oxidize to an aldehyde via the hydroxy radical attack mechanism and formation of a new π-bond (forming FFCA; Figure 12), before proceeding via the geminal diol intermediate and β-elimination to form FDCA (Figure 13).

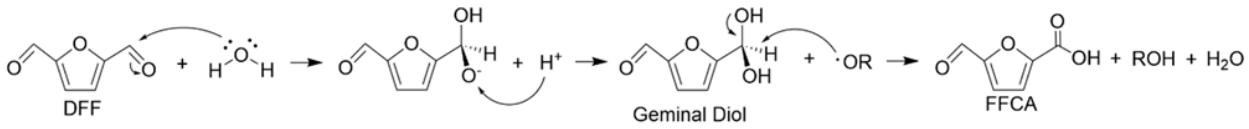

Figure 11. Reaction mechanism for oxidation of DFF to FFCA. The conversion of an aldehyde to a carboxylic acid progresses through the geminal diol intermediate before a β-hydride elimination allows the formation of a new C=O bond.

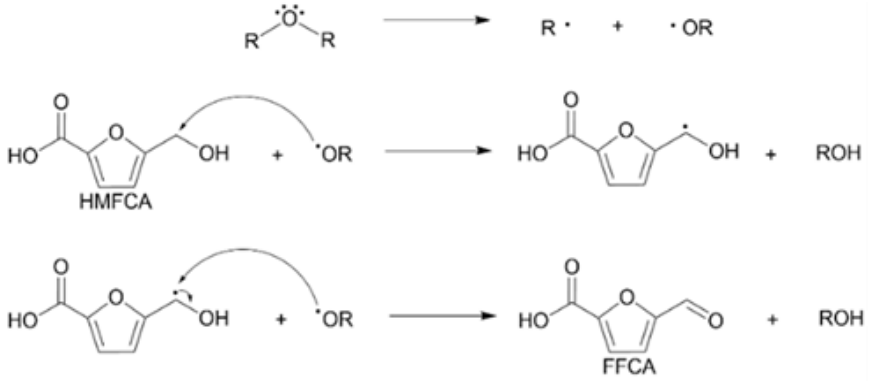

Figure 12. Reaction mechanism for the oxidation of HMFCA to FFCA. A hydroxy radical attack first targets the carbinol carbon of the alcohol group before a second oxidant results in the formation of a π-bond.

As reported by the mechanistic and kinetic studies of Chen et al., the activation energies necessary to proceed along the reaction pathway increase with each subsequent oxidation step, likely increasing with molecular bulkiness and increasing steric hindrance. (Figure 8) Following this trend, the limiting step of the overall HMF to FDCA process is the final aldehyde oxidation of FFCA to FDCA.[101] Starting with HMF and progressing through either DFF or HMFCA to FFCA and ultimately FDCA, the oxidation process leaves significant opportunity for intricate reaction engineering through alteration of solvents, catalysts, and reaction conditions.

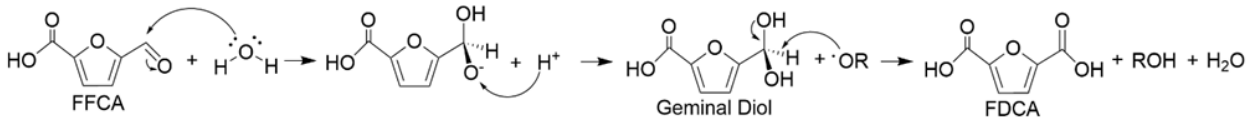

Figure 13. Reaction mechanism for the oxidation of FFCA to FDCA. The remaining aldehyde of FFCA is converted to a carboxylic acid via a geminal diol intermediate a β-hydride elimination.

2.6 Aqueous Reactions

Water, with or without the addition of a base (such as NaOH) is the most reported solvent for the oxidation of HMF to FDCA due to its low cost, availability, and in the case of bases, increased solubility of FDCA.[24, 25] Water has been shown an effective solvent for HMF oxidation, often achieving FDCA yields exceeding 80% across a range of reaction conditions. This is largely due to water's donation of hydroxy radicals and its low interactivity with the functional groups present in furan compounds (Figure 8).[36]

Despite high HMF conversion and FDCA yields, purely water-based reactions are typically run at low HMF concentrations (<1.25 wt% HMF) due to the low solubility of FDCA which can precipitate on the catalyst surface and deactivate the catalyst.[108, 115, 116] Adding bases to form the corresponding FDCA salt has been shown to increase solubility across a range of additives including $KHCO_3$,[117] $NaHCO_3$,[118] Na_2CO_3,[20] and, most commonly, NaOH,[30, 119] which helps avoid catalyst deactivation resulting in higher FDCA yields when operating at HMF concentrations greater than 2 wt%. However, the use of an excess of base should be carefully considered. It has been shown that a 0.3 M NaOH solution converted 10% HMF even without catalyst present (t = 0.5 h; T = 295 K),[120] and too caustic of a reaction solution can cause HMF degradation to formic acid and 2,5-bis(hydroxymethyl)furan (BHMF).[120] Vuyyuru and Strasser

reported that during a 10 h observation period at 333 K, nearly 80% of HMF degraded in the presence of NaOH (pH 13).[119] Caustic reaction solvents also lead to increased safety hazards, reactor vessel and piping material considerations, and additional processing steps to neutralize solvents before discharge. While increased base content and the subsequent presence of hydroxide ions improves FDCA solubility and catalytic activity, carbon loss due to furan degradation must be considered.

A growing movement towards base-free oxidation has focused on using specially engineered catalysts or non-caustic additives to improve reaction efficiency.[108, 121-123] For example, with the addition of metal or oxide catalysts, higher HMF conversions and FDCA yields have been shown possible at comparable temperatures and at higher initial HMF concentrations (>2 wt% HMF) in batch reactors.[78, 83, 102, 124] In the following sections, the impact of additives, catalyst type, and reaction conditions will be discussed to determine key trends for improving HMF conversion and FDCA yields in aqueous solvent systems.

Noble Metal Catalysts

Noble metal catalysts, such as platinum (Pt), palladium (Pd), gold (Au), silver (Ag), and ruthenium (Ru), are commonly used in industrial processes for the upgrading of organic molecules.[125, 126] This is true for HMF oxidation as well, with many publications prior to 2020 focusing on the use of noble metals as catalysts, which offer advantages such as achieving high reaction activation energy and better reusability, while non-noble metal catalysts are desirable for their lower cost and lesser environmental impact. Noble metals also have significant advantages such as improved catalytic activity, anticorrosion properties, and stability. These properties are corollary behaviors to the highly stable structures of noble metals, with fully filled or mostly

filled d-electron orbitals and only two or three possible oxidation states (Table 1).[24] The exception to this statement is Ru, which has been frequently applied in HMF catalysis in unique ways compared to other noble metals.

Metal	Possible Oxidation States	Electron Orbital Configuration
Pt	0, +2, +4	[Xe] $4f^{14}$ $5d^{9}$ $6s^{1}$
Pd	0, +2, +4	[Kr] $4d^{10}$
Au	0, +1, +3	[Xe] $4f^{14}$ $5d^{10}$ $6s^{1}$
Ag	0, +1	[Kr] $4d^{10}$ $5s^{1}$
Ru	0, +2, +3, +4, +6, +8	[Kr] $4d^{7}$ $5s^{1}$

Table 1. Oxidation states and electron orbital configuration of different noble metals.

These metals can be supported by a range of materials including activated carbon (AC), transition metal oxides, or non-oxide ceramics. Such materials often enhance the catalytic activity of the metals on the support by increasing electron transfer, particle distribution, or increasing the available surface area for reactant adsorption.

Platinum

Platinum catalysts typically provide high HMF conversion, high FDCA yields, and are resistant to fouling, allowing hydroxide ions to adsorb and interact with reactants more efficiently.[127] They have been effectively applied to the oxidation of HMF for a range of solvents and reaction conditions and often serve as a baseline for novel catalyst development. In regards

to HMF oxidation, Pt catalysts have been used at a range of temperatures and have shown to be active on various supports.

Index	Catalyst	Support	Base	t (h)	T (K)	O_2 P (MPa)	$C_{HMF,i}$ (wt%)	HMF/Cat. (mol/mol)	HMF Conv. (%)	FDCA Yield (%)	Ref.
1	Pt	Carbon	-	2.5	393	1	1.00	50	100	89.7	[36]
2	Pt	Carbon	-	3	393	1	3.00	75	100	80	[36]
3	Pt	NC-400	$NaHCO_3$	24	383	0.5	0.63	200	98.8	1.3	[128]
4	Pt	NC-600	$NaHCO_3$	24	383	0.5	0.63	200	99.9	2.5	[128]
5	Pt	NC-800	$NaHCO_3$	24	383	0.5	0.63	200	100	83.9	[128]
6	Pt	Carbon	$NaHCO_3$	24	383	0.5	0.63	200	100	66.8	[128]
7	Pt	UiO-66	-	14	408	0.5	0.31	200	99	68	[123]
8	Pt	MIL-101 (Cr)	-	14	408	0.5	0.31	200	98	28	[123]
9	Pt	Boehmite	-	14	408	0.5	0.31	200	98	19	[123]
10	Pt	PVP-UiO-66	-	14	408	0.5	0.31	200	99	46	[123]

Table 2. Platinum catalysts that have been studied for aqueous based HMF oxidation.

On a carbon support with no base addition, a recent study by Ryu et al. observed that higher catalyst to HMF ratios for shorter reaction times (Table 2, index 1) resulted in 10% more FDCA compared to longer reactions at lower catalyst loadings (Table 2, index 2), with yields ranging from 80-90%.[36] In another study, Yang et al. prepared platinum catalysts supported by nitrogen-doped carbon (NC), then stabilized the Pt nanoparticles (NPs) using polyvinyl alcohol (PVA).[128] The NC supports were made from pomelo peel and attained different surface areas based on the carbonization temperature (673, 873, or 1073 K). The reactions used $NaHCO_3$ as a base additive.

The supports studied, NC-400 (Table 2, index 3), NC-600 (index 4), and NC-800 (index 5), had S_{BET} values of 513, 740, and 809 m^2/g, respectively, with both pore volume and average pore diameter increasing in parallel to overall surface area. Compared to both a traditional,

commercially available AC support (Table 2, index 6) and the lower S_{BET} prepared supports (indices 3 and 4), the NC-800 support (index 5) that was synthesized with the highest carbonization temperature, reported the highest FDCA yields of 83.9% at 100% HMF conversion and lower percentages of intermediates.[128]

A base-free study by Hou et al.[108] found that although the surface area of the catalyst did trend with FDCA yield, in most cases, the amount of phosphorous (P) on the support also contributed to the activity of the catalyst (Figure 3). Maintaining standard reaction conditions, levels of P doping on a manganese (Mn) oxide support were varied and compared to non-doped MnO2, which converted 100% of the HMF with 67% FDCA selectivity. Increased ratios of P/Mn on the catalyst surface peaked at the highest P/Mn surface ratio evaluated and resulted in 98% FDCA selectivity at 100% HMF conversion (Figure 14). However, this catalyst did not have the highest P/Mn bulk ratio (determined by ICP-MS). Increasing the P/Mn ratio from the optimal 0.50 to 0.55 and 0.59 decreased the FDCA yield to 73% (0.57 P/Mn surface ratio) and 66% (0.42 P/Mn surface ratio), respectively, while increasing the FFCA yield.

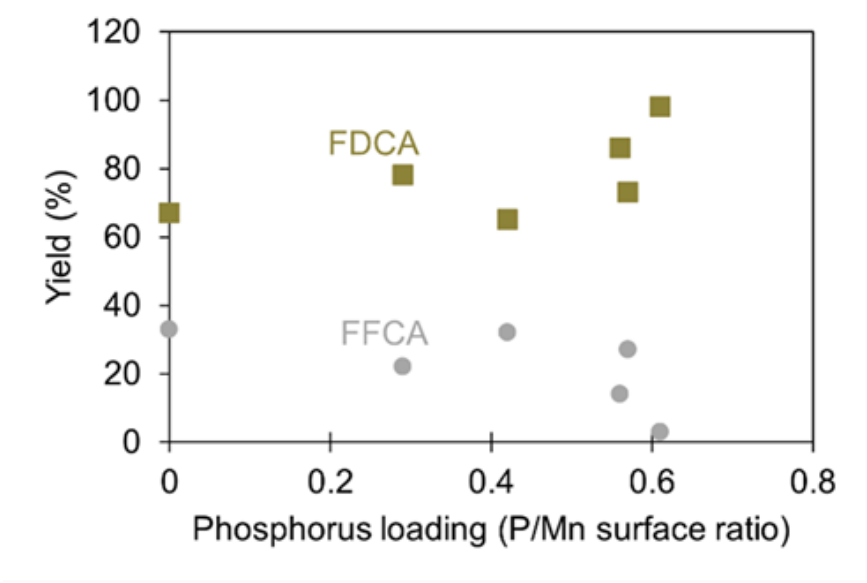

Figure 14. Impact of P dopant amount on the surface of the catalyst (determined by XPS) on FDCA (■) and FFCA (●) yields for the MnP_yO_x catalyst (100% HMF conversion for all). Reaction conditions: 100: 1 HMF: Pt molar ratio, 1.25 wt% HMF, T = 383 K, P_{O2} = 1 MPa, 24 h.[108]

The decreased activity of the catalyst at increased P concentrations may be due to the lower P amount at the surface or the formation of stronger Mn-P-O interactions that decrease the availability of oxygen for use as an oxidizing agent. The presence of phosphorous in the support was noted to help maintain the metallic (Pt^0) state of Pt and facilitate the reduction of MnO_x to stabilize at Mn^{4+} and Mn^{3+} states.[108] This aligns well with prior discussion of P-doping and its impact on catalytic activity elsewhere in the literature.[129]

The importance of maintaining Pt in its metallic (Pt^0) state was also reported by Seehamongkol et al.,[123] who investigated the catalytic activity of Pt nanoparticles (NPs) on metal-organic frameworks (MOFs). At 98-99% HMF conversion, Pt without surfactant on a zirconium oxide MOF (UiO-66) support resulted in the highest FDCA yields of near 70% (T =

408 K, PO2 = 0.5 MPa; Table 2, index 7). Comparatively, a MIL-101 (Cr) MOF reported a 28% yield (index 8), Boehmite reported a 19% yield (index 9), and polyvinylpyrrolidone (PVP)-stabilized Pt on UiO-66 reported a 46% yield (index 10). Both catalysts with and without PVP-stabilization produced 2% FFCA as a side product whereas the Boehmite and MIL-101 (Cr) supported catalysts resulted in 7% and 20% FFCA, respectively.[123] Much like the supports studied by Hou et al., the UiO-66 MOF was proposed to offer the greatest availability of basic sites and adsorbed oxygen species. Also, in the case of Pt/UiO-66, the relative oxidation state distribution of Pt^0 was higher compared to Pt-PVP/UiO-66 and Pt/MIL-101(Cr) resulting in higher FDCA production. Additionally, the researchers hypothesized that the PVP-stabilized catalyst had lower activity due to the limited substrate accessibility as a result of polymers blocking active sites,[123] which has also been seen in prior literature.[20, 130]

Temperature is another relevant factor in FDCA selectivity, as reported in multiple place in the literature, as kinetic studies on the decomposition of HMF showed that the decomposition rate constant doubles with every 25 K of increasing temperature.[131] When the $Pt/MnP_{0.50}O_x$ catalyst was tested across a range of temperatures, an expected increase in FDCA yield occurred (Figure 15; filled squares).[108] A similar increase in FDCA yield from 11% (368 K) to 68% (408 K) was observed when using the previously discussed Pt/UiO-66 catalyst; however, at 423 K, the FDCA yield decreased to 62% (Figure 15; open squares).[123] This decrease in yield was hypothesized to be due to HMF degradation at the higher temperature,[123] which has been shown in other studies as well. HMF degradation has been reported to typically begin around 403 K with some variability due to reaction conditions like solvent selection or the presence of

additives, decreasing selectivity. Similar observations have been reported in the literature, with downturns in FDCA production at 423 K in methanol[81] and above 393 K in ACN.[84]

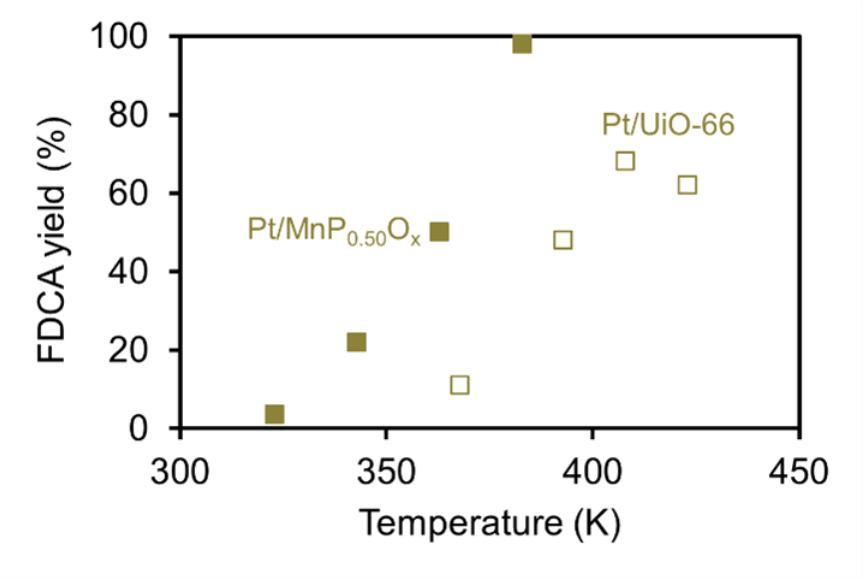

Figure 15. Effect of reaction temperature on FDCA yield with a Pt/UiO-66 catalyst (□)[123] and a Pt/MnP0.50Ox catalyst (■).[108] [43] Reaction conditions for Pt/UiO-66 catalyst: HMF: Pt 200: 1 molar ratio, PO2 = 0.5 MPa, t = 14 h[123] and for $Pt/MnP_{0.50}O_x$ catalyst: HMF: Pt 100: 1 molar ratio, P_{O2} = 1 MPa, t = 24 h.[108]

Among the most significant factors impacting catalyst activity were overall surface area, the addition of stabilizers such as PVA or PVP, and reaction temperature. Polymeric stabilizers run the risk of reduced yields, as they can block active sites and reduce effective catalyst surface area. Higher surface areas for a given catalyst type correlated with higher FDCA yields due to an increased number of active sites and capacity for reactant adsorption to the surface of the catalyst. Additionally, the availability of Lewis-base sites and surface-adsorbed oxygen species to promote the oxidation of furan compounds must be considered. Pt was most effective in its

metallic state (Pt^0), likely since it was most capable of accepting or donating a d-orbital electron. Increasing temperature and time improved HMF conversion and yield, but with diminishing returns as temperatures above approximately 408 K resulted in lower FDCA yields, likely due to HMF degradation.

Gold and Palladium

In recent years, Au has been commonly reported for the catalytic oxidation of HMF,[20, 115] often as a bimetallic catalyst with Pd,[78, 132] Ag,[118] Ni, Fe, and Cu[122] as secondary metals. The additional metal stabilizes Au NPs, as pure Au tends to leach from supports or sinter into larger particles at elevated temperatures.[20] Larger particles tend to be less evenly dispersed, have lower surface area to volume ratios, and have fewer active sites compared to an equivalent weighting of smaller, more evenly distributed particles.

Kharlamova et al.[132] evaluated multiple synthesis techniques that resulted in different average particle sizes of Au, Pd, and bimetallic AuPd over a ZrO_2 support (Table 3). They found that for pure Au, decreasing particle size correlated with increasing FDCA yields. Deposition-precipitation had the smallest grain size (9 nm) and highest yield (13.4%), followed by impregnation-reduction under basic conditions (15 nm; 12.3%), impregnation-reduction under acidic conditions (30 nm; 5.0%), and incipient wetness impregnation (70 nm; 5.9%). Somsri et al. similarly noted higher yields with smaller particle sizes when comparing Au catalysts on CaZSM-5 supports synthesized via two different methods, incipient wetness (IW; Table 4, index 1) and deposition-precipitation (DP; Table 4, index 2). The catalysts produced using an incipient-wetness method resulted in a smaller average size of Au particles and led to significantly higher FDCA yields compared to catalysts synthesized with a deposition-precipitation method (Table

3).[20] The contrast in particle size relative to preparation method in the two studies indicates that there are additional factors influencing the effectiveness of the preparation method but highlights the importance of smaller Au particles for increasing FDCA yields.

	Au				Pd				AuPd			
Synthesis Method	Wt%	Particle Size (nm)	HMF Conv. (%)	FDCA Yield (%)	Wt%	Particle Size (nm)	HMF Conv. (%)	FDCA Yield (%)	Wt%	Particle Size (nm)	HMF Conv. (%)	FDCA Yield (%)
IW	2.1	70	74.5	5.9	2.0	2.3	6.5	0.1	1.2/0.9	NR	10.5	0.6
IW*	0.8	3.6	100	75.1	-	-	-	-	-	-	-	-
DP	1.2	9	100	13.4	2.5	2.2	15.5	0.8	0.4/0.9	NR	26.3	1.3
DP*	0.84	1.3	99.8	20.6	-	-	-	-	-	-	-	-
IRB	1.2	15	93.6	12.3	1.6	5.2	72.5	6.4	1.3/0.9	NR	95.2	37.3
IRA	2.0	30	91	5	1.6	25	76.9	6.5	1.4/0.7	24	100	77.9

Table 3. Effects of different catalyst synthesis techniques for aqueous HMF oxidation using ZrO2 supports[118] and CaZSM-5 supports (marked with *).[82] For synthesis methods: IW = incipient wetness impregnation; DP = deposition-precipitation; IRB = impregnation-reduction under basic conditions; IRA = impregnation-reduction under acidic conditions.

The same correlation between particle size and FDCA yield was not seen with Pd (Table 3), where larger particle sizes resulted in the highest FDCA yields. In most Pd reactions, the conversion of HMF was low and for both the single metal Au and Pd reactions the majority of HMF converted to HMFCA and FFCA (Figure 16).[132] The alkaline conditions were more effective for the pure Au catalyst while the acidic chemical reduction technique resulted in higher FDCA yields for both the pure Pd and the bimetallic AuPd catalyst. For the bimetallic AuPd catalysts, the synthesis method had a much larger impact, where incipient wetness and deposition-precipitation methods resulted in low FDCA yields, but impregnation-reduction methods resulted in higher conversions and yields (Table 3).

Index	Catalyst	Support	Base	t (h)	T (K)	O_2 P (MPa)	$C_{HMF,i}$ (wt%)	HMF/Cat. (mol/mol)	HMF Conv. (%)	FDCA Yield (%)	Ref.
1	Au-Pd(imp)	ZrO_2	$NaHCO_3$	24	353	0.5	0.63	100	13.8	0.5	[132]
2	Pd-Au(imp)	ZrO_2	$NaHCO_3$	24	353	0.5	0.63	100	59.1	4.6	[132]
3	$Au_{1.5}Pd$	C	NaOH	6	333	0.3	5.93	110	99	70	[78]
4	$Au_{1.5}Pd$	C	$NaHCO_3$	6	363	0.3	5.93	110	96	27	[78]
5	Au	MnO_2	-	12	373	0.1	0.99	20.9	75.7	52	[115]
6	Au	MnO_2	-	12	373	0.1	0.99	9.3	99	93.2	[115]

Table 4. Gold and palladium catalysts studied for aqueous HMF oxidation.

For basic conditions the FDCA yield was 37.3% and for acidic conditions, impregnation-reduction synthesis resulted in FDCA yields of 77.9%. The researchers attributed this higher activity to the presence of $Au_{1-x}Pd_x$ nanoparticles that cause a synergistic effect due to the electron redistribution of the metals, which favors initial HMF oxidation through the hydroxyl group (Scheme 2) versus the HMFCA intermediate.[132]

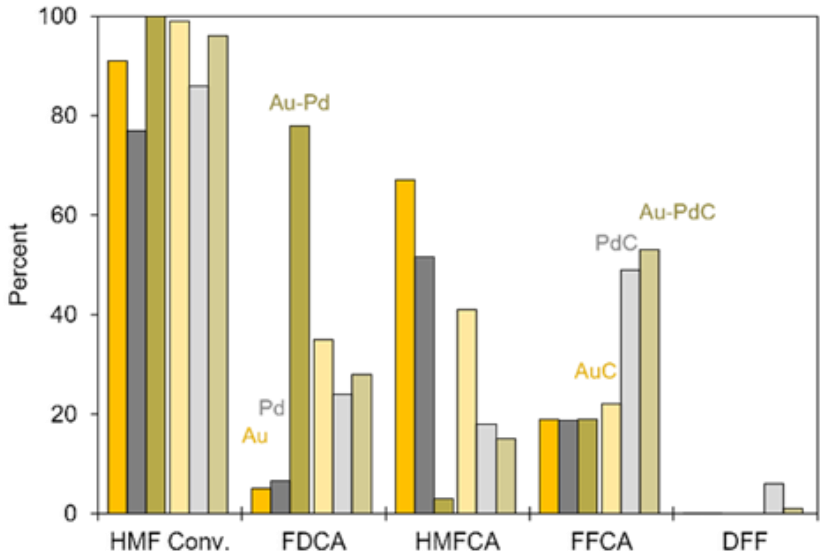

Figure 16. Product yields for reactions using impregnation-reduction under acidic conditions synthesized catalysts using Au (■), Pd (■), and Au-Pd (■) on ZrO_2[118] and deposition-precipitation method on Au/C (■), Pd/C (■), and Au-Pd/C (■) catalysts.[78] Reaction conditions for impregnation-reduction catalyst: 100:1 HMF:catalyst molar ratio, 0.2 mol $NaHCO_3$, 0.63 wt% HMF, T = 353 K, P_{O2} = 0.5 MPa, and t = 24 h.[132] For deposition-precipitation catalyst: 110:0.93:0.07 HMF:Pd:Au molar ratio, 20 mmol $NaHCO_3$, 5 mmol HMF, T = 363 K, P_{O2} = 0.3 MPa, and t = 6 h.[78]

When comparing the Au/Pd catalysts produced by impregnation-reduction under acidic conditions on ZrO_2 supports to those produced by depositing Au on a commercial Pd/C catalyst using a deposition-precipitation method, both achieved high HMF conversion, but the product distributions differ. (Figure 16) On the ZrO_2 support, single metal catalysts of Au and Pd showed low FDCA yields, favoring HMFCA and FFCA under the reaction conditions. In contrast, the bimetallic Au-Pd/ZrO_2 catalyst exhibited high selectivity to FDCA.[132] On carbon supports, both single metal and bimetallic Au and Pd catalysts produced FDCA yields ranging from 24-35%. Pure Au produced more HMFCA (41% yield) while both Pd and Au/Pd catalysts generated more FFCA (49% and 53% yields, respectively) after 6 h. Extending the reaction time for the Pd/C

catalyst to 9 h increased both HMF conversion and FDCA yield by approximately 4% while the FFCA, HMFCA, and DFF yields all decreased slightly.[78] Kharlamova et al. ran reactions for 24 h and achieved higher FDCA yields, comparatively. However, when the Au-Pd/ZrO_2 catalyst was run at shorter times (4 h), the HMF conversion (~78%) and FDCA yield (~5%) were lower while yields of intermediate products increased: HMFCA (~18%) and FFCA (~55%).[132] This indicates that the intermediates may have been converted to FDCA if the reaction was run for longer time over the carbon supported catalysts.

Another option to increase the reaction is to add base. When a strong base, NaOH, was used, the HMF conversion increased to nearly 100% for both single metal Au and Pd catalysts and all ranges of the Au-Pd catalysts. Additionally, the FDCA yields increased to approximately 70% for the bimetallic Au-Pd catalysts with single digit percents of HMFCA forming and no detectable DFF or FFCA present (Table 4; index 3). This was attributed to the presence of hydroxide ions from the strong base, which resulted in the formation of a geminal diol intermediate and a preference for the HMFCA pathway as shown in Scheme 3.[78] Peng et al. also evaluated different Au loadings onto the 10% Pd/C catalyst, ranging the percent of Au from 0.75 to 4.5 wt%. Changing the Au loading had limited effect on the HMF conversion (92- 97%) or the FDCA yield (23-31%) when NaOH (Table 4, index 3) or $NaHCO_3$ (Table 4, index 4) bases were added. However, when they evaluated the rate of reaction with $NaHCO_3$ as the base, the reaction rate increased as the amount of Au on the catalyst increased.[78] Zeng et al. also studied the effect of metal loading by investigating Au catalysts on an MnO_2 support at loadings of 2.5 and 5.6 wt% Au. Increasing the loading of Au from 2.5 wt% (Table 4, index 5) to 5.6 wt% (Table 4, index 6) increased HMF conversion from 75.7% to 99%, and FDCA yields from 70.2% to

97.7%.[115] As the number of active sites available increased with Au loading, the catalytic performance also increased. They also attributed improved catalytic activity to the higher ratio of Au:Mn as metal-metal interactions were reported to form superoxide ions (O_2^-), leading to enhanced oxidation.[115]

Su et al. also used a metal oxide support, $MgAlO_x$, which held Au particles in a negative state and improved oxidation.[122] Additionally, they created Au-based bimetallic catalysts that contained approximately 1.1 wt% Au and 0.018 to 0.031 wt% of the additive metal, finding that the metal altered product selectivity and changed the electron density of Au species. Across all bimetallic Au-M catalysts studied, FDCA yields were observed to increase, except for Au-Cu. The Au-Ni catalyst achieved the highest conversion (100%) and yield (76.6%) amongst the studied bimetallic catalysts (Figure 17).[122] Fe and Ni were both observed to promote HMF and HMFCA oxidation, while Pd was more effective at the promotion of FFCA oxidation. Pd has been previously cited as enhancing the stability of Au catalysts through improved electron transfer and modulation of electron structure in bimetallic catalysts,[133] making it a commonly used additive metal to Au. The lower activity of the Au-Cu catalyst may be attributed to the similar electron structures of the two metals, which are both group 11 elements with one valence electron. Differing valence structures, such as those observed in the Au-Ni catalyst (with 1 and 2 valence electrons, respectively), may lead to greater electron density and thus catalyst activity. Furthermore, the improved FDCA yields over Au-Ni compared to Au-Pd may also relate to the atomic structures of the dopant metal. Ni, a smaller atom, has three less electron shells than Pd, making it more reactive even though they are both group 10 metals. This higher reactivity may

correlate to better reactant adsorption compared to the more stable Pd, allowing the Au portion of the catalyst to more effectively oxidize towards FDCA.

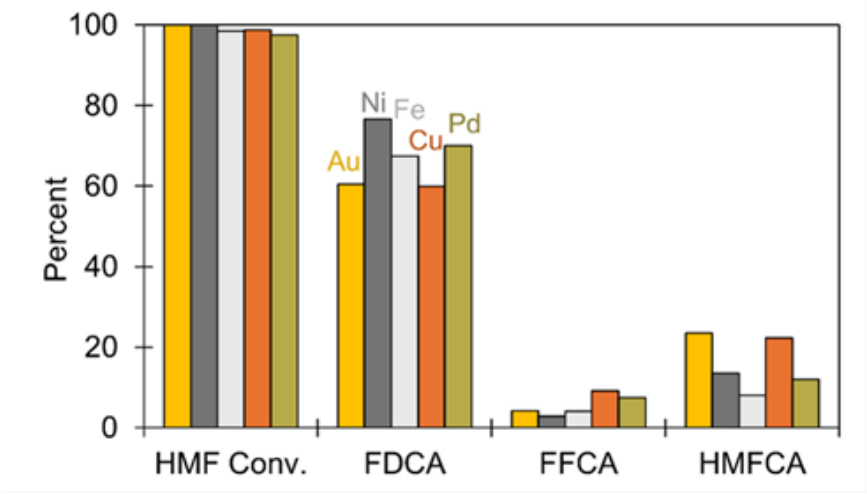

Figure 17. Yields and conversion of adding metals to an Au/$MgAlO_x$ catalyst. Reaction conditions: 70:1 HMF:metal molar ratio, 0.25 wt% initial HMF, T = 363 K, P_{O2} = 0.5 MPa, and t = 2 h.[122]

Using an SiO_2 support, de Boed et al.[118] synthesized bimetallic catalysts using various amounts of Au and Ag but maintained an HMF:catalyst molar ratio of 72:1. They found with a pure Au catalyst the HMF conversion was 100% and that approximately 40% FDCA and 60% HMFCA were produced. When Ag was added up to 0.18 mass fraction, the HMF conversion remained at 100%, but the FDCA yields increased to over 90% while the HMFCA dropped proportionately (Figure 18a). Increasing the mass fraction of Ag to over 0.2 decreased the HMF conversion and FDCA yield, again favoring HMFCA production. Using only Ag on SiO2, there was no FDCA or HMFCA produced even though the HMF conversion was 81%.[118] Ke at al.[110] also found that using a pure Ag catalyst resulted in no FDCA production. Continuing to add up to

0.4 mg of Pt to the initial 0.1 mg of $AgNO_3$, decreasing the mass fraction of silver to 0.2, still did not produce FDCA (Figure 18b). Below the Ag mass fraction of 0.2, as the Pt loading and the overall ratio of catalyst to reactant increased, both conversion of HMF and selectivity to FDCA increased. The initial metal ratio of 2.8:1 Pt:Ag (143:1 HMF:catalyst) resulted in 26% HMF conversion, primarily to HMFCA. However, increasing the Pt loading further while keeping the $AgNO_3$ at 0.1 mg (12:1 HMF:catalyst), increased FDCA yields up to approximately 86% FDCA at 100% HMF conversion.[110] As previously observed during discussion of mechanistic insights, Ag^{+1} negatively impacted FDCA selectivity by targeting HMFCA production instead.

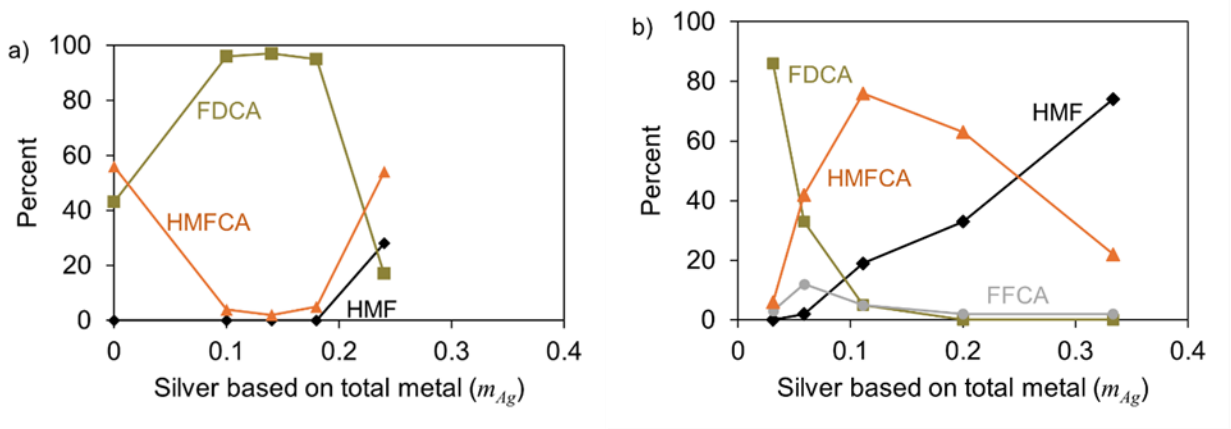

Figure 18. Effect of silver loading on a bimetallic a) Au/Ag SiO_2 catalyst (conditions: 79:1 HMF:Au molar ratio, 0.4 mmol $NaHCO_3$, T = 353 K, P_{O2} = 1 MPa, and t = 6 h)[118] and b) Pt/Ag catalyst where the x-axis represents the mass fraction of Ag of the total mass of the metals. Reaction conditions: 50:1 HMF:Pt molar ratio, 0.8 mmol $NaHCO_3$, T = 373 K, O_2 bubbling at 75 mL/min, and t = 1 h.[110]

As noted in the Pt section, temperature can also affect the reaction. Zeng et al.[115] studied temperature effects over a range of 333 K to 373 K using the previously mentioned 5.6 wt% Au/MnO_2 catalyst. As the temperature increased, the HMF conversion stayed relatively constant

around 90% until 373 K, at which point it was almost 100% (Figure 19). However, the product selectivity varied across the temperature range. At low temperatures, HMFCA was present in significant amounts with lower yields of FDCA and little FFCA, but as the temperature increased, higher amounts of FDCA and FFCA were produced, reaching 94.1% FDCA selectivity at 373 K,[115] which indicates that the higher temperatures were critical for proceeding along the reaction pathway.

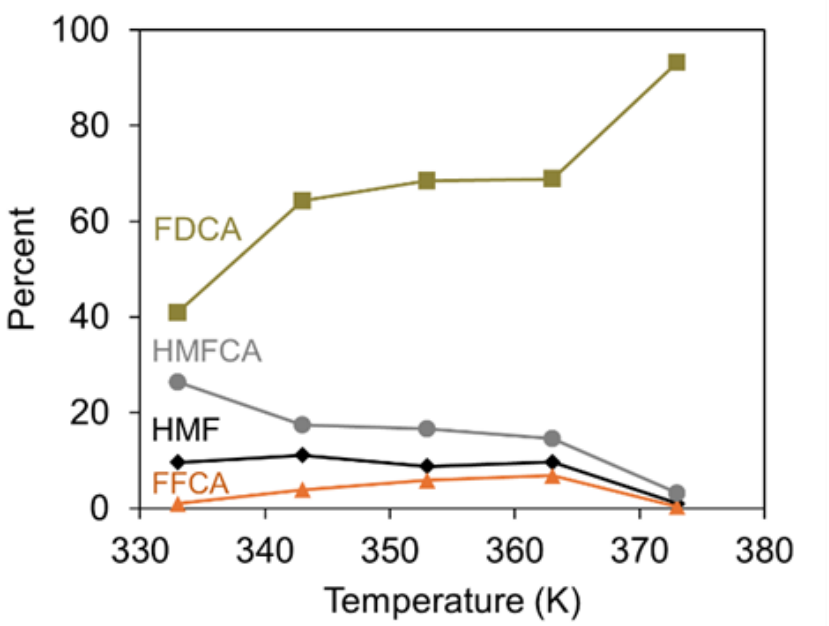

Figure 19. Remaining HMF (♦) and product yields of FDCA (■), HMFCA (●), and FFCA (▲) for a 5.6 wt% Au catalyst on MnO_2. Reaction conditions: 9.3:1 HMF:catalyst molar ratio, and t = 12 h.[115]

In summary, Au is an effective single metal catalyst but can suffer from stability issues at elevated temperatures. At these higher temperatures, Au may leach from the support surface or sinter, leading to a reduction in catalyst surface area and thus, a lower number of active sites to

facilitate furan conversion. Particularly when stabilized by other metals or organic compounds, the stronger that Au NPs interact with the support, the less likely sintering and catalyst deactivation is.[134] The addition of other metals, particularly elements that are not a part of the same group on the periodic table, to create bimetallic catalysts can improve yields. From the example of Su et al.,[122] Cu/Au both have one valence electron and did not perform as well as Ni/Au catalysts, which had different numbers of valence electrons. The addition of bases over Au catalysts reported significant HMF degradation, though they typically also bolstered FDCA selectivity. As was observed with Pt, many different types of support could be used to achieve high FDCA yields.

Ruthenium

Aside from Au, Ru is the most common metal studied for application in HMF oxidation in recent years. Ru is unique among noble metals due to its vast range of potential oxidation states (Table 1), high stability, and relatively low cost compared to other noble metals. They also tend to be more resistant to some of the issues that impact other noble metals, including sintering, leaching, and oxidation. Across several studies that recycled Ru-based catalysts, FDCA yields were found to decrease by less than 5% when used for 4-6 cycles.[116, 124, 135] Such recyclability was attributed in one case to polymeric stabilizing agents,[135] but more commonly to the interactions between Ru and the support that helped stabilize Ru NPs.[19] These catalytic properties make Ru an attractive metal for HMF oxidation.

Index	Catalyst	Support	Base	t (h)	T (K)	$C_{HMF, i}$ (wt%)	HMF/Cat. (mol/mol)	FDCA Yield (%)	Ref.
1	Ru	C	$Mg(OH)_2$	8	383	0.5	40	97.3	[19]
2	Ru	ZrO_2	$Mg(OH)_2$	8	383	0.5	30	82.2	[19]
3	Ru	TiO_2	$Mg(OH)_2$	8	383	0.5	30	80.8	[19]
4	Ru	Al_2O_3	$Mg(OH)_2$	8	383	0.5	30	86.1	[19]
5	Ru	Cr2- Fe1-O	$KHCO_3$	16	373	0.5	5.1	99.9	[124]
6	Ru	N- doped C	$CaCO_3$	6	413	0.6	30	97	[21]
7	Ru	N- doped C	$CaCO_3$	2	413	0.6	30	45	[21]

Table 5. Ruthenium catalysts studied for aqueous HMF oxidation using 1 MPa O2 at 100% HMF conversion.

Many different supports have been used with Ru catalysts to achieve high yields (Table 5). Zheng et al.[19] investigated a range of metal oxide supports, comparing activated carbon (Table 5, index 1) to ZrO_2 (index 2), TiO_2 (index 3), and Al_2O_3 (index 4) with 5 wt% Ru^0 and average NP diameters of ~1 nm. All of the oxide-supported catalysts yielded 81-86% FDCA. However, even at a lower Ru loading the Ru/C catalyst (40:1) achieved the highest yield of 97% compared to the oxide-supported catalysts (30:1).[19] Other metal oxide supports have also been used with Ru with increased oxygen availability being noted as a key component in effective HMF upgrading.[116] Zhang et al.[116] studied oxide supports containing Cu, Co, and Mg oxides and found that a 4 wt% Ru^0/Cu_xCo_yO catalyst with a 1:1 molar ratio of Cu:Co oxides (CuO and Co_3O_4; Ru/Cu1-Co1-O in Figure 20) had a significantly lower FDCA yield than a 4 wt% Ru/MgO catalyst, which they attributed to a lack of basic sites. However, when using the Cu:Co support that was doped with 6 mmol of MgO, a yield of almost 80% FDCA was achieved (Ru/Cu1-Co1-O·MgO, Figure 20) This mixture most effectively activated oxygen due to the synergistic effects between the Cu and Co oxides, with MgO playing a key role in structural

effects. For the catalysts with Cu:Co ratios of 1:2 and 2:1, the FDCA yields were less than 40%, indicating that 1:1 was the optimum ratio. Running just the Cu1-Co1-O·MgO support resulted in only 3.5% FDCA, but 25.7% FFCA (Figure 20), showing the need for Ru to drive the oxidation of HMF.[116]

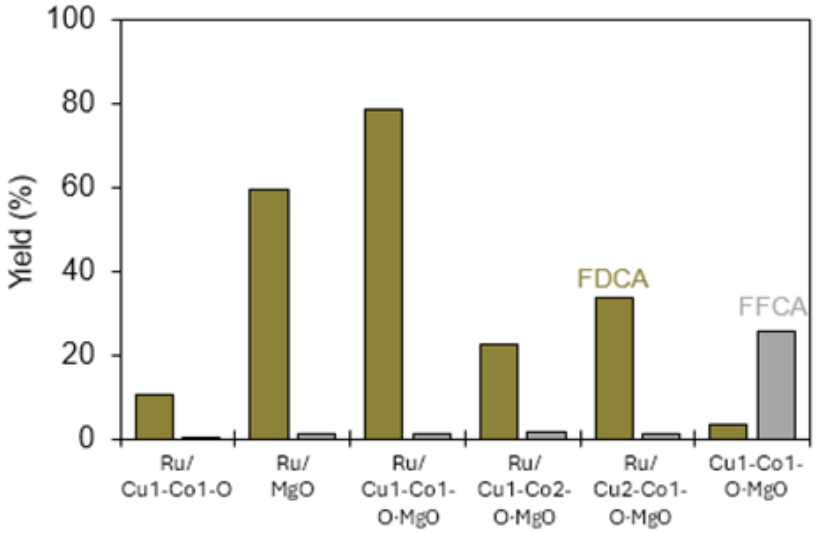

Figure 20. Support and metal effects on FDCA (■) and FFCA (■) yields for HMF oxidation using 4 wt% Ru (when noted) on various Cu, Co, and Mg oxides supports. Reaction conditions: 0.5 wt% HMF, T = 383 K, P_{O2} = 1 MPa, t = 12 h.[116]

When studying the impact of Ru loading on the Cu1-Co1-O·MgO support, Zhang et al.[116] evaluated the impact of 1-5 wt% Ru, which they had also studied previously on a Cr2-Fe1-O support with Ru loading ranging from 1-4 wt%.[124] In both studies, FDCA yields increased with Ru loading up to 4 wt% Ru, with yields of around 80% for the Cu1-Co1-O·MgO support[116] and near 100% with the Cr2-Fe1-O support (Figure 21).[124] Increasing the Ru loading further to 5 wt% was hypothesized to result in an excess of Ru blocking pores and reducing surface area, allowing fewer active sites.[116] A different study that used Ru^0 on nitrogen-doped activated carbon

catalysts saw a similar effect regarding the amount of Ru, with the highest amount of Ru resulting in lower FDCA yields (Ru/NC; Figure 21).[21] In the 2023 study with the 4 wt% Ru/Cr2-Fe1-O catalyst, $KHCO_3$ was used as a liquid base, which led to high FDCA yields as mentioned when 0.06 g was added. (Table 5, index 5) Decreasing the amount of $KHCO_3$ to 0.04, 0.02, and 0 g resulted in FDCA yields of 54%, 30.3%, and 6.6%, respectively, verifying that the base additive was necessary when using the Cr2-Fe1-O supported catalyst.[124] A significant advantage of the Ru/Cu1-Co1-O·MgO catalyst was that no liquid base was required, eliminating potential HMF degradation as a result of alkalinity.[116]

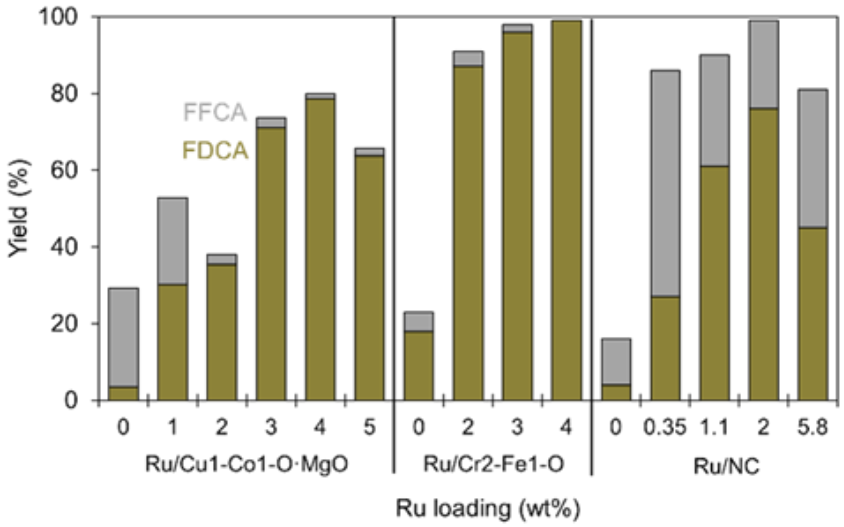

Figure 21. The effect of Ru loading on FDCA (■) and FFCA (■) yields on a Cu1-Co1-O·MgO,[116] Cr2-Fe1-O,[124] and NC support.[21] Reaction conditions for Ru/Cu1-Co1-O catalyst: 0.5 wt% HMF, T =383 K, P_{O2} = 1 MPa O_2, t = 12 h,[116] for Ru/Cr2-Fe1-O catalyst: 6 mmol $KHCO_3$ additive, 0.5 wt% HMF, T = 373 K, P_{O2} = 1 MPa, t = 16 h,[124] and for Ru/NC catalyst: 0.6 wt% HMF, 0.25 mmol $CaCO_3$ additive, T = 413 K, P_{O2} = 1 MPa, t = 2 h.[21]

In the case of the Ru/Cu1-Co1-O·MgO catalyst, the MgO was hypothesized to contribute the basic sites needed to complete conversion of HMF to FDCA. Zhang et al.[116] evaluated the effect the of MgO loading and found that the FDCA yield increased up to 6 mmol MgO to 78.6% and then decreased at 8 mmol to near 40% (Figure 22), which was attributed to a reduction of CuCo content, hampering catalytic activity.[116] The addition of Mg to Ru catalysts was found to assist in FDCA production not only as part of a support, but as a base additive as well. Another research group compared a wide range of base additives and found that $Mg(OH)_2$ resulted in the best mass balances and highest FDCA yields. The second most effective base, hydrotalcite (HT), also contained high amounts of Mg.[19] The exact mechanism by which Mg enhances furan oxidation has not been reported, but other alkaline earth metals such as Ca have been previously reported to enhance HMF oxidation reactions as well.[20] Regarding the amount of dopant added, Perumal et al.[135] made similar observations in their study of a Nb-doped Ru^0 catalyst supported by a mesoporous silicon structure, SBA-15. Increasing the amount of Nb improved FDCA yields to up to 2.5 Nb atoms per 100 Si atoms, but increasing the loading further decreased FDCA yields (Figure 22). The authors proposed that excess Nb dopant decreased surface effects and surface acidity, which negatively impacted furan conversion.[135] Using nitrogen as the dopant, Zhang et al.[21] also reported high yields over Ru NPs supported by a nitrogen-doped activated carbon, achieving 97% FDCA yield after 6 h of reaction time. (Table 5, index 6) This was significantly higher than the 45% FDCA yield achieved after 2 h (Table 5, index 7) even though the HMF conversion was 100%. Doping the carbon support with nitrogen improved electron density in the Ru NPs and prevalence of basic sites on the support. The increased electron density amongst the metal particles, particularly surface atoms, resulted in the transfer of 3d

electrons to the π* orbitals of O_2. Such a process weakened the oxygen-oxygen bond and primed the molecules for oxidation reactions.[21] The primary features of these carbon supports are their high surface areas, which have been observed across other noble metal catalysts,[108, 124, 128, 135] the activation of O_2, and the stabilization of Ru NPs to guard against sintering.

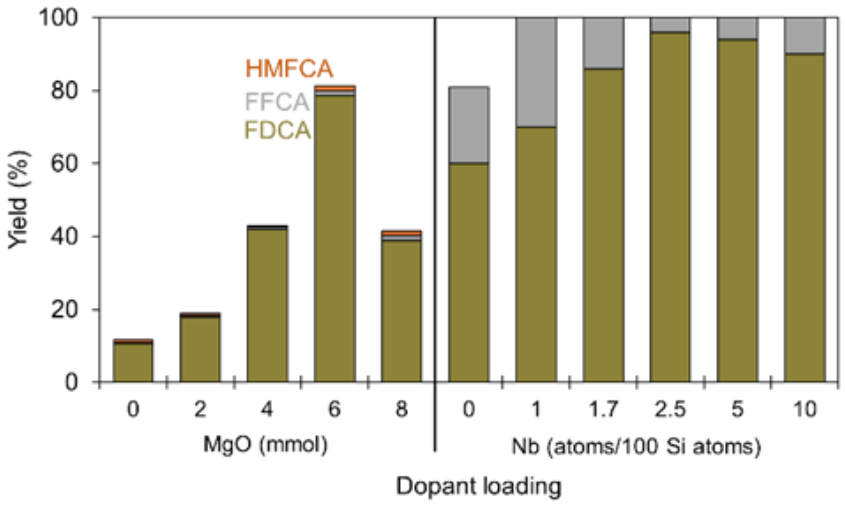

Figure 22. Impact of dopant amount on FDCA (■), FFCA (■), and HMFCA (■) yields for a MgO dopant loaded on a 4% Ru/ Cu1-Co1-O·MgO catalyst (100% HMF conversion for all)[116] and Nb loading on a Ru/SBA-15 catalyst.[135] Reaction conditions: P_{O2}= 1 MPa, t = 12 h and for Cu1-Co1-O·MgO catalyst: 0.5 wt% HMF, T= 383 K,[116] and for Nb-SBA-15 catalyst: 1.25 wt% HMF, T = 393 K.[135]

Although most of the previously discussed HMF oxidation studies reported stable catalysts with minimal deactivation upon reuse,[116, 124, 135] a study by Mani et al.[83] reported the leaching of Mn under certain conditions for a Ru^0/MnO_2 catalyst. They studied multiple supports including MnO_2, $CoMn_2O_4$, $MnFe_2O_4$, and $CuOFe_2O_3$ and found that the MnO_2 catalyst resulted in the highest FDCA yields (91% compared to 82, 87, and 15%, respectively) and that higher

initial HMF concentrations significantly decreased FDCA yields (Figure 23). The decrease in yield was directly proportional to decreasing carbon balances, which was attributed to the low solubility of FDCA in the aqueous solution leading to precipitation of FDCA. After treating the 2 wt% HMF reaction effluent with base and added organic solvent (MeOH), the FDCA yield increased markedly from 59% yield to 83%, indicating the presence of insoluble or precipitated FDCA that wasn't detected with the initial analysis. Also using 2 wt% HMF, the study found that Mn leached from the Ru/MnO_2 catalyst, which they attributed to the production of FDCA, an acidic product.[83] The stability of the catalyst in acidic medium is an important consideration if a base is not added to the reaction. FDCA has a relatively low pKa ± 3 which acidifies the medium as the reaction proceeds and as reported by Mani et al.,[83] this effect is more pronounced at high HMF concentrations and can be a reason for catalyst deactivation due to metal leaching. When stoichiometric amounts of base ($NaHCO_3$) were added to the reaction, the amount of Mn detected significantly decreased from 988 ppm to 7 ppm, but small amounts of Ru (4 ppm) were also detected.[83]

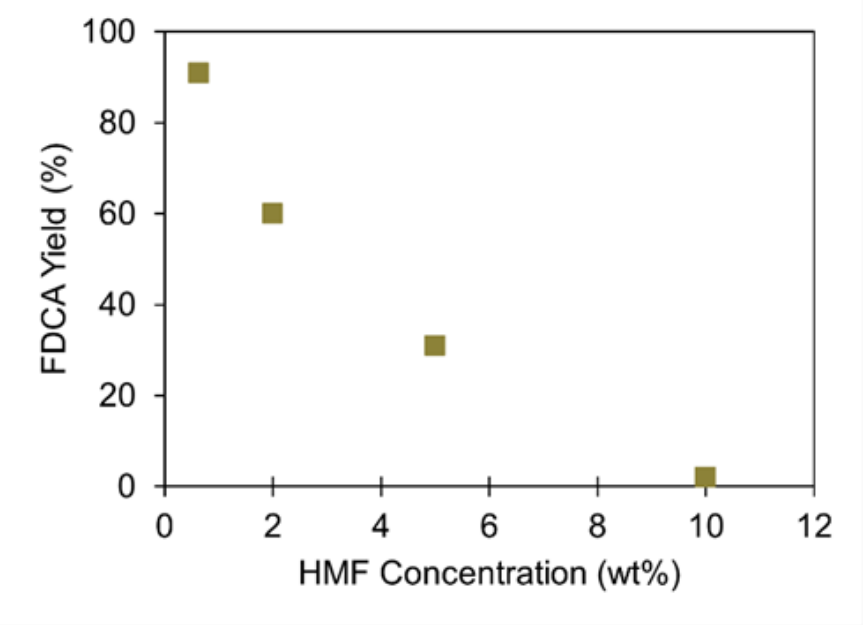

Figure 23. Effect of initial HMF concentration on final FDCA yields observed in an aqueous system using a Ru/MnO_2 catalyst without the addition of base. Reaction conditions: 2:1 HMF:catalyst weight ratio, T = 373 K, P_{O2} = 3 MPa, t = 24 h.[25]

Ruthenium catalysts, studied in aqueous systems as Ru^0, attained higher yields with smaller NP diameter, greater NP distribution, and higher catalyst surface area. However, for furan compounds to adsorb onto the catalyst surface and interact with these NPs, greater catalyst loading or surface area can become detrimental when it is at the expense of sufficient pore sizes or active site availability. If excessive Ru NPs begin to block pores, it may restrict the access of reactants to the electron-dense catalyst. Dopants such as MgO or Nb are useful for improving Lewis acidic/alkaline properties, but the correct ratio of dopant to catalyst must be found for the best results. Accessibility of acidic or alkaline sites continues to be relevant, with the addition of bases being useful, but not necessary, for increased yields. To that end, weak bases containing Mg were found to be particularly effective at maintaining high mass balances and attaining high

FDCA selectivity. The reason for this is not completely understood but could correlate to Mg's group (II) or its row on the periodic table since the addition of Ca in other reactions has been seen beneficial. Decreased initial HMF concentration was definitively shown to correlate to higher yields at constant reaction conditions.

Non-noble Metal Catalysts

Non-noble metals (NNM) such as Mn, Fe, Bi, Co, and Cu tend to be less active and less stable than noble metals; however, they have been extensively studied as catalysts because of their low cost and availability. NNM, particularly first row metals (Mn-Zn), are easily oxidized in the presence of oxygen and these metal oxides can have their relative Lewis acidity change depending on surface adsorption. As such, NNM catalysts favor the HMFCA pathway (Schemes 3 and 5). The Mars-van Krevelen reaction mechanism is facilitated by oxygen atoms acting as Lewis acids. Additionally, oxygen vacancies in the metal oxide matrix generate strong Lewis base sites that attract water molecules. These water molecules react with the metal ion(s) surrounding the vacancy to complete the matrix, filling in the missing oxygen. This reaction mechanism can be tuned by replacing metal ions with a metal ion of a different valency or oxidation state.[136] This creates a change in the Lewis acid-base nature of the area and makes a catalytic hotspot where oxygen is either more easily exchanged with the adsorbed product or water can be more easily reacted with the resulting vacancy. There is a tradeoff, however; the easier a matrix oxygen atom is removed to oxidize a furan, the harder it is to replace the removed oxygen in the matrix and vice versa.[137, 138] Another way to affect the catalytic potential of the metal oxide is by depositing metal on the surface. The deposited metal on the surface has its

relative Lewis acidity promoted, and the metal also lowers the energy needed to form an oxygen vacancy in the immediate area.

Single Metal Non-Noble Catalyst

Few studies report the use of single metal NNM catalysts, as bimetallic catalysts take advantage of the different catalytic properties of the metals used. Using a zeolite support, Herlina et al.[139] impregnated ZSM-5 with NiO and CuO oxides separately and reported that the optimal HMF oxidation temperature for these catalysts was 303 K using H_2O_2 as an oxidant. For the Ni-impregnated catalyst (Table 6, index 1), 79% FDCA yield was achieved after 5 h and for the Cu-impregnated catalyst (index 2), 70% FDCA yield was achieved compared to 50% FDCA with a non-impregnated ZSM-5 catalyst (index 3). The formation of oxides allowed the transition metals to have a higher oxidation state as both the Ni and Cu were held at a [+2] oxidation state, which resulted in higher activity.[139]

Index	Catalyst	Support	Base	t (h)	T (K)	P (MPa)	$C_{HMF,i}$ (wt%)	Oxidant	HMF/Cat. (mol/mol)	HMF Conv. (%)	FDCA Yield (%)	Ref.
1	NiO	ZSM-5	K_2CO_3	5	403	atm	3.6	H_2O_2	10	100	79	139
2	CuO	ZSM-5	K_2CO_3	5	403	atm	3.6	H_2O_2	10	80	70	139
3	-	ZSM-5	K_2CO_3	5	403	atm	3.6	H_2O_2	10	35	50	139
4	FeTPP-1	NC	NaOH	5	353	1	0.25	O_2	11	82	28	140
5	Co	NC-900	$NaCO_3$	12	338	0.5	0.12	O_2	0.024	100	82	141
6	Co	NC-900-a	$NaCO_3$	12	338	0.5	0.12	O_2	0.024	100	71	141
7	Co	NC-900-a	$NaCO_3$	16	338	0.2	0.52	O_2	0.12	100	94	141

Table 6. Non-noble single metal catalysts studied for aqueous HMF oxidation.

Another way to increase the oxidation state of a NNM catalyst is by forming ligands. Chelating compounds trap and form ligands with metals, forcing them into a higher oxidation state and pulling electrons away from the metal atom. When in a higher oxidation state, the electronegative elements like oxygen are attracted to the less shielded nucleus. This allows water to adhere to the surface of the metal in the center of the chelate and oxidize, forming a hydroxide. This hydroxide can then interact with other molecules, causing them to oxidize as well.[140] Gao et al.[140] deposited iron tetraphenylphosphonium (FeTPP) to form a ligand on the surface of activated carbon and used this as the catalyst for HMF oxidation to form HMFCA. The iron chelates reacted to cyano- groups on the surface of the N-doped activated carbon rather than crystalizing on the surface. Using temperatures ranging from 333-373 K and higher concentrations of NaOH to stabilize the intermediate, the FDCA yield was 28% with 41% HMFCA (Table 6, index 4).[140]

Cobalt (Co) has also been investigated for HMF oxidation as a single metal catalyst. Y. Gao et al.[141] deposited Co on activated carbon, graphitized it, and achieved 81.8% FDCA yield (Table 6, index 5). They showed that Co NPs were the main catalytic site by acid etching away the surface Co and revealing previously carbon-bound Co sites resulting in the NC-900-a catalysts (Table 6, indices 6 and 7). Using ICP, the concentration of Co on the unetched catalyst was 28.2%, while the concentration of Co after acid etching was only 0.71%. Using the etched catalyst resulted in a 16% decrease FDCA yield after 12 h (Table 6, index 6) compared to the unetched catalyst. However, when using the same amount of the etched catalyst but 5 times the HMF (50 mM), a lower O_2 pressure, and increased reaction time of 16 h, 94% FDCA yield was

achieved (Table 6, index 7).[141] Similarly to what was seen with Ru catalysts,[116] an excess of Co on the catalyst surface decreased the FDCA yield.

The Co catalysts used graphitized carbon as a support, a factor shown to influence FDCA yield. Gao et al. defined the degree of graphitization as the ratio of random, unorganized carbons (D peak in Raman spectroscopy; ID) divided by the number or organized or graphitic carbons (G peak in Raman spectroscopy; IG).[141] The degree of graphitization that resulted in the highest FDCA yield was determined to be 0.6 for the etched Co-catalyst and 0.7 for the unetched (Figure 24). The acid etching of the Co/NC-900-a catalyst reportedly removed some of the disorganized carbon, leading to a higher ratio of graphitized carbon and had a higher surface area,[141] which could be the reason there was not a large decrease in the catalytic activity after much of the surface Co was removed.

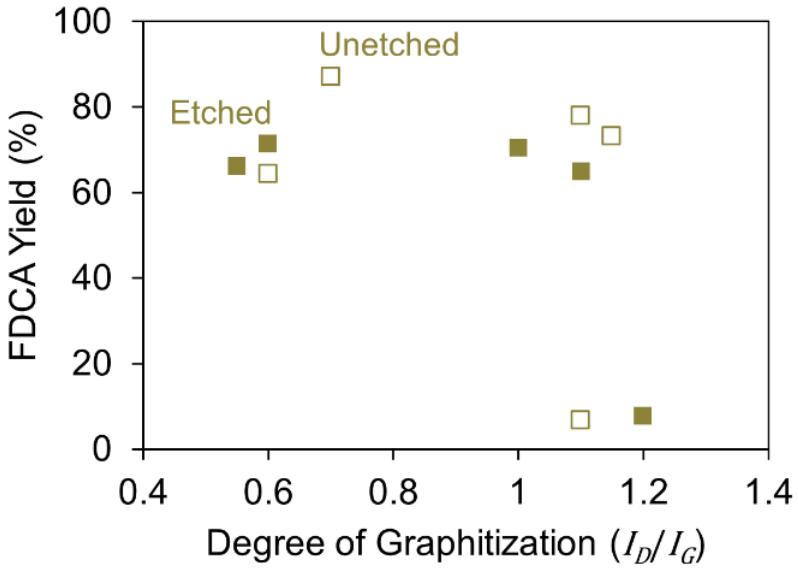

Figure 24. The effect of graphitization on FDCA yields. Reaction conditions: 0.024 HMF:catalyst molar ratio, T = 338 K, P_{O2} = 0.5 MPa, t = 12 h.[141]

Bimetallic Non-Noble Catalysts

Single metal NNM catalysts have been shown to be effective for the oxidation of FDCA, but using bimetallic catalysts can greatly increase catalytic activity. When using two oxides of differing charge densities, the effects of the individual metals can be amplified by being chemically bonded to each other. For example, Cu oxide is a strong oxidizing catalyst but has little selectivity, while Co has high selectivity but lower activity.

Rao et al.[142] compared Cu and Co at two different oxidation states each, Co and Cu oxides physically mixed, and a CuO_x-CoO_y nanoparticle both randomly deposited and organized using polyvinylpyrrolidone (PVP) as catalysts for HMF oxidation. Using the same reaction conditions, all catalysts achieved high (greater than 95% HMF conversions), but the FDCA yields varied significantly (Figure 25). The Cu oxides achieved a maximum FDCA yield of 39%, while the Co oxide achieved 54%. Using both the CuO_x and CoO_x together as a physical mixture resulted in 55% FDCA yield, but a one-pot synthesis method using both Cu and Co oxide, the FDCA yield increased to 67% showing the enhancement of properties using both oxides. Rao et al. also deposited the Cu-Co oxide catalyst onto graphite and the FDCA yield increased to 80% and using PVP to organize the structure on the surface of graphite increased the FDCA yield to 91%.[142] Separately, both Cu and Co were active catalysts, but when combined into a single metal oxide, both of their catalytic properties were enhanced, leading to higher selectivity.

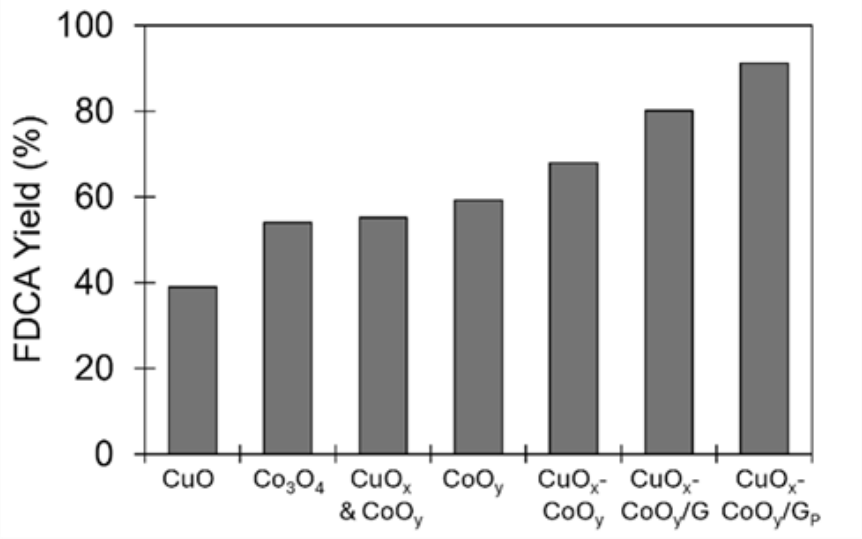

Figure 25. FDCA yields of various Cu- and Co-based catalysts where G represents graphite deposited catalysts and GP represents the PVP-organized catalyst on graphite. All HMF conversions were greater than 95%. Reaction conditions: 0.525:1 HMF:catalyst by weight, 3.2 mmol NaClO, 0.5 mmol HMF, T = 303 K, P = atm, t =1 h.[142]

This higher selectivity and conversion could be due to the ability of CoO to form H_2O_2 in the presence of water and O_2. Zhang et al.[143] looked at Cu-Co oxide catalysts as well but focused on the oxygen being added to the reaction media. They found that under alkaline conditions, CoO could reduce O_2 to hydrogen peroxide. This was also observed in Cu-Co oxide catalysts as well. They then showed that Cu could oxidize the H_2O_2 into copper peroxide. This copper superoxide would then be reduced by a furan, causing the furan to oxidize.[143]

Index	Catalyst	Support	t (h)	T (K)	P_{O2} (MPa)	$C_{HMF,i}$ (wt%)	HMF/Cat. (mol/mol)	HMF Conv. (%)	FDCA Yield (%)	Ref.
1	Bi_2O_3	-	3	383	0.6	0.083	0.17	97	0.5	[144]
2	Co_3O_4	-	3	383	0.6	0.083	0.05	100	20	[144]
3	12 Co:Bi	-	3	383	0.6	0.083	0.06	99.9	98.2	[144]
4	10%Bi-CeO_2	-	12	383	1	0.14	0.21	98	30	[80]
5	10%Bi-CeO_2	NC -800C	12	383	1	0.14	0.14	100	55	[80]

Table 7. Non-noble bimetallic catalysts that have been studied for aqueous-based HMF oxidation with NaOH base additive.

Cobalt has been used with other metal oxides as well. Zhang et al.[144] used a bimetallic Co and bismuth (Bi) oxide catalyst since pure Bi oxide converted 98% HMF but resulted in little FDCA yield (Table 7, index 1). The results using Co oxide were better with 100% HMF conversion and 20% FDCA yield (Table 7, index 2), but using these same conditions and a binary metal oxide consisting of 12 mol% Bi and the remainder Co (CoBi-12), the FDCA yield increased to 98.2 % at 100% HMF conversion (index 3).[144] This Co-Bi catalyst was an improvement on previous work using Bi and cerium (Ce) oxide that achieved 30% FDCA yield at 100% HMF conversion (Table 7, index 4).[80] However, similar to Rao et al.,[142] when Wei et al.[80] deposited the Ce-Bi metal oxide on activated carbon, which increased the surface area, the FDCA yield increased from 30% to 55% using only 1.6 mmol NaOH (Table 7, index 5). Zhang et al.[144] also studied the effect of alkalinity on the production of FDCA using the CoBi-12 catalyst by increasing the amount of NaOH with respect to initial HMF concentrations. They found that a molar ratio of 2:1 NaOH to HMF was optimal, resulting in near ideal selectivity of 98% FDCA (Figure 26). Increasing the NaOH ratio further resulted in decreased FDCA yields, likely due to HMF degradation as mentioned previously.

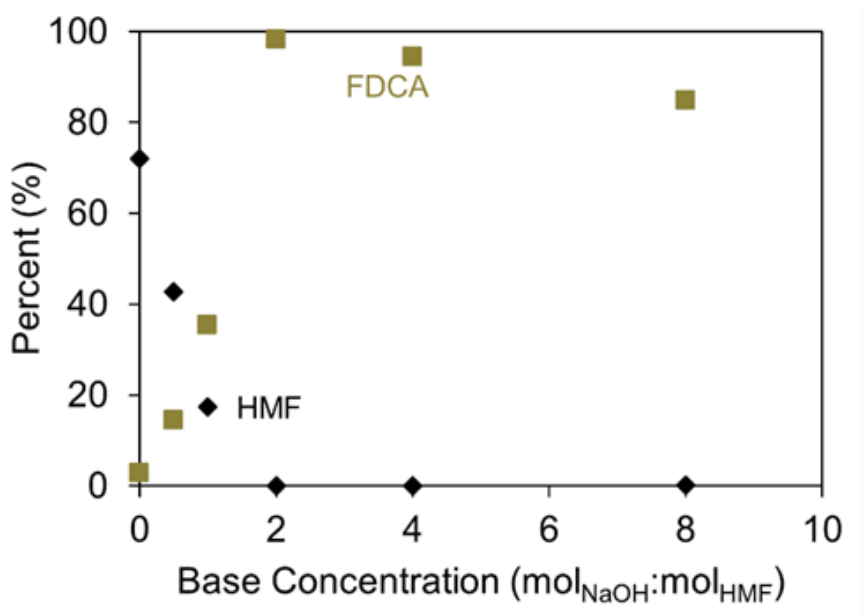

Figure 26. The effect of NaOH on HMF conversion (♦) and FDCA yield (■) using a Co-Bi oxide catalyst. Reaction conditions: 0.056 HMF:catalyst molar ratio, 0.8 mmol of NaOH, T = 380 K, P_{O2} = 0.6 MPa, t = 3 h.[144]

As single-metal non-noble catalysts, transition metal oxide catalysts typically have low effectiveness in aqueous systems. However, by increasing the surface area of the catalyst significantly increases the activity of the catalyst. A consideration when using carbon-based supports is that having graphitic carbon on the surface increases the effectiveness of the catalyst but tends to reduce the surface area. Metal oxide catalysts also greatly benefit as from the addition of another transition metal oxide. These mixed metal oxides amplify the properties of both individual metals rather than just averaging out the two oxide's properties.

2.7 Organic Solvent Reactions

Using water as a solvent results in high HMF conversion and FDCA selectivity typically at low HMF concentrations. However, there are several reasons to consider using organic solvents as the reaction medium for the HMF to FDCA reaction. Firstly, economic and sustainable production of FDCA is linked to the production of HMF, which is produced from the dehydration of C_6 sugars in acidic medium.[75, 145-148] An important consideration is that in the presence of water and acid catalyst, HMF reacts to produce levulinic and formic acid and can polymerize to form humins. To avoid HMF degradation, biphasic and/or organic monophasic systems have been used, so that the HMF is extracted and produced in an organic solvent.[105, 149-152]

Another important reason to study the oxidation of HMF in organic solvents is to increase FDCA solubility, as concentrations around 10 wt% are necessary to consider the process industrially relevant.[153] In order to improve FDCA solubility, many solvent blends involving water and an additional organic solvent have been studied[27-29, 31, 36] with researchers showing that organic solvents can solubilize up to 31 wt% FDCA compared to 0.12 wt% for water at STP.[32] However, solvents must also be stable at the reaction conditions, offer a sufficient source of oxygen for reaction progress, and not interact with furan compounds in such a way that hinders the oxidation process. These issues can be mitigated by selecting an organic solvent or blend of solvents with the correct physical and chemical characteristics to promote both solubility and reaction progress.

In the case of solvent interactions, several research groups have discussed the importance of solvent selection in HMF to FDCA reaction design.[36, 154, 155] As shown in Scheme 1, furan

compounds contain carbonyl (C=O) and alcohol (O-H) groups, which are capable of forming hydrogen bonds with organic solvents, both as hydrogen bond donors (O-H) and acceptors (C=O). There are multiple ways to measure solvent properties for evaluation; two options that have been used previously are the Hansen Solubility Parameters (HSPs)[29, 32] of hydrogen bonding (δ_H), dispersion (δ_D), and polarity (δ_P),[52] and the Kamlet-Abboud-Taft (KT) parameters[36] of hydrogen bond acceptor basicity (β), hydrogen bond donor acidity (α), and polarizability (π*).[156] In particular, hydrogen bond contribution and polarity have been identified to be of interest for HMF oxidation. The hydrogen bond contribution has been shown to positively impact the capacity of a solvent to solubilize FDCA, but can also negatively impact the forward progress of HMF oxidation through strong solvent-reactant intermolecular interactions with intermediates.[36] Polarity impacts reaction progress by facilitating the dissolution of oxygen and HMF conversion.[154] Additionally, a holistic parameter, the radius of interaction ($R_{i,j}$), compares all the HSPs of the solute (i; FDCA in this case) to the solvent (j) and has been identified to show a strong correlation between the maximum FDCA solubility and the minimum $R_{i,j}$ of a solvent.[32] This trend was found to be weak for pure solvents, as demonstrated in Figure 27a, but were significantly stronger in aqueous/organic solvent blends (Figure 27b).

These variables of interest are listed in Table 8 for a range of organic solvents that have been reported in the literature, including γ-valerolactone (GVL),[27, 32, 36] dimethyl sulfoxide (DMSO),[32, 36] acetonitrile (ACN),[32, 42] tert-butyl alcohol (TBA),[102] 1,2-dimethoxyethane (DME), diglyme (DG), and 1,4-dioxane (DX).[36, 105] Additionally, other studies mention improved solubility in dimethylformamide (DMF), ethanol (EtOH),[157] methanol (MeOH), acetone

(ACE),[104] n-propanol (n-PrOH), and isopropanol (i-PrOH)[154] without reporting pure solvent FDCA solubilities.

Solvent	Pure solvent FDCA solubility (wt%)	KT hydrogen bond acceptor (β)[d]	KT hydrogen bond donor (α)[d]	HSP hydrogen (δ_H)[e]	HSP polarity (δ_P)[e]	HSP $R_{i,j}$
DX	0.42[a]	0.37	0.00	9.0	1.8	7.8
DME	0.3[b]	0.41	0.00	4.9	4.9	12.9
TBA	-	0.93	0.42	14.7	5.1	10.0
DG	0.3[b]	0.40	0.00	6.5	6.1	10.6
i-PrOH	-	0.84	0.76	16.4	6.1	9.0
n-PrOH	-	0.90	0.84	17.4	6.8	8.9
EtOH	0.92[c]	0.75	0.86	19.4	8.8	9.8
ACE	-	0.43	0.08	7.0	10.4	9.8
MeOH	1.59[c]	0.66	0.98	22.3	12.3	13.4
DMF	23.0[b]	0.69	0.00	11.3	13.7	5.5
H_2O	0.12[c]	0.47	1.17	42	16	30.6
DMSO	30.7[c]	0.76	0.00	10.2	16.4	6.7
GVL	0.19[c]	0.58	0.00	6.7	16.5	5.9
ACN	0.02[c]	0.40	0.19	6.1	18.0	10.6

Table 8. Overview of properties and FDCA solubility at 303 K[a] or 293 K for various solvents. [a]Xu et al.,[158] [b]Ryu et al.,[36] [c]Molinaro et al.,[34] [d]R. Stenutz,[159] [e]HSPiP Software Package.[56]

Pure DMSO had the highest reported FDCA solubility of over 30 wt% at 293 K (Table 8),[32, 36] which was attributed to the strong dipole-dipole interactivity of DMSO and its high capacity for hydrogen bond acceptance.[160, 161] It is worth noting that Table 8 lists the FDCA solubility for the pure solvent, and not for aqueous/organic blends, which in most cases achieved higher FDCA solubilities. For example, FDCA solubility was shown to increase nearly four-fold in binary mixtures of water and DX compared to the pure solvent, which was attributed to the hydroxyl groups on FDCA acting as Lewis acids or hydrogen bond contributors, while the carbonyl groups can function as hydrogen bond acceptors.[29] The correlation between FDCA solubility and ability of a solvent to hydrogen bond was noted to be true across all ether-type solvents and solvent blends and can largely be extended to other solvent types as well, with

correlation made most strongly to the KT β parameter.[36] Additionally, FDCA solubility has also been shown to correlate with an increased heat of mixing (ΔH_{mix})[27] and a lower $R_{i,j}$ (Figure 27).[32]

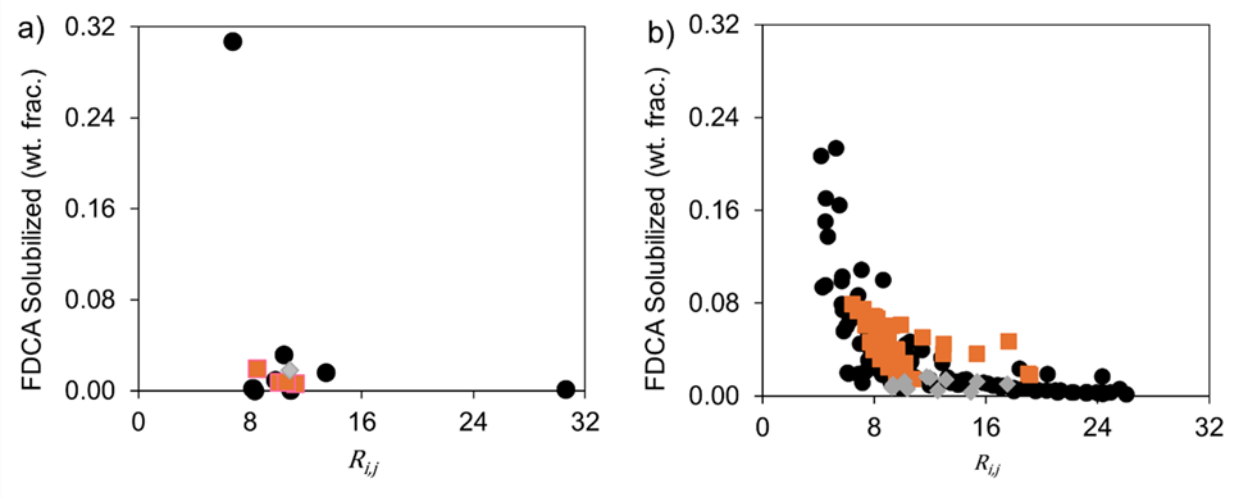

Figure 27. Relationship between the $R_{i,j}$ parameter and FDCA solubility in a) pure solvents and b) binary aqueous/organic mixtures, and ternary aqueous/organic/organic mixtures from (●),[32] (■),[29] and (♦).[31]

However, high FDCA solubility is not the only consideration, as ideally the solvent would also promote HMF oxidation. In some cases, solvents have high FDCA solubility, but low FDCA yields due to interactions of the solvents with the reactant and/or intermediates.[36] For example, DMSO is of great interest for application in HMF upgrading due to its high capacity to solubilize furan compounds. However, Fourier-transform infrared analysis (FTIR) studies on HMF-DMSO pairings showed DMSO interacts strongly with both the alcohol and carbonyl groups of HMF through hydrogen bonding and dipole – induced dipole effects, limiting reaction progress beyond DFF. The tendency of DMSO to interact strongly with the furanic solute

molecules resulted in reduced capacity for oxidants and catalysts to facilitate reaction progress. Similarly, in the case of GVL, strong interactions with the C=O groups in DFF and FFCA limited forward progress to FDCA.[36] This trend of organic solvents interacting with the C=O and O-H groups of HMF and DFF and having limited selectivity to FFCA or FDCA has also been reported elsewhere in the literature.[154, 157]

Additionally, consideration of the stability of the organic solvent is important. A common organic solvent, tetrahydrofuran (THF), is not regularly applied in HMF oxidation reactions despite a relatively high FDCA solubility of 3.2 wt% at STP[32] because of its tendency to convert to γ-butyrolactone (GBL). In a reaction with a $ZnFe_2O_4$ catalyst at 353 K, nearly 50% of the THF converted to GBL in 12 h.[162] Other solvents are more resistant to reaction such as GVL, for example. At 373 K and in acidic conditions, GVL was found to reach equilibrium after the formation of only 4 mol% 4-hydroxyvaleric acid (4-HVA) as a side product.[163] Although it would be most desirable to have no solvent react, minimizing its degradation should be a key consideration.

Based on the solubility and process benefits of organic and aqueous/organic solvent systems, there has been a recent influx of publications focusing on organic reaction media for HMF oxidation. In the following sections, the impact of solvent, catalyst type, and reaction conditions will be discussed to determine key trends for improving HMF conversion and FDCA yields in organic solvent systems.

Noble Metal Catalysts

As in aqueous systems, the application of the noble metals Pt, Pd, Au, and Ru as catalysts for HMF upgrading has been commonly reported. Since Prasad et al. completed their review in

2023,[25] several papers have focused on noble metal catalysis in organics and show similar trends to those observed in aqueous systems described previously, including improved FDCA yields using catalysts containing the metallic (zero-valence state) forms of metals, those with increased oxygen content, and those with smaller diameter particles that are more evenly distributed across the surface of the catalyst.

Both Ryu et al.[36] and Motagamwala et al.[27] used Pt^0 for reactions run in organic solvents. Ryu et al.[36] found that the overall product selectivity remained low and FDCA yields remained below 30% in pure solvents including DMSO (0%), DMF (0%), GVL (0.7%), DG (27%), DME (6.9%), and DX (1.4%) (Table 9, indices 1-6).[36] Low selectivity towards FDCA in pure organic solvents relates to prior discussion of solvent-reactant intermolecular interactions, particularly corresponding to hydrogen bond acceptance (β). In the study by Ryu et al., DMSO, DMF, and GVL have high β values relative to the other solvents (Table 8) and decreasing β values corresponded to increasing HMF conversion and, in the case of any FDCA production at all, increasing FDCA production (Table 9, indices 1-6).

Index	Catalyst	Solvent (w/w)	t (h)	T (K)	P_{O2} (MPa)	$C_{HMF,i}$ (wt%)	HMF/Cat. (mol/mol)	HMF Conv. (%)	FDCA Yield (%)	Ref.
1	Pt	DMSO	2.5	393	1	1	50	2.6	0	36
2	Pt	DMF	2.5	393	1	1	50	5.1	0	36
3	Pt	GVL	2.5	393	1	1	50	78.9	0.7	36
4	Pt	DG	2.5	393	1	1	50	82	27	36
5	Pt	DME	2.5	393	1	1	50	93.2	6.9	36
6	Pt	DX	2.5	393	1	1	50	86.8	1.4	36
7	Pt	GVL/ H_2O (80/20)	20	383	4	0.5	15	97	95	27
8	Pt	GVL/ H_2O (80/20)	20	383	4	5	20	100	11	27
9	Pt	GVL/ H_2O (50/50)	20	383	4	7.5	30	100	94	27
10	Ru	DX/H_2O (50/50)	12	393	1	3.2	15.8	100	89	105

Table 9. Noble metal catalysts on carbon supports studied in organic solvent systems for HMF oxidation.

Although some FDCA yields were seen with pure organic solvents, using aqueous mixtures of organics led to higher FDCA yields. In a separate study by Motagamwala et al.,[27] they used a Pt/C catalyst, 80/20 w/w GVL/water, and low concentrations of HMF (0.5 wt%) to achieve 95% FDCA yield (Table 9, index 7). However, when the HMF concentration was increased to 5 wt%, the FDCA yield decreased to 11% (Table 9, index 8). They determined that the 80/20 w/w GVL/water solvent did not have sufficient water to provide oxygen to facilitate the formation of the intermediate geminal diol.[27] However, using a 50/50 w/w GVL/water solvent blend and an HMF concentration of 7.5 wt% resulted in FDCA yields near 95% (Table 9, index 9), highlighting the need for sufficient water to be present in organic solvents.[27]

Using a solvent with low hydrogen bond acceptance (β) capacity and low polarity, Chen et al.[105] investigated a Ru/C catalyzed system in 50/50 w/w DX/water. Binary mixtures of DX and water have been previously shown to address solubility concerns,[29, 36, 158] while the lack of solvent-reactant interactions was proposed to be beneficial for the two-step upgrading of fructose to FDCA. As mentioned previously, the two-step process with first upgrading the sugar to HMF and then further converting to FDCA in the same solvent would be beneficial. Chen et al.[105] consistently achieved fructose to HMF yields of approximately 90% in 85/15 w/w DX/water before extracting the HMF and diluting to 3.15 wt% HMF in 50/50 DX/water. The resulting oxidation saw 100% HMF conversion with an 89% selectivity to FDCA (Table 9, index 10).

While many researchers have reported high HMF conversion and FDCA selectivity over Pt and Ru single metal catalysts, research has also been done on bimetallic catalysts. Rao et al.[104] studied Ru-doped Ni-manganite catalysts and found that higher Mn content facilitated the formation of Ru^{3+} and Ru^{4+} versus higher ratios of Ru^{0} at lower Mn content.[104] The catalyst with

the most manganese-rich support, Ru/Ni_1Mn_6, had increased oxygen content, which led to higher oxidative activity and yields of FDCA (Figure 28). Similar findings were also reported by Qian et al.[164] when studying non-noble bimetallic catalysts containing Ni and Co, which will be discussed in more detail in the NNM catalyst section below.

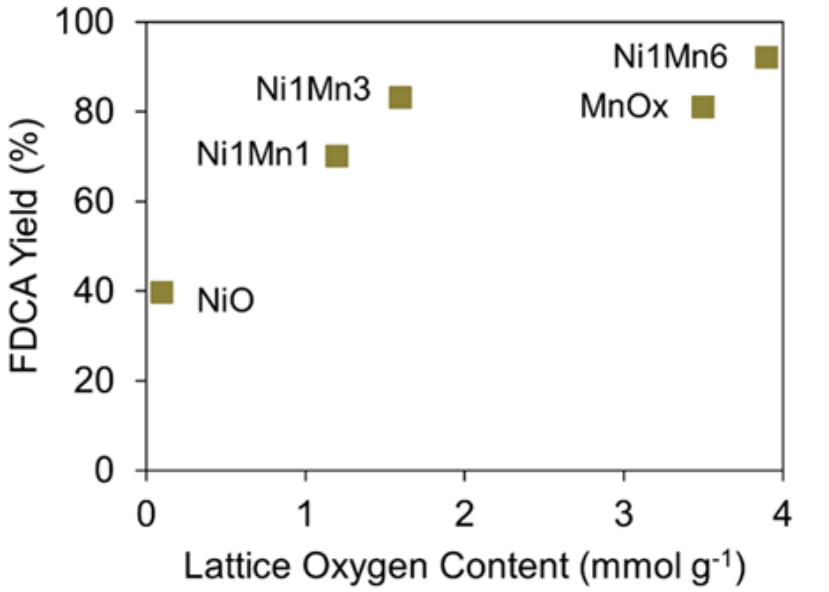

Figure 28. Effect of lattice oxygen content of Ru catalysts supported by a range of Ni-Mn supports on FDCA yield at an HMF conversion of 100% (excluding Ru/NiO where the HMF conversion was 63%). Reaction conditions: 1.43:1 catalyst:HMF by weight; 70/30 H_2O/ACE w/w; 5 wt% initial HMF; T = 383 K; P_{O2} = 1 MPa; t = 12 h.[104]

Rao et al.[104] found that metal surface area, as determined using CO-chemisorption, positively correlated with FDCA yields (Figure 29a) while Ru particle size negatively correlated (Figure 29b). Particle dispersion was also measured and observed to positively correlate with greater selectivity to FDCA. The support that resulted in the highest yield (92%), Ni_1Mn_6, had 72% dispersion of Ru NPs, compared to 53% dispersion on the next most active support,

Ni_1Mn_3.[104] As with aqueous reactions, increased surface area and decreased particle size were seen to improve catalytic activity for a given type of catalyst.

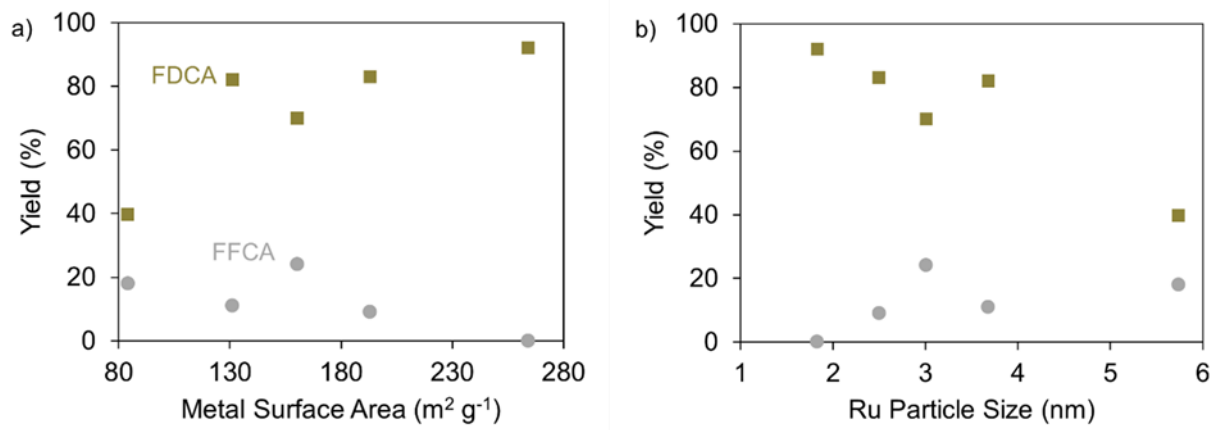

Figure 29. Comparison of the effect of catalyst a) metal surface area and b) Ru particle size on an HMF oxidation reaction. Reaction conditions: 1:1.43 HMF:catalyst by weight, 70/30 w/w water/ACE, 5 wt% initial HMF, T = 383 K, P_{O2} = 1 MPa, t = 12 h.[104]

Trends amongst noble metal catalysts using organic and aqueous/organic solvent systems paralleled those observed in purely aqueous systems. Correlations were found between increased FDCA yields and decreased active particle size, increased FDCA yields and decreased active particle size, increased particle dispersion, and increased lattice oxygen content. The catalyst surface area improved FDCA yields, but only within a given catalyst design. The addition of organic solvents to the reaction system impacted product selectivity through interactions with furan intermediates like DFF and HMFCA, primarily via hydrogen bond formation at high concentrations of organic solvent. Improved solubility of furans through the addition of organics also allowed for high FDCA yields at initial HMF concentrations greater than 5 wt%.

Non-Noble Metal Catalysts

As was true for aqueous systems, NNM catalysts are of increasing interest in organic and organic/aqueous systems. Though generally less active than NM catalysts, metals like Co, Fe, Cu, V, Mn, and Ni are lower in cost and more readily available, potentially providing new paths to commercialization for a process limited by its economic feasibility. This is particularly true in conjunction with the use of organic solvent systems, combining lower cost metal catalysts with the capacity for operating at higher HMF concentrations. From a broad perspective, NNM catalysts can form many different valence states (Table 10), and such versatility lends itself well to bimetallic catalysts, oxide catalysts, and other unique catalytic approaches that are not possible with noble metals. A wide range of NNM catalysts have been studied on a variety of supports and in different solvents blends, showing several of the same trends that were observed in water.

Metal	Possible Oxidation States	Electron Orbital Configuration
V	+2, +3, +4, +5	[Ar] $3d^3$ $4s^2$
Mn	+2, +3, +4, +6, +7	[Ar] $3d^5$ $4s^2$
Fe	+1, +2, +3, +4, +5, +6	[Ar] $3d^6$ $4s^2$
Co	+1, +2, +3, +4, +5	[Ar] $3d^7$ $4s^2$
Ni	-1, 0, +1, +2, +3, +4	[Ar] $3d^8$ $4s^2$
Cu	+1, +2, +3, +4	[Ar] $3d^{10}$ $4s^1$

Table 10. Oxidation and electron orbital configurations of different non-noble metals.

Similar to aqueous phase reactions, bimetallic NNM catalysts have more activity compared to single-NNM catalysts. Four recent studies used single-metal NNM catalysts as controls to study bimetallic catalysts, and the bimetallic catalysts consistently outperformed the single metal catalysts with respect to both HMF conversion and FDCA yield.

For example, Demet et al.[42] studied a range of atomic metal ratios for both Mn-Cu and Fe-Co catalysts in a pure ACN solvent system. The pure metals, shown at either end of Figure 30, represent FDCA yield minima for all bimetallic systems. For bimetallic systems, FDCA yields increased to nearly 30% for the Mn-Cu catalyst and nearly 25% for the Fe-Co catalyst. When present in smaller proportions relative to the less charged component, the more highly charged metal - Mn in the Mn-Cu system (Mn^{3+}/Mn^{4+}) and Fe in the Fe-Co system (Fe^{3+}) - produced higher yields.[42] Liu et al.[157] saw that the pure metal catalysts of Cu and VO on a nitrogen-containing polymer support (PDVTA) had high FDCA yields of approximately 61 and 78% in a DMSO/TBA solvent, respectively (Figure 30). Similar to the other catalysts presented in Figure 30, when a bimetallic catalyst was used, FDCA yields were higher, and in the case of Cu-VO/PDVTA, FDCA yields were almost 90%. The authors attributed this increased yield to the synergistic effects of the two metals.[157]

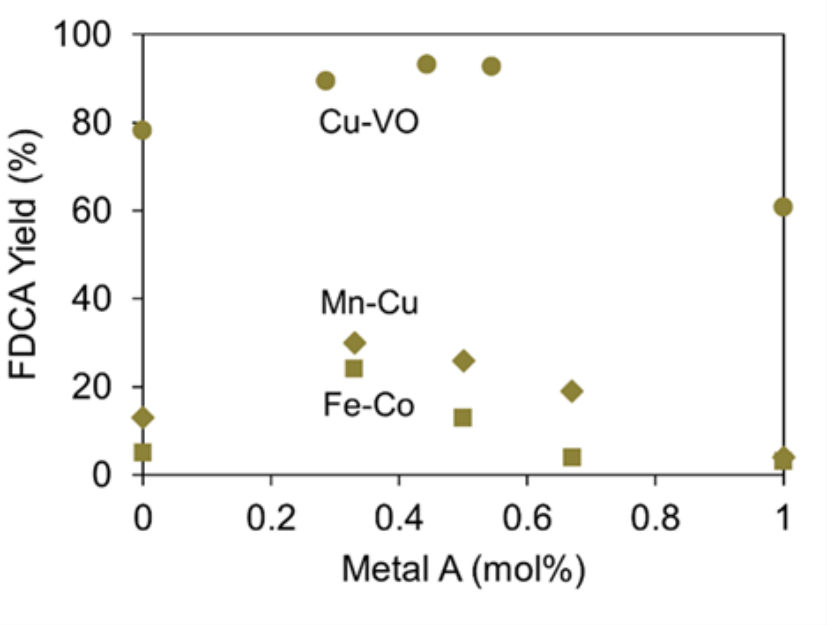

Figure 30. Comparison of FDCA yields on single metal and bimetallic catalysts containing Mn-Cu (♦), Fe-Co (■),[42] and Cu^{2+}-VO^{2+} over a PVDTA support (●).[157] Reaction conditions for the Mn-Cu and Fe-Co catalysts: 1:4 HMF:catalyst by weight, pure ACN, 13:1 TBHP:HMF molar ratio, 3.5 wt% initial HMF, T = 333 K, P = atm, t = 3 h,[42] and for the Cu-VO/PVDTA catalyst: 32/68 w/w DMSO/TBA, 0.37 wt% initial HMF, T = 363 K, P = atm, t = 5 h.[157]

The disparity in activity between two Cu bimetallic catalysts,[42, 157] highlights the importance of both the secondary metal and of the support. The catalysts studied by Demet et al.[42] were unsupported, acting as mixtures of metallic oxides rather than as deposited particles on a support like those prepared by Liu et al. The PVDTA support allowed for an increase in particle dispersion,[157] a factor previously observed to impact catalyst activity by Rao et al.[104] The use of VO as a secondary metal may have also impacted the activity of the catalyst for similar reasons as those discussed regarding bimetallic Au catalysts; primarily, factors such as electron density, reactivity, and reactant adsorption capacity.

Yang et al.[102] also studied Mn, Cu, and V catalysts, varying the supports across a range of MoO_3 polymorphs in a TBA solvent. Like Liu et al.,[157] they found that the V-doped catalyst had the highest FDCA yields, also correlating both surface area (Figure 31a) and pore volume (Figure 31b) to these high yields. The high activity of the catalyst was further attributed to a balance of acidic and basic sites due to the incorporation of V onto the support, and the structure of the support itself. The polymorph of MoO_3 had a significant effect on both the HMF conversion and the FDCA yields, with α-MoO_3 having the highest activity as a catalyst without the addition of metal, but FDCA yields were only around 30%. (Figure 31a) This was attributed to the [010] crystal plane of α-MoO_3 being favorable for contact with the substrate. The same correlations to surface area and pore size held true for the non-doped supports as were seen on the metal-doped catalysts. (Figure 31b).[157]

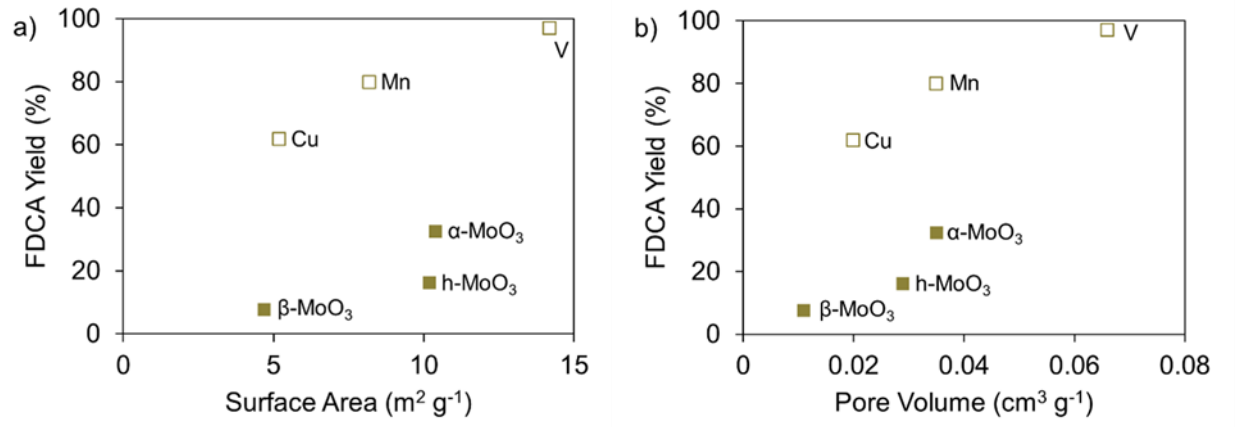

Figure 31. The relationship between FDCA yield and a) surface area and b) pore volume for NNM catalysts on α-MoO_3 supports (□) and different MoO_3 phases without additional metal (■) (Reaction conditions: 4 mL TBA solvent, 4 mmol TBHP, 0.4 wt% HMF, T = 353 K, P = atm, t = 12 h).[102]

The importance of basic sites to facilitate HMF conversion observed by Yang et al.[102] was also noted by Liu et al.[157] and Hameed et al.[85] In the first case, basic amine groups at the surface of the catalyst helped to coordinate metal ions (Cu^{2+} and VO^{2+}) and improve catalytic efficiency.[157] In the second case, a Fe-N-C catalyst was supported on a range of metal oxides that led to a range of Lewis acid-base chemistries present at the surface of the catalysts, with Al_2O_3 leading to the highest FDCA yield (99.8%) and MgO the lowest (7.5%). NH_3-TPD analysis showed increasing intensity of acidic sites in the order of MgO < ZrO_2 < TiO_2 < Al_2O_3 (Figure 32), while CO_2-TPD analysis showed an increasing intensity of basic sites in identical order.[85] Another study by Zheng et al.[19] also reported the highest yields of FDCA for their Ru-based system over an Al_2O_3 support.

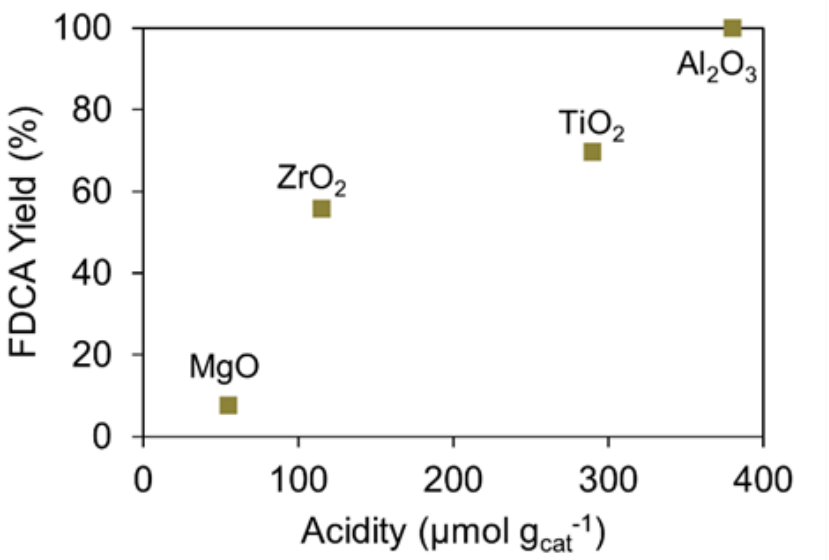

Figure 32. Relationship between catalyst surface acidity and FDCA yield. Reaction conditions: 30:1 HMF:Catalyst molar ratio, 50/50 w/w DMSO/water, 0.95 wt% HMF, T = 383 K, P = atm, t = 15 h.[85]

Hameed et al.[85] also highlighted the catalytic importance of nitrogen in the catalyst structure, emphasizing its ability to exhibit electron-withdrawing and donating effects. Nitrogen atoms acted as the primary ligands by which the single-atom Fe catalyst, operating in 50/50 w/w DMSO/H_2O, was attached to a carbon backbone. Furthermore, the nitrogen stabilized the Fe into a higher valence state, Fe^{5+}, than would typically be observed through formation of FeN_5 structures. These penta-coordinated structures were hypothesized to be the most active part of the catalyst, generating active oxygen species for the conversion of HMF towards FDCA.[85] Rao et al.[81] also upgraded HMF over a N-doped catalyst, a carbonized bamboo sawdust catalyst doped with melamine as a nitrogen source using MeOH as the solvent. The lack of metal in the catalyst allowed for a more direct study of the impact of nitrogen on the catalyst structure and activity at a range of carbonization temperatures (873 – 1173 K). Pyridinic, pyrrolic, and graphitic nitrogen were all observed in the catalyst structures, at varying concentrations dependent upon the carbonization temperature. While no correlation was observed between the presence of pyridinic or pyrrolic nitrogen content, increased abundance of graphitic nitrogen did correlate to both increased presence of acidic and basic sites as well as increased yields of FDCA (Figure 33).[81]

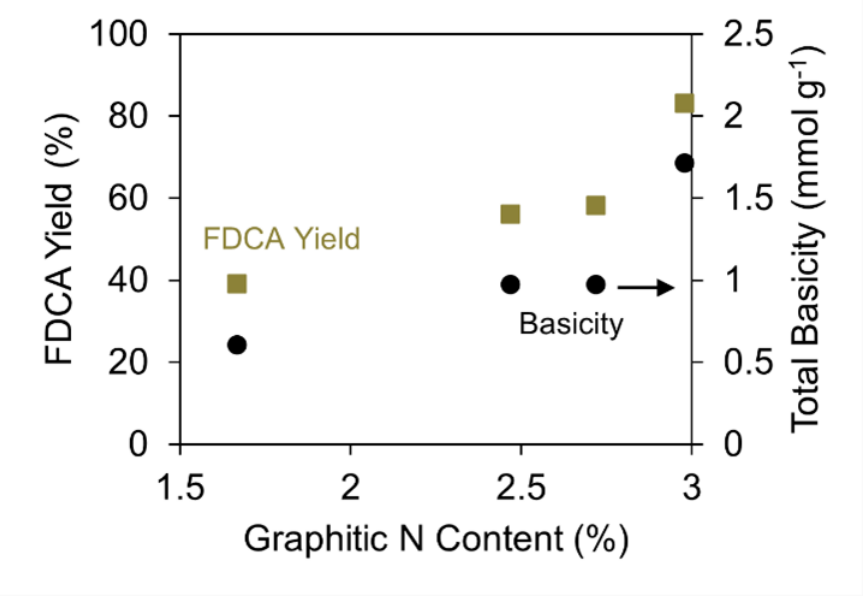

Figure 33. Impact of graphitic N content on FDCA yield (■) and total catalyst basicity (●). Reaction conditions: MeOH solvent, 0.1 M K_2CO_3 weak base additive, 0.89 wt% HMF, T = 433 K, P_{O2} = 2 MPa, t = 6 h.[81]

Gao et al.[84] also reported improved yields due to an increased availability of basic sites while investigating Co-Fe catalysts supported by hydrotalcite doped with either sulfur (S) or phosphorous (P). While layered double hydroxide (LDH) supports are more commonly applied in electrocatalytic systems,[165, 166] where they excel due to their tunable redox properties, their use in thermochemical oxidation also shows high HMF conversions and FDCA yields. Distribution of Co and Fe on the LDH hydrotalcite support allowed for improved electron transfer ability between $Co^{2+/3+}$ and $Fe^{2+/3+}$, particularly with the introduction of S or P dopants. The addition of these non-metal elements created three-dimensional structures in the LDH, increasing catalyst surface area, pore diameter, and pore volume.[84] These physical attributes were maximized for the catalyst with the highest FDCA yield, a P-doped Co-Fe/LDH catalyst (Co-Fe-P-400/LDH) that converted 98% of HMF with 61% selectivity to FDCA in ACN (Table 11, index 1). When

studying reaction temperature, the difference in catalytic activity between the S- and P- doped catalysts was similar (Figure 34), suggesting that both S- and P- doping had similar effects and that the enhanced catalytic activity correlated more strongly to the availability of basic sites.[84]

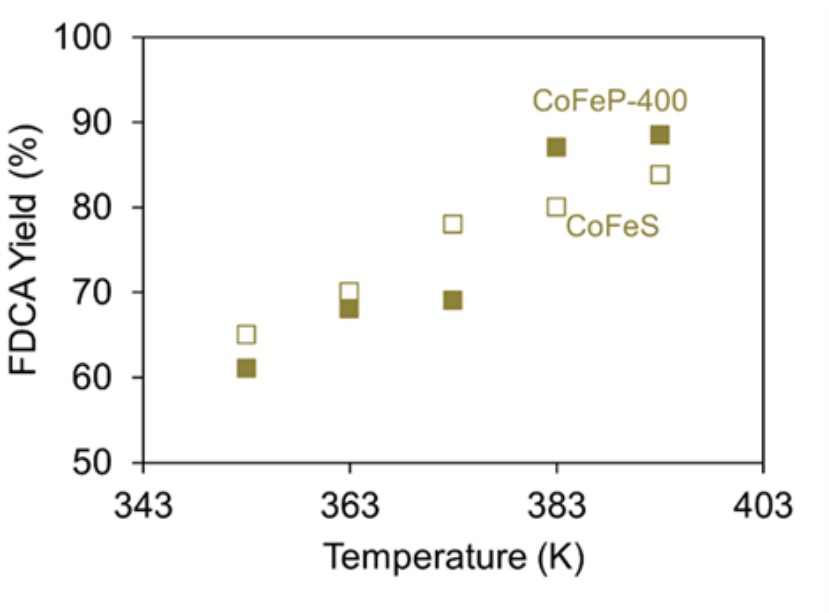

Figure 34. Temperature effect on FDCA yield of doped Co-Fe catalysts on a layered double hydroxide hydrotalcite support. Reaction conditions: 1:1 HMF:catalyst by weight, ACN solvent, 0.61 wt% initial HMF, P = atm, t = 6 h.[84]

Using the CoFeP-400/LDH catalyst, Gao et al.[84] studied the oxidation of HMF in several different solvents including ACN, DMF, DMSO, and EtOH (Table 11, indices 1-4). As had been observed by Ryu et al.,[36] the molecular properties and interactivities of the solvent impacted the distribution of products obtained from HMF oxidation. In this selection of solvents, the effect of hydrogen bond acceptance capacity was less clear. The solvent with the lowest β value, ACN (0.4), achieved the highest HMF conversion and FDCA yield. In contrast, DMF, DMSO, and

EtOH, with β -values ranging from 0.69 – 0.76 (Table 8), were more selective towards primary intermediates like HMFCA. However, these three solvents did not follow a clear trend in HMF conversion (Figure 35a) as data presented by Ryu et al. had, where lower β values corresponded to further reaction progress. For example, DMF (β = 0.69) had 42% HMF conversion, while EtOH (β = 0.75) achieved 78%. Conversion and yields trended more consistently with increasing polarity (Table 8, δ_P), however. ACN, the most polar solvent studied (δ_P = 18.0), had the highest FDCA yields while EtOH (δ_P = 8.8), the least polar, favored primary intermediates like HMFCA and DFF (Figure 35b).

Index	Catalyst	Support	Solvent	t (h)	$C_{HMF,i}$ (wt%)	HMF/ Cat (mol/mol)	HMF Conv. (%)	FDCA Yield (%)	Ref.
1	Co-Fe-P-400	LDH	ACN	6	0.61	NR	98	60	[84]
2	Co-Fe-P-400	LDH	DMF	6	0.51	NR	42	4.2	[84]
3	Co-Fe-P-400	LDH	DMSO	6	0.44	NR	66	6.6	[84]
4	Co-Fe-P-400	LDH	EtOH	6	0.60	NR	78	14	[84]
5	$NiCo_2O_4$	-	ACN/TBHP	12	2.2	10.4	100	60	[164]

Table 11. Non-noble metal catalysts studied in organic solvent systems for HMF oxidation at 353 K.

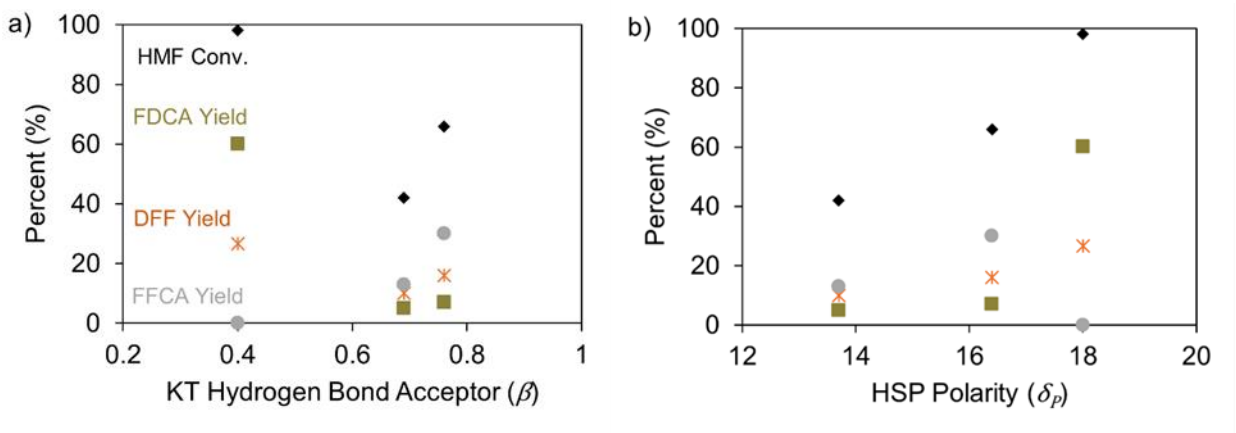

Figure 35. Effect of solvent a) hydrogen bond acceptance capacity and b) polarity on HMF conversion (♦) and FDCA (■), DFF (✳), and FFCA (●) yields for ACN, DMF, and DMSO solvents. Reaction conditions: CoFeP-400/LDH catalyst, 0.36 mL TBHP oxidant additive, 0.44-0.61 wt% HMF, T = 353 K, P_{O2} = 1 MPa, t = 6 h.[84]

Yu et al.[154] conducted a similar study into a solvent's impact on HMF conversion and product yields. In pure organic solvent systems, all reactions were limited to low FDCA yields (0-6%) with primary selectivity to DFF (Figures 36a and b) even in alcohol-based solvents (Figures 36c and d). Considering all solvents, as the β-value increased, both the HMF conversion and DFF yield increased (Figures 36a and c), which was the opposite trend seen with δ_P (Figures 36b and d). No significant trends were observed between solvent characteristics and FDCA yields, though insufficient water and O_2 pressure, or the lack of an added oxidant to provide a source of oxygen may have dominated any solvent effects. When the same reaction conditions were applied to a system with more available oxygen, water containing 0.0235 M Na_2CO_3 base additive, HMF conversion improved to 95% and FDCA yield to 88.3%.[154] Increased oxygen availability was also noted as important by Qian et al.,[164] who studied the impact of TBHP dosage on FDCA yields in ACN, and by Pandey et al.[167] who studied a bimetallic Mn_1Fe_1 catalyst in 46/54 w/w GVL/H_2O both with and without the pretreatment of HMF with ozone.

Additionally, adding an ozone pretreatment improved FDCA yields from 40% to 60%, with all other conditions held constant.[167] Qian et al.[164] also found that the catalyst with the largest number of surface defects, and thus the largest amount of adsorbed oxygen in these defects, resulted in the highest yield of FDCA. In their specific study, the 'flaky' morphology of a $NiCo_2O_4$ catalyst contained the highest percentage of adsorbed surface oxygen out of the catalyst variations investigated. This higher oxygen concentration corresponded to the highest FDCA yield, 60.1%.

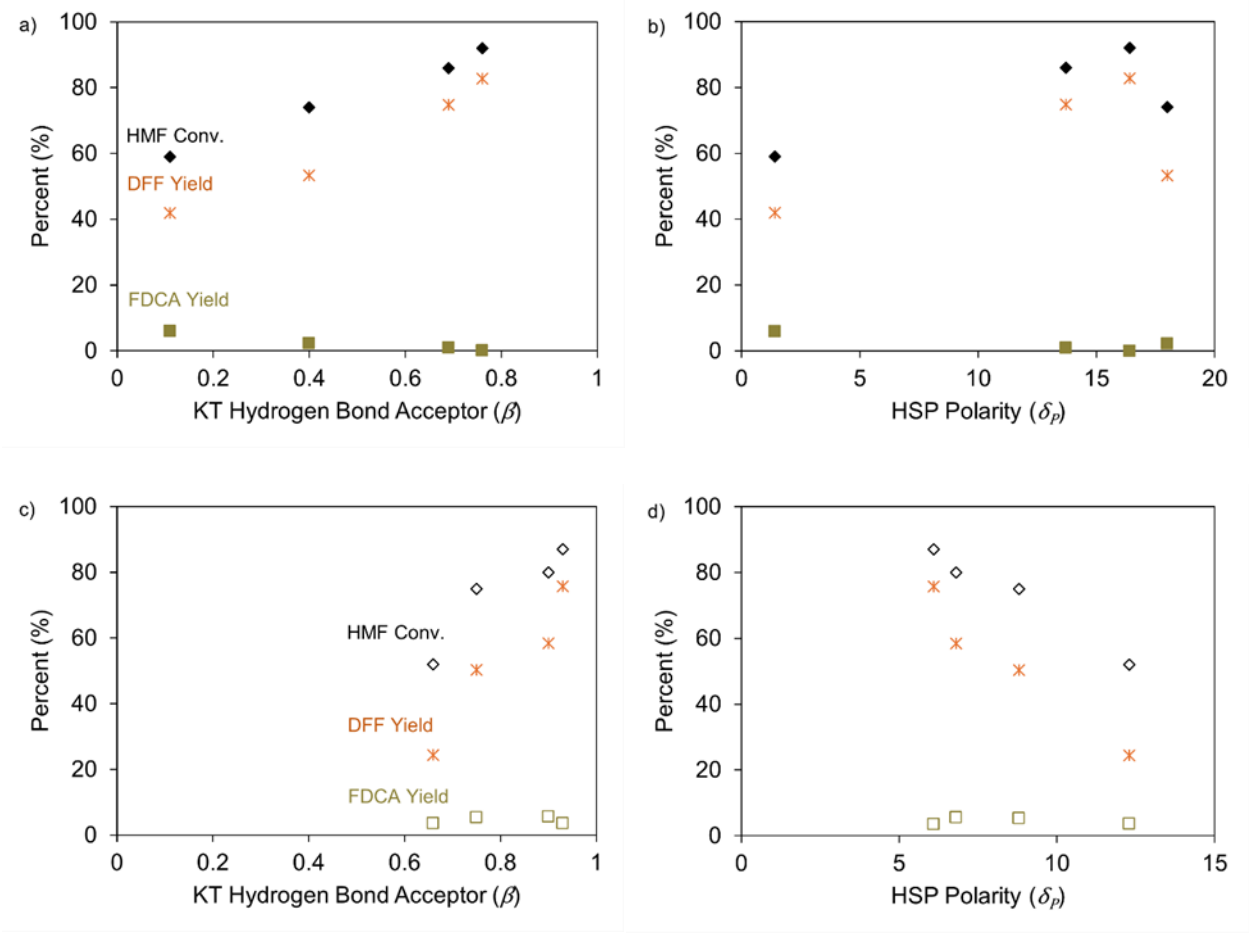

Figure 36. Trends of HMF conversion (◊), DFF (✳), and FDCA (□) yields for toluene, ACN, DMF, and DMSO pure solvents compared to a) the KT β parameter and b) the HSP polarity parameter and the same trends for MeOH, EtOH, n-PrOH,, and i-PrOH in figure c) and d), respectively. Reaction conditions: Co/MnO_2 catalyst, 0.57-0.80 wt% HMF, T = 413 K, P_{O2} = 0.3 MPa, t = 4 h.[154]

Qian et al.[164] also found that the catalyst with the largest number of surface defects, and thus the largest amount of adsorbed oxygen in these defects, resulted in the highest yield of FDCA. In their specific study, the 'flaky' morphology of a $NiCo_2O_4$ catalyst contained the highest percentage of adsorbed surface oxygen out of the catalyst variations investigated. This

higher oxygen concentration corresponded to the highest observed FDCA yield, 60.1% (Table 11, index 5).[164]

The presence and quantity of acidic/basic sites at the surface of a catalyst remains an important factor in HMF conversion even in organic solvents. For the catalysts reviewed, the presence of graphitic nitrogen and the use of an optimal carbonization temperature for AC supports correlated with increased FDCA yields. When using metal oxide supports, the selection of the correct metal oxide, particularly Al_2O_3, seemed to have the largest impact on such acidic/basic sites. Choosing compatible metals for bimetallic catalysts and implementing them in optimal ratios is also important to effectively oxide HMF over NNM catalysts. Additionally, similar to observations with NM catalysts and organics in general, the choice of solvent can significantly impact product selectivity, with solvents prone to accepting hydrogen bonds being more likely to interact with furan functional groups, leading to decreased reactant adsorption at the catalyst surface and hindered reaction progress. Finally, ensuring sufficient oxygen to support the formation of intermediate products and, ultimately, FDCA may be a limiting factor in organic reactions, outweighing the influence of solvent effects.

2.8 Conclusions and Future Outlook

The sustainable and economical production of FDCA is a critical challenge to be addressed in the development of bio-derived materials like PEF. In order to find a solution, novel solvents, catalysts, and catalyst supports have been investigated in systems both with and without base additives. Recent TEAs and LCA analyses[13, 76, 168, 169] have concluded that the HMF production step is a more critical process than FDCA production. This is mostly because FDCA yields close to 100% can be achieved with many catalysts using different reaction conditions,

while HMF yields are just 60-90% when using fructose ($600-800 per MT) and 30-60% when using glucose or cellulose ($100-400 per MT). Based on this, future improvements to the commercialization of FDCA should also focus on production of HMF, not only the oxidation of HMF to FDCA. Developing catalysts that may be less active but more tolerant to biomass-derived impurities and using similar solvents for the production of both FDCA and HMF may improve the economics of the process. The use of similar or the same solvents for both processes would eliminate or reduce HMF purification and/or recovery requirements and save the energy required for solvent recovery.

From a catalytic perspective, water remains the best solvent, with low intermolecular solvent-furan interactions and the ability to donate oxygen to the reaction while being low-cost and readily available. Organic solvents can improve FDCA solubility or allow for the two-step upgrading of sugars directly to FDCA, removing costly purification steps. However, without the presence of water, obtaining FDCA yields close to 100% is more challenging and is unfeasible in many pure-organic systems. Aqueous/organic solvent mixtures seem to be the most promising option for future research. These systems offer the unique advantage of higher FDCA solubility, which reduces catalyst fouling due to FDCA crystallization, while retaining sufficient water to facilitate high selectivity towards FDCA. Solvent mixtures containing organics with low KT hydrogen bond acceptance basicity (β) and low to moderate polarity (δ_P) tend to correlate with the highest yields of FDCA likely due to minimal interference with furan adsorption to catalyst surfaces.

When sustainability is taken into consideration, the use of organic solvents has both economic and environmental advantages as working at higher HMF concentrations decreases

energy expenditure considerably; however, solvent stability at reaction conditions, solvent recovery strategies, and catalyst selection need to be carefully studied in the future. A poor organic solvent management strategy may result in higher energy demand compared to aqueous systems, but in either case purification and recovery must be accounted for in LCA and come at a significant cost. Finally, solvent toxicity must also be considered, and in this sense, articles are starting to appear to guide solvent selection. For example, Al Ghatta et al.[13] evaluated solvents and concluded that DMSO and ionic liquids would be considered safer than solvents such as methyl isobutyl ketone (MIBK). Other studies, however, indicate that MIBK would be advised before DMSO.[170] Lack of consensus is in part due to differing criteria for the definition of a 'safe' or 'sustainable' solvent. Therefore, establishing clear criteria for evaluation is necessary in order to compare different systems and make conclusions concerning scale-up.

Noble metal catalysts such as Pt, Pd, Au, and Ru continue to play a significant role in HMF oxidation, particularly when paired with transition metal oxide or nitrogen-doped carbon supports. Such pairings often result in high conversion of HMF with high selectivity to FDCA. Catalyst characteristics such as high surface area, low metal particle size, even particle distribution, and high concentration of Lewis acidic and basic sites correlate strongly with improved yields. Within the last few years, non-noble metal catalysts such as Ni, Cu, V, Co, Fe, Bi, and Mn, have seen a significant increase in study due to the low cost and lower environmental impact compared to noble metals. These non-noble metal catalysts show high conversion and selectivity towards FDCA, particularly when used as bimetallic catalysts. Specifically, the combined use of metals with different physical properties and valence states has

been found to enhance catalytic performance by facilitating better electron transfer and improving reactant adsorption to active sites.

While non-noble metal catalysts may require longer reaction times or higher temperatures compared to noble metal catalysts, catalyst composition, beneficial doping, and selection of compatible supports has allowed for competitive performance in select cases. Similarly, though aqueous systems offer the highest FDCA selectivity, they are hindered by low FDCA solubility. Organic solvents improve solubility and allow for higher HMF concentrations but can sometimes interfere with reaction progress through solvent-reactant interactions. The application of aqueous/organic solvent blends, such as GVL/H_2O and DX/H_2O, offer a promising compromise by maintaining selectivity towards FDCA while improving product solubility.

Both noble and non-noble metal catalysts are often reported as stable catalysts. However, most studies do not include extensive stability studies. Out of 19 studies that included catalyst deactivation performance, only three were done as continuous flow operations, which is necessary to properly evaluate the applicability of a catalyst at commercial scale.[153] The remaining studies were conducted as repeated batch reactions. Even amongst the flow reactors investigated, experiments lasted only 40-60 h, which may not have been sufficient time to observe deactivation. Additionally, purified HMF and/or low concentrations of HMF were used as the feedstock, eliminating the effects of impurities on catalyst activity and stability. Longer stability studies at high HMF concentrations and in the presence of biomass-derived impurities should be performed to properly evaluate catalysts for commercial use.

The development of these studies may have a significant effect on TEAs and LCAs. Currently, catalyst selection seems to have a relatively minor effect on both, with catalysts

assumed to be stable for years with just minor need for replacement (i.e. 10% catalyst make-up).[171] Kim et al.[76] reported an increase of 7.9% on the minimum selling price when catalyst stability was reduced from 6 to 3 months (2000 h). In this sense, noble metal catalysts will likely always be more stable than non-metals and future research should consider focusing on reducing necessary metal loading on catalysts via new synthesis techniques that allow for better utilization of noble metals, or by using bimetallic catalysts that find synergies between noble and non-noble metal catalysts.

Reaction conditions, including temperature, pH, and reaction time, must be optimized to maximize FDCA yield while minimizing HMF degradation. The synergistic interplay of solvent, catalyst, support, additives, and reaction conditions ultimately dictate the efficiency of HMF conversion and selectivity towards FDCA. Continued research into non-noble metal catalysts and aqueous/organic solvent mixtures for HMF upgrading presents ongoing opportunities to enhance FDCA yields and ultimately achieve the economic viability of FDCA production.

Future research in the field of HMF oxidation to produce FDCA will likely focus on the key areas of improvement highlighted in this review, mainly catalyst activity and reusability, particularly for non-noble metal systems, solvent selection that mitigates negative solvent-reactant interactions, and the expanded application of alternate oxidative techniques like electrocatalysis and photocatalysis. This research will have to be integrated with TEAs and LCAs where the oxidation of HMF is studied alongside its production.

CHAPTER THREE

SOLUBILITY OF 2,5-FURANDICARBOXYLIC ACID IN PURE AND MIXED ORGANIC SOLVENT SYSTEMS AT 293 K PREDICTED USING HANSEN SOLUBILITY PARAMETERS

3.1 Contributions of Authors and Co-Authors

Author: Jacob M. Molinaro

Contributions: Methodology, Data curation, Writing - Original manuscript preparation.

Co-Author: Matthew R. Carroll

Contributions: Data curation and Methodology.

Co-Author: Annabelle S. Young

Contributions: Data curation.

Co-Author: Stephanie G. Wettstein

Contributions: Conceptualization, Supervision, Funding acquisition, Methodology, Writing - Original manuscript preparation.

Manuscript in Chapter 3.

3.2 Manuscript Information

Jacob M. Molinaro, Matthew R. Carroll, Annabelle S. Young, and Stephanie G. Wettstein

ACS Omega

Status of Manuscript:

_____ Prepared for submission to a peer-reviewed journal

_____ Officially submitted to a peer-reviewed journal

_____ Accepted by a peer-reviewed journal

__X__ Published in a peer-reviewed journal

ACS Publications

27 June 2024

3.3 Abstract

Central to the production of polyethylene furanoate (PEF), a bioplastic that could potentially replace petroleum-derived plastics, is 2,5-furandicarboxylic acid (FDCA). FDCA is a chemical derived from biomass that has low solubility in traditionally used solvents such as water. Thus, identifying solvents that can solubilize significant amounts of FDCA could allow for lower PEF production costs. In this study, FDCA solubility was investigated in nine pure solvents including H_2O, acetonitrile (ACN), γ-valerolactone (GVL), γ-butyrolactone (GBL), ethanol (EtOH), methanol (MeOH) , dimethyl sulfoxide (DMSO), sulfolane (SULF), and tetrahydrofuran (THF), eight binary, and three ternary solvent blends at 293 K. For all binary systems excluding DMSO and MeOH, the solubility of FDCA increased 1.5 to 65 times compared to the pure organic solvent, and the FDCA solubility was at least 10 times higher when compared to pure water. Specifically, the 20/80 w/w H_2O/DMSO system solubilized 23.1 wt% FDCA, the highest of any binary blend studied, and 190 times more solubility than in pure water. In 20/80 w/w H_2O/THF, the FDCA solubility was 60 times higher than pure water. In ternary blends that included DMSO, H_2O, and either GVL, THF, or SULF, solubility increased by at least 6.6 times relative to the pure secondary organic component and 54 times relative to pure water. Using Hansen Solubility Parameters (HSPs), the radius of interaction ($R_{i,j}$) was found to be more strongly correlated to FDCA solubility than individual HSPs or the total solubility parameter. A MATLAB-based optimization code was developed and successful in minimizing the $R_{i,j}$ of a solvent blend to maximize FDCA solubility in binary and ternary aqueous solvents.

3.4 Introduction

As a biomass-derived platform chemical, 2,5-furandicarboxylic acid (FDCA) has diverse applications that could help build a sustainable future. With the diminishing availability of nonrenewable resources, there is a growing emphasis on sustainable production methods for consumer goods. One area affected by this is the petrochemical and plastics industry, as everyday products like food containers, shipping packaging, and water bottles are made from polyethylene terephthalate (PET).[3] Though extremely useful, PET products are manufactured from petroleum derivatives and are significant contributors to pollution and long-term environmental damage when not recycled.[172] One solution to this problem is the introduction of bio-based plastics like polyethylene furanoate (PEF),[8] which can be synthesized from lignocellulosic biomass-derived FDCA. Economical production of FDCA is of great importance to PEF production, but the low solubility of FDCA[27-30] a challenge. In solvents such as water[27] and ethanol[31] the solubility of FDCA is less than 1 wt% at STP. Therefore, either large amounts of solvent or additives, like sodium hydroxide, are required to improve solubility, which increases the financial barrier to scale up.[34, 35]

Although the literature is limited, research has reported that organic solvents show promise for improving FDCA solubility. Zhang et al.[28] reported FDCA solubilities in eight pure and two binary mixtures from 313 to 363 K and correlated increased solubility to increased temperature. Additionally, mixtures achieved higher solubilization of FDCA than pure components. For example, at 323 K the FDCA solubility in acetic acid (AA) and acetonitrile (ACN) were 0.09 wt% and 0.04 wt%, respectively, which is lower than the solubility they reported in pure water (0.25 wt%). However, in aqueous/organic mixtures, the maximum

reported solubilities were 0.70 wt% (at 40/60 w/w H_2O/AA) and 2.5 wt% (at 39/62 w/w H_2O/ACN), representing at least a twofold increase over pure components. Thermodynamic models were able to predict the H_2O/AA and H_2O/ACN binary mixture solubility data using both the non-random two liquid (NRTL) and universal quasichemical (UNIQUAC) models.[28]

In other studies by Motagamwala et al.[27] and Ban et al.,[31] similar or higher FDCA solubilities were observed. In an 20/80 w/w H_2O/γ-valerolactone (GVL) solvent system, Motagamwala et al. increased FDCA solubility an order of magnitude from 0.2 wt% in pure water to 2.4 wt% at 303 K. At 373 K, the same solvent blend solubilized over 9 wt% FDCA compared to just over 1 wt% in pure water. They hypothesized that the increase in solubility within binary aqueous/organic mixtures was related to a higher enthalpy of mixing between solvents.[27] Ban et al. studied binary mixtures of H_2O/AA, H_2O/ethanol (EtOH), and H_2O/methanol (MeOH). Findings showed that for AA, binary mixtures yielded higher solubility than the pure component, but that MeOH and EtOH both showed the highest solubility as pure components, though the range of mixtures studied only included 0 to 30 wt% H_2O.[31]

Zhuang et al.,[29] in a similar study, found that all binary aqueous/organic mixtures they studied (tetrahydrofuran (THF), 1,4-dioxane (DX), 1,2-dimethoxyethane (DME), and diethylene glycol dimethyl ether (DGDE)) had higher solubility than pure components. They proposed the use of several thermodynamic models, including Hansen Solubility Parameters (HSPs), to provide a useful approach for finding ideal solvents. Specifically, using the Hansen Total Solubility Parameter, δ_T, a strong correlation was found between solvents and solutes of similar δ_T and FDCA solubility.

Compared to NRTL and UNIQUAC models, HSPs are convenient since data for thousands of common solutes and solvents is available, mixtures of solvents can be easily considered, and they can be adjusted for temperature. HSPs were originally developed to assess solvent compatibility within the paint and coatings industry, where they were found to be effective for developing surface coatings.[53] Since then, HSPs have been effectively applied in the selection of green extraction solvents,[173] solvent choice for the solubilization of cellulose,[49] and identification of ideal solvents for lignin dissolution.[50] Despite this, to the best of the authors' knowledge no further work has been done applying HSPs to FDCA solubility beyond that reported by Zhuang et al.[29] It is hypothesized that by identifying what HSP parameter correlates best to FDCA solubility, solvent blends could be optimized leading to improved efficiency in PEF production. Additionally, the findings presented herein may apply to solute-solvent combinations at a much broader scale.

For this work, nine solvents were selected based on prior application in the production of furan compounds[64] or the upgrading of HMF[25, 31] to determine FDCA solubility in pure and blended solvent mixtures. These solvents were H_2O, ACN, GVL, γ-butyrolactone (GBL), EtOH, MeOH, dimethyl sulfoxide (DMSO), sulfolane (SULF), and THF. Using these solvents, we not only build upon existing research, but also provide new insights into the relationship between HSPs and FDCA solubility and report HSPs and FDCA solubilities for ternary solvent blends.

3.5 Theory

The work conducted by Motagamwala et al.,[27] Zhang et al.,[28] and Zhuang et al.[29] all cite thermodynamic explanations and correlations for FDCA solubility, specifically correlating

solubility to temperature and enthalpy. Such thermodynamic principles state that mixing occurs when there is a negative Gibb's Free Energy (ΔG), which is given for an isothermal system by:

$$\Delta G = \Delta H - T\Delta S \qquad (Eqn. 20)$$

where H is enthalpy, T is temperature, and S is entropy. Smaller ΔH and/or higher T would thus increase the likelihood of ΔG being negative. The enthalpy change (ΔH) can be expressed through HSPs, which decompose ΔH into three distinct components: atomic dispersion forces (δ_D), dipole-dipole polarization (δ_P), and molecular hydrogen bonding (δ_H).[51] Each chemical has unique values for these components, which can be found in the literature or are calculable using the HSPiP software.

The HSP dispersion component, δ_D, is rooted in nonpolar atomic interactions, also referred to as London dispersion forces. These forces capture fluctuations in the electric field of molecules resulting from interactions with neighboring molecules. The dipole-dipole polarization value, δ_P, addresses varying charge densities influencing molecular organization while the molecular hydrogen bonding value, δ_H, represents the electrostatic forces between a hydrogen atom and the dipole of another molecule. Both the polarity and hydrogen bonding parameters share a strictly molecular nature, while the dispersion parameter relies on induced dipole interactions with other molecules.[51] HSPs have been previously explored as a promising method for predicting solubility of many components including FDCA,[29] cellulose,[49] and other ring-containing organic compounds and pharmaceuticals[174-176] with an overall focus on "like dissolves like."[29, 51, 52]

The pure component HSP values can then be used to determine the HSPs for solvent mixtures using:

$$\delta_{X_{Blend}} = \sum_i (\varphi_i * \delta_{X_i}) \quad (Eqn. 21)$$

where φ_i is volume fraction and δ_{X_i} is the pure component HSP value. This calculates the mixture values as volume weighted averages of each component and sets the foundation for further applications in solubility estimation. Then, utilizing the solvent parameters, various methods can be used to estimate solute solubility. One of these methods, which was used by Zhuang et al.,[29] compares the total solubility parameter[52] δ_T calculated with:

$$\delta_T = \sqrt{\delta_D^2 + \delta_P^2 + \delta_H^2} \quad (Eqn. 22)$$

for both solvent and solute, and then calculating the difference between solute and solvent δ_T using:

$$\Delta\delta_T = \delta_{T,i} - \delta_{T,j} \quad (Eqn. 23)$$

where *i* and *j* represent the solvent and solute, respectively. According to HSP theory, substances with similar total solubility parameters, and therefore lower $\Delta\delta_T$ values, are more likely to solubilize each other.[52]

A second method to determine the likelihood of solubilization between a solvent and solute is the radius of interaction $R_{i,j}$, which is defined by:

$$R_{i,j} = \sqrt{4 * (\delta_{D,i} - \delta_{D,j})^2 + (\delta_{P,i} - \delta_{P,j})^2 + (\delta_{H,i} - \delta_{H,j})^2} \quad (Eqn. 24)$$

where *i* and *j* represent the properties of the solvent and solute, respectively.[52] Similar to $\Delta\delta_T$, the lower the value of $R_{i,j}$, the more likely that the solute is soluble in the solvent.[57] However, the key difference between the two variables is that the $\Delta\delta_T$ parameter represents an unweighted comparison of each solubility vector, while the $R_{i,j}$ incorporates a weighting factor of 2 on δ_D, a

coefficient determined through experimental findings.[51, 58] The experimental data found that the δ_D, which arises from atomic induced dipole interactions rather than as a function of molecular structure (like δ_P or δ_H), required a coefficient of 4 in the $R_{i,j}$ equation to create a spherical shape to the interaction plot. Furthermore, $R_{i,j}$ explicitly compares individual HSP values rather than the overall solubility vectors of the two components. With $\Delta\delta_T$ it is possible for a solvent-solute pairing to have drastically different values of multiple HSP components while maintaining similar values of δ_T. For both methods, since the HSP values of a mixture are weighted by volume fractions of the individual components, mixing two individual solvents in different proportions can minimize the $R_{i,j}$ and $\Delta\delta_T$ in order to maximize solubility.

3.6 Experimental Methods

Solubility Determination

FDCA solubility was determined for pure components (Table 12) as well as binary and ternary solvent blends using H_2O, ACN, GVL, GBL, EtOH, MeOH, THF, DMSO, and SULF. The sample solution was prepared in a 3.0 to 10.0 g sample in a conical vial with weight determined using an analytical balance. FDCA was then added incrementally to the vial at room temperature (293 K, accuracy ±0.3 K) while the solution was stirred at 800 rpm until FDCA was left visibly undissolved in the vial. Temperature was assessed using a K-type thermocouple and Omega Engineering OM-EL-USB-TC-LCD thermocouple data logger. If FDCA was still present in the vial after a minimum of 1 h of stirring, saturation was assumed to be reached, 6 and the solution was allowed to settle for a minimum of 20 min., or until visibly clear, before sampling. In the case of any uncertainty with solution conditions, additional stirring or settling time was

allowed up to 24 hours. Procedures for the assessment of experimental conditions such as temperature (T) and pressure (P) are available in the Supplemental Materials.

Chemical Name	Chemical Abbreviation	CAS No.	Molecular Formula	Structure	Source[a]	Purity
2,5-Furandicarboxylic acid	FDCA	3238-40-2	$C_6H_4O_5$	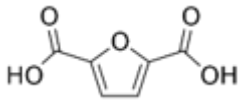	AK	98%
Acetonitrile	ACN	75-05-08	CH_3CN		FS	≥ 99%
Water	H_2O	7732-18-5	H_2O	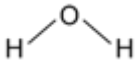	-	18.2Ω
γ-valerolactone	GVL	108-29-2	$C_5H_8O_2$	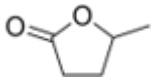	SA	≥ 99%
γ-butyrolactone	GBL	96-48-0	$C_4H_6O_2$	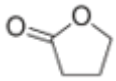	SA	≥ 99%
Ethanol	EtOH	64-17-5	CH_3CH_2OH		AO	≥ 99%
Methanol	MeOH	67-56-1	CH_3OH	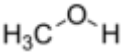	FS	≥ 99%
Tetrahydrofuran	THF	109-99-9	C_4H_8O		FS	≥ 99%
Dimethyl sulfoxide	DMSO	67-68-5	C_2H_6SO		SA	≥ 99%
Sulfolane	SULF	126-33-0	$C_4H_8O_2S$		SA	99%

Table 12. Solvents and solute used in experiments. [a]AK = AK Scientific, SA = Sigma-Aldrich, FS = Fisher Scientific, AO = Acros Organics

For sampling, a 1.0 mL sample of the FDCA-saturated solvent was diluted with 18.2Ω H_2O to prevent FDCA recrystallization in the HPLC. The amount of water added was determined by diluting the FDCA sample concentration to below the FDCA saturation point in pure water (a molarity of 0.0075). The diluted sample was filtered using a 0.2 μm membrane and then analyzed using an Agilent 1100 HPLC with DAD and RID detectors running trifluoroacetic acid buffer at a pH of 2 and flowrate of 0.6 mL/min on an Aminex HPX-87H (300 mm x 7.8 mm) column. Using the HPLC peak areas (A), the mass fraction of FDCA (w_{FDCA}) could be calculated using:

$$w_{FDCA} = \frac{0.001 \times k \times A \times D \times V \times M_W}{m_s} \qquad (Eqn. 25)$$

where k is the HPLC standard calibration value, D is the dilution ratio, V is the total sample volume, M_W is the molecular weight of FDCA, and m_s is the total sample mass. Assessment of uncertainty on solubility values is reported in the Supplemental Materials (Appendix A).

HSP Calculations

The mixture HSP values for solvents were calculated using Eqns. 21-23 with pure component values retrieved from the HSPiP software package (Table 13) at the same temperature as experiments were conducted, 293 K.[56]

MATLAB Modeling Methods

To determine ideal solvent blends based on minimizing $R_{i,j}$, a MATLAB program was created using version R2023a. The relevant solvent names and HSP parameters for the system under study were input to the code as a matrix. Once these variables were defined, the minimum $R_{i,j}$ (Eqn. 5) was found between FDCA and the stated solvent blend. The optimal mixture was

identified using the 'fmincon' function, which employs advanced nonlinear optimization methods to calculate the volume proportions of each solvent in the ideal blend. This function seeks to minimize the $R_{i,j}$ value while being constrained by lower and upper bounds ranging from 0.0 to 1.0 for each solvent and a sum of the individual volume fractions totaling 1.0. The code outputs the names and volume fractions of each solvent that were then manually converted to a mass basis using densities. A full version of the code is available in the Supplemental Materials (Appendix A).

Chemical	δ_D	δ_P	δ_H	δ_T	$\Delta\delta_D$	$\Delta\delta_P$	$\Delta\delta_H$	$\Delta\delta_T$	$R_{i,j}$
FDCA	19.4	10.3	12.9	25.5	-	-	-	-	-
DMSO	18.4	14.6	8.1	24.8	1	4.3	4.8	0.6	6.8
GVL	16.8	11.4	6.7	21.4	2.6	1.1	6.2	4.1	8.2
GBL	17.5	15.5	7.8	24.6	1.9	5.2	5.1	0.8	8.2
SULF	18.1	16.8	8.4	26.1	1.3	6.5	4.5	0.6	8.3
EtOH	15.8	8.8	19.4	26.5	3.6	1.5	6.5	1.1	9.8
THF	16.7	4.9	5.8	18.3	2.7	5.4	7.1	7.1	10.4
ACN	15.6	16.6	8.3	24.2	3.8	6.3	4.6	1.2	10.9
MeOH	14.7	12.3	22.3	29.4	4.7	2	9.4	3.9	13.4
H_2O	15.6	16	42	47.6	3.8	5.7	29.1	22.1	30.6

Table 13. HSP Parameter Data ($MPa^{1/2}$) for Pure Compounds at $T = 293$ K as Determined Using the HSPiP Software Where Δ Calculates the Difference Between the Pure Component and FDCA.

3.7 Results and Discussion

Binary Aqueous/Organic Solvent Systems

The eight organic solvents were studied in binary aqueous mixtures ranging from 20 to 90 wt% organic (Figure 37), and the maximum FDCA solubility for most solvents was approximately 2 wt% with the exception of THF (Figure 37; solid, black triangles) and DMSO (Figure 37; gray, unfilled triangles plotted on the secondary axis). THF solubilized a maximum of 7.2 wt% FDCA in a mixture of 20/80 w/w H_2O/THF and pure DMSO solubilized 30.7 wt% FDCA. Both results are significantly more than have been previously reported at higher temperatures,[27-29] or observed for the other solvents in this study.

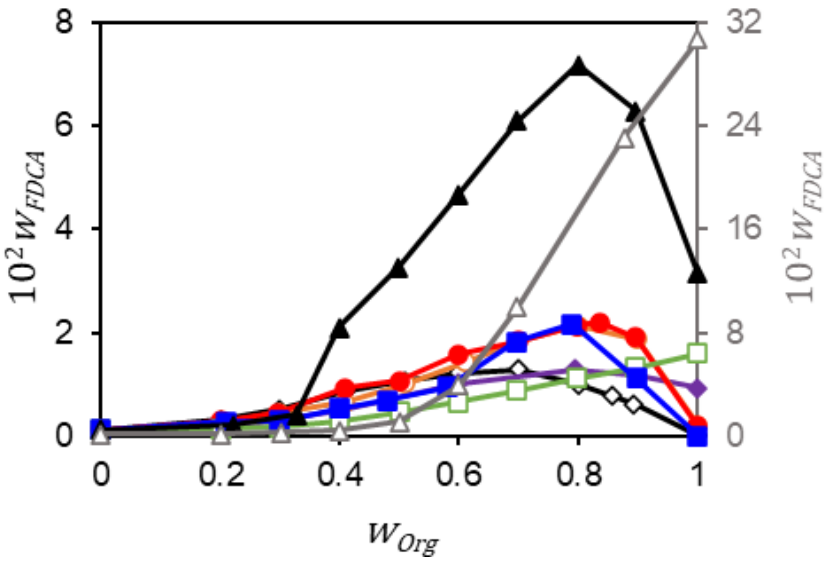

Figure 37. Plot of the mass fraction of FDCA solubilized (w_{FDCA}) in varying binary mixtures of H_2O and organic solvent (THF (▲), SULF (■), MeOH (□), EtOH (♦), ACN (◊), GVL (●), or GBL (○)) with the organic mass fraction (w_{Org}) on the horizontal axis. Solubility data for DMSO is shown on the secondary axis (△). Lines are provided to guide the eye. Raw data is provided in the Supplemental Materials (Appendix A, Tables 18 to 25).

DMSO and MeOH had the highest FDCA solubility as pure solvents, which may be explained by their molecular structures. MeOH is a small molecule that readily forms hydrogen bonds with water, forming a framework of hydrogen bonds and thus increasing the overall volume of the solution.[177] This nonideal behavior is paired with a positive heat of solution, or an increase in overall system enthalpy. This increase moves the system further from a state of ideal mixing as previously defined in the theory section, meaning that as water is added the overall system enthalpy increases, leading to reduced solubility. The same behavior, of MeOH exhibiting the highest solubility as a pure component, has previously been observed by Ban et al. and was similarly correlated to hydrogen bonding interactions (Appendix A, Figure 56a).[31]

DMSO has also been shown to form strong hydrogen bonding networks with water, particularly at DMSO mass fractions less than 68 wt%.[178] This may explain why FDCA solubility in H_2O/DMSO mixtures starts to exponentially increase in the DMSO mass fraction range of 60 to 70 wt% (Figure 37) since the hydrogen bond network may begin to weaken. When considering hydrogen bonding, Figure 38a shows the FDCA solubilities of all aqueous/organic solvent systems plotted against δ_H of the solvent. For a given solvent system, the maximum solubility occurs near the δ_H of FDCA (12.9; indicated by the red dashed line). Considering the other HSP parameters, δ_D (Figure 38b) also shows an increasing trend as the δ_D of the solvent approaches the δ_D of FDCA, but in the case of δ_P, no overall trends are seen for the solvent systems (Figure 38c).

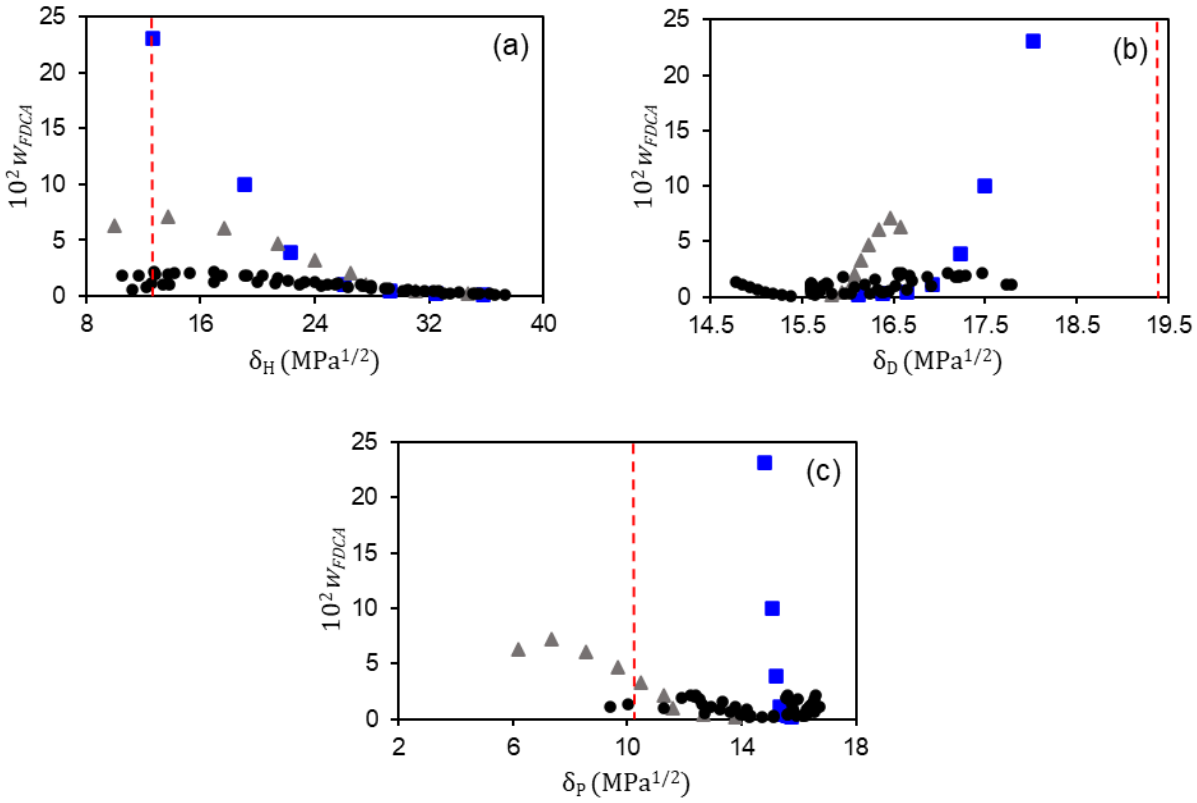

Figure 38. Mass fraction of FDCA solubilized (w_{FDCA}) in aqueous/organic binary solvent systems plotted versus a) δ_H, b) δ_D, and c) δ_P. Markers represent H_2O/DMSO (■), H_2O/THF (▲), and all other components (●) with the dashed lines (---) representing the respective HSP value of FDCA.

The observation that the maximum FDCA solubility aligns closely with its δ_H and δ_D values indicates that adopting a more comprehensive approach using the differences in parameters, like $R_{i,j}$ or $\Delta\delta_T$, may yield better correlations. This approach is supported by findings in the binary aqueous mixture data, where the highest FDCA solubility often matched the lowest $R_{i,j}$ values (Figure 39). For $\Delta\delta_T$, there were slight deviations in some instances as shown in Figure 39b, c, g, and h.

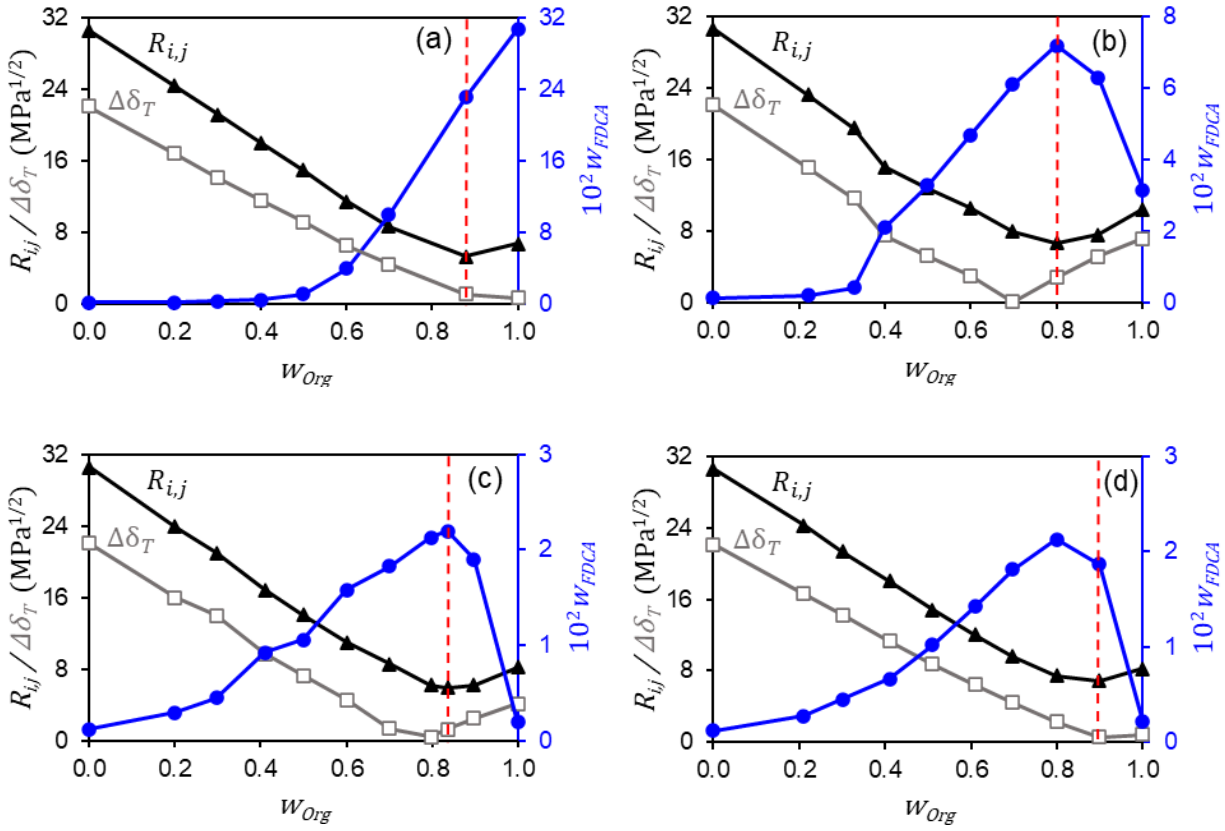
(a)
(b)
(c)
(d)
$R_{i,j}$
$\Delta\delta_T$
$R_{ij}\,/\,\Delta\delta_T$ (MPa$^{1/2}$)
$10^2\,w_{FDCA}$
w_{Org}
0.0
0.2
0.4
0.6
0.8
1.0
0
8
16
24
32
1
2
3
4
6

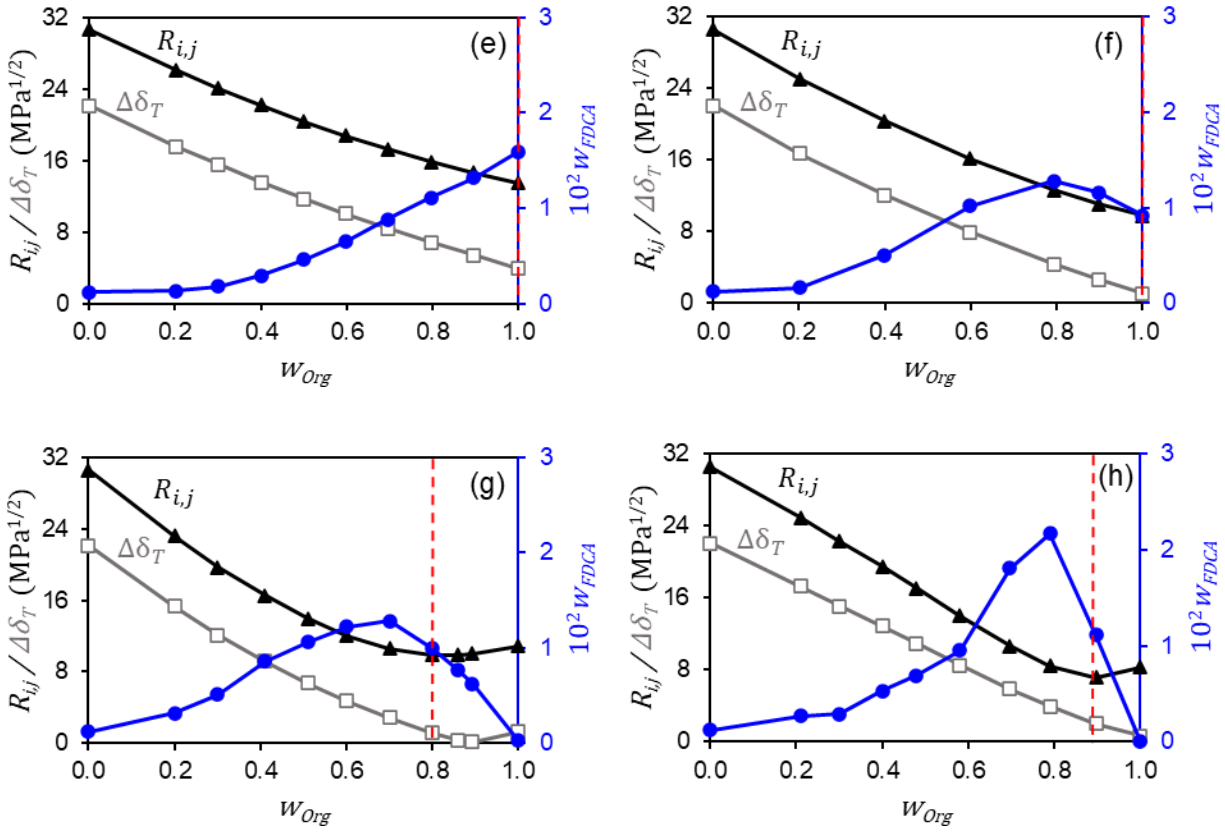

Figure 39. The $R_{i,j}$ (▲), $\Delta\delta_T$ (□), and the mass fraction of FDCA solubilized (w_{FDCA}; ●, secondary axis) versus the mass fraction of organic (w_{Org}) in binary mixtures of H_2O and (a) DMSO, (b) THF, (c) GVL, (d) GBL, (e) MeOH, (f) EtOH, (g) ACN, or (h) SULF where the dashed line indicates the minima of $R_{i,j}$ (---). Data collected at $T = 293$ K and $P = 0.1$ MPa.

Building on the findings of Zhuang et al.,[29] which identified the difference in total HSP ($\Delta\delta_T$) as a predictor for FDCA solubility in aqueous/organic mixtures - a finding corroborated by this work – it was found that in seven of the eight binary systems currently studied, $R_{i,j}$ offers a better or equivalent prediction of maximum FDCA solubility compared to $\Delta\delta_T$ (Figure 39). Further comparison of the data presented in the paper by Zhuang et al.[29] also indicates a better correlation with $R_{i,j}$ in three out of four cases (Appendix A, Figure 55). The same observation can be made of the data presented by Ban et al.,[31] wherein H_2O/MeOH and H_2O/EtOH data are

seen to correlate high solubility to low $R_{i,j}$ more strongly than to low $\Delta\delta_T$ (Appendix A, Figure 56).

Aggregating the data from Figure 39 into a single plot reveals the correlation between $R_{i,j}$ and FDCA solubility, as shown in Figure 40 using three markers: blue squares for H_2O/DMSO mixtures, gray triangles for H_2O/THF mixtures, and black circles for all other H_2O/organic mixtures. As the $R_{i,j}$ decreased from approximately 27, the FDCA solubility increased across all solvent systems. However, while FDCA solubility consistently increased with decreasing $R_{i,j}$ from approximately 20 to 13 across all solvents, the rate of increase becomes markedly varied below $R_{i,j}$ values of 12. The high solubilization in DMSO and THF may be explained by a combination of intramolecular solvent properties and intermolecular interactions with FDCA and H_2O. Both solvents are highly polar and aprotic. While this alone does not distinguish them relative to the other solvents studied, both are known to report strong dipole-dipole interactivity and to readily form strong hydrogen bonds with water and organic compounds.[160, 161] DMSO has further been identified as having an unusually high dielectric constant, which allows for easy charge separation and excellent solvation capacity,[179] and to excel at disrupting crystalline lattices.[160] These combined effects may lead to a unique ability to solubilize much more FDCA than the other the solvents studied.

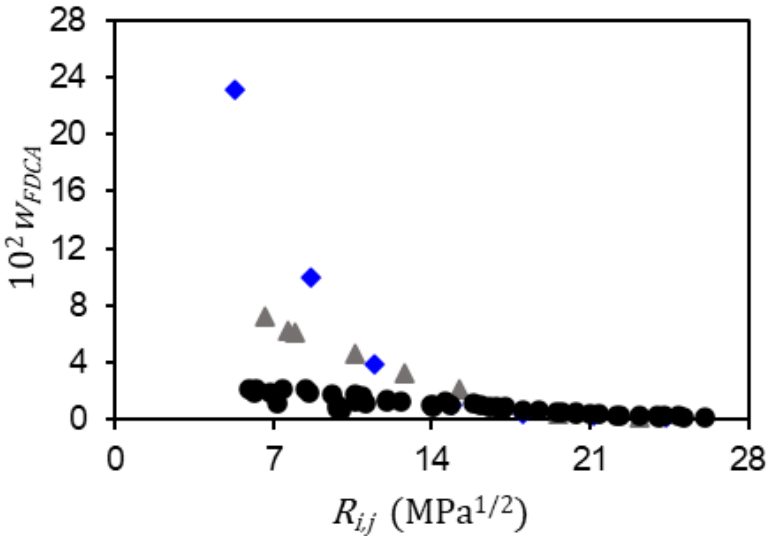

Figure 40. The $R_{i,j}$ for H_2O/DMSO (♦), H_2O/THF (▲), all other H_2O/organic (●) mixtures plotted against mass fraction of FDCA solubilized (w_{FDCA}).

While the trend in $R_{i,j}$ with binary solvents suggests a correlation, the highest FDCA solubility was not consistently observed at the lowest $R_{i,j}$ for pure solvents. In pure solvents, the FDCA solubility varied significantly, ranging from 0.02 wt% in ACN to 30.7 wt% in DMSO at 293 K. Notably, all solvents except ACN had higher solubilities than water (0.12 wt%), as listed in Table 14. Sulfolane, being solid at 293 K, could not be evaluated as a pure solvent. When considering HSP predictions by $\Delta\delta_T$ and $R_{i,j}$, the pure solvents would be ordered differently and there were several notable discrepancies against HSP solubility predictions (Table 14).

Chemical	$10^2 w_{FDCA}$	$\Delta\delta_T$ Ranking	$R_{i,j}$ Ranking
DMSO	30.7	1	1
THF	3.15	7	5
MeOH	1.59	5	7
EtOH	0.92	3	4
GBL	0.21	2	2
GVL	0.19	6	3
H_2O	0.12	8	8
ACN	0.02	4	6

Table 14. The Amount of FDCA Solubilized in Each Pure Solvent Ranked from Highest to Lowest FDCA Solubility at 293 K and the Ranking Predicted by $\Delta\delta_T$ and $R_{i,j}$ with 1 Being the Highest Expected Solubility and 8 the Lowest.[a]
[a]Standard uncertainties were $u(T)$ = 0.3 K, $u(P)$ = 0.1 kPa and relative uncertainties were $u_r(w_{FDCA})$ = 0.061 (for $10^2 w_{FDCA} < 5$), 0.128 (for $10^2 w_{FDCA} > 5$).

DMSO was predicted to have the highest FDCA solubility and, indeed, has the lowest $\Delta\delta_T$ and $R_{i,j}$. However, GBL, GVL, MeOH, and ACN would be predicted to have higher solubilities based on their HSP values relative to the other solvents evaluated. In the case of MeOH and ACN, previous literature mentions that molar volume can significantly impact solubility, stating that compounds with very small molar volumes may not conform to HSP predictions.[52] Specifically, small molecules like MeOH or ACN may exhibit solubility behaviors that diverge from those anticipated based on their HSP values. MeOH, at 0.380 nm in molecular diameter,[180] has been specifically cited as falling into this boundary effect category.[52]

Regardless of the FDCA solubility in pure components, in binary aqueous mixtures, a minimized $R_{i,j}$ typically corresponds to the maximum or near-maximum FDCA solubility for a given aqueous/organic solvent system. Notably, H_2O/DMSO and H2O/THF blends demonstrated

particularly high FDCA solubilities, with low $R_{i,j}$ values closely matching the points of highest FDCA solubility. While trends were observed between FDCA solubility and HSPs in binary mixtures, these trends did not extend to the prediction of FDCA solubility in pure solvents. This observation aligns with findings from non-aqueous binary mixture data as well (Appendix A: Figure 57, Table 29). The absence of a similar predictive trend in pure solvents and non-aqueous mixtures evaluated suggests that while HSPs can guide solubility optimization in aqueous binary mixtures, their applicability may be subject to greater variability in other solvent mixtures.

Ternary Aqueous/Organic/Organic Solvent Systems

Due to the high FDCA solubility of DMSO and H_2O/DMSO mixtures, ternary mixtures were evaluated that focused on H_2O/DMSO combined with a second organic solvent of GVL, THF, or SULF. The use of DMSO in ternary mixtures can optimize the $R_{i,j}$ of the solvent mixture due to the differences in HSPs, theoretically leading to higher solubility.

For the ternary H_2O/DMSO/organic mixtures, FDCA solubilities ranged from less than 1 wt% at high $R_{i,j}$ values to over 10 wt% for ternary mixtures that have an $R_{i,j}$ less than 5, as seen in Figure 5. The ternary blends at 293 K exhibited higher FDCA solubility compared to the binary blends studied by Zhuang et al. at higher temperatures (333 K).[29] For example, ternary blends containing 80 wt% total organic (DMSO and secondary organic) had FDCA solubilities exceeding 20 wt%. In the binary mixtures studied by Zhuang et al., those containing 80 wt% organic only reported a maximum of 7.9 wt% FDCA solubilized at 303 K (20/80 w/w H_2O/THF) and 10.5 wt% at 333 K (20/80 w/w H_2O/THF).[29] The other mixtures studied by Zhuang et al., H_2O/DX, H_2O/DME, and H_2O/DGDE, had maximum solubilities of 5.1, 6.7, and 6.9 wt%,

respectively, at 303 K. The FDCA solubilities reported in this study are over a twofold increase compared to these previously reported literature values.

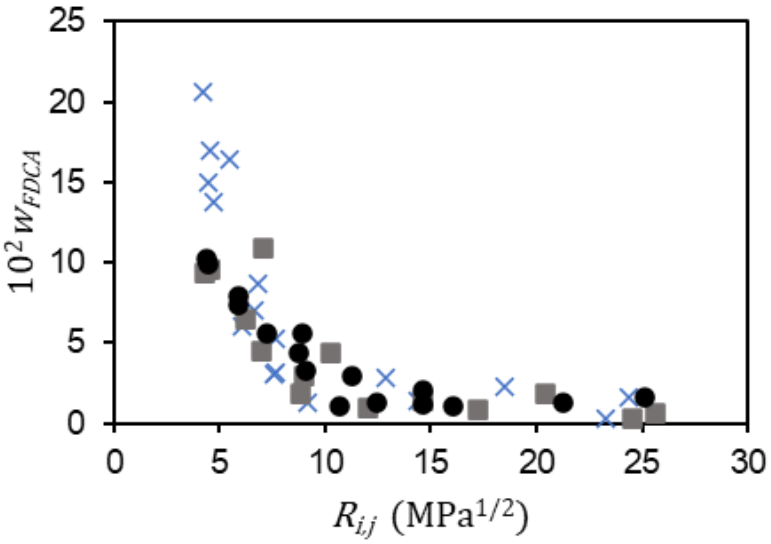

Figure 41. Mass fraction of FDCA solubilized (w_{FDCA}) in ternary mixtures of H_2O/DMSO/organic, where the second organic was either GVL (●), THF (X), or SULF (■), plotted against $R_{i,j}$.

As was the case with the binary solvent mixtures, $R_{i,j}$ and FDCA solubility correlated (Figure 41) and indicated that minimizing $R_{i,j}$ for a solvent system maximizes solubility. Across the three solvent systems, H_2O/DMSO with GVL, THF, or SULF, the trend of maximum FDCA solubility at minimum $R_{i,j}$ held true for the solvent blends studied (Appendix A, Table 30). There was a slight deviation in the case of H_2O/DMSO/SULF at 20/40/40 w/w/w as the FDCA solubility was slightly higher than at the minimum $R_{i,j}$ value, but still within the margin of error. The consistency of $R_{i,j}$ being able to predict the maximum FDCA solubility for both binary and ternary aqueous mixtures could enable a more precise approach to solvent selection.

Solvent Selection Optimization Using MATLAB

Building on the trends seen in the experimental data, a MATLAB model was developed that minimized $R_{i,j}$ based on the volume fractions and HSPs of the solvents with FDCA as the solute. Initially, the code was used to find the minimum $R_{i,j}$ for a mixture of H_2O/DMSO/THF and determined mass fractions of 14/59/27 would maximize FDCA solubility. When the optimized ternary blend was evaluated experimentally, the FDCA solubility was found to be 20.7 wt%, which was the highest of any ternary blend studied (Figure 41). The two other ternary blends, H_2O/DMSO/GVL and H_2O/DMSO/SULF, as well as all binary systems studied, were inputted into the code to find the minimum $R_{i,j}$ blends and assess their solubility relative to experimentally found maxima (Table 15).

Chemical	Maximum Solubility				Difference Between Predicted[b] and Experimental	
	Experimental		MATLAB Predicted[b]			
	10^2 $(w_w/w_1/w_2)$	$10^2 w_{FDCA}$	10^2 $(w_w/w_1/w_2)$	$10^2 w_{FDCA}$	$10^2 w_1$	$10^2 w_{FDCA}$
ACN	30/70/0	1.3	17/83/0	~1.0	- 13	-0.3
GBL	20/80/0	2.1	12/88/0	~1.9	- 8	-0.2
EtOH	21/79/0	1.4	0/100/0	0.9	- 21	-0.5
MeOH	0/100/0	1.6	0/100/0	1.6	0	0
DMSO	0/100/0	30.7	15/85/0	~23.1	+ 15	-7.6
GVL	16/84/0	2.2	16/84/0	2.2	0	0
THF	20/80/0	7.2	23/77/0	~7.2	+ 3	0
SULF	21/79/0	2.2	11/89/0	1.1	- 10	-1.1
DMSO/GVL	20/60/20	10.3	12/66/22	-	- 8/+6/+2	
DMSO/THF	14/59/27	20.7	14/59/27	20.7	0	0
DMSO/SULF	20/40/40	10.9	11/89/0	1.1	-9/49/-40	-9.8

Table 15. Comparison of Experimental Maximum Solubility to MATLAB Predicted Maximum Solubility in Binary and Ternary Mixtures at $T = 293$ K and $P = 0.1$ MPa.[a]
[a]Standard uncertainties were $u(w_1, w_2, w_w) = 0.002$, $u(T) = 0.3$ K, $u(P) = 0.1$ kPa and relative uncertainties were $u_r(w_{FDCA}) = 0.061$ (for $10^2 w_{FDCA} < 5$), 0.128 (for $10^2 w_{FDCA} > 5$).
[b]The $10^2 w_{FDCA}$ "predicted" values represent the experimentally determined solubility at the predicted solvent composition.

The MATLAB optimization code accurately predicted mixture compositions, often achieving results within 10 wt% of the composition determined experimentally, and almost always within 15 wt%. There were two exceptions, which were H_2O/EtOH and the ternary blend of H_2O/DMSO/SULF. The challenge with the EtOH mixture may be due to its molar volume being near the boundary region for HSP predictions, as previously discussed, but the FDCA solubility was low as well, which has been previously reported as well.[31] For the ternary mixture

involving SULF, the exclusion of SULF in the predicted mixture was due to its HSP values increasing $R_{i,j}$, which was an issue for the optimization code. From a research perspective, the optimization process narrows the range of experimental work needed, thereby allowing for more efficient experimentation. By limiting the experimental range to more targeted solvent blends, computational optimization can save time and resources in identifying optimal solvent mixtures to maximize FDCA solubility.

3.8 Conclusions

This study marks a significant advancement in the understanding of FDCA solubility by systematically analyzing its behavior in pure, binary, and ternary solvent blends of H_2O, ACN, DMSO, THF, SULF, GVL, GBL, MeOH, and EtOH at 293 K. The FDCA solubility was found to increase with decreasing values of both $\Delta\delta_T$ and $R_{i,j}$ within a set solvent system. Of these two HSP-based parameters, the correlation between FDCA solubility and $R_{i,j}$ was stronger. Notably, mixtures containing DMSO were found to have the lowest $R_{i,j}$ values and the highest FDCA solubility values (30.7 wt% maximum), followed by mixtures containing THF (7.2 wt% maximum). All other binary solvents investigated had less than 2.5 wt% of FDCA solubilized, but maximum solubility still correlated with the minimum $R_{i,j}$. The same trend was observed for ternary solvent blends, which saw solubilities exceeding 20 wt% at low values of $R_{i,j}$. In contrast, no correlation was found between using HSP parameters to predict the baseline solubility of pure solvent systems.

The MATLAB code developed in this study effectively optimized solvent blends by minimizing $R_{i,j}$, predicting a narrow range of mass fractions that contained the maximum FDCA

solubility for various solvent combinations. In the future, the code could readily be expanded to different solutes or solvents for additional applications. Identifying solvents that have increased solubility may allow for more efficient upgrading of chemicals such as FDCA and PEF, and the MATLAB code could be used to optimize a diverse range of solvent systems.

CHAPTER FOUR

USING ARTIFICIAL NEURAL NETWORKS TO PREDICT 2,5-FURANDICARBOXYLIC ACID SOLUBILITY FOR SOLVENT SELECTION

4.1 Contributions of Authors and Co-Authors

Author: Jacob M. Molinaro

Contributions: Conceptualization, Data curation, Analysis, Investigation, Methodology, Project Administration, Software, Undergraduate supervision, Validation, Visualization, Writing – original manuscript preparation, revision, and formatting

Co-Author: Van W. Ledger

Contributions: Data curation, Methodology, Software, Visualization, Writing – review and editing

Co-Author: Karlene A. Hoo

Contributions: Conceptualization, Data curation, Analysis, Investigation, Methodology, Software, Validation, Visualization, Writing – original manuscript preparation

Co-Author: Stephanie G. Wettstein

Contributions: Conceptualization, Data curation, Analysis, Investigation, Methodology, Project Administration, Software, Supervision, Validation, Visualization, Writing – original manuscript preparation, revision, and formatting

Manuscript in Chapter 4.

4.2 Manuscript Information

Jacob M. Molinaro, Van W. Ledger, Karlene A. Hoo, and Stephanie G. Wettstein

Chemical Engineering Journal Advances

Status of Manuscript:

__X__ Prepared for submission to a peer-reviewed journal

_____ Officially submitted to a peer-reviewed journal

_____ Accepted by a peer-reviewed journal

_____ Published in a peer-reviewed journal

Elsevier B.V.

8 April 2025

4.3 Abstract

This study developed two separate feed-forward artificial neural network (ANN) models to correlate Hansen Solubility Parameters (HSPs) to 2,5-furandicarboxylic acid (FDCA) solubility, in alcohol-type solvents (with four hidden nodes) and in non-alcohol solvents (with seven hidden nodes). HSPs have been previously shown to correlate to FDCA solubility, and the solubility of FDCA is of critical importance to improved bioplastics production, but the exact influence of each solubility parameter has not been previously understood. Further, the most important thermodynamic factors influencing FDCA solvation have not been identified. Through training and assessment of ANNs, as well as thermodynamic correlations from the Conductor-like Screening Model for Realistic Solvents (COSMO-RS), the influence of each of the individual HSPs and of excess enthalpy on FDCA solvation prediction are identified, providing a rational method for selecting solvents for FDCA solubilization.

4.4 Introduction

The ongoing transition towards a more efficient, bio-based economy has identified 2,5-furandicarboxylic acid (FDCA) as an important platform chemical across several industries.[1, 2] FDCA is made by upgrading the C_6 sugars present in lignocellulosic biomass and serves as the monomeric precursor to useful biomaterials like polyethylene furanoate (PEF), which could be a sustainable replacement for petroleum-derived polyethylene terephthalate (PET) in packaging, textiles, and other consumer products.[67] While significant effort has been made to develop viable methods for FDCA production in the past two decades,[24-26] the economic feasibility of the process still prevents widespread adoption of FDCA and PEF.

Technoeconomic analyses have identified low product concentration as a critical barrier to cost-effective FDCA synthesis,[7, 74-76, 153] with the poor solubility of FDCA in common solvents being a recurring issue.[27-29, 32] For example, Iglesias et al.,[153] estimated that for production to be industrially relevant, operating conditions producing 10 wt% FDCA in solution must be achieved. The most promising process design to date, the AMOCO process,[72, 73] currently operates in acetic acid, which has an FDCA solubility value of 0.63 wt% at 303 K.[31] Some researchers have noted the impact of solvent selection on effective reaction design for FDCA synthesis,[36, 154, 155, 157] but less research has focused on understanding the molecular factors behind FDCA solvation behavior.

Three recent studies have investigated FDCA solubility at a fundamental level, Zhang et al.,[28] Zhuang et al.,[29] and Molinaro et al.[32] Zhang et al.[28] examined eight pure solvents (water, methanol, acetonitrile, acetic acid, ethyl acetate, methyl isobutyl ketone, 1-butanol, iso-butanol) and two aqueous/organic solvent blends (water/acetonitrile, water/acetic acid). They found that solubility increased with temperature across all systems and that methanol had the highest FDCA solubility of the pure solvents, while acetonitrile had the lowest. The pure solvents correlated most closely to the Non-Random Two Liquid (NRTL), Wilson, and Universal Quasi-chemical (UNIQUAC) models. In the binary solvent mixtures, solubility improved with increasing mole fractions of water up to 0.6 in water/acetonitrile and 0.7 in water/acetic acid. The authors suggested that these results correlated to non-ideal mixing behavior in both binary solvent blends that were better captured by the NRTL and UNIQUAC models than the Wilson model.[28]

Zhuang et al.[29] conducted a thermodynamic analysis of FDCA solubility in aqueous/organic mixtures of water and 1,4-dioxane, tetrahydrofuran (THF), 1,2-

dimethoxyethane, and diethylene glycol dimethyl ether. They studied the Wilson and NRTL models, as well as Hansen Solubility Parameter (HSP) and Kamlet-Abboud-Taft methods. Key findings included the identification of the Wilson model as most applicable to FDCA solubility modeling in the systems studied, as well as a clear enthalpic driving force behind FDCA solvation.[29] This contrasts with Zhang's work,[28] where the Wilson model exhibited the lowest performance in binary solvent blends, highlighting the system-specific applicability of different models. However, the enthalpy-driven solubility behavior agrees with the early findings of Motagamwala et al.,[27] who identified an increased enthalpy of mixing as leading to increased FDCA solubility.

Finally, research that investigated binary and ternary blends of water and eight organic solvents (acetonitrile, methanol (MeOH), ethanol (EtOH), THF, sulfolane, dimethyl sulfoxide (DMSO), γ-valerolactone (GVL), and γ-butyrolactone (GBL)), found that the holistic Hansen Radius of Interaction ($R_{i,j}$) parameter[52] could, within a given system, accurately predict the ratio of solvents that would result in the highest FDCA solubility without a need for complex modeling software, but could not predict the FDCA solubility outside a given solvent system.[32]

This prior experimental and modeling work has allowed researchers to better understand and, in a limited sense, predict FDCA solubility within a given blend of solvents. The computational studies conducted with the NRTL,[28, 29] UNIQUAC,[28] and Wilson models,[29] as well as the work done with HSPs,[29, 32] showed that fundamental mixing thermodynamics describe FDCA solubility, particularly properties like solution enthalpies, though the exact reason for this behavior remains unclear. Activity coefficient-style models like NRTL and UNIQUAC are built upon such thermodynamic concepts but can be time consuming and mathematically complex to

apply whereas HSPs can be calculated using HSPiP software or commonly found in the literature.[52, 56]

The HSPs divide the enthalpy of mixing within a system into three parameters that represent the London dispersion forces (δ_D), polarity (δ_P), and capacity to form hydrogen bonds (δ_H) of each compound.[52] Thus, they retain a clear connection to fundamental thermodynamic principles while also providing insight into the important physiochemical properties of the solvents. Additionally, holistic variables that are combinations of all three HSPs can be calculate and prior work showed that one of these, the radius of interaction ($R_{i,j}$), correlated with maximum FDCA solubility within a selected organic solvent/water mixture.[32] However prediction of FDCA solubility was not achievable outside a given solvent system due to complex solvent-solute interactions and therefore, a combination of thermodynamic modeling with consideration of chemical properties may be required.

These types of complex solvent-solute systems have previously been described using Artificial Neural Network (ANN) models.[59, 60] In prior work, ANN models were used to correlate input data, such as physiochemical or thermodynamic properties, to output data like experimental solubility values. In this manner, the solubility of pharmaceutical compounds[61, 62] and proteins[63] were effectively estimated in a range of solvents. However, the application of ANNs as a modeling tool in the field of biomass engineering is less widespread. In 2021, Job et al.[64] used a two-layer feed-forward ANN to estimate the yield of furfural from biomass-derived sugars based on solvent polarity (δ_P) and severity, but to the best of our knowledge, the solubility of FDCA has never been studied with ANN models.

As part of this work, ANN models were developed using HSPs as inputs. Additionally, a physiochemically-informed thermodynamic method, the Conductor-like Screening Model for Realistic Solvents (COSMO-RS), was used for the numerical calculation of solvent and system thermodynamic properties including system enthalpies.[181] The COSMO-RS model accounts for solute-solvent interactions by calculating molecular surface charge densities based on similar molecular properties as those underlying the HSP model. COSMO-RS has previously been used to assess solubility of organic or pharmaceutical compounds,[182-186] and recently, to understand the solubility behavior of furan compounds in organic solvents.[187] Working with the furan compound 2,2'-bifuran-5,5'-dicarboxylic acid, Castilla-Acevedo et al. found that the COSMO-RS solvation model largely overestimated solubility in different solvents but did qualitatively rank the solvents.[187]

In the present work, FDCA solubility was predicted from HSPs using two ANN models, COSMO-RS thermodynamic data, and within a select system with $R_{i,j}$. Two ANN models were built, one based on alcohol/water mixtures and the other, non-alcohol organic/water mixtures. FDCA solubility measurements in water mixtures with N,N-dimethylacetamide (DMAc), acetone, or 2-propanol (2-PrOH) were used in the training and testing of the ANN models that were selected based on the accuracy of FDCA solubility prediction and the corrected Akaike Information Criterion (AIC). Thermodynamic insights using COSMO-RS are also discussed. The combined approach of COSMO-RS, ANN modeling, and the $R_{i,j}$-based solvent ratio estimation from our prior work allows for a rational solvent selection to effectively solubilize FDCA.

4.5 Methods

Chemicals

Chemicals were used as received without further purification including 2-propanol (2-PrOH, Fisher Scientific, 99.9%), acetone (Fisher Scientific, 99.9%), and N,N-dimethylacetamide (DMAc, Fisher Scientific, 99.5%). Water for experiments was 18.2Ω from a MilliporeSigma Milli-Q Advantage A10 system.

Solubility Assessment

Solubility was evaluated following a previously described method.[32] Solvents were measured in 10.0 g samples into conical vials with weight determined using an OHAUS Discovery analytic balance. Incrementally, FDCA was added to the vials at room temperature (293 K, accuracy ±0.3 K) and the mass was recorded after each addition. The vials were allowed to stir at 1000 rpm until no FDCA was visible, or in the case that the FDCA did not solubilize, overnight (≥20 h) to ensure saturation. The saturated solutions were then removed from stirring and allowed to settle (≥12 h) before sampling. In the case of any uncertainty concerning solution saturation or settling, additional stirring or settling time was added up to 48 h.

The saturated sample was then diluted with a known quantity of 18.2Ω water such that the FDCA concentration was less than that of saturation in pure water (0.12 wt% or 0.0075 M) and filtered with a 0.2 μm filter syringe. The samples were then injected into a Thermo Scientific Vanquish High Performance Liquid Chromatography (HPLC) System with both UV and RI detectors. The system utilized a 0.01 M trifluoroacetic acid buffer solution (pH 2) at a flow rate of 0.600 mL/min with product separation occurring on an Aminex HPX-87H (300 mm x 7.8 mm) column. The mass fraction of FDCA present in the sample was determined against a

prepared set of FDCA standards, (Appendix C, Figure 58) using the resulting HPLC UV peak areas collected via peak integration in the Chromeleon 7 software. Data were found to have a relative uncertainty of 0.061 on reported experimental solubility values below 5 wt%, and 0.128 on solubility values above 5 wt%.

Data were also used from previously published solubility studies including aqueous/organic blends of water and THF, acetonitrile, MeOH, EtOH, sulfolane, GVL, and GBL, wherein solubility values were determined by the method described above.[32] Solubilities are expressed as the mass fraction (w_{FDCA}) of FDCA solubilized in the system.

Artificial Neural Network

To capture the nonlinear, multivariable relationships between solvent properties and FDCA solubility, two-layer, feed-forward ANN models were developed using MATLAB 2023a (Mathworks®) and the Neural Net Fitting Tool from the Deep Learning Toolbox. Based on previous work,[29, 32] the inputs considered included the base three HSPs (δ_D, δ_P, and δ_H) and the comprehensive HSPs (δ_T, $\Delta\delta_T$, and $R_{i,j}$), while the output variable was FDCA solubility. The ANN parameters also included the transfer functions between the layers, which were selected as a hyperbolic tangent function between the input and hidden layers, and a linear summation function between the hidden and output layers.

The dataset was split into two groups, alcohols and non-alcohol solvents, based on prior work.[32] A 102 data point non-alcohol solvents model was developed using a dataset containing HSPs (inputs) and FDCA solubility (output) from pure and binary blends containing water, THF, sulfolane, GVL, GBL, and acetonitrile. The alcohol dataset contained alcohol-type compounds or mixtures where the primary organic component was an alcohol (MeOH, EtOH, and binary

mixtures of alcohol and GVL or THF; n = 44). Acetone, 2-PrOH, and DMAc were not in the initial dataset but were used as independent test sets to determine the predictability of the ANN. These test sets remained within the HSP ranges of the trained model (Table 16; Appendix C, Table 31).

	Alcohol Model		Non-alcohol Model	
Input	Dataset Low Value	Dataset High Value	Dataset Low Value	Dataset High Value
δ_D	14.70	16.55	13.87	17.79
δ_P	5.70	16.00	4.90	16.70
δ_H	9.90	42.00	5.80	42.00
δ_T	21.96	47.57	18.35	47.57
$R_{i,j}$	6.14	30.61	6.09	30.61

Table 16. Ranges of values for ANN model training inputs.

The non-alcohol solvent dataset consisted of 102 data points while the alcohol dataset contained 44 data points with a range of HSP values (Table 16). Since the accuracy and repeatability of ANN models tend to improve with increased number of inputs and outputs,[188] the datasets were doubled by including randomized variability from within the normal distributions of experimental error as has been done in prior research.[64, 149] The Levenberg-Marquardt algorithm was selected for training the ANN with splits of 70/15/15 that were randomly determined for training, validation, and testing data.

Selection of the final ANN model was based on a normalized distribution of error amongst datasets (Appendix C, Figure 59) and minimization of the corrected Akaike Information Criterion (AICc). A well-normalized error profile across all three data subsets (training, validation, and testing) is indicative of adequate capturing of patterns within the data and avoidance of bias or skewing within the dataset. To help prevent overfitting and identify the optimal number of hidden nodes, the AICc[65] was used as the basis for final model selection. Performance measures to determine the fit of the model to the validation data were the sum of square error (SSE), root mean squared error (RMSE), and the coefficient of determination (R^2), all of which are commonly used for evaluating predictive accuracy.[59, 64] Equations and details are listed in the supplemental materials (Appendix C, Eqns. 25-29). For the correlation analysis, each configuration was trained five times, and model performance was evaluated based on the average R^2 and RMSE values across the combined datasets.

COSMO-RS

Values of excess enthalpy (H^E) were determined at 298.15 K using COSMO-RS software through the Ternary Mixture VLE/LLE feature. The relationship between HSPs and H^E are described in the Supplemental Materials (Appendix C, Derivation 1). Data were calculated across a range of solvent compositions. For each system, the mass fraction of the organic solvent (w_i) varied from 0 to 1 in 0.01 increments. Calculations were performed for mixtures containing a fixed FDCA mass fraction, w_{FDCA} = 0.01, in binary aqueous/organic solvent blends (w_{Org} = 0 – 0.99; w_{H2O} = 0 – 0.99).

4.6 Results and Discussion

Solubility Data

Although some of the solubility data used in the ANN model development can be found in the literature,[32] several additional solvents were evaluated to increase the number of data points. The aqueous/organic solvent systems were studied in weight percent of organic (w_{Org}) ranging from 20 to 100 wt% for acetone, 2-PrOH, and DMAc. Non-alcohol systems followed the previously reported trend[32] where the maximum solubility correlated with the minimum $R_{i,j}$, with 6.89 wt% FDCA solubilized in 20/80 water/DMAc (Figure 42a) and 3.28 wt% in 20/80 water/acetone (Figure 42b). In the case of 2-PrOH, the minimum $R_{i,j}$ occurred at 100 wt% organic solvent, which was not where the maximum solubility was seen (80 wt% alcohol, Figure 42c). 2-PrOH had a maximum FDCA solubility of just over 1.14 wt% (Figure 42c) compared to 0.53 wt% with pure solvent, showing a distinct difference compared to the $R_{i,j}$ behavior of the non-alcohols.

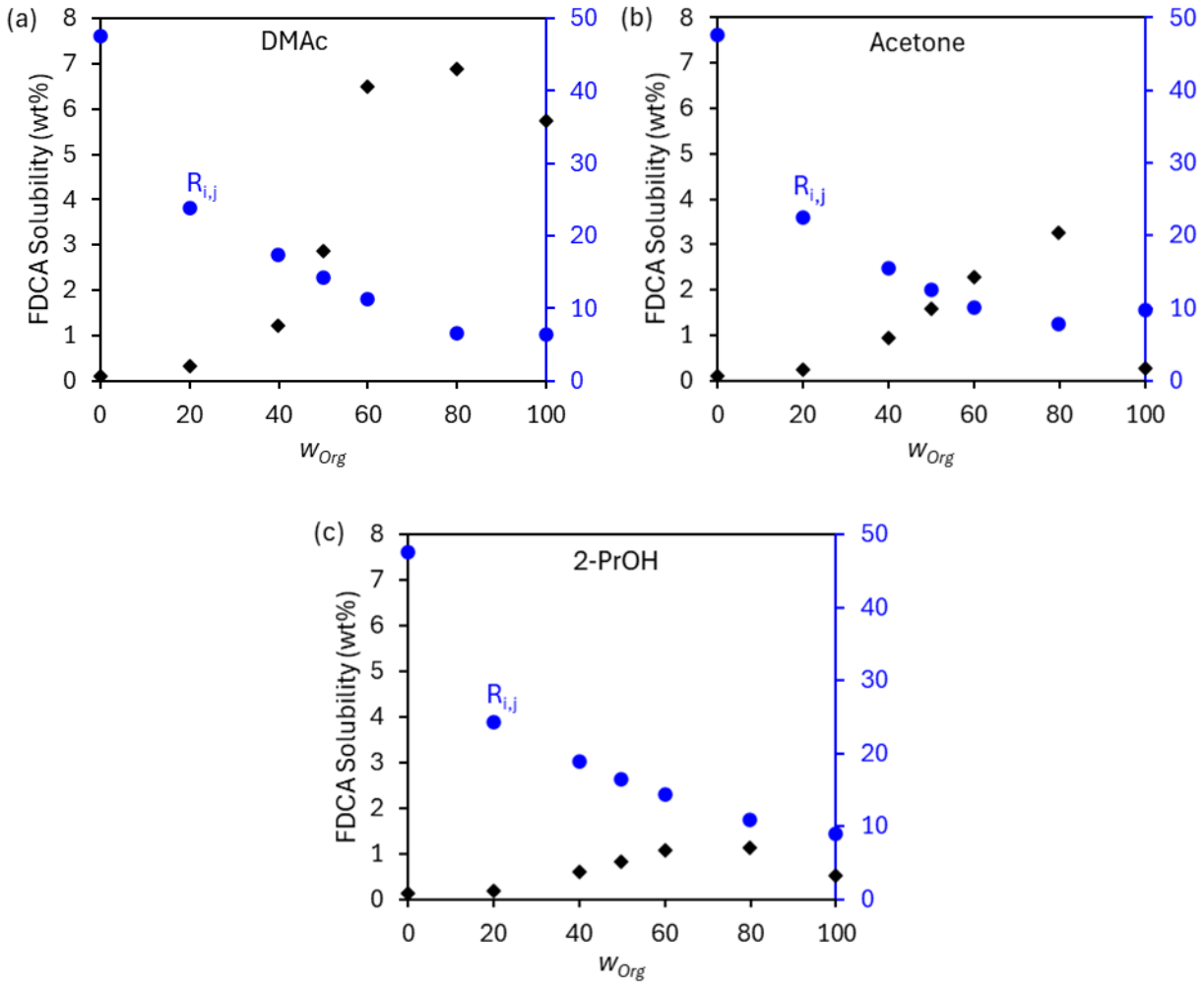

Figure 42. Solubility data for mixtures of water and (a) DMAc, (b) acetone, and (c) 2-PrOH presented on the left (black) axis (♦). The $R_{i,j}$ of the solvent blend at that composition is shown on the right (blue) axis (●).

A possible reason the alcohol data does not correlate with the minimum $R_{i,j}$ may be due to differing solvation behavior in alcohols compared to other mixed solvent systems.[32, 189] For example, MeOH has been shown to form strong hydrogen bonds in mixed systems containing water, forming hydrogen-bond networks that lead to an increase in total system volume.[177] MeOH has also been observed to act contrary to the predictions of the HSP model, which is

hypothesized to be due to its small molecular diameter[180] and low molar volume.[52] Other researchers have more broadly found that alcohols, particularly those attached to just a hydrocarbon chain of one or more carbons, exhibit extremely high capacity for forming hydrogen bonds.[58] In one model using group contribution theory to develop solubility parameters, the contribution of an alcohol functional group (-OH) was found to be triple the magnitude of the next closest functional group when calculating the hydrogen bond contribution parameter.[58] Given these discrepancies within the alcohol data, it was decided that the data would be split into two categories for ANN development: alcohols and non-alcohols.

ANN Models Using Hansen Solubility Parameters

The ANN models were built using the three primary HSPs (δ_D, δ_P, δ_H) as inputs to allow for a focused analysis of the impact of intermolecular forces on solubility without duplication of parameters in the holistic variables. The ANN models that most accurately predicted FDCA solubility from the HSPs ($R^2 > 0.99$; Appendix C, Table 32) required seven hidden nodes for the non-alcohol model and four hidden nodes for the alcohol model. The number of hidden nodes reflects the nonlinearity of the input to output relationship in these systems.

For the non-alcohol data, as seen in Figure 43a (unfilled diamonds), all points in the training dataset fell within the 95% confidence interval on a predicted versus experimental chart excluding one point that was marginally outside the interval. This datapoint was randomly generated from the variability within the dataset for 90/10 THF/water and since the model accurately predicted the experimental 90/10 THF/water point, the reasoning is likely a larger shift in randomly varied inputs relative to the variation applied to the output.

For the independent test sets that consisted of water mixtures that included acetone or DMAc, 64% of the independent test data (7 out of 11) fell within or on the line of the 95% confidence interval (Figure 43a). The four points that fell significantly outside the confidence interval were the high mass fraction organic points (50 wt% or more DMAc and 80 wt% acetone). The poor predictability may be due to the structure of the test solvents. Previous researchers have noted that for solvents like DMAc, the interactions and structuring of the solvent with respect to water varies significantly depending on the Organic:Water ratio.[190]

The organics in the training set consist of five-membered ring compounds (GVL, GBL, THF, and sulfolane) and a nitrile (acetonitrile). However, acetone is a ketone, DMAc is an amide, and both have a trigonal planar geometry. DMAc has been previously shown to interact strongly with water up to approximately 50 wt% in DMAc/water blends, at which point the influence of water decreases exponentially.[191] This change in behavior above 50 wt% DMAc may explain both the rapidly increasing solubility, and the challenges the model had with accurately predicting solubility. A similarly structured molecule, dimethyl sulfoxide (DMSO), also exhibits this effect where the organic begins to dominate intermolecular behavior, again, at 50 wt% organic.[32, 178] In an additional test presented in the Supplemental Materials, the non-alcohol model accurately predicted FDCA solubilities up to 50 wt% DMSO before experimental and predicted values sharply diverged (Appendix C, Figure 60). Similar behavior has been seen in acetone mixtures starting at approximately 80 wt% acetone.[192] These effects may explain why the model predicted well at low proportions of organic and poorly at high proportions of organic, and highlights the importance of a solvent's molecular structure to FDCA solubility.

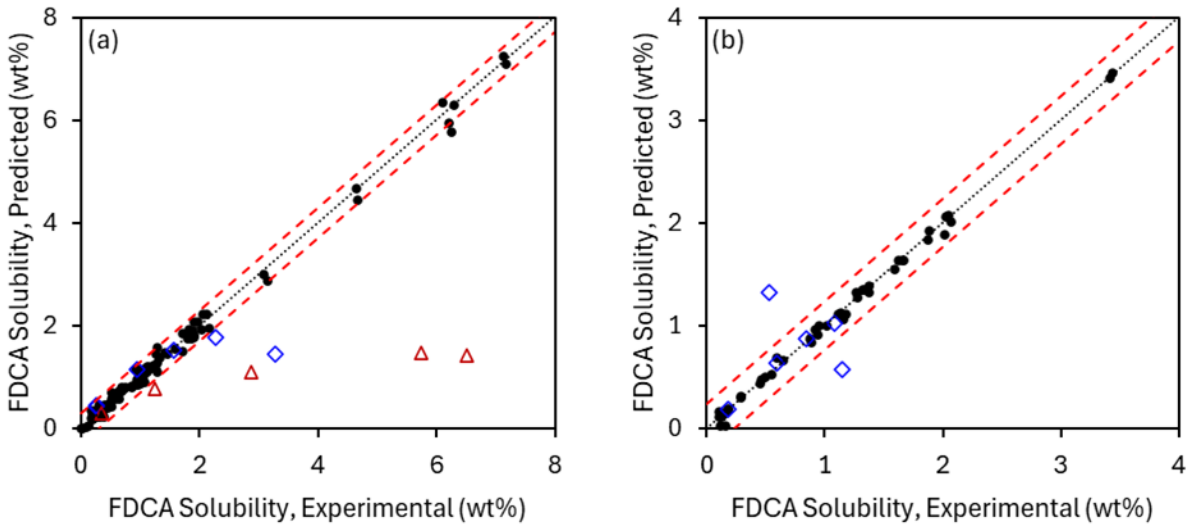

Figure 43. Comparison of the experimental and predicted FDCA solubilities for the training set (●) and independent test sets of acetone (◊), 2-PrOH (◊), and DMAc (Δ) for the non-alcohol (a) and alcohol (b) ANN models. Also shown are the 95% confidence intervals (---) on either side of the parity line (⋯).

For the alcohol ANN model, all data points from the training set were within the 95% confidence interval (Figure 43b). Additionally, only two independent test point of 2-PrOH fell outside the intervals. These datapoints represented 80/20 w/w 2-PrOH/water and pure 2-PrOH. As is commonly known, pure alcohols behave differently than mixtures of alcohols and water,[189] which may also be why pure 2-PrOH fell outside of the confidence interval.

Overall, the results demonstrate that ANN models are highly effective at capturing the nonlinear relationships between solubility and solvent properties as represented by HSPs in both alcohol and non-alcohol systems. However, although variable weights can be extracted from the ANN, relationships between the variables are difficult to determine. To determine the impact of the different HSPs and combinations of HSPs have on FDCA solubility prediction, a correlation

analysis was conducted by training ANN models using all combinations of the three selected HSPs.

For the alcohol dataset, δ_H had the greatest predictive ability of the individual HSPs, and when paired with δ_P, had the highest R value of the paired variables (Figure 44). For the non-alcohol dataset, δ_D was the best predictor as an individual HSP and when paired with δ_P, produced the highest predictive power of the two-input systems. These results indicate that in the non-alcohol model, the aprotic solvents are most strongly influenced by dispersion forces, while hydrogen bond formation is more critical in the protic alcohol model solvents. Ultimately, the best predictability and most consistent models were found when all three parameters were used as inputs, but the difference in how parameters impacted each model ($\delta_H > \delta_P >> \delta_D$ for alcohols; $\delta_D > \delta_P > \delta_H$ for non-alcohols) highlight the distinct intermolecular drivers of FDCA solubility in different types of solvents and reinforce the importance of input variable selection for ANNs.

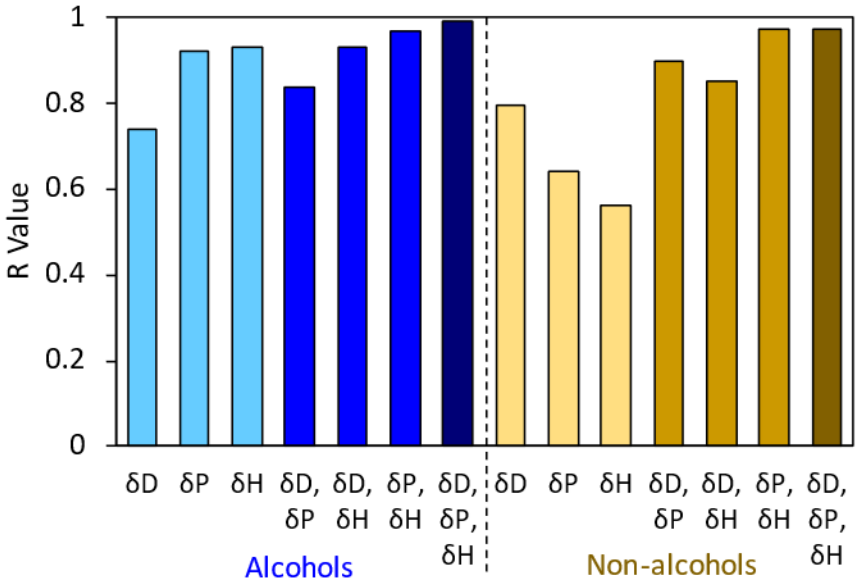

Figure 44. Median R values from two-layer feed forward ANNs trained with different combinations of HSPs as input variables for alcohol (blue) and non-alcohol (gold) models. Each value represents the median R from five training runs using the final model design and the complete dataset with the shading within a color representing one, two, and three inputs (from light to dark).

Graphs of individual HSPs against solubility values for the training data provide insight to the directionality of these effects (Figure 45). Specifically, the alcohol data show an increase in solubility with decreasing values of δ_P and δ_H, while the relationship between solubility and δ_D is less clear (Figure 45d-f). In the non-alcohol system, decreasing values of δ_P and δ_H also corresponded to increased FDCA solubility, while increased values of δ_D correlated to increasing FDCA solubility (Figure 45a-c).

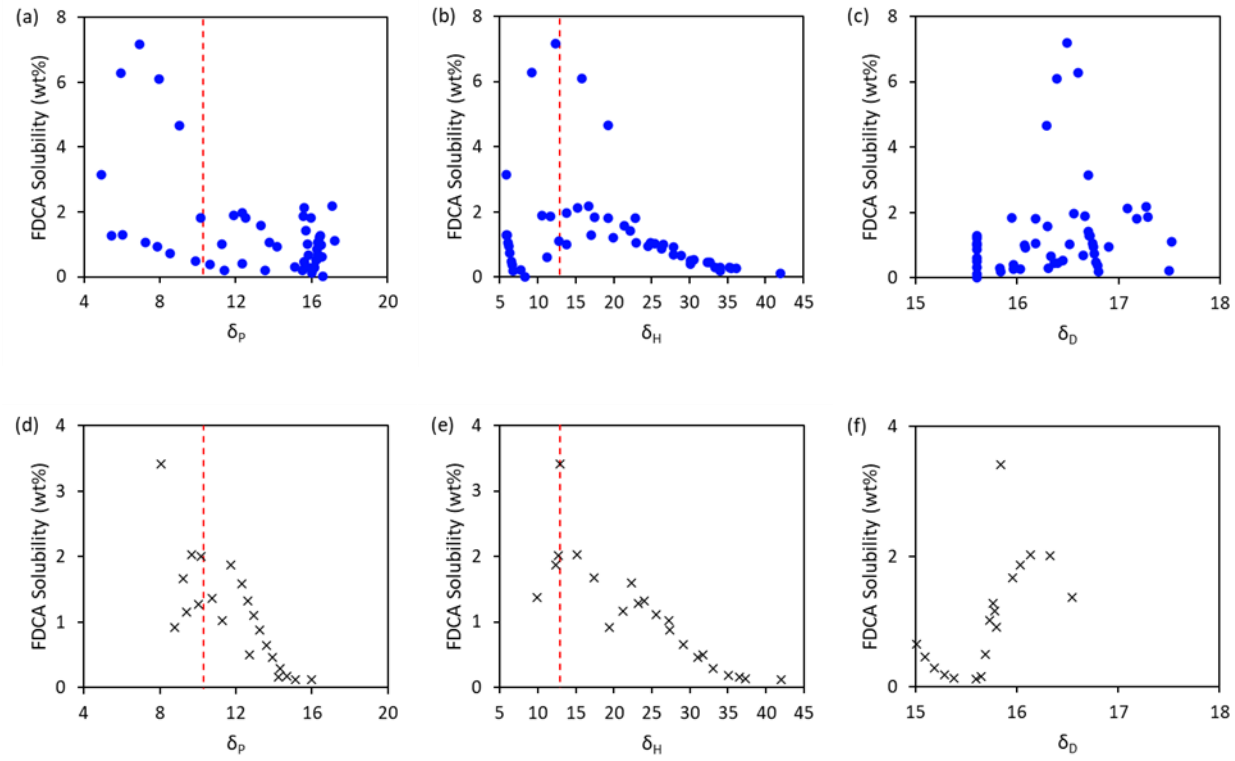

Figure 45. Plots of individual HSPs versus FDCA solubility for non-alcohol (●) and alcohol (×) datasets. A line denoting the HSP value for FDCA is shown in red (---); the value for δ_D occurs at at 19.4.

The fact that in both systems, δ_P and δ_H trended together suggests a physical connection between the two variables. These trends are consistent with the nature of mixed-solvent systems, where the addition of water (high δ_H and δ_P, low δ_D; Appendix C, Table 31) shifts the overall solubility parameters accordingly. The correlation between δ_P and δ_H reflects the physical and chemical behavior of the solvent systems. Hydrogen bonds arise from interactions between molecular dipoles, which occur because of increased molecular polarity. More nonpolar molecules or molecular regions, like the alkyl chains present in higher-carbon alcohols, have a relatively even electron density distribution, whereas polar molecules concentrate electron

density at their more negative dipole(s). This suggests that solvents with stronger hydrogen bonding capacity also tend to be more polar but exhibit weaker dispersion interactions.

In looking at the individual HSPs, increasing δ_H was associated with reduced FDCA solubility for the alcohols (Figure 45f). This trend likely reflects the formation of hydrogen bond associations and networks amongst the binary solvent components. Additionally, higher values of δ_H typically correspond to higher proportions of water in a mixed solvent system. Water has been repeatedly shown to have poor FDCA solubility, and to reduce solubility in organic systems where mass fractions of water exceed ~0.2.[27-29, 31, 32] A similar trend is seen in the non-alcohol dataset (Figure 45c), where increasing δ_H is also associated with decreasing solubility. While the non-alcohol solvents are themselves mostly aprotic, the inclusion of water as a cosolvent likely drives this trend. In contrast, δ_D is positively correlated with solubility in the non-alcohol model, suggesting that stronger London dispersion, or induced dipole – induced dipole forces, may enhance FDCA-solvent compatibility. Given that FDCA is strongly influenced by dispersion forces (δ_D = 19.4),[32, 56] this observed trend makes sense. This may be explained by favorable dispersion-based interactions between the non-polar, p-electron rich regions of the FDCA molecule and chemically similar environments found in high-δ_D solvents. For example, DMSO has the highest δ_D value of any solvent discussed (δ_D = 18.4), and also reported the highest FDCA solubility (30.7 wt%).[32] This strong solvation ability may be in part due to its compact, highly polarizable structure that allows for strong dispersion interactions with FDCA's central aromatic ring.

The impact of dispersion forces was less clear in the alcohol system, seeming to trend with water concentration more than physical phenomena. The solubility of FDCA in MeOH systems in Figure 45d (δ_D < 15.5) decreases with increasing values of δ_D. However, other alcohol systems (EtOH, 2-PrOH, and binary blends with water or THF) show increased solubility with increasing values of δ_D. The inconsistencies here may be in part due to MeOH's divergence from typical HSP behavior, as previously discussed, but may also be in part due to the overwhelming contribution of δ_H to explaining alcohol phenomena. Previous research has shown that the intermolecular interactions of alcohols, particularly short-chain alcohols like MeOH or EtOH, are dominated by hydrogen bond formation. The strengths of hydrogen bonds in MeOH have been measured in a range from -11 to -20 kJ/mol,[193] while the total dispersion contributions are typically much lower. Kumar et al. found that the contributions of induced dipole forces were approximately -6.95 kJ/mol for MeOH at the C_6 term, with an additional, smaller term of -0.38 kJ/mol at the C_9 distance.[194] These data support the idea that δ_H dominates alcohol behavior, especially in small, strongly associating alcohols like MeOH. The positive, negative, or negligible impacts of each HSP on FDCA solubility are shown in Figure 45.

A further observation from the alcohol dataset is that FDCA solubility decreases with increasing carbon chain length in the pure alcohols: MeOH (1.59 wt%) > EtOH (0.92 wt%) > 2-PrOH (0.53 wt%) > 1-BuOH (0.36 wt%). This trend correlates strongly with both decreasing values of δ_P (12.3, 8.8, 6.1, 5.7, respectively) and δ_H (22.3, 19.4, 16.4, and 15.8, respectively), which are all lower than for water (16 and 42, respectively). As the carbon chain length increases the alcohols become less polar and less capable of strong hydrogen bond interactions. The decrease in both δ_P and δ_H with increasing alkyl chain length is a natural result of substituting

polar hydroxyl groups with increasingly non-polar hydrocarbon chain, which reduces both dipole strength and hydrogen bonding potential.

Taken together, these observations support a broader conclusion that solubility in alcohol systems is governed in part by polarity and hydrogen bonding capacity, both of which diminish as the alkyl group increases in size. This indicates the importance of considering not only absolute HSP values but also how the chemical features that they represent, like alkyl chains of varying length, affect solubility behavior. The identification of δ_H and δ_P as dominant contributors for alcohol solvents reinforce the chemical rationale behind observed trends.

More importantly, such models serve not only as predictive tools, but as frameworks to reinforce chemical theory and identify the dominant forces in complex solvation environments. A sensitivity analysis on inputs revealed distinct solvation drivers for each model: hydrogen bond interactions for alcohols, and dispersion forces for non-alcohols. The directional impact of these forces, negative for δ_H and positive for δ_D, was consistent with experimental trends and aligns with known solvation behavior previously observed. Particularly, the negative impact of increasing water content in aqueous/organic blends and the high solubility of FDCA in high-δ_D solvents like DMSO.

COSMO-RS Data

The ANN models and consideration of physical phenomena within systems identified relationships between solubility and HSPs, highlighting the strong roles of dispersion and hydrogen bond interactions in determining FDCA solubility and the supporting role of polarity. However, as has previously been discussed, solubility trends can also be linked to more

fundamental thermodynamic properties. Analysis using COMSO-RS revealed a strong exponential relationship between FDCA solubility and excess enthalpy (H^E) (Figure 46), mirroring the trend previously observed with $R_{i,j}$ (Appendix C, Figure 61). As derived in the Supplemental Materials (Appendix C, Derivation 1), a direct thermodynamic link connects HSPs to excess enthalpy, where enthalpy scales exponentially with δ_T (Eqn. 2). Since both $R_{i,j}$ and δ_T quantify solute-solvent compatibility, an exponential relationship between FDCA solubility and excess enthalpy is theoretically expected and quantitatively confirmed by COSMO-RS data.

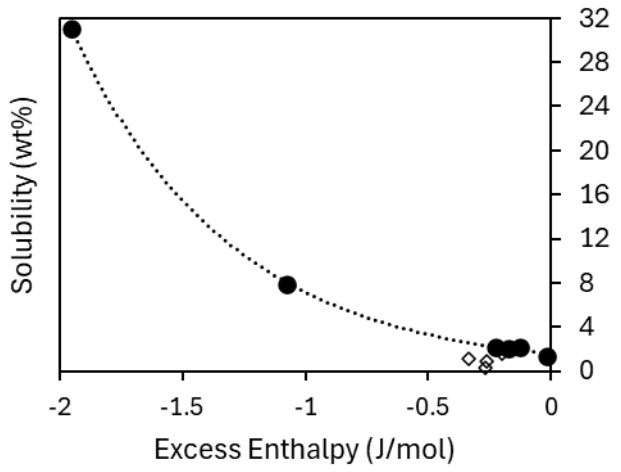

Figure 46. Relationship between the minimum excess enthalpy value for aqueous/organic blends of non-alcohol solvents (●; DMSO, THF, acetone, GBL, GVL, sulfolane, acetonitrile) and alcohol solvents (◊; MeOH, EtOH, 2-PrOH, 1-BuOH) at a consistent FDCA concentration (1 wt%). Trendline added to guide the eye.

To evaluate the usefulness of excess enthalpy as a predictive tool, minimum values for each binary aqueous/organic non-alcohol solvent system were compared at a fixed FDCA concentration of 1 wt%. Using a standardized solute concentration allowed for consistent thermodynamic comparisons across systems, independent of concerns with saturation limits

(Figure 46). This analysis revealed a clear exponential relationship as more negative excess enthalpy values corresponded to higher FDCA solubility, while systems with near-zero or positive values showed negligible solubility (<0.02 wt%, Figure 47). Trends were examined with both ANN training set data and additional data for a high solubility solvent, dimethyl sulfoxide (DMSO), from the literature.[32] The trend correctly predicted DMSO and THF as the top-performing solvents, as was consistent with experimental data.[32] Likewise cyclohexane, a highly nonpolar solvent previously reported to have negligible solubility of FDCA,[93] was found to be a poor solubilizer from an excess enthalpy modeling perspective.

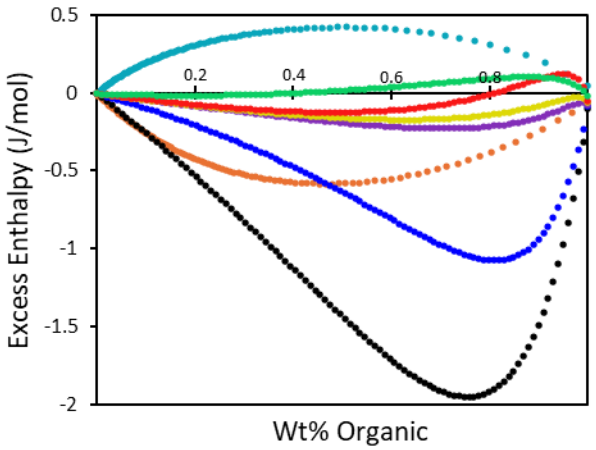

Figure 47. Excess enthalpy values for ternary mixtures of constant FDCA (1 wt%) and variable aqueous/organic solvent ratios of water and (●) DMSO, (●) THF, (●) acetone, (●) GVL, (●) GBL, (●) sulfolane, (●) acetonitrile, and (●) cyclohexane.

While excess enthalpy values were effective at ranking solvents (Table 17), the water to organic ratio that minimized excess enthalpy did not always match the composition that yielded maximum FDCA solubility. In several cases, such as THF and acetone, the compositions fell with ±10 wt% of each other: 19/81 water/organic vs. 20/80 and 26/74 water/organic vs. 20/80,

respectively. However, deviations were larger for other systems, ranging from 13 wt% in GVL to as much as a 51 wt% difference from experimental findings in water/acetonitrile systems. These discrepancies indicate that though excess enthalpy minimization offers a strong thermodynamic marker for ranking solvents for increasing FDCA solubility, a question left unanswered in our prior publication,[32] it may not fully capture the nuanced factors influencing optimized solvent ratios. In our prior work, we showed that $R_{i,j}$ provides a more accurate prediction of composition-dependent solubility behavior, a trend reinforced by the current non-alcohol solubility studies (Figures 42a, b).

Experimental Solub. Ranking	**Maximum Solubility (wt%)**	**Max. Solub. Org/H_2O Ratio (w/w)**	**Ranking by H^E**	**Min/Max H^E at Low FDCA; w_{FDCA} = 0.01 (J/mol)**	**Min. H^E Org/H_2O Ratio (w/w)**
DMSO	30.7	100/0	DMSO	-1.95325	76/24
THF	7.9	80/20	THF	-1.07495	81/19
Acetone	3.3	80/20	Acetone	-0.58401	74/26
GVL	2.2	84/16	GVL	-0.22783	71/29
Sulfolane	2.1	79/21	GBL	-0.17195	63/37
GBL	2.1	80/20	Sulfolane	-0.12459	49/51
Acetonitrile	0.02	70/30	Acetonitrile	-0.01637	19/81
Cyclohexane	<0.02	-	Cyclohexane	0.42197	83/17

Table 17. Ranking of differing solvents by maximum system FDCA solubility and minimum system excess enthalpy.

Among the solvents studied, both acetonitrile and the alcohol systems showed significant deviations from excess enthalpy-based solvent ratio predictions, suggesting a common set of physiochemical factors that invalidate enthalpy as a dominant predictor of solubility. Acetonitrile exhibited the most significant difference between the experimentally observed highest solubility blend (30/70 water/acetonitrile) and the one predicted by excess enthalpy minimization (81/19 water/acetonitrile). Reports in the literature may attribute this discrepancy to acetonitrile's unique solvation behavior in aqueous mixtures.[195-198] Rather than existing as uniformly dispersed

molecules, acetonitrile tends to form molecular clusters instead.[197] In mixtures where one solvent is the significant majority, the minority solvent forms localized, homogeneous domains, while in near-equimolar mixtures (~50/50 n/n) large clusters of both acetonitrile and water exist, leading to the appearance of homogeneity at the macro-scale but exhibiting distinct inhomogeneities at the microscopic scale.[195] These structural inhomogeneities disrupt ideal mixing assumptions and alter solvent-solute interactions in ways that are not captured by an enthalpy-only model. Similar to MeOH, acetonitrile also has a low molar volume (0.053 L/mol)[56] and has been shown to increase total system volumes due to excluded volume effects.[199] Compounding these effects, acetonitrile can also alter the hydrogen bond network of water, introducing additional factors to solvation behavior.[195, 196]

Similar inconsistences emerged in alcohol systems. Based on the trends seen in non-alcohol mixtures, it would be expected that a more negative value of excess enthalpy would correlate with increased FDCA solubilization. However, this relationship did not hold (Figure 48). MeOH, despite having the least negative value of excess enthalpy (-0.201 J/mol), solubilized the most FDCA (1.59 wt%). In contrast, 2-PrOH had significantly lower solubility and the highest values of excess enthalpy (H^E = -0.337 J/mol, 1.14 wt% FDCA solubilized). This reversal of the previously observed trend suggests that in alcohol-rich systems, excess enthalpy is not a dominant factor governing solubility. Instead, hydrogen bond structuring and self-association phenomena are more likely drivers. Wakisaka and Ohki[189] reported that alcohol molecules strongly self-associate, particularly in the presence of small amounts of water. These self-associated clusters were also reported to disrupt water's hydrogen bond network. The clustering behavior observed in alcohols closely resembles that present in water/acetonitrile

mixtures and is likely to have a similar effect on enthalpy-based predictions. Across both alcohol and acetonitrile systems, microscale inhomogeneities and hydrogen bond driven structuring appear to limit the accuracy of the excess enthalpy minimization model, emphasizing the need for additional molecular-level descriptors such as HSPs when evaluating solubility in these systems.

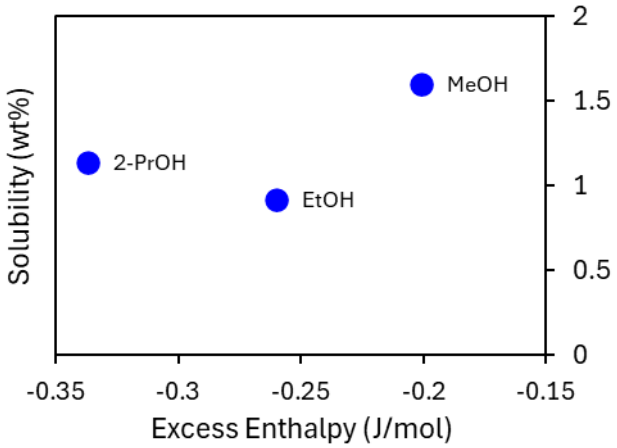

Figure 48. Relationship between the minimum excess enthalpy value for blends of alcohol solvents (2-PrOH, EtOH, MeOH), water, and 1 wt% FDCA and the maximum FDCA system solubility.

The findings across both alcohol and non-alcohol systems show the value of excess enthalpy as a thermodynamic indicator for evaluating FDCA solubility, particularly in non-alcohol systems where a strong exponential relationship between excess enthalpy and solubility was consistently observed. This trend parallels previous results using $R_{i,j}$ and aligns with the theoretical connection between excess enthalpy and holistic HSPs. The ability of the enthalpy-based model to correctly rank solvents like DMSO, THF, and acetone as highly effective solubilizers, while also identifying poor solvents such as anisole and cyclohexane, confirms its

usefulness for solvent screening. However, the model's failure to predict optimal solvent blending ratios in systems like acetonitrile and its breakdown in mixtures containing alcohols reinforces the importance of solvent-specific structural effects like clustering or the disruption of hydrogen bond networks. These structural effects cannot be fully captured by an excess enthalpy minimization model and are better captured by the ANN models presented before. Overall, the strong correlations between excess enthalpy, HSPs, and solubility further validate the use of HSPs as input parameters for the ANN models and affirm the theoretical decision to divide the models into alcohol and non-alcohol systems.

4.7 Conclusions

In solubility systems relevant to FDCA production, we demonstrated that HSPs and thermodynamic metrics like excess enthalpy show strong nonlinear correlations with FDCA solubility in non-alcohol aqueous/organic solvent systems. The solvation capacity of solvents ranked with decreasing values of excess enthalpy, while minimizing the $R_{i,j}$ allowed for the prediction of optimized water to organic ratios. In alcohol systems, neither the enthalpy-based solvent ranking nor $R_{i,j}$ minimization for blend prediction proved reliable, likely due to structural effects like solvent self-association and hydrogen bond network formation that are not captured by the excess enthalpy model.

Two-layer, feed-forward ANN models were developed using the base HSPs of δ_D, δ_P, and δ_H, achieving high predictive accuracy ($R^2 > 0.99$) for both alcohol and non-alcohol systems. Analysis of these models revealed that FDCA solubility in alcohol-based systems is primarily influenced by a decrease in δ_H, while increasing dispersion forces were the dominant

factor in non-alcohol systems. In both cases, δ_P was observed to be a complimentary driving force towards increased solubility.

Conclusively, these results demonstrate that FDCA solubility behavior in complex solvent systems can be effectively modeled through the integration of machine learning with intermolecular theory and thermodynamics. The combined ANN and COSMO-RS framework enables more accurate solvent screening and blending for improved FDCA solubility and provides insight into the distinct physical interactions driving solubility in two different solvent systems, while a connection to former work with the Hansen $R_{i,j}$ parameter allows for even more precise solvent selection. Application of these insights could allow for rational solvent selection in FDCA production or other related biomass upgrading processes, decreasing the barrier towards an economically viable bio-based economy.

CHAPTER FIVE

NOVEL SOLVENT SYSTEMS FOR THE BASE-FREE OXIDATION OF 5-HYDROXYMETHYLFURFURAL TO 2,5-FURANDICARBOXYLIC ACID

5.1 Contributions of Authors and Co-Authors

Author: Jacob M. Molinaro

Contributions: Conceptualization, Data curation, Analysis, Investigation, Methodology, Project Administration, Undergraduate supervision, Validation, Visualization, Writing – original manuscript preparation, revision, and formatting

Co-Author: Van W. Ledger

Contributions: Data curation, Methodology, Software, Visualization, Writing – review and editing

Co-Author: Stephanie G. Wettstein

Contributions: Conceptualization, Analysis, Methodology, Project Administration, Supervision, Visualization, Writing – original manuscript preparation, revision, and formatting

Manuscript in Chapter 5.

5.2 Manuscript Information

Jacob M. Molinaro, Van W. Ledger, and Stephanie G. Wettstein

Applied Catalysis A: General

Status of Manuscript:

_____ Prepared for submission to a peer-reviewed journal

__X__ Officially submitted to a peer-reviewed journal

_____ Accepted by a peer-reviewed journal

_____ Published in a peer-reviewed journal

Elsevier B. V.

8 April 2025

5.3 Abstract

The bio-derived monomer, 2,5-furandicarboyxlic acid (FDCA), is of significant interest for applications in sustainable materials. Production of FDCA is currently hindered by low product solubility in pure solvents, as well as low product yields as the result of initial reactant concentrations less than 1 wt%. The base-free oxidation of 5-hydroxymethylfurfural (HMF) to 2,5-furandicarboxylic acid (FDCA) was investigated using a 5% Pt/C catalyst in a range of aqueous/organic solvent systems including dimethyl sulfoxide, tetrahydrofuran, sulfolane, acetonitrile, γ-valerolactone (GVL), and γ-butyrolactone (GBL) with a focus on identifying blends that balance solubility, selectivity, and solvent stability. Most systems showed the highest FDCA yields in 20/80 organic/water blends, highlighting the critical role of water in promoting full oxidation. However, sulfolane/water mixtures deviated from this trend, achieving a maximum FDCA yield of 76.4% in a 50/50 blend. At higher HMF concentrations, sulfolane enabled significantly higher mass balances compared to water. Optimal FDCA yields were achieved between 373–383 K, though product recovery declined above this range. Importantly, sulfolane exhibited no degradation under reaction conditions, unlike other solvents studied. These results suggest sulfolane/water systems offer a promising solvent platform for high-yield, scalable FDCA production and may enable integrated biomass-to-FDCA processing through one-pot synthesis.

5.4 Introduction

A key biomass-derived platform chemical is 2,5-furandicarboxylic acid (FDCA)[1, 2] that has applications in sustainable materials, particularly as the monomeric precursor for polyethylene furanoate (PEF).[67, 200] PEF is a bio-based alternative to polyethylene terephthalate (PET), a common petroleum-based plastic and a leading contributor to plastic waste.[3, 8-10] In addition to improved environmental impact, PEF offers material advantages such as greater thermal stability,[14] superior O_2 and CO_2 barrier properties,[13] the ability to compost under industrial conditions,[201] and full recyclability within existing PET infrastructure.[202] However, despite its significant promise and growing corporate investment,[5, 7] industrial-scale production of FDCA has two main challenges: low solubility in many common solvents[26, 28, 29, 32, 153] and low selectivity towards FDCA in reaction systems.[26, 153] Addressing these limitations requires an improved understanding of solvent selection for increased solubility, reaction promotion, and improved catalytic performance in the oxidation of 5-hydroxymethylfurfural (HMF) to FDCA (Figure 49).

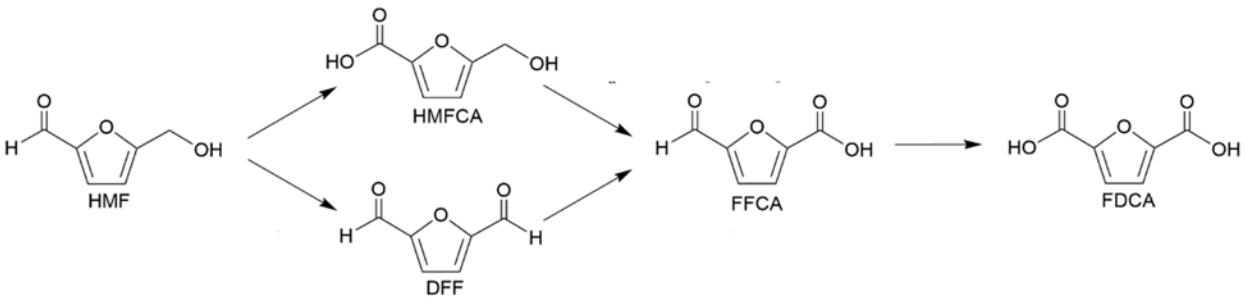

Figure 49. Reaction schematic for the oxidative upgrading of HMF to FDCA.

The first of these primary obstacles, solvent selection, requires a balancing of FDCA solubility with the effects of the solvent on reaction progress. Many conventional solvents have low solubility of FDCA at standard temperatures and pressures, including water (0.12 wt% FDCA solubility),[32] ethanol (0.92 wt% FDCA solubility),[32] and acetic acid (0.63 wt% FDCA solubility).[31] Low solubility necessitates the use of large reactor vessels and solvent volumes, or the use of bases like NaOH[120] or $KHCO_3$[117] to improve solubility. The addition of bases leads to challenges with furan degradation,[108, 121] product separations,[122] and safety[123] while the use of large equipment and solvent volumes requires significant start-up and operational costs due to low concentrations. A techno-economic analysis by Iglesias et al.[153] cited that FDCA concentrations of approximately 10 wt% would be necessary for the process to be competitive with PET production.

Recent studies have explored organic and aqueous/organic solvent blends as alternative systems and demonstrated that some solvents and mixtures lead to high FDCA solubility.[27-29, 32, 36] Zhuang et al.,[29] for example, demonstrated three to sixfold increases in FDCA solubility in aqueous/organic blends of ethers (1,4-dioxane (DX), 1,2-dimethoxyethane (DME), diethylene glycol dimethyl ether (DGDE)) compared to the pure organics. Molinaro et al.[32] observed even greater solubility increases in solvent blends, with sixfold increases in blends containing γ-valerolactone (GVL), tetrahydrofuran (THF), or sulfolane and up to sixty-fivefold in blends containing dimethyl sulfoxide (DMSO) relative to the pure organic. The significant solubility advantages of blends compared to pure water or pure organic have been cited as a promising path towards higher concentration FDCA production on the industrial scale.[26]

Solvent selection affects more than just solubility, and the effect on the reaction needs to be considered. In 2018, Motagamwala et al.[27] used a Pt/C catalyst with a GVL/water solvent for HMF oxidation and achieved high FDCA yields at low initial HMF weight percentages[27] showing that organic solvents may improve the process. In 2024, Ryu et al.[36] studied mixed solvent systems containing water and DMSO, N,N-dimethylformamide (DMF), GVL, DX, DGDE, and DME to determine the effect of solvent choice on the HMF to FDCA reaction. They investigated the impacts of FDCA solubility, solvent polarity, and hydrogen bond acceptance or donation using Kamlet-Abboud-Taft (KT) parameters on reaction yields. Their results showed that solvents with moderate solubility (2 – 5 wt% maximum FDCA solubility), low polarizability ($\pi^* < 0.7$), and low hydrogen bond interactions ($\beta < 0.5$) like DX or DME are desirable for FDCA production.[36] Despite these findings, there remains limited information of how solvent-reactant interactions influence oxidative selectivity in mixed aqueous/organic systems. Additionally, solvent stability under oxidative conditions needs to be evaluated as some organics like tetrahydrofuran (THF) undergo degradation or conversion to secondary products[162] that may interfere with the HMF to FDCA reaction.

To better understand these challenges, this study investigates the oxidation of HMF to FDCA in seven pure and six binary aqueous/organic solvent systems (DMSO, THF, GVL, γ-butyrolactone (GBL), acetonitrile, and sulfolane) using a 5% Pt/C catalyst. These organic solvents have unique FDCA solubilities, polarities, hydrogen bond formation, and molecular organization and clustering when mixed with water and how solvent composition influences reaction conversion, product selectivity, and FDCA yield is reported. This study provides new insights into the role of solvent-reactant interactions within FDCA production and contribute to a

broader understanding of how solvent selection impacts reaction efficiency, offering a valuable resource for improving FDCA production in future research and, potentially, industry-scale synthesis.

5.5 Materials and Methods

Chemicals

All chemicals were used as received without further purification or processing: 5-HMF (98%, AK Scientific), FDCA (98%, AK Scientific), 2,5-furandicarbaldehyde (DFF; 98%, AK Scientific), 5-hydroxymethyl-2-furancarboxylic acid (HMFCA; ≥99%, MedChemExpress), 5-formyl-2-furancarboxylic acid (FFCA; 98%, Tokyo Chemical Industry Co.), DMSO (≥99.9%, Millipore Sigma), THF (≥99%, Fisher Scientific), GVL (≥99%, Sigma Aldrich), GBL (≥99%, Sigma Aldrich), acetonitrile (≥99%, Fisher Scientific), sulfolane (99%, Sigma Aldrich), and Milli-Q water (18.2Ω; MilliporeSigma Milli-Q Advantage A10 system).

Catalysts

All catalysts were used as received without further purification or processing: 5% Pt/C (Thermo Scientific) and 10% Pt/C (Thermo Scientific).

HMF Oxidation Procedure

Batch oxidation experiments were conducted in a 30 mL Parr stainless steel reactor equipped with an electric heater regulated by an Omega CN7500 PID controller. Temperature was measured using a K-type thermocouple, with independent logging performed using an

Omega USB-TC-LCD Data Logger and EasyLog USB software. Stirring was maintained at 1000 rpm by placing the Parr reactor on a Fisher Scientific Isotemp stir plate.

For each reaction, unless otherwise specified, 0.106 g of HMF (1 wt% relative to solvent mass), 10 g of solvent, and catalyst (either 0.437 g of 5 or 10 wt% Pt/C) were added to the reactor along with a stir bar. The reactor was then purged three times with O_2 to remove air before being pressurized to 580 psi O_2. Stirring was set to 1000 rpm and the Parr heated to the reaction temperature (363 K) using a ramp time of 2 h, followed by a temperature hold for the reaction duration. Upon completion of the reaction, the vessel was cooled by removing it from the heating jacket and air-cooled. The final pressure was recorded once the vessel cooled to 298 K, and reaction temperature and duration data were logged.

The reaction mixture was then diluted and rinsed with 20 mL of DMSO followed by 200 mL of deionized water. The catalyst was recovered using vacuum filtration through Whatman 44 (70 mm) filter paper. The permeate was filtered through a 0.2 μm PTFE syringe filter before high-performance liquid chromatography (HPLC) analysis using a Thermo Scientific Vanquish HPLC system equipped with an Aminex HPX-87H column (300 mm × 7.8 mm). The mobile phase consisted of 0.01 M trifluoroacetic acid (TFA, pH = 2) at a flow rate of 0.600 mL min^{-1}. Both ultraviolet (UV) and refractive index (RI) detectors were used, with UV peak integration performed against calibration standards (Appendix D). Comprehensive, step-by-step instructions for running and analysis of batch HMF oxidation reactions are available in Appendix B.

Solvent Degradation Assessment

The effect of reaction conditions on solvent stability was evaluated by performing control reactions under identical conditions to those described in ‘Batch Oxidation Reactions’, excluding

HMF: 4 h at 363 K with 1000 rpm stirring and 580 psi O_2. A DMSO rinse was omitted to prevent interference with HPLC-RI analysis and therefore, the solvent was diluted with 200 mL of deionized water and filtered as previous described. Additionally, a control sample was prepared by diluting an equivalent amount of pure, unreacted solvent (10 g) in 200 mL of deionized water. The control sample was filtered using the same procedure to ensure consistency in sample preparation. and both the reacted solvent and control samples were analyzed using HPLC as described previously.

5.6 Results and Discussion

Solvent Effects

The product distribution and mass balance of HMF base-free oxidation over a 5% Pt/C catalyst (363 K; 4 h) was significantly affected by solvent composition as seen in Figure 2. The solvents studied included pure water, DMSO (Figure 50a), acetonitrile (50b), sulfolane (50c), GBL (50d), GVL (50e), and THF (50f), with each studied in aqueous/organic blends containing 20, 50, and 80 wt% organic composition. In all cases, the pure organic solvents had low FDCA yields with acetonitrile (Figure 50b) and THF (Figure 50f) having the highest yields of 3.87% and 3.92%, respectively. Additionally, excluding pure DMSO, the pure solvents had lower HMF conversion and high selectivity to DFF, the primary intermediate following HMF (Figure 49). These incomplete oxidations compared to 20/80 water/organic blends indicate that water has a critical role in the oxidation of HMF as mentioned previously.[27, 32, 42] When mixed with 20 wt% water, even the lowest of the binary blends (80/20 DMSO/Water, 20.29%, Figure 50a) had more than five times the FDCA yield of the pure solvent (Figure 50).

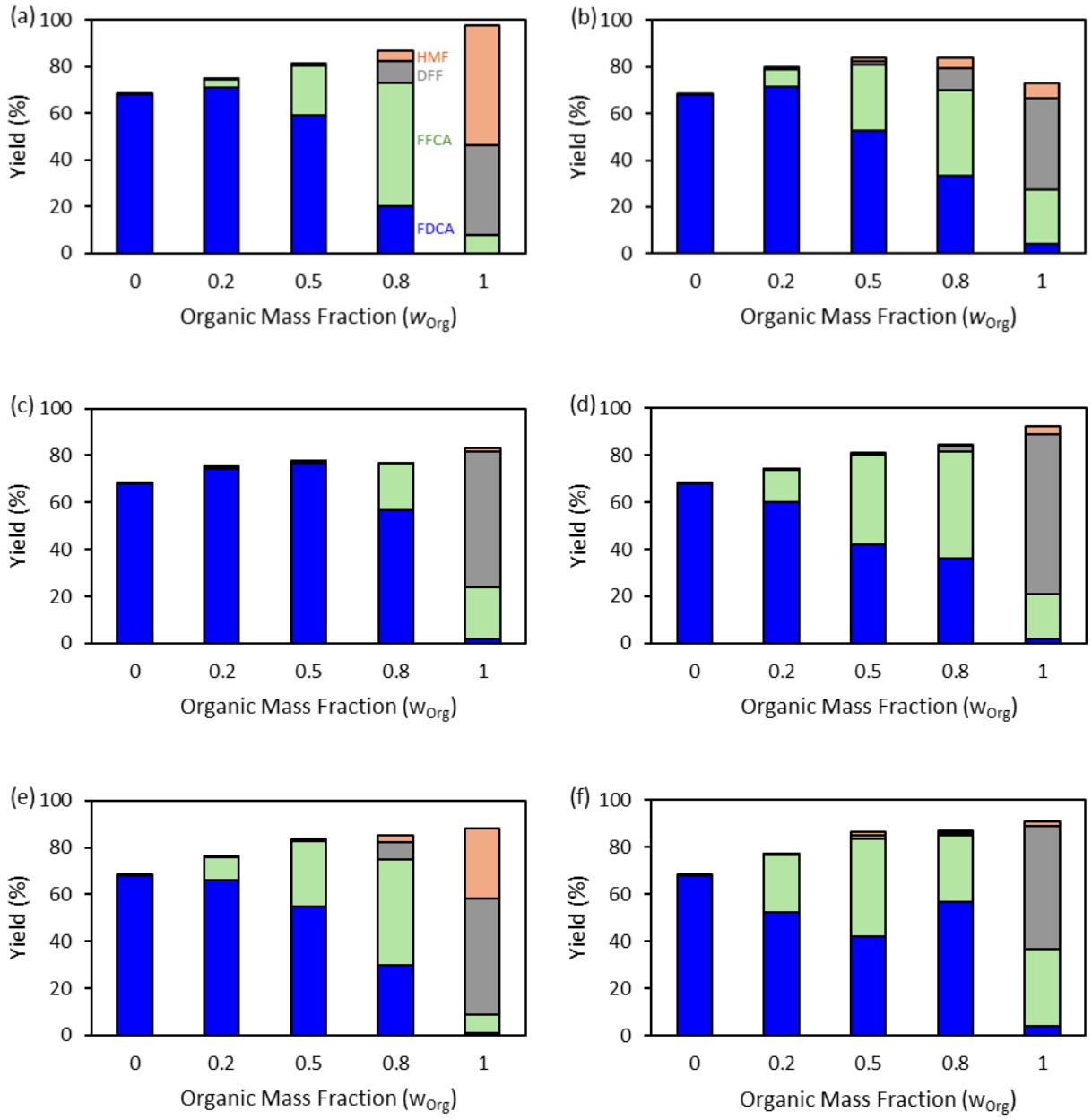

Figure 50. Final compositions of HMF oxidation reactions in DMSO (a), acetonitrile (b), sulfolane (c), GBL (d), GVL (e), and THF (f). Product yields are represented as FDCA (■), FFCA (■), DFF (■), and remaining HMF (■). Total bar height indicates final mass balance value. Reaction conditions: 363 K, 4 h, 40 bar O_2, 1000 rpm stirring, 1 wt% HMF concentration, 7.5:1 HMF:Pt.

This phenomenon has been attributed to the role of water in forming a geminal diol intermediate during the conversion of DFF or FFCA to FDCA,[26, 112] whereas no intermediate forms in the conversion of HMF to DFF. Formation of the geminal diol has been previously cited as the rate determining step in the overall reaction,[78] particularly in the oxidation of FFCA to FDCA. This mechanistic insight is supported by experimental work from Motagamwala et al.[27] that attributed low selectivity towards FDCA (11% yield) in mixtures of 80/20 GVL/water to insufficient water, citing geminal diol formation as the mechanistic reason for low yields.[27] In a follow up experiment using a 50/50 GVL/water mixture, the researchers reported a 94% FDCA yield compared to pure water resulting in 67.9% FDCA. Given the strong dependence of reaction progress on this water-facilitated intermediate, the finding of this present study that pure organics resulted in majority DFF formation follows expected reaction behavior.

Increasing the amount of water further to 50 and 80 wt% saw increasing selectivity towards FDCA in almost all systems (Figure 50). In the case of DMSO (Figure 50a) and acetonitrile (50b), the maximum FDCA yield was observed in 20 wt% organic solvent and indicates that the organic solvent facilitated an improved oxidation environment. Additionally, in both systems, the final mass balance is higher in the 20/80 w/w organic/water system than in pure water, 79.2% in 20/80 acetonitrile/water and 74.6% in 20/80 DMSO/water compared to 68.5% in pure water (Figure 51). Interestingly, DMSO has the highest reported solubility of organic solvents tested, 30.7 wt%, while acetonitrile has one of the lowest at 0.02 wt%.[32] Both DMSO and THF enhance hydrogen bond stability in biomass-derived compounds and form solvation shells around them.[203, 204] These strong solvent-solute interactions were suggested to reduce the frequency of furan-furan interactions and result in pronation of oxygen atoms, which

are a leading cause of HMF degradation to humins in the system.[203] In the later work of Ryu et al., analysis via ATR-FTIR observed strong interactions between DMSO and HMF, as well as between GVL and HMF.[36] Evidence of solvent-reactant interactions in solvents like DMSO, GVL, and THF may explain the increasing mass balances and decreasing formation of FDCA with increasing proportions of organic solvent (Figure 50a, e, f).

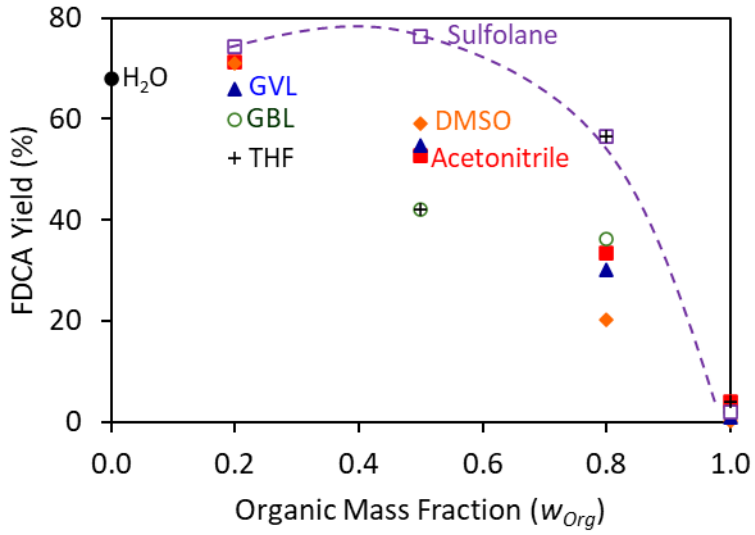

Figure 51. Maximum FDCA yields from HMF oxidation reactions in water (●), DMSO (♦), acetonitrile (■), sulfolane (□), GBL (○), GVL (▲), and THF (+). Lines were added to guide the eye. Reaction conditions: 363 K, 4 h, 40 bar O_2, 1000 rpm stirring, 1 wt% HMF concentration, 7.5:1 HMF:Pt.

In contrast, acetonitrile has the lowest capacity for hydrogen bond acceptance of the solvents previously studied for HMF oxidation.[26] In combination with a tendency for self-association in aqueous mixtures,[195] this suggests that acetonitrile is unlikely to shield furan compounds from the degradation as described above. This may explain why in all binary systems except for acetonitrile (max at for 50/50 acetonitrile/water), mass balances increase with organic

content with the highest mass balances occurring at 100% organic (Figure 50). Mass recovery improved from 68.5% in pure water to above 80% GBL, GVL, and sulfolane and above 90% in DMSO, GBL, and THF; however, FDCA yields were in the single digits or lower for the pure organic solvents.

As seen in Figure 51, maximum FDCA yields were observed in 20/80 organic/water blends containing acetonitrile (71.4%), DMSO (71.0%), GVL (65.8%), and GBL (59.9%). Sulfolane produced a similarly high yield at 20/80 organic/water (74.3%), but also had high FDCA yields at higher organic weight percents, 76.4% in 50/50 and 56.5% in 80/20 sulfolane/water. This suggests that sulfolane has unique properties that allow for increased organic content while still achieving high FDCA yields unlike other solvents, whose FDCA yields typically declined as water content decreased. Additionally, presented in detail in the Supplemental Materials (Appendix D), analysis showed that DMSO, sulfolane, and GBL are the most resistant to degradation.

Prior HMF oxidation research has highlighted the tradeoff between improving solubility (strong solvent-solute interactions) and reaction progress (availability of water).[36] Sulfolane may help to resolve this conflict as 50/50 sulfolane/water had approximately ten times the FDCA solubility of pure water, while 80/20 mixtures had over 20 times the solubility and both mixtures led to high FDCA yields. This aligns with prior studies such as Wang et al.[205] [REF: Wang, K. 2020] who previously used 90/10 sulfolane/water mixtures for the conversion of cellulose to levulinic acid and furfural. Sulfolane/water mixtures produced higher yields faster and at higher reactant concentration than organic/aqueous blends containing DMSO, THF, or GVL. The

authors attributed this to "synergistic" effects between sulfolane and water that were driven by the high dipole moment, dielectric constant, and solvation effects of sulfolane.[205]

In another study of levulinic acid and HMF production in organic/aqueous mixtures, Mikola et al.[206] found that increasing the sulfolane content up to 90 wt% significantly improved the rate of reaction, particularly in the HMF reaction. Similar observations were made in a one-pot upgrading of bamboo biomass in 90/10 sulfolane/water solvent, where a 47.8% HMF yield was achieved.[207] One-pot synthesis methods, where biomass can be converted through intermediates to FDCA in a single reactor system, are amongst the most desirable approaches for reducing the overall cost of FDCA production[26, 105] since using the solvent from the previous upgrading step could significantly improve the process economics.

Effect of HMF Concentration

Reactant concentration has been cited as a barrier to economical FDCA production[153] as FDCA yields in pure aqueous reactions are usually low without the addition of a base. Catalyst fouling due to reactant or product adsorption on active sites is a frequently reported concern in high-concentration reactions,[87] and as such a solvent that improves solubility to inhibit adsorption is desirable. For this work, increased HMF concentrations were evaluated in pure water and compared to the top-performing aqueous/organic blend, 50/50 sulfolane/water by analyzing samples directly from the reactor vessel without (Figure 52a) and with (Figure 52b) the catalyst rinsing procedure described in the methods to assess the extent of furan adsorption on the surface of the catalyst.

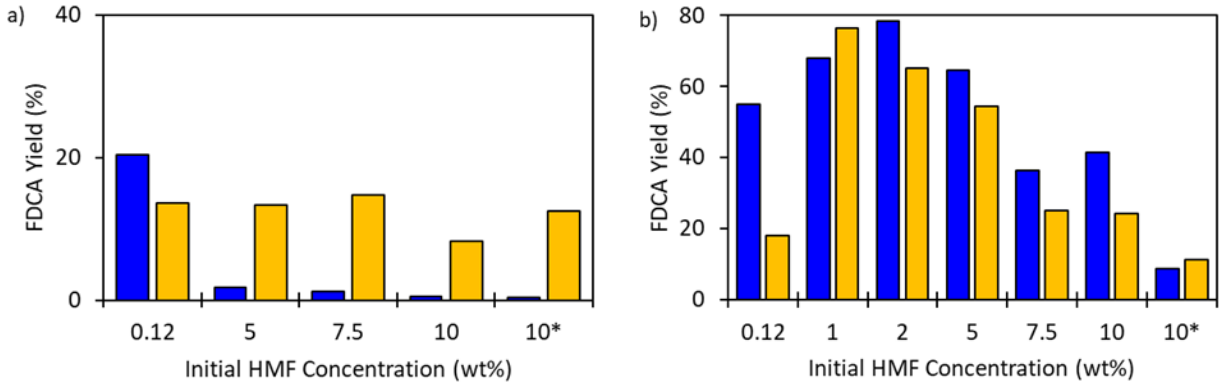

Figure 52. The effect of initial HMF concentration on yields of FDCA in pure water (■) and 50/50 sulfolane/water (■) sampled immediately after the reaction (a) and after catalyst and reactor rinsing (b). Reaction conditions: 363 K, 4 h, 40 bar O_2, 1000 rpm stirring, 0.437 g of 5% Pt/C catalyst, varying HMF concentration. A * indicates that a 10% Pt/C catalyst was substituted at the same catalyst weight.

The impact of catalyst rinsing was substantial across both solvent systems, with the aqueous system showing the most dramatic differences (Figure 52). In the unrinsed aqueous system, FDCA yields and mass recoveries were minimal with just 20% of FDCA being recovered at 0.12 wt% HMF and less than 2% at concentrations higher than 5 wt% HMF (Figure 52a). In contrast, the sulfolane/water system retained 13.7% of the FDCA without rinsing under the same conditions. When the reactor and catalyst were rinsed (Figure 52b), FDCA yield in the aqueous system at 7.5 wt% HMF improved to 36.5%, while in the sulfolane/water system, rinsing only increased the FDCA yield from 14.7% to 25.0%.This suggests that in aqueous media, substantial adsorption of furan products onto the catalyst surface limits product recovery and reaction progress, whereas sulfolane mixtures significantly reduce this interaction.

Although rinsing was necessary, high FDCA yields (78.2%) were achieved in the aqueous system starting with 2 wt% HMF but trended downward with increasing concentration (Figure

53a). At 10 wt% HMF and using a 5 wt% catalyst, the FDCA yield was similar to 7.5 wt% HMF and more FFCA was formed. This was hypothesized to be due to mass-transfer limitations in the viscous reactor mixture not allowing reactants and products to adsorb to the catalyst. When using a 10 wt% Pt/C catalyst at half the weight as the 5% Pt/C catalyst (Figure 53a; "10*"), the FDCA yield fell to 8.7%, suggesting that catalyst fouling and humin formation did in fact inhibit conversion. The sulfolane/water system, meanwhile, reached a maximum FDCA yield of 76.4% at 1 wt% HMF. At higher HMF concentrations, FDCA yields dropped more rapidly than in water (Figure 52b), but mass recovery remained high (Figure 53b). This trend suggests that while sulfolane mixtures may reduce degradation, additional time or elevated temperatures may be necessary to drive complete oxidation to FDCA due to the high yields of FFCA and DFF seen. Regardless, even at higher HMF concentrations, sulfolane systems consistently recovered more product and experienced less degradation, likely due to reduced furan-furan interactions and stronger solvent stabilization of intermediates.

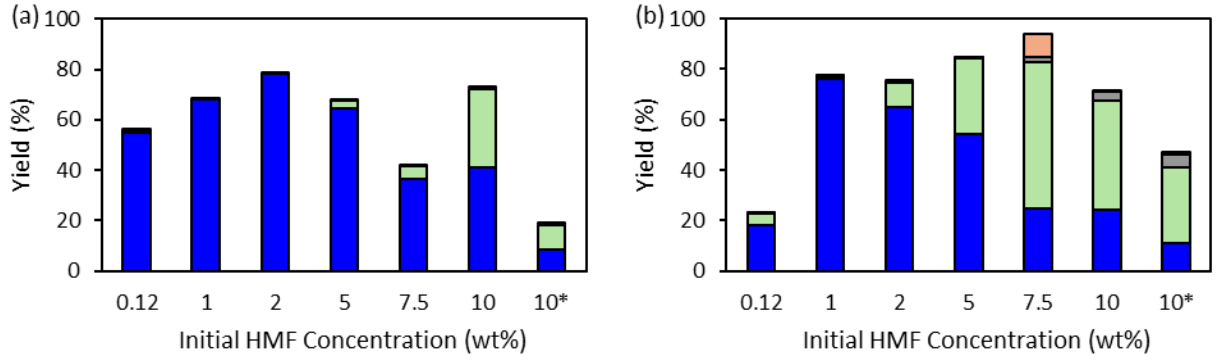

Figure 53. Product yields for different initial HMF concentration for FDCA (■), FFCA (■), DFF (■), and remaining HMF (■) in water (a) and 50/50 sulfolane/water (b). Reaction conditions: 363 K, 4 h, 40 bar O_2, 1000 rpm stirring, 0.437 g of 5% Pt/C catalyst, varying HMF concentration and the catalyst was rinsed after reaction. A * indicates that a 10% Pt/C catalyst was substituted at the same catalyst weight.

In the aqueous system (Figure 53a), overall product recovery decreased significantly at initial HMF concentrations great than 2 wt% (Figure 3a; excluding the 10 wt% point as discussed previously). A similar trend was observed by Mani et al.[83] in a base-free aqueous system (Ru/MnO_2). Starting with over 2 wt% HMF, product yields and mass balances decreased significantly with less than 5% of the mass and negligible FDCA recovered at 10 wt% HMF.[83] In contrast to the aqueous system, the 50/50 sulfolane/water mixture saw improved mass balances up to 7.5 wt% HMF (Figure 53b). At 7.5 wt% HMF concentration, 94.2% of the mass in the system was recovered compared to only 41.8% in the pure water system. Though only 25.0% of the product yield was FDCA, the high recovery of intermediates like FFCA indicate that potentially with reaction optimization, such as additional reaction time or an increase in temperature, higher yields may be achieved.

Effect of Reaction Temperature

In order to evaluate the effect of temperature, 7.5 wt% HMF was used in 50/50 sulfolane/water with 5% Pt/C catalyst across a temperature range of 363 K to 403 K (Figure 54). Increasing the temperature from 363 K to 373 K, conversion of HMF improved from 90.6% to 99.7% and FDCA yield improved from 25.0% to 32.9%, following the expected trend,[84, 108, 115, 123] while the FFCA yield remained consistent (Figure 5). Increasing the temperature to 403 K resulted in yields of approximately 50% FDCA with no significant amounts of intermediates, therefore leading to low mass balance.

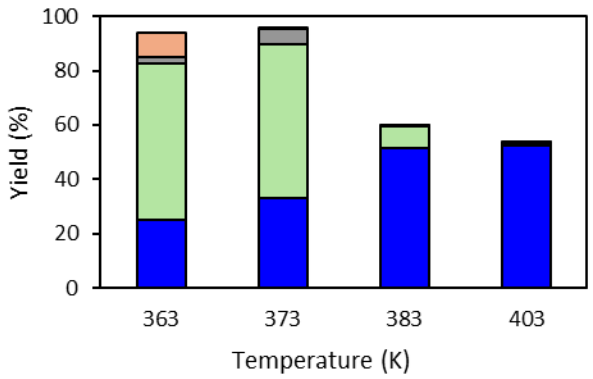

Figure 54. Impact of temperature on product distribution of FDCA (■), FFCA (■), DFF (■), and remaining HMF (■). Reaction conditions: 7.5 wt% HMF concentration, 50/50 SULF/water solvent, 4 h, 40 bar O_2, 1000 rpm stirring, 0.437 g of 5% Pt/C catalyst.

This is likely explained by previous work which reported temperatures exceeding 403 K resulted in decreased FDCA yield due to temperature-driven furan degradation.[123] Gao et al.[84] saw similar results when they studied a non-noble metal catalyst in acetonitrile and observed increasing yields up to approximately 90% at 393 K. These results indicate that the ideal

temperature range for upgrading 7.5 wt% HMF in 50/50 sulfolane water over a 5% Pt/C catalyst lies somewhere between 373 and 383 K. At higher temperatures, though the majority product recovered is FDCA, there is a significant loss of mass (Figure 54).

5.7 Conclusions

This work investigated the oxidative upgrading of HMF to FDCA using a 5% Pt/C catalyst across a diverse range of solvent systems, with a specific focus on aqueous/organic solvent mixtures. Reaction yields show the critical role of water in forming a geminal diol intermediate and promoting full oxidation of HMF to FDCA in most aqueous/organic solvent systems. With the exception of pure water and sulfolane mixtures, blends containing 20/80 organic/water resulted in the highest FDCA yields due to high water availability and the shielding effects of highly interactive organic solvents. The distinct behaviors seen in DMSO, THF, and acetonitrile show the effects of intermolecular solvent-solute interactions such as hydrogen bonding and self-association on reactions outcomes.

Among the solvent blends tested, sulfolane was unique in facilitating high FDCA yields at elevated organic content, achieving a 76.36% yield in a 50/50 sulfolane/water, the highest observed in any system. This was notable since all other solvents achieved maximum FDCA yields in 20/80 organic/water blends, in line with prior work indicating the importance of water to the production of FDCA. Sulfolane was unique in enabling higher FDCA yields than those seen in pure water even at elevated proportions of organic solvent, indicating a balance between improved solubility and reaction kinetics. These findings indicate that high organic content blends of sulfolane and water could be a promising candidate for combined biomass-to-FDCA reactions.

Sulfolane's ability to promote reaction progress at higher weight fractions of organic is advantageous because increased organic content correlates with increased FDCA solubility, allowing for reactions to be run at higher initial HMF concentrations. The 50/50 sulfolane/water system reported significantly higher mass recovery than the pure water system for all systems greater than 2 wt% HMF. At most concentrations, aqueous systems showed higher selectivity to FDCA, with approximately 90% of the mass recovered being FDCA, but low overall mass recovery. When tested at 7.5 wt% HMF, the 50/50 sulfolane/water system achieved 25.0% FDCA yield and a 94.2% mass balance, significantly outperforming the 41.8% mass balance in water. These results indicate that sulfolane systems are capable of handling high reactant loading without substantial losses to degradation or side reactions, both of which are important considerations for practical, scalable FDCA production. While objective yields of FDCA were lower in sulfolane/water systems, the high recovery of intermediate products leaves room for reaction design to enhance progress towards FDCA.

Temperature was also found to have a key role in determining product distributions for sulfolane/water systems, with a balance required between higher yields and reduced product recovery. At 373 K, a 32.87% yield of FDCA was achieved with the remainder of the product being FFCA (56.86%) and DFF (5.46%). At 383 K FDCA yields improved to 51.47%, but with a reduced mass balance from 95.51% to 59.71%. Above 383 K yields did not significantly improve, but overall product recovery decreased, suggesting that the 373 – 383 K range represents ideal operating temperatures for high concentration HMF oxidation in this solvent and catalyst system.

Sulfolane exhibited no detectable degradation under the reaction conditions studied, in contrast to other solvents like THF, GVL, and ACN. This robustness, paired with proven applications in upstream biomass-to-HMF conversion, makes a binary aqueous/sulfolane solvent system a promising candidate for a one-pot synthesis of FDCA directly from biomass. Such a process, if proven, could address key challenges with economical FDCA production for bioplastics by simplifying reactor design and eliminating intermediary purification or separation steps.

Conclusively, this work demonstrates that sulfolane/water mixtures not only enhance FDCA yields and mass balance at high proportions of organic but also offer high solubility and solvent stability under oxidative conditions. These findings represent novel avenues for process design and suggest that further exploration of sulfolane-based systems, particularly for streamlined biomass-to-FDCA processing, warrant further investigation.

CHAPTER SIX

CONCLUSIONS AND FUTURE OUTLOOK

The work presented in this dissertation addresses two of the main challenges limiting the economical production of 2,5-furandicarboxylic acid (FDCA) for application in sustainable materials like polyethylene furanoate (PEF). First, the poor solubility of FDCA was addressed through the collection of new solubility data in relevant solvents and solvent mixtures. This data was then correlated to the Hansen Solubility Parameter (HSP) model and excess enthalpy values. Key physiochemical attributes of a mixed solvent system were identified as they related to improved solubility. A methodology for selecting a high-solubility solvent mixture with ideal ratios of water to organic was demonstrated. Second, the effects of aqueous/organic solvent blends on reaction progress in the oxidation of 5-hydroxymethylfurfural (HMF) to FDCA were explored. These effects were quantified and explained, and the solvent system with the highest proportion of organic solvent was assessed at a range of initial HMF concentrations and temperatures.

FDCA solubility was assessed in pure, binary, and ternary solvent systems containing water and eight organic solvents. Some of the organics tested had previously been assessed for FDCA solubility, but several were novel to the literature. Across these blends, FDCA solubility increased with decreasing values of holistic HSPs, typically maximizing at approximately 80 wt% organic solvent composition. The application of minimizing the Radius of Interaction ($R_{i,j}$) parameter for solubility maximization was a novel technique in FDCA solubility research, introducing an accessible, easily applicable methodology for improving mixture compositions. Furthermore, the $R_{i,j}$ predicted maximum-solubility solvent mixtures more accurately than the

previously proposed difference in total HSP ($\Delta\delta_T$), typically predicting within ±10 wt% organic solvent of experimentally identified solubility maxima. Using the $R_{i,j}$ as the target of an optimization function, a MATLAB code was written to optimize combinations of input solvents for FDCA solubility. Use of this code was demonstrated by optimizing blends of dimethyl sulfoxide (DMSO), tetrahydrofuran (THF), and water for a highest-observed FDCA solubility of 20.7 wt%.

This improved methodology for assessing FDCA solubility was further refined through numerical methods and machine learning models. This not only allowed for solvent optimization within a blend of water and an identified organic solvent but also presented an approach by which the baseline solubility of any organic solvent could be estimated. Further, the physical basis of FDCA solubility within different classes of solvent (mainly, alcohols and non-alcohols) was assessed. Artificial neural network (ANN) models were able to correlate input variables consisting of δ_D, δ_P, and δ_H, the three base HSPs, to FDCA solubility with correlation coefficients (R^2) exceeding 0.99. These ANN models were then able to predict the FDCA solubility of independent test sets for solvents governed by similar intermolecular behaviors (of the same "solvent class") within the 95% confidence band. For alcohol type solvents, the main drivers of FDCA solvation were identified to be decreasing values of δ_H and δ_P, correlating to reduced water content, smaller carbon chain lengths, and decreasing instances of solvent self-association. In the non-alcohol systems, FDCA solvation was determined to be more strongly influenced by increasing dispersion forces (δ_D) and decreasing values of δ_H.

Numerical approximations for excess enthalpy were calculated using the COSMO-RS software package. More negative values of excess enthalpy, indicating increasingly non-ideal

mixing behavior between cosolvents, were correlated strongly to increasing FDCA solubility in non-alcohol systems regardless of molecular structure. Using this approach for determining baseline solubility, high-solubility solvents like DMSO and THF were correctly predicted, and eight organic solvents were accurately ranked from least to greatest FDCA solubility. The combined approach of understanding key molecular interactions influencing solubility to inform solvent selection, followed by excess enthalpy minimization to select a solvent and $R_{i,j}$ minimization to blend that solvent with water presents a simple but effective technique for identifying solvent systems with high FDCA solubility, without the need for physical experimentation.

Based on this improved understanding of FDCA interactions and solubility in a range of solvent systems, solvent effects were assessed during the oxidation of HMF to produce FDCA in batch reactions. Six aqueous/organic systems were systematically assessed at 0%, 20%, 50%, 80%, and 100% organic using a 5% Pt/C catalyst. In nearly all systems, the influence of water in promoting reaction progress overwhelmed results, with the highest FDCA yields observed in either pure water or 20/80 organic/water systems. A shielding effect of certain organics, mainly DMSO, THF, γ-valerolactone (GVL), γ-butyrolactone (GBL), and sulfolane, was observed with increasing mass recovered correlating to increased organic content. Further, degradation studies on the solvents identified DMSO, GBL, and sulfolane as the most resistant to oxidative conditions.

Sulfolane was seen to be unique amongst the solvents studied, showing high FDCA yields up to 80% organic solvent composition. Higher proportions of organic allowed for improved FDCA solubility and increased reactant concentrations. The ability of reaction systems

to handle increased loadings of HMF was assessed, comparing a 50/50 sulfolane/water system to a purely aqueous system from 0.12 wt% HMF to 10 wt% HMF. The blended sulfolane system showed high mass balances (>94%) up to 7.5 wt% initial HMF concentration, whereas the aqueous system showed reduced recoveries above 2 wt%. Increasing FDCA yields were further correlated to increasing temperatures up to 403 K during a study of temperature effects. The identification of sulfolane/water blends as effective for HMF oxidation was identified to be of particular importance due to prior work using the same solvents for the upgrading of biomass to HMF. The use of a single-solvent system for the production of FDCA directly from biomass is of great interest for improving process economics through removal of costly purification and separation steps.

Finally, a comprehensive literature review was conducted, written, and published, identifying trends in catalyst design and solvent selection for the oxidation of HMF to inform future research. This review identified critical opportunities for future research to improve the efficiency of FDCA production. These opportunities include those potentially applicable within the Wettstein Laboratory, as well as several to be addressed by the larger scientific community and by the bioplastics industry on a commercial scale.

First, due to recent improvements in the production of FDCA from HMF, several techno-economic analyses (TEAs) have identified the conversion of biomass to HMF as more costly than the upgrading of HMF to FDCA. To improve the economics of both processes, effectively addressing two problems at the same time, one-pot synthesis of FDCA directly from biomass should be investigated. Within the Wettstein Laboratory, further investigation of blended sulfolane/water systems should be studied for their balance of product solubility, selectivity

towards FDCA, resistance to degradation, and prior application in biomass to HMF reactions. Ideally, these studies would move from the batch scale to a flow reactor system to improve applicability in industry. The $R_{i,j}$, ANN, and excess enthalpy models developed in this dissertation could be used to investigate alternate solvents, or improved to more accurately predict in solvent systems of differing geometries – trigonal planar, tetrahedral, or others. The excess enthalpy model could be of particular interest for further study, potentially collecting additional data to develop an empirically-informed equation for solubility modeling.

On a broader scale, investigation of more solvents should be conducted, including over a wider range of catalysts. While noble metal catalysts like the carbon-supported platinum studied here offer high selectivity to FDCA, non-noble metals such as Mn, Cu, Ni, and Co are gaining popularity due to their lower cost and relative abundance. Bimetallic systems have shown synergistic effects and may reduce metal loading requirements, which could further improve the economics of FDCA production. However, extended catalyst stability studies, particularly in continuous flow and with realistic feeds containing impurities, are currently lacking. Such studies are needed to inform TEAs and life-cycle assessments and determine the true lifetime cost of different solvent and catalyst systems.

In conclusion, this work develops novel approaches for identifying promising solvents for the oxidative upgrading of HMF to FDCA. Solvent-solute and solvent-solvent interactions have been carefully assessed and discussed, providing a three-step approach for selecting high solubility aqueous/organic solvent blends. First, molecular geometries and physiochemical properties are considered based on HSPs, followed by a minimization of excess enthalpy. Finally, the Hansen $R_{i,j}$ parameter is minimized to determine the ratio of water to organic in the specified

system. The effects of different solvents on reaction progress were also studied, identifying sulfolane/water systems as extremely promising for both high-concentration HMF oxidation, but also one-pot or continuous flow upgrading of biomass directly to FDCA. These combined findings represent potential for reduced cost of commercial FDCA production, and if successfully applied could help bridge the gap between laboratory-scale innovation and industrial-scale sustainability, ultimately bringing bioplastics like PEF into mainstream use. Such a transition from the petroleum-based economy to a bio-based one could reduce carbon emissions and pollution, improving the environmental impact of necessary materials like plastics.

REFERENCES CITED

1. T. P. Werpy, G.; Aden, A.; Bozell, J.; Holladay, J.; White, J.; Manheim, A., *Journal*, 2004, **1**.
2. J. J. Bozell and G. R. Petersen, *Green Chem*, 2010, **12**, 539-554.
3. M. Tamoor, N. A. Samak, M. H. Yang and J. M. Xing, *Molecules*, 2022, **27**.
4. R. Geyer, J. R. Jambeck and K. L. Law, *Sci Adv*, 2017, **3**, e1700782.
5. A. Jasi, *Journal*, 2019, **July/August 2019**, 21.
6. J. Louw, S. Farzad and J. F. Görgens, *Biofuel Bioprod Bior*, 2023, **17**, 135-152.
7. E. de Jong, H. A. Visser, A. S. Dias, C. Harvey and G.-J. M. Gruter, *Polymers-Basel*, 2022, **14**, 943.
8. J. G. Rosenboom, D. K. Hohl, P. Fleckenstein, G. Storti and M. Morbidelli, *Nat Commun*, 2018, **9**.
9. J. K. Schachter, R., *Journal*, 2022.
10. Y. D. Cui, C.; Fan, L.; Qiu, Y.; Zhao, L., *Green Chem*, 2023, **25**, 5836-5857.
11. A. Dormer, D. P. Finn, P. Ward and J. Cullen, *Journal of Cleaner Production*, 2013, **51**, 133-141.
12. A. J. J. E. Eerhart, A. P. C. Faaij and M. K. Patel, *Energ Environ Sci*, 2012, **5**, 6407-6422.
13. A. Al Ghatta, J. D. E. T. Wilton-Ely and J. P. Hallett, *Green Chem*, 2021, **23**, 1716-1733.
14. N. Poulopoulou, D. Smyrnioti, G. N. Nikolaidis, I. Tsitsimaka, E. Christodoulou, D. N. Bikiaris, M. A. Charitopoulou, D. S. Achilias, M. Kapnisti and G. Z. Papageorgiou, *Polymers-Basel*, 2020, **12**.
15. S. K. Burgess, J. E. Leisen, B. E. Kraftschik, C. R. Mubarak, R. M. Kriegel and W. J. Koros, *Macromolecules*, 2014, **47**, 1383-1391.

16. V. P. Kashparova, D. V. Chernysheva, V. A. Klushin, V. E. Andreeva, O. A. Kravchenko and N. V. Smirnova, *Russ Chem Rev+*, 2021, **90**, 750-784.

17. O. Casanova, S. Iborra and A. Corma, *ChemSusChem: Chemistry & Sustainability Energy & Materials*, 2009, **2**, 1138-1144.

18. S. E. Davis, A. D. Benavidez, R. W. Gosselink, J. H. Bitter, K. P. De Jong, A. K. Datye and R. J. Davis, *J. Mol. Catal. A: Chem.*, 2014, **388**, 123-132.

19. L. Zheng, J. Zhao, Z. Du, B. Zong and H. Liu, *Sci. China Chem.*, 2017, **60**, 950-957.

20. S. Somsri, A. Prasertsab, P. Pornsetmetakul, N. Maineawklang, M. T. Nguyen, T. Yonezawa and C. Wattanakit, *Microporous Mesoporous Mater.*, 2023, **354**, 112559.

21. J. Zhang, P. Chen, H. Liu, R. Zhang, W. Jia, J. Zhang and L. Peng, *Appl. Catal., A*, 2024, **676**, 119663.

22. 1951.

23. C. Chen, L. Wang, B. Zhu, Z. Zhou, S. I. El-Hout, J. Yang and J. Zhang, *J. Energy Chem.*, 2021, **54**, 528-554.

24. J. Cai, K. Li and S. Wu, *Biomass Bioenergy*, 2022, **158**, 106358.

25. S. K. Prasad, A. J.; Narishetty, V.; Kumar, V.; Dutta, S.; Ahmad, E., *Mater Sci Energy Technol*, 2023, **6**, 501-521.

26. J. M. Molinaro, J. Swartzentruber, Z. T. Fredericks, V. W. Ledger, D. Alonso and S. G. Wettstein, *EES Catalysis*, 2025.

27. A. H. Motagamwala, W. Y. Won, C. Sener, D. M. Alonso, C. T. Maravelias and J. A. Dumesic, *Sci Adv*, 2018, **4**, eaap9722.

28. Y. Z. Zhang, X. Guo, P. Tang and J. Xu, *J Chem Eng Data*, 2018, **63**, 1316-1324.

29. N. H. Zhuang, J. C. Wang, S. Ma, Q. Liu, W. L. Jia, X. Yu, Z. Li, S. L. Yang, Y. Sun, X. Tang, X. H. Zeng and L. Lin, *J Chem Eng Data*, 2023, DOI: 10.1021/acs.jced.2c00730.

30. H. B. Rose, T. Greinert, C. Held, G. Sadowski and A. S. Bommarius, *J Chem Eng Data*, 2018, **63**, 1460-1470.

31. H. P. Ban, T.; Cheng, Y.; Wang, L.; Li, X., *J Chem Eng Data*, 2018, **63**, 1987-1993.

32. J. M. Molinaro, M. R. Carroll, A. S. Young and S. G. Wettstein, *ACS Omega*, 2024, **9**, 30708–30716.

33. S. M. Payne and F. M. Kerton, *Green Chem*, 2010, **12**, 1648-1653.

34. C. Megías-Sayago, A. Lolli, S. Ivanova, S. Albonetti, F. Cavani and J. A. Odriozola, *Catal Today*, 2019, **333**, 169-175.

35. L. Sanabria, C. Lederhos, M. Quiroga, J. Cubillos, H. Rojas and J. J. Martinez, *Ing Compet*, 2017, **19**, 37-43.

36. G. Y. Ryu, D. Park, Y. Jo, C. C. Truong, D. K. Mishra and Y.-W. Suh, *Biomass Bioenergy*, 2024, **180**, 107022.

37. G. T. Yi, S. P.; Zhang, Y., *Green Chq*, 2016, **18**, 979-983.

38. H. E. Choudhary, K., *Chem. Lett.*, 2016, **45**, 613-615.

39. C. D. Zhou, W.; Wan, X.; Zhang, Q.; Yang, Y.; Wang, Y., *ChemCatChem*, 2015, **7**, 2853-2863.

40. X. G. Han, L.; Guo, Y.; Jia, R.; Liu, X.; Zhang, Y.; Wang, Y., *Green Chem*, 2016, **18**, 1597-1604.

41. X. Z. Wan, C.; Chen, J.; Deng, W.; Zhang, Q.; Yany, Y.; Wang, Y., *ACS Catal.*, 2014, **4**, 2175-2185.

42. A. E. G. Demet, O.; Arletti, R.; Tanchoux, N.; Sougratti, M. T.; Stievano, L.; Quignard, F.; Venti, G.; Perathoner, S.; Di Renzo, F., *Catalysts*, 2022, **12**, 814-839.

43. K. D. W. Rasmussen, H.; Bangs, C.; Petavratzi, E.; Liu, G., *Environmental Science & Technology*, 2019, **53**, 11541-11551.

44. R. Fittig, *Berichte der deutchsen chemischen Gesellschaft*, 1876, **9**, 1189-1199.

45. E. E. Harris, E. Beglinger, G. J. Hajny and E. C. Sherrard, *Ind Eng Chem*, 1945, **37**, 12-23.

46. F. N. Peters Jr, *Industrial & Engineering Chemistry*, 1939, **31**, 178-180.

47. K. Laird, *Journal*, 2011.

48. C. Group, Carlsberg makes bio-based and fully recyclable bottles available to consumers in its largest ever trial, (accessed 24 March, 2024).

49. J. Y. Lang, N. Wang, X. H. Wang, Y. L. Wang, G. R. Chen and H. Zhang, *Bioresources*, 2021, **16**, 7111-7120.

50. Q. Z. Ma, C. Q. Yu, Y. R. Zhou, D. G. Hu, J. B. Chen and X. J. Zhang, *Int J Biol Macromol*, 2024, **256**.

51. H. A. Yamamoto, S.; Hansen, C. M., presented in part at the Hansen Solubility Parameters 50th Anniversary Conference, York, UK, 2017.

52. C. M. Hansen, *Hansen Solubility Parameters: A User's Handbook*, CRC Press, Boca Raton, FL, 2 edn., 2007.

53. C. M. Hansen, Ph. D. Dissertation, Technical University of Denmark, 1967.

54. J. H. Hildebrand and R. L. Scott, *(No Title)*, 1950.

55. J. Hildebrand and R. Scott, *Englewood Cliffs, NJ*, 1962.

56. S. Y. Abbott, H.; Hansen, C. M., *HSPiP Software*, 2020.

57. N. P. Cheremisinoff, *Industrial Solvents Handbook*, CRC Press, Boca Raton, FL, Second edn., 2003.

58. D. Mathieu, *ACS Omega*, 2018, **3**, 17049-17056.

59. A. Eslamimanesh, F. Gharagheizi, A. H. Mohammadi and D. Richon, *Chemical engineering science*, 2011, **66**, 3039-3044.

60. M. A. Sedghamiz, A. Rasoolzadeh and M. R. Rahimpour, *Journal of CO2 Utilization*, 2015, **9**, 39-47.

61. J. Huuskonen, M. Salo and J. Taskinen, *Journal of pharmaceutical sciences*, 1997, **86**, 450-454.

62. E. M. Tosca, R. Bartolucci and P. Magni, *Pharmaceutics*, 2021, **13**, 1101.

63. A. D. Naik and S. S. Bhagwat, *Journal of Chemical & Engineering Data*, 2005, **50**, 460-467.

64. A. L. S. Job, S. M.; Umhey, C. E.; Hoo, K. A.; Wettstein, S. G., *ACS Sustain. Chem. Eng.*, 2022, **10**, 177-181.

65. O. M. Akpa and E. I. Unuabonah, *Desalination*, 2011, **272**, 20-26.

66. S. Fogler, *Elements of Chemical Reaction Engineering*, Prentice Hall, 5 edn., 2006.

67. J. Stanley, Z. Terzopoulou, P. A. Klonos, A. Zamboulis, E. Xanthopoulou, S. Koltsakidis, D. Tzetzis, L. F. Zemljič, D. A. Lambropoulou, A. Kyritsis, G. Z. Papageorgiou and D. N. Bikiaris, *Polymers-Basel*, 2023, **15**, 2707.

68. E. C. Forestier, C.; Guigo, N.; Sbirrazzuoli, N., *Polymers-Basel*, 2023, **15**, 661-678.

69. M. Plum et al., Case Studies Based on Peer-reviewed Life Cycle Assessments - Carbon Footprints on Different Renevwable Carbon-based Chemicals and Materials, https://renewable-carbon.eu/publications/product/rci-scientific-background-report-2023/, (accessed October 13, 2024).

70. P. Lokhande, K. Sonone and P. L. Dhepe, *New J. Chem.*, 2023, **47**, 15325-15335.

71. P. Stegmann, T. Gerritse, L. Shen, M. Londo, Á. Puente and M. Junginger, *J. Cleaner Prod.*, 2023, **395**, 136426.

72. Y. Lu, C. Lin, H. Yang, P. Ma, J. Chen, Z. He, H. Wu, F. Cao, K. Chen and P. Ouyang, *Biomass Convers. Biorefin.*, 2024, **14**, 20105-20115.

73. X. Zuo, P. Venkitasubramanian, D. H. Busch and B. Subramaniam, *ACS Sustain. Chem. Eng.*, 2016, **4**, 3659-3668.

74. C. Chen, M. Lv, H. Hu, L. Huai, B. Zhu, S. Fan, Q. Wang and J. Zhang, *Advanced Materials*, 2024, **36**, 2311464.

75. M. G. Davidson, S. Elgie, S. Parsons and T. J. Young, *Green Chem*, 2021, **23**, 3154-3171.

76. H. Kim, S. Baek and W. Won, *Renew. Sust. Energ. Rev.*, 2022, **157**, 112059.

77. S. Li, S. Wang, Y. Wang, J. He, K. Li, Y. Xu, M. Wang, S. Zhao, X. Li and X. Zhong, *Adv. Funct. Mater.*, 2023, **33**, 2214488.

78. Y. Peng, B. Qiu, S. Ding, M. Hu, Y. Zhang, Y. Jiao, X. Fan and C. M. Parlett, *ChemPlusChem*, 2024, **89**, e202300545.

79. K. Wadaugsorn, K.-Y. Lin, A. Kaewchada and A. Jaree, *RSC Adv.*, 2022, **12**, 18084-18092.

80. Y. Wei, C. Li, C. Zhu, Y. Zhang, Z. Zhu, Y. Chen, X. Li and Y. Yan, *J. Taiwan Inst. Chem. Eng.*, 2022, **138**, 104439.

81. K. T. V. Rao, Y. Hu, Z. Yuan, Y. Zhang and C. C. Xu, *Chem. Eng. J.*, 2021, **404**, 127063.

82. W. Guan, Y. Zhang, Y. Chen, J. Wu, Y. Cao, Y. Wei and P. Huo, *J. Catal.*, 2021, **396**, 40-53.

83. M. Mani, M. Mariyaselvakumar, S. Tothadi, A. B. Panda, K. Srinivasan and L. J. Konwar, *Mol. Catal.*, 2024, **554**, 113811.

84. D. Gao, F. Fang, G. I. Waterhouse, F. Han and Y. Li, *Catal. Sci. Technol.*, 2024, **14**, 1191-1200.

85. S. Hameed, W. Liu, Z. Yu, J. Pang, W. Luo and A. Wang, *Green Chem*, 2024, **26**, 7806-7817.

86. G. Lin, W. Lin, J. Wu, Y. Zhan, F. Okejiri, M. Weng and J. Fu, *Chem. Eng. Sci.*, 2022, **249**, 117343.

87. Y. Jin, S. Sarina, H. Liu, W. Martens, E. R. Waclawik, E. Peiris, J. Jia, J. Shang, L. Kou and C. Guo, *ACS Catalysis*, 2022, **12**, 11226-11238.

88. N. Thiensuwan, S. Sankaranarayanan, T. Yokoi and C. Ngamcharussrivichai, *ACS Sustainable Chemistry & Engineering*, 2023, **11**, 11424-11436.

89. Clarivate, Web of Science, (accessed January 25, 2025).

90. J. Kim, J.-C. Kim, Y.-M. Cho, C.-H. Yoon, H. W. Kwak, J.-H. Choi, H. Kim and I.-G. Choi, *Biomass Bioenergy*, 2024, **181**, 107049.

91. L. Yu, H. Chen, Z. Wen, X. Ma, Y. Li and Y. Li, *Ind. Eng. Chem. Res.*, 2021, **60**, 13485-13491.

92. Z. Ma, L. Wang, G. Li and T. Song, *Catalysts*, 2024, **14**, 157.

93. F. Pardo Pardo, H. Oorts, A. M. Urtiaga Mendia, J. Esteban Serrano and G. Zarca Lago, *J. Mol. Liq.*, 2024, **409**.

94. G. Nawaz, M. Fatima, Z. Ahmad, K. S. Joya, M. A. Assiri, S. I. A. Shah, F. Yasmeen and M. N. Khan, *Fuel*, 2024, **362**, 130828.

95. W. Wang, H. Xu, T. Sang, D. Ji, J. Hao and Z. Li, *Chem. Commun.*, 2024, **60**, 4214-4217.

96. T. Wei, W. Liu, S. Zhang, Q. Liu, J. Luo and X. Liu, *Chem. Commun.*, 2023, **59**, 442-445.

97. Z. Lin, L. Wang, T. Jia, X. Wang, C. Li, H. Wang, L. Li, Y. Zhou, C. Zhai and H. Tao, *Chem. Eng. J.*, 2024, **481**, 148429.

98. Y. Wang, H. Chen, Y. Tang and Y. Li, *Int. J. Hydrogen Energy* 2024.

99. Y. Lin, H. Wang, Y. Zhou and Y. Wu, *J. Mol. Struct.*, 2025, **1322**, 140404.

100. M. Umair, C. M. Pecoraro, F. Di Franco, M. Santamaria, L. Palmisano, V. Loddo and M. Bellardita, *Sustainable Mater. Technol.*, 2025, **43**, e01188.

101. S. G. Chen, X.; Ban, H.; Pan, T.; Zheng, L.; Cheng, Y.; Wang, L.; Li, X., *Ind. Eng. Chem. Res.*, 2021, **60**, 16887-16898.

102. L. Yang, J. Liu, F. Cheng, S. Zhou, Q. Xu, D. Yin and X. Liu, *Renewable Energy*, 2024, **226**, 120409.

103. S. Das, G. Cibin and R. I. Walton, *ACS Sustain. Chem. Eng.*, 2024, **12**, 5575-5585.

104. B. S. Rao, M. J. Hidajat, G.-N. Yun and D. W. Hwang, *Catal. Sci. Technol.*, 2023, **13**, 6921-6936.

105. G. Chen, L. Zheng, Q. Sun and B. Zong, *Mol. Catal.*, 2024, **552**, 113677.

106. J. Xie, J. Nie and H. Liu, *Chin. J. Catal.*, 2014, **35**, 937-944.

107. Z. Li, E. Du, P. Hao, L. Huai, Y. Zhong, S. I. El-Hout, C. Chen and J. Zhang, *Catal Today*, 2023, **423**, 114277.

108. Q. Hou, T. Gao, H. Zhang, Q. Tang and W. Fang, *Catal Today*, 2025, **443**, 114990.

109. J. O. P. Broekman and P. J. Deuss, *Organometallics*, 2024.

110. M.-K. Ke, Y. Min, S.-C. Mei, H.-W. Zeng, Z.-H. Wang, T.-W. Hua, J.-J. Chen, G.-X. Huang and H.-Q. Yu, *Appl. Catal., B*, 2024, **358**, 124431.

111. S. Kar, Q.-Q. Zhou, Y. Ben-David and D. Milstein, *J. Am. Chem. Soc.*, 2022, **144**, 1288-1295.

112. D. Zhao, T. Su, Y. Wang, R. S. Varma and C. Len, *Mol. Catal.*, 2020, **495**, 111133.

113. A. Laurell Nash, R. Hertzberg, Y. Q. Wen, B. Dahlgren, T. Brinck and C. Moberg, *Chem. Eur. J.*, 2016, **22**, 3821-3829.

114. Z. Zhang, B. Liu, K. Lv, J. Sun and K. Deng, *Green Chem*, 2014, **16**, 2762-2770.

115. D. Zeng, W. Wang, B. Cui, B. Jiang, C. Zhang, L. Zhang and W. Wang, *Fuel*, 2025, **381**, 133238.

116. S. Zhang, G. Chu, S. Wang, J. Ma and C. Wang, *Molecules*, 2024, **29**, 3213.

117. B. Chen, Y. Abe, H. Guo and R. L. Smith Jr, *Fuel*, 2024, **376**, 132745.

118. E. J. de Boed, H. L. Nolten, N. Masoud, R. Vogel, F. Wang, Z. Xu, E. J. Doskocil, B. Donoeva and P. E. de Jongh, *ChemCatChem*, 2024, **16**, e202301436.

119. K. R. Vuyyuru and P. Strasser, *Catal Today*, 2012, **195**, 144-154.

120. S. E. Davis, L. R. Houk, E. C. Tamargo, A. K. Datye and R. J. Davis, *Catal Today*, 2011, **160**, 55-60.

121. H. Moradi, S. A. Kulinich, W. Wunderlich and M. Ghiaci, *ChemistrySelect*, 2024, **9**, e202303246.

122. J. Su, Z. Liu, Y. Tan, Y. Xiao, N. Zhan and Y. Ding, *Molecules*, 2024, **29**, 2724.

123. T. Seehamongkol, B. Rungtaweevoranit, P. Chakthranont, T. Butburee, W. Nimsaila and K. Faungnawakij, *ChemNanoMat*, 2024, **10**, e202400037.

124. S. Zhang, Y. Yang, G. Chu, S. Wang, C. Wang, Y. Zhang, L. Zhang and J. Mei, *Chem. Eng. J.*, 2023, **474**, 145670.

125. V. Parmon, V. Simagina and L. Milova, *Catalysis in Industry*, 2010, **2**, 199-205.

126. J. D. Hayler, D. K. Leahy and E. M. Simmons, *Organometallics*, 2018, **38**, 36-46.

127. S. E. Davis, B. N. Zope and R. J. Davis, *Green Chem*, 2012, **14**, 143-147.

128. C. Yang, X. Li, Z. Zhang, B. Lv, J. Li, Z. Liu, W. Zhu, F. Tao, G. Lv and Y. Yang, *Fuel*, 2020, **278**, 118361.

129. C. Chen, X. Li, L. Wang, T. Liang, L. Wang, Y. Zhang and J. Zhang, *ACS Sustainable Chem. Eng.*, 2017, **5**, 11300-11306.

130. Y. Zhao, J. Baeza, N. K. Rao, L. Calvo, M. Gilarranz, Y. Li and L. Lefferts, *J. Catal.*, 2014, **318**, 162-169.

131. K. D. Baugh and P. L. McCarty, *Biotechnol. Bioeng.*, 1988, **31**, 50-61.

132. T. S. Kharlamova, K. L. Timofeev, D. P. Morilov, M. A. Salaev, A. I. Stadnichenko, O. A. Stonkus and O. V. Vodyankina, *React. Chem. Eng.*, 2024, **9**, 2691-2709.

133. S. Xie, H. Tsunoyama, W. Kurashige, Y. Negishi and T. Tsukuda, *ACS Catal.*, 2012, **2**, 1519-1523.

134. R. Zanella and C. Louis, *Catal Today*, 2005, **107**, 768-777.

135. S. K. Perumal, S. Lee, H. Yu, J. Heo, M. J. Kang, Y. Kim, M. Park, H. Lee and H. S. Kim, *ACS Appl. Mater. Interfaces*, 2024, **16**, 7353-7363.

136. R. Mu, Z.-j. Zhao, Z. Dohnálek and J. Gong, *Chem. Soc. Rev.*, 2017, **46**, 1785-1806.

137. A. Ruiz Puigdollers, P. Schlexer, S. Tosoni and G. Pacchioni, *ACS Catal.*, 2017, **7**, 6493-6513.

138. H. Metiu, S. Chrétien, Z. Hu, B. Li and X. Sun, *J. Phys. Chem. C*, 2012, **116**, 10439-10450.

139. I. Herlina, Y. K. Krisnandi and M. Ridwan, *S. Afr. J. Chem. Eng.*, 2024, **47**, 75-82.

140. D. Gao, F. Han, G. I. Waterhouse, Y. Li and L. Zhang, *Biomass Convers. Biorefin.*, 2024, **14**, 13707-13719.

141. Y. Gao, S. Fan, B. Zhu, S. I. El-Hout, J. Lyu, J. Zhang and C. Chen, *Catal Today*, 2024, **440**, 114847.

142. M. Rao, M. Wang, X. Zheng, D. Pan, C. Hong, K. Chen and L. Lin, *Chem. Eng. Sci.*, 2022, **262**, 118004.

143. M. Zhang, P. Che, H. Ma, X. Liu, S. Zhang, Y. Luo and J. Xu, *Chinese Journal of Catalysis*, 2024, **67**, 144-156.

144. Q. Zhang, A. Chen, W. Pan and H. Zhu, *New J. Chem.*, 2024, **48**, 4054-4062.

145. Z. Wang, S. Xia, X. Wang, Y. Fan, K. Zhao, S. Wang, Z. Zhao and A. Zheng, *Renew. Sust. Energ. Rev.*, 2024, **196**, 114332.

146. H. S. Le, Z. Said, M. T. Pham, T. H. Le, I. Veza, B. Deepanraj and L. H. Nguyen, *Fuel*, 2022, **324**, 124474.

147. Y. Wang, C. A. Brown and R. Chen, *AIMS Microbiol.*, 2018, **4**, 261.

148. M. J. Antal Jr, W. S. Mok and G. N. Richards, *Carbohydr. Res.*, 1990, **199**, 91-109.

149. J. E. Romo, N. V. Bollar, C. J. Zimmermann and S. G. Wettstein, *ChemCatChem*, 2018, **10**, 4805-4816.

150. S. G. Wettstein, D. M. Alonso, E. I. Gürbüz and J. A. Dumesic, *Curr. Opin. Chem. Eng.*, 2012, **1**, 218-224.

151. Y. Román-Leshkov and J. A. Dumesic, *Top. Catal.*, 2009, **52**, 297-303.

152. Y. Román-Leshkov, J. N. Chheda and J. A. Dumesic, *Science*, 2006, **312**, 1933-1937.

153. J. Iglesias, I. Martínez-Salazar, P. Maireles-Torres, D. M. Alonso, d. R. Mariscal and M. L. Granados, *Chem. Soc. Rev.*, 2020, **49**, 5704-5771.

154. L. Yu, J. Mao, Y. Chen, G. Zhang and X. Chen, *Catal. Lett.*, 2024, **154**, 5555-5560.

155. B. Tharat, L. Ngamwongwan, T. Seehamongkol, B. Rungtaweevoranit, J. Nonkumwong, S. Suthirakun, K. Faungnawakij, N. Chanlek, A. Plucksacholatarn and W. Nimsaila, *Nanoscale*, 2024, **16**, 678-690.

156. M. J. Kamlet, J. L. M. Abboud, M. H. Abraham and R. Taft, *J. Org. Chem.*, 1983, **48**, 2877-2887.

157. J. Liu, F. Cheng, S. Zhou, L. Zhu, Q. Xu, D. Yin and X. Liu, *Mol. Catal.*, 2024, **560**, 114141.

158. L. Xu, J. Fu, C. Du, Q. Xu, B. Liu and Z. Bao, *Processes*, 2022, **10**, 2480.

159. R. Stenutz, Kamlet-Taft solvent parameters, https://www.stenutz.eu/chem/kamlettaft.php?s=1&p=0, 2024).

160. C. F. Brayton, *Cornell Vet.*, 1986, **76**, 61-90.

161. P. Góralski, *J. Chem. Soc., Faraday Trans. 1*, 1988, **84**, 4311-4316.

162. N. A. Abduh, A. Al-Kahtani, T. S. Algarni and A.-B. Al-Odayni, *Catalysts*, 2023, **13**, 692.

163. C. Y. Y. Wong, A. W.-T. Choi, M. Y. Lui, B. Fridrich, A. K. Horváth, L. T. Mika and I. T. Horváth, *Struct. Chem.*, 2017, **28**, 423-429.

164. H. Qian, Y. He, Q. Hou, C. Xie, R. Lai, G. Yu, T. Xia, X. Bai, H. Xie and M. Ju, *Green Energy Environ.*, 2024.

165. B. Liu, S. Xu, M. Zhang, X. Li, D. Decarolis, Y. Liu, Y. Wang, E. K. Gibson, C. R. A. Catlow and K. Yan, *Green Chem*, 2021, **23**, 4034-4043.

166. M. Zhang, Y. Liu, B. Liu, Z. Chen, H. Xu and K. Yan, *Acs Catalysis*, 2020, **10**, 5179-5189.

167. S. Pandey, M. Mottoul, V. Orsat, J.-F. Morin and M.-J. Dumont, *J. Environ. Chem. Eng.*, 2024, **12**, 112763.

168. S. Bello, P. Méndez-Trelles, E. Rodil, G. Feijoo and M. T. Moreira, *Separation and Purification Technology*, 2020, **233**, 116056.

169. P. Patel, D. Schwartz, X. Wang, R. Lin, O. Ajao and A. Seifitokaldani, *ACS Sustainable Chem. Eng.*, 2022, **10**, 4206-4217.

170. D. Prat, A. Wells, J. Hayler, H. Sneddon, C. R. McElroy, S. Abou-Shehada and P. J. Dunn, *Green Chem*, 2016, **18**, 288-296.

171. S. M. Sen, D. M. Alonso, S. G. Wettstein, E. I. Gürbüz, C. A. Henao, J. A. Dumesic and C. T. Maravelias, *Energ Environ Sci*, 2012, **5**, 9690-9697.

172. T. Tiso, T. Narancic, R. Wei, E. Pollet, N. Beagan, K. Schröder, A. Honak, M. Y. Jiang, S. T. Kenny, N. Wierckx, R. Perrin, L. Avérous, W. Zimmermann, K. O'Connor and L. M. Blank, *Metab Eng*, 2021, **66**, 167-178.

173. A. D. Sánchez-Camargo, M. Bueno, F. Parada-Alfonso, A. Cifuentes and E. Ibáñez, *Trac-Trend Anal Chem*, 2019, **118**, 227-237.

174. E. Behboudi, J. Soleymani, F. Martinez and A. Jouyban, *Phys Chem Liq*, 2022, **60**, 892-909.

175. M. A. Peña-Fernández, G. Spanò, N. S. Torres-Pabón and F. Martínez, *Ars Pharm*, 2023, **64**, 329-341.

176. J. Sha, Z. D. Cao, X. R. Hu, Z. B. Huang, Y. G. Chang, Y. M. Wan, R. R. Sun, G. L. Jiang, H. X. He, Y. Li, T. Li and B. Z. Ren, *J Chem Thermodyn*, 2021, **158**.

177. *Journal*, 2002, **80**, 24.

178. A. Chand and S. Chowdhuri, *J Chem Sci*, 2016, **128**, 991-1001.

179. W. S. MacGregor, New York, NY, 1967.

180. A. Ikeda, C. Abe, W. Matsuura and Y. Hasegawa, *Membranes-Basel*, 2021, **11**.

181. A. Klamt, *The Journal of Physical Chemistry*, 1995, **99**, 2224-2235.

182. A. Klamt, F. Eckert, M. Hornig, M. E. Beck and T. Bürger, *Journal of computational chemistry*, 2002, **23**, 275-281.

183. W. Hu, Z. Shang, N. Wei, B. Hou, J. Gong and Y. Wang, *The Journal of Chemical Thermodynamics*, 2021, **152**, 106272.

184. I. W. Cordova, G. Teixeira, P. J. Ribeiro-Claro, D. O. Abranches, S. P. Pinho, O. Ferreira and J. A. Coutinho, *Industrial & Engineering Chemistry Research*, 2024, **63**, 9565-9575.

185. B. Schröder, L. M. Santos, I. M. Marrucho and J. A. Coutinho, *Fluid Phase Equilibria*, 2010, **289**, 140-147.

186. B. Schröder, L. M. Santos, M. A. Rocha, M. B. Oliveira, I. M. Marrucho and J. A. Coutinho, *Chemosphere*, 2010, **79**, 821-829.

187. S. F. Castilla-Acevedo, A. Pallais-Leclair, D. T. Melfi, P. Bhalode, B. Mellein, A. M. Scurto, D. G. Vlachos and A. M. Allgeier, *Fluid Phase Equilibria*, 2025, **594**, 114355.

188. A. B. Çolak, *International Journal of Energy Research*, 2021, **45**, 478-500.

189. A. Wakisaka and T. Ohki, *Faraday discussions*, 2005, **129**, 231-245.

190. L.-H. ZHU, L. PING and Y. LEI, *Acta Chimica Sinica*, 2005, **63**, 1293.

191. G.-Z. Jia and J.-C. Liu, *Phys Chem Liq*, 2014, **52**, 608-617.

192. D. S. Venables and C. A. Schmuttenmaer, *The Journal of Chemical Physics*, 2000, **113**, 11222-11236.

193. C. Czeslik and J. Jonas, *Chemical physics letters*, 1999, **302**, 633-638.

194. A. Kumar, B. Jhanwar and W. J. Meath, *Collection of Czechoslovak chemical communications*, 2005, **70**, 1196-1224.

195. J. Chen and P. H.-L. Sit, *Chemical Physics*, 2015, **457**, 87-97.

196. H. Kovacs and A. Laaksonen, *Journal of the American Chemical Society*, 1991, **113**, 5596-5605.

197. C. Oldiges, K. Wittler, T. Tönsing and A. Alijah, *The Journal of Physical Chemistry A*, 2002, **106**, 7147-7154.

198. K. L. Rowlen and J. M. Harris, *Analytical chemistry*, 1991, **63**, 964-969.

199. I. Bakó, T. Megyes and G. Pálinkás, *Chemical physics*, 2005, **316**, 235-244.

200. J. Stanley, E. Xanthopoulou, M. Kostoglou, L. Fras Zemljič, D. A. Lambropoulou and D. N. Bikiaris, *Polymers-Basel*, 2024, **16**, 3305.

201. G.-J. Gruter, *Avantium https://www. avantium. com/wp-content/uploads/2019/06/20190606-Technology-Day_CTO_Gert-Jan_Gruter_breakout_final_. pdf*, 2019.

202. V. Kumar, A. Pellis, R. Wimmer, V. Popok, J. d. C. Christiansen and C. Varrone, *ACS Sustainable Chemistry & Engineering*, 2024, **12**, 9658-9668.

203. L. Shuai and J. Luterbacher, *ChemSusChem*, 2016, **9**, 133-155.

204. V. Vasudevan and S. H. Mushrif, *Rsc Advances*, 2015, **5**, 20756-20763.

205. K. Wang, J. Ye, M. Zhou, P. Liu, X. Liang, J. Xu and J. Jiang, *Cellulose*, 2017, **24**, 1383-1394.

206. M. Mikola, J. Ahola and J. Tanskanen, *Chemical Engineering Research and Design*, 2019, **148**, 291-297.

207. C. Liu, M. Wei, F. Wang, L. Wei, X. Yin, J. Jiang and K. Wang, *Journal of the Energy Institute*, 2020, **93**, 1642-1650.

208. M. U. Alzueta, M. Guerrero, Á. Millera, P. Marshall and P. Glarborg, *Proceedings of the Combustion Institute*, 2021, **38**, 575-583.

209. P. Jusner, M. Bacher, H. Hettegger, H. Q. Lê, A. Potthast, H. Sixta and T. Rosenau, *Green Chem*, 2021, **23**, 5832-5848.

210. A. T. Zoghi, M. Shokouhi, M. Abbasghorbani, M. Vahidi, M. Zare and S. Daripour, *International Journal of Thermophysics*, 2020, **41**, 1-16.

APPENDICES

APPENDIX A

SUPPLEMENTAL MATERIALS FOR SOLUBILITY OF 2,5-FURANDICARBOXYLIC ACID IN PURE AND MIXED ORGANIC SOLVENT SYSTEMS AT 293 K PREDICTED USING HANSEN SOLUBILITY PARAMETERS

Error Assessment

Standard deviation was determined for FDCA solubility data found using HPLC analysis. Four solvent blends were prepared in triplicate and assessed for FDCA solubilization. Two of these blends had FDCA solubility below 0.05 g/g and two had FDCA solubility above 0.05 g/g. The standard deviation for each blend was calculated and then converted to relative uncertainty by dividing the standard deviation by the number of samples. These relative uncertainties were then averaged, and for samples with FDCA solubility below 0.05 g/g, a relative uncertainty of 0.061 (or 6.1% error) was determined, and for samples with FDCA solubility above 0.05 g/g, a relative uncertainty of 0.128 (or 12.8% error) was determined. The larger uncertainty in samples that solubilized more FDCA was likely due to the larger amount of dilution required before analysis.

HSP values retrieved from the HSPiP database were only impacted by temperature, varying by 0.1 MPa1/2 with temperature fluctuations of greater than ±2 K. The temperature at the lab bench was recorded twice for a period of four hours each time using an Omega Engineering OM-EL-USB-TC-LCD thermocouple data logger and K-type thermocouple. The temperature at the lab bench were found to only fluctuate by ±0.3 K across 3640 data points collected at 10 second intervals. Similarly, hourly atmospheric pressure data was analyzed and a standard deviation of 0.1 kPa was determined across 72 data points collected at hourly intervals. Thus, HSP values are considered absolute. Mixture values, however, are subject to errors in the massing of solvents and subsequent conversions to volume percentages. A standard uncertainty of 0.2 was found for reported values of $10^2\ w_i$ across 110 samples considered.

MATLAB Code

A MATLAB code was prepared for the purpose of minimizing the $R_{i,j}$ of a specified solvent blend. The code was written using MATLAB version R2023a and was created in such a way that other solvents and solutes can readily be substituted into the program. The complete MATLAB code is listed below (Code 1), with comment statements that instruct the user on its application and modification.

Code 1

```
%Define solvent names as an array
%This section may be edited to account for other solvents of interest:
%Replace the existing solvent names with those of interest in the solventNames vector below
solventNames = ['Solvent 1', 'Solvent 2', 'Solvent 3'];


%Define solvent properties as a matrix: [dD, dP, dH]
%This section may be edited to account for other solvents of interest!
%Replace the existing HSP values with those of interest in the solventProps matrix %below,
keeping in order with the solvent names input above
%Solvent:  dD,   dP,   dH
%Water:  [15.6, 16.0, 42.0;
%MeOH:    14.7, 12.3, 22.3;
%ACN:     15.6, 16.6, 8.30;
%THF:     16.7, 4.90, 5.80;
%EtOH:    15.8, 8.80, 19.4;
```

```
%SULF:    18.1, 16.8, 8.40;
%GBL:     17.5, 15.5, 7.80;
%GVL:     16.8, 11.4, 6.70;
%DMSO:    18.4, 14.6, 8.10];

solventProps = [18.4, 14.6, 8.10;
                16.7, 4.90, 5.80;
                15.6, 16.0, 42.0];
%Input HSP properties are for a sample mix of DMSO, THF, and Water

%Define Objective function: Radius of Interaction
%FDCA's HSP values are hardcoded into the rij function as [19.4, 10.3, 12.9].
% For use with other solutes, these values will need to be altered.
rij = @(weights) sqrt(4 * (19.4 - dot(weights, solventProps(:, 1))).^2 ...
    + (10.3 - dot(weights, solventProps(:, 2))).^2 ...
    + (12.9 - dot(weights, solventProps(:, 3))).^2);

%
% DO NOT EDIT BELOW THIS LINE
%

%Define Constraints
```

```
A = ones(1, numel(solventNames));  % Constraint: Sum of solvent percentages must equal
100%
b = 1;
lb = zeros(size(solventNames));  % Lower bound: 0% for each solvent
ub = ones(size(solventNames));   % Upper bound: 100% for each solvent

%Call fmincon optimization function to minimize the radius of interaction
%Define R_ij primarily as a function of Vol% of solvent
weights = fmincon(rij, ones(size(solventNames))/numel(solventNames), A, b, [], [], lb, ub);

% Display optimized solvent blend
disp('Optimized Solvent Blend (v/v/v):');
for i = 1:numel(solventNames)
    disp([solventNames[i] ': ' num2str(weights(i)*100) '%']);
end
disp(['Minimum Radius of Interaction: ' num2str(rij(weights))]);
```

Additional Tables and Data

Solvent	w_1[a]	$10^2 w_{FDCA}$[b]	δ_D	δ_P	δ_H	$\Delta\delta_T$	$R_{i,j}$
Water	1	0.12	19.4	10.3	12.9	22.1	30.6
ACN	0.20	0.31	15.6	16.1	34.0	15.3	23.2
	0.30	0.51	15.6	16.2	30.1	12.1	19.7
	0.41	0.86	15.6	16.3	26.3	9.2	16.5
	0.51	1.06	15.6	16.3	22.9	6.7	14.0
	0.60	1.22	15.6	16.4	20.0	4.7	12.0
	0.70	1.28	15.6	16.4	17.0	2.9	10.6
	0.80	0.99	15.6	16.5	13.8	1.1	9.9
	0.86	0.77	15.6	16.5	12.2	24.7	9.9
	0.89	0.62	15.6	16.5	11.2	0.1	10.0
	1	0.02	15.6	16.6	8.3	1.2	10.9

Table 18. Experimental Mass Fraction Solubilities of FDCA (w_{FDCA}), HSP Values, and Values of $\Delta\delta_T$ and $R_{i,j}$ in Binary Mixtures of Water and ACN at Varying Organic Mass Fractions (w_{Org}) at $T = 293$ K and $P = 0.1$ MPa.[a]

[a]Standard uncertainties were $u(w_{Org}) = 0.002$, $u(T) = 0.3$ K, $u(P) = 0.1$ kPa and relative uncertainties were $u_r(w_{FDCA}) = 0.061$ (for $10^2 w_{FDCA} < 5$), 0.128 (for $10^2 w_{FDCA} > 5$).

Solvent	w_1[a]	$10^2 w_{FDCA}$[b]	δ_D	δ_P	δ_H	$\Delta\delta_T$	$R_{i,j}$
Water	1	0.12	19.4	10.3	12.9	22.1	30.6
GVL	0.20	0.29	15.8	15.1	35.2	16.0	23.9
	0.30	0.45	16.4	15.6	32.3	14.0	21.0
	0.41	0.92	16.1	14.2	27.9	9.7	16.8
	0.50	1.06	16.2	13.8	24.9	7.2	14.0
	0.60	1.58	16.3	13.3	21.4	4.6	11.0
	0.70	1.83	15.9	12.5	17.5	1.3	8.6
	0.80	2.13	16.5	12.4	14.2	0.4	6.2
	0.84	2.20	16.6	12.2	12.8	1.2	5.9
	0.90	1.90	16.7	11.9	10.5	2.4	6.2
	1	0.19	16.8	11.4	6.7	4.1	8.2

Table 19. Experimental Mass Fraction Solubilities of FDCA (w_{FDCA}), HSP Values, and Values of $\Delta\delta_T$ and $R_{i,j}$ in Binary Mixtures of Water and GVL at Varying Organic Mass Fractions (w_{Org}) at $T = 293$ K and $P = 0.1$ MPa.[a]

[a]Standard uncertainties were $u(w_{Org}) = 0.002$, $u(T) = 0.3$ K, $u(P) = 0.1$ kPa and relative uncertainties were $u_r(w_{FDCA}) = 0.061$ (for $10^2 w_{FDCA} < 5$), 0.128 (for $10^2 w_{FDCA} > 5$).

Solvent	w_1[a]	$10^2 w_{FDCA}$[b]	δ_D	δ_P	δ_H	$\Delta\delta_T$	$R_{i,j}$
Water	1	0.12	19.4	10.3	12.9	22.1	30.6
EtOH	0.20	0.16	15.6	14.3	36.5	16.7	25.1
	0.40	0.50	15.7	12.7	31.7	12.1	20.3
	0.60	1.02	15.7	11.3	27.2	7.9	16.1
	0.79	1.28	15.8	10.0	23.3	4.4	12.7
	0.90	1.16	15.8	9.4	21.3	2.6	11.1
	1	0.92	15.8	8.8	19.4	1.0	9.8

Table 20. Experimental Mass Fraction Solubilities of FDCA (w_{FDCA}), HSP Values, and Values of $\Delta\delta_T$ and $R_{i,j}$ in Binary Mixtures of Water and EtOH at Varying Organic Mass Fractions (w_{Org}) at $T = 293$ K and $P = 0.1$ MPa.[a]

[a]Standard uncertainties were $u(w_{Org}) = 0.002$, $u(T) = 0.3$ K, $u(P) = 0.1$ kPa and relative uncertainties were $u_r(w_{FDCA}) = 0.061$ (for $10^2 w_{FDCA} < 5$), 0.128 (for $10^2 w_{FDCA} > 5$).

Solvent	w_1[a]	$10^2 w_{FDCA}$[b]	δ_D	δ_P	δ_H	$\Delta\delta_T$	$R_{i,j}$
Water	1	0.12	19.4	10.3	12.9	22.1	30.6
GBL	0.21	0.27	16.0	15.9	35.5	16.6	24.3
	0.30	0.45	16.4	15.6	32.7	14.3	21.4
	0.41	0.66	16.3	15.8	28.9	11.3	18.0
	0.51	1.02	16.5	15.8	25.4	8.7	14.8
	0.61	1.42	16.7	15.7	22.1	6.4	12.0
	0.70	1.81	17.2	15.9	19.2	4.4	9.6
	0.80	2.13	17.1	15.6	15.2	2.2	7.4
	0.90	1.87	17.3	15.6	11.7	0.5	6.9
	1	0.21	17.5	15.5	7.8	0.8	8.2

Table 21. Experimental Mass Fraction Solubilities of FDCA (w_{FDCA}), HSP Values, and Values of $\Delta\delta_T$ and $R_{i,j}$ in Binary Mixtures of Water and GBL at Varying Organic Mass Fractions (w_{Org}) at $T = 293$ K and $P = 0.1$ MPa.[a]

[a]Standard uncertainties were $u(w_{Org}) = 0.002$, $u(T) = 0.3$ K, $u(P) = 0.1$ kPa and relative uncertainties were $u_r(w_{FDCA}) = 0.061$ (for $10^2 w_{FDCA} < 5$), 0.128 (for $10^2 w_{FDCA} > 5$).

Solvent	w_1[a]	$10^2 w_{FDCA}$[b]	δ_D	δ_P	δ_H	$\Delta\delta_T$	$R_{i,j}$
Water	1	0.12	19.4	10.3	12.9	22.1	30.6
THF	0.22	0.20	15.8	13.8	34.7	15.1	23.2
	0.33	0.41	15.9	12.6	31.0	11.6	19.6
	0.40	2.09	16.1	11.3	26.5	7.5	15.2
	0.50	3.27	16.1	10.5	24.0	5.3	12.8
	0.60	4.66	16.2	9.7	21.4	3.0	10.6
	0.70	6.10	16.3	8.5	17.7	0.1	8.0
	0.80	7.18	16.5	7.3	13.8	2.8	6.6
	0.90	6.29	16.6	6.2	9.9	5.2	7.6
	1	3.15	16.7	4.9	5.8	7.1	10.4

Table 22. Experimental Mass Fraction Solubilities of FDCA (w_{FDCA}), HSP Values, and Values of $\Delta\delta_T$ and $R_{i,j}$ in Binary Mixtures of Water and THF at Varying Organic Mass Fractions (w_{Org}) at $T = 293$ K and $P = 0.1$ MPa.[a]

[a]Standard uncertainties were $u(w_{Org}) = 0.002$, $u(T) = 0.3$ K, $u(P) = 0.1$ kPa and relative uncertainties were $u_r(w_{FDCA}) = 0.061$ (for $10^2 w_{FDCA} < 5$), 0.128 (for $10^2 w_{FDCA} > 5$).

Solvent	w_1[a]	$10^2 w_{FDCA}$[b]	δ_D	δ_P	δ_H	$\Delta\delta_T$	$R_{i,j}$
Water	1	0.12	19.4	10.3	12.9	22.1	30.6
MeOH	0.20	0.13	15.4	15.1	37.3	17.6	26.1
	0.30	0.18	15.3	14.7	35.1	15.5	24.1
	0.40	0.29	15.2	14.3	33.0	13.6	22.2
	0.50	0.46	15.1	13.9	31.0	11.7	20.4
	0.60	0.65	15.0	13.6	29.2	10.0	18.8
	0.70	0.88	14.9	13.3	27.4	8.4	17.3
	0.80	1.11	14.9	12.9	25.6	6.8	15.8
	0.90	1.32	14.8	12.6	24.0	5.4	14.6
	1	1.59	14.7	12.3	22.3	3.9	13.4

Table 23. Experimental Mass Fraction Solubilities of FDCA (w_{FDCA}), HSP Values, and Values of $\Delta\delta_T$ and $R_{i,j}$ in Binary Mixtures of Water and MeOH at Varying Organic Mass Fractions (w_{Org}) at $T = 293$ K and $P = 0.1$ MPa.[a]

[a]Standard uncertainties were $u(w_{Org}) = 0.002$, $u(T) = 0.3$ K, $u(P) = 0.1$ kPa and relative uncertainties were $u_r(w_{FDCA}) = 0.061$ (for $10^2 w_{FDCA} < 5$), 0.128 (for $10^2 w_{FDCA} > 5$).

Solvent	w_1[a]	$10^2 w_{FDCA}$[b]	δ_D	δ_P	δ_H	$\Delta\delta_T$	$R_{i,j}$
Water	1	0.12	19.4	10.3	12.9	22.1	30.6
SULF	0.21	0.27	16.2	16.2	33.5	17.3	24.9
	0.30	0.29	16.5	16.3	30.5	15.1	22.3
	0.40	0.53	16.6	16.3	27.9	12.8	19.5
	0.48	0.69	16.9	16.4	24.5	10.9	17.1
	0.58	0.95	17.2	16.5	20.3	8.5	14.0
	0.70	1.81	17.5	16.6	16.9	5.9	10.6
	0.79	2.17	17.7	16.7	13.3	4.0	8.4
	0.90	1.11	17.8	16.7	12.6	2.0	7.2
	1	0.00	18.1	16.8	8.4	0.6	8.3

Table 24. Experimental Mass Fraction Solubilities of FDCA (w_{FDCA}), HSP Values, and Values of $\Delta\delta_T$ and $R_{i,j}$ in Binary Mixtures of Water and SULF at Varying Organic Mass Fractions (w_{Org}) at $T = 293$ K and $P = 0.1$ MPa.[a]

[a]Standard uncertainties were $u(w_{Org}) = 0.002$, $u(T) = 0.3$ K, $u(P) = 0.1$ kPa and relative uncertainties were $u_r(w_{FDCA}) = 0.061$ (for $10^2 w_{FDCA} < 5$), 0.128 (for $10^2 w_{FDCA} > 5$).

Solvent	w_1[a]	$10^2 w_{FDCA}$[b]	δ_D	δ_P	δ_H	$\Delta\delta_T$	$R_{i,j}$
Water	1	0.12	19.4	10.3	12.9	22.1	30.6
DMSO	0.20	0.17	16.1	15.7	35.7	16.8	24.4
	0.30	0.28	16.4	15.6	32.5	14.1	21.2
	0.40	0.41	16.7	15.5	29.3	11.6	18.0
	0.50	1.07	16.9	15.3	26.0	9.2	14.9
	0.60	3.93	17.2	15.2	22.3	6.5	11.4
	0.70	9.97	17.5	15.1	19.0	4.4	8.6
	0.88	23.12	18.0	14.8	12.6	1.0	5.3
	1	30.71	18.4	14.6	8.1	0.6	6.7

Table 25. Experimental Mass Fraction Solubilities of FDCA (w_{FDCA}), HSP Values, and Values of $\Delta\delta_T$ and $R_{i,j}$ in Binary Mixtures of Water and DMSO at Varying Organic Mass Fractions (w_{Org}) at $T = 293$ K and $P = 0.1$ MPa.[a]

[a]Standard uncertainties were $u(w_{Org})$ = 0.002, $u(T)$ = 0.3 K, $u(P)$ = 0.1 kPa and relative uncertainties were $u_r(w_{FDCA})$ = 0.061 (for $10^2 w_{FDCA} < 5$), 0.128 (for $10^2 w_{FDCA} > 5$).

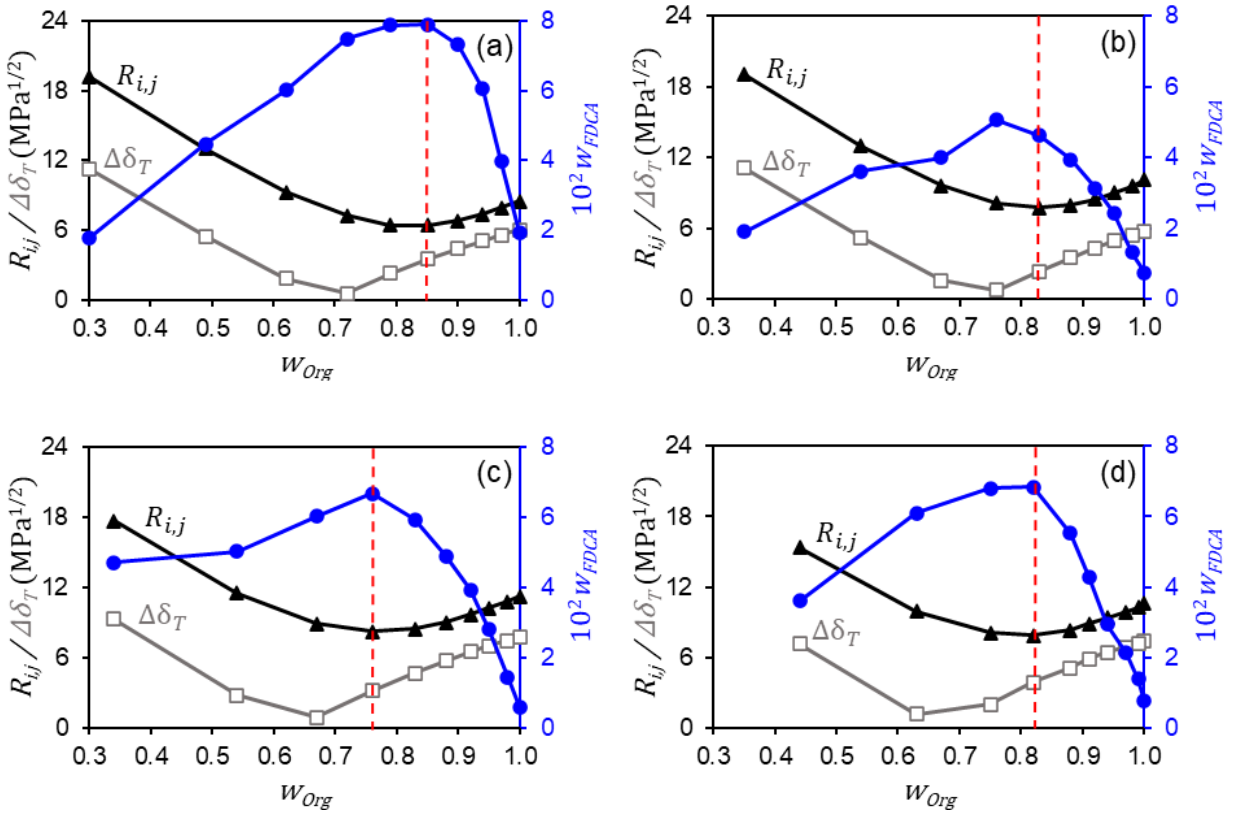

Figure 55. The $R_{i,j}$ (▲), $\Delta\delta_T$ (□), and the mass fraction of FDCA solubilized (w_{FDCA}; ●, secondary axis) collected at 303 K by Zhuang, et al.[29] versus mass fraction organic (w_{Org}) present in binary mixtures of H_2O and (a) THF, (b) 1,4-dioxane, (c) 1,2-dimethoxyethane, and (d) diethylene glycol dimethyl ether. The dashed red line indicates the minima of the $R_{i,j}$ curve (- - -).

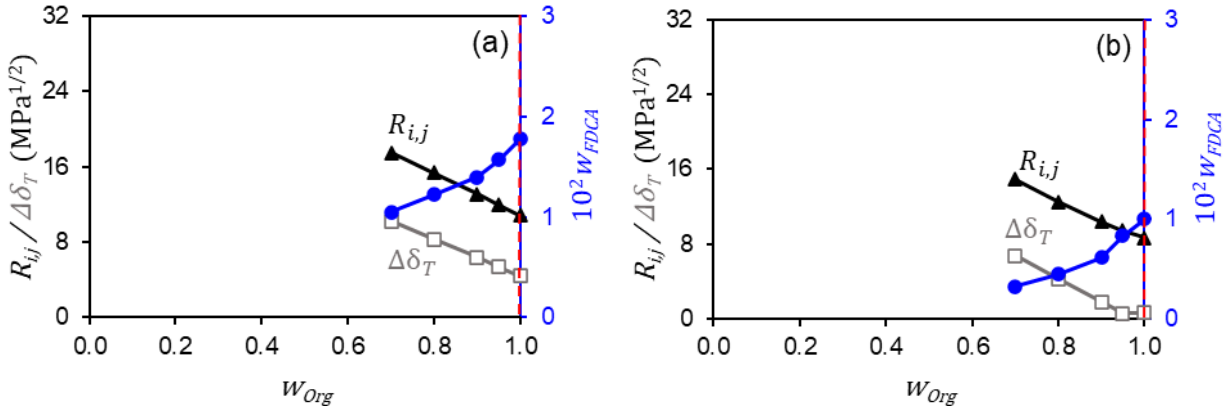

Figure 56. The $R_{i,j}$ (▲), $\Delta\delta_T$ (□), and the mass fraction of FDCA solubilized (w_{FDCA}; ●, secondary axis) collected at (a) 297 K and (b) 299 K by Ban, et al.[31] versus mass fraction organic (w_{Org}) present in binary mixtures of H_2O and (a) MeOH and (b) EtOH. The dashed red line indicates the minima of the $R_{i,j}$ curve (---).

HSP Values at 303 K

Chemical	δ_D	δ_P	δ_H	δ_T
H_2O	15.4	16	41.7	47.2
THF	16.7	5.7	7.9	19.3
DX	17.4	1.8	8.9	19.6
DME	15.3	6.3	6.0	17.6
DGDE	15.6	6.1	6.5	18.0

Table 26. HSP Values for Chemicals Studied by Zhuang et al. at $T = 303$ K and $P = 0.1$ MPa, as Retrieved from the HPSiP Software.[a]
[a]Standard uncertainties were $u(T) = 0.05$ K and $u(P) = 5$ kPa.

Solvent	w_{Org}	$10^2 w_{FDCA}$	$\Delta\delta_T$	$R_{i,j}$	Solvent	w_{Org}	$10^2 w_{FDCA}$	$\Delta\delta_T$	$R_{i,j}$
THF	1	1.93	6.0	8.5	DME	1	0.60	7.8	11.2
	0.97	3.97	5.6	8.0		0.98	1.44	7.4	10.8
	0.94	6.05	5.1	7.4		0.95	2.82	7.0	10.2
	0.90	7.31	4.4	6.8		0.92	3.92	6.5	9.6
	0.85	7.89	3.5	6.4		0.88	4.88	5.7	9.0
	0.79	7.88	2.3	6.4		0.83	5.93	4.7	8.5
	0.72	7.49	0.6	7.3		0.76	6.66	3.2	8.2
	0.62	6.02	1.8	9.3		0.67	6.01	0.9	8.9
	0.49	4.46	5.5	13.0		0.54	5.01	2.8	11.5
	0.30	1.77	11.3	19.2		0.34	4.71	9.3	17.6
DX	1	0.75	5.7	10.1	DGDE	1	0.76	7.4	10.6
	0.98	1.32	5.4	9.6		0.99	1.39	7.1	10.2
	0.95	2.44	4.9	9.0		0.97	2.12	6.8	9.8
	0.92	3.14	4.3	8.5		0.94	2.93	6.4	9.4
	0.88	3.95	3.5	8.0		0.91	4.28	5.9	8.8
	0.83	4.62	2.4	7.7		0.88	5.52	5.1	8.3
	0.76	5.07	0.7	8.1		0.82	6.85	3.9	7.9
	0.67	4.00	1.6	9.6		0.75	6.80	2.0	8.1
	0.54	3.61	5.2	13.0		0.63	6.10	1.2	9.9
	0.35	1.90	11.1	19.1		0.44	3.61	7.1	15.4

Table 27. Solubility ($10^2 w_{FDCA}$) Data Calculated from Zhuang et al. for H_2O/Organic (w_{Org}) Mixtures at 303 K.[29] Temperature Corrected $\Delta\delta_T$ and $R_{i,j}$ Values Calculated from HSP Values Determined Using the HSPiP Software (Table S1).[a]

[a]Standard uncertainties were $u(T)$ = 0.05 K, $u(P)$ = 5 kPa.

Solvent	w_{Org}	$10^2 w_{FDCA}$	$\Delta\delta_T$	$R_{i,j}$	Solvent	w_{Org}	$10^2 w_{FDCA}$	$\Delta\delta_T$	$R_{i,j}$
MeOH	1	1.78	4.4	10.8	EtOH	1	1.00	0.66	8.6
	0.95	1.57	5.4	12.0		0.95	0.83	0.57	9.4
	0.90	1.40	6.4	13.1		0.90	0.61	1.8	10.4
	0.80	1.22	8.3	15.4		0.80	0.45	4.3	12.6
	0.70	1.05	10.2	17.5		0.70	0.32	6.7	14.9

Table 28. Solubility ($10^2 w_{FDCA}$) Data Calculated from Ban et al. for H_2O/Organic (w_{Org}) Mixtures at 303 K. [31] Temperature Corrected $\Delta\delta_T$ and $R_{i,j}$ Values Calculated from HSP Values Determined Using the HSPiP Software.[a]

[a]Standard uncertainties were $u(T)$ = 0.02 K, $u(P)$ = 5 kPa.

Organic/Organic Binary Mixtures

Seven organic/organic systems were also investigated: DMSO/MeOH, DMSO/THF, EtOH/GVL, GVL/DMSO, GVL/MeOH, GVL/THF, and THF/MeOH. The minimum R_(i,j) correlated with the maximum FDCA solubility (Figure S1) or was within the specified uncertainty values for four of the systems but was not within error for the DMSO/MeOH, DMSO/THF, and GVL/THF systems, where neither Δδ_T and R_(i,j) identified the maximum solubility.

For all non-DMSO organic/organic solutions, the maximum FDCA solubilization was less than 0.04 g/g, while the GVL/THF system had higher solubility that correlated with higher R_(i,j). The reason for this is unknown, but the presence of GVL appears to suppress THF's high solubility, decreasing from 0.032 g/g to 0.013 g/g when the GVL mass fraction increases to just 0.10.

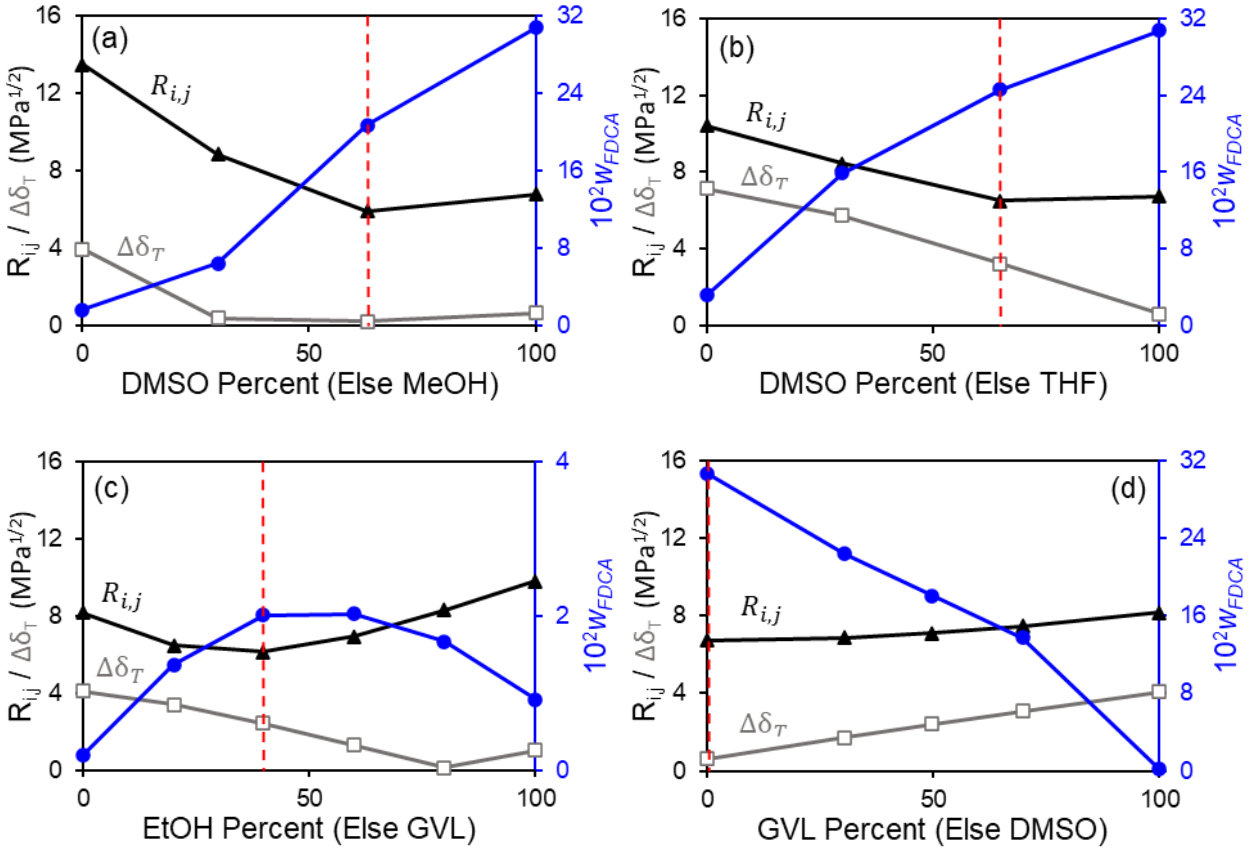
(a)
$R_{i,j}$
$\Delta\delta_T$
$R_{i,j}$ / $\Delta\delta_T$ (MPa$^{1/2}$)
$10^2 w_{FDCA}$
DMSO Percent (Else MeOH)
(b)
$R_{i,j}$
$\Delta\delta_T$
$R_{i,j}$ / $\Delta\delta_T$ (MPa$^{1/2}$)
$10^2 w_{FDCA}$
DMSO Percent (Else THF)
(c)
$R_{i,j}$
$\Delta\delta_T$
$R_{i,j}$ / $\Delta\delta_T$ (MPa$^{1/2}$)
$10^2 w_{FDCA}$
EtOH Percent (Else GVL)
(d)
$R_{i,j}$
$\Delta\delta_T$
$R_{i,j}$ / $\Delta\delta_T$ (MPa$^{1/2}$)
$10^2 w_{FDCA}$
GVL Percent (Else DMSO)

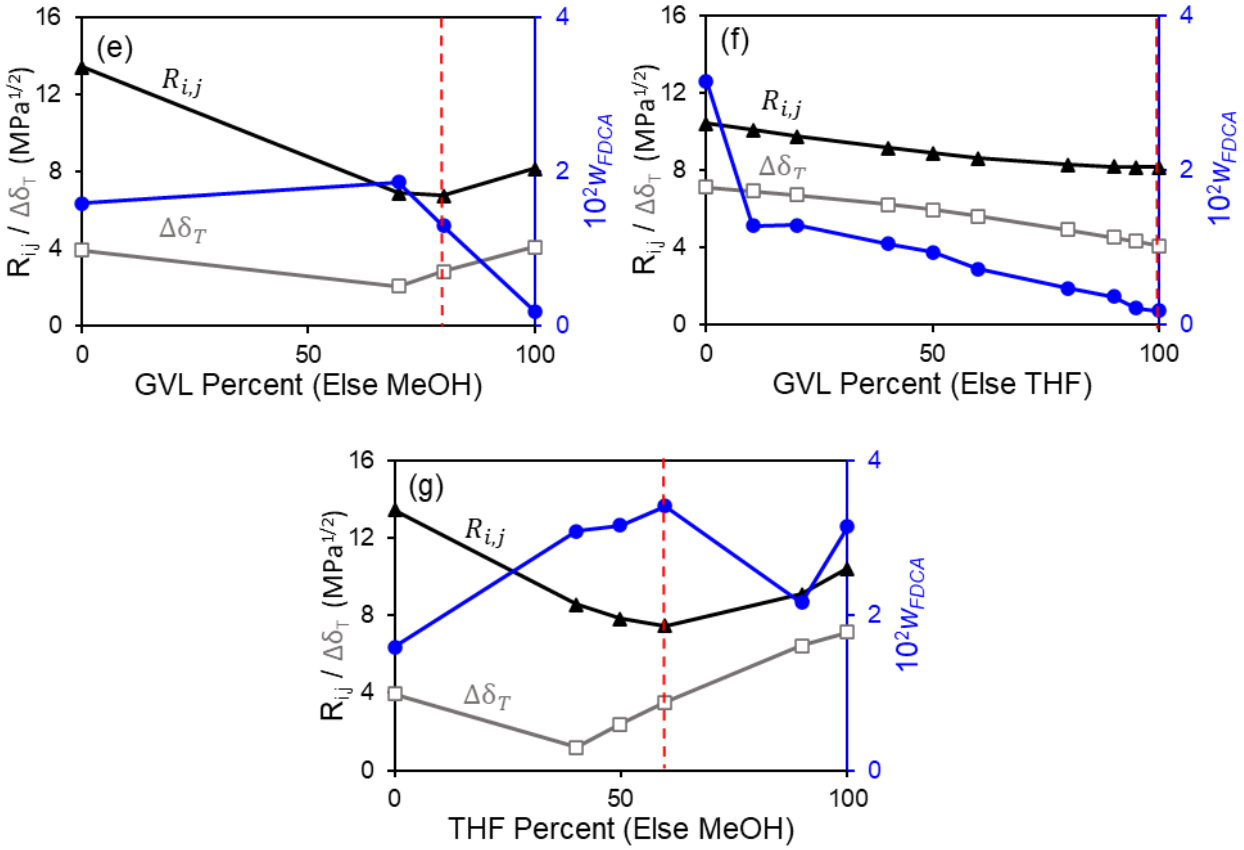

Figure 57. Comparison of solubility, $R_{i,j}$, and $\Delta\delta_T$ in Organic/Organic binary systems. (a) DMSO/MeOH (b) DMSO/THF (c) EtOH /GVL (d) GVL/DMSO (e) GVL/MeOH (f) GVL/THF (g) THF/MeOH. A dashed red line (---) indicates the minimum $R_{i,j}$ to help guide the eye.

Solvent Blend	w_{Org}	$10^2 * w_{FDCA}$	$\Delta\delta_T$	$R_{i,j}$	Solvent Blend	w_{Org}	$10^2 * w_{FDCA}$	$\Delta\delta_T$	$R_{i,j}$
DMSO/ MeOH	0	1.59	3.9	13.4	GVL/MeOH	0	1.59	3.9	13.4
	29.98	6.40	0.4	8.8		69.99	1.87	2.1	6.9
	62.86	20.64	0.2	5.9		79.88	1.30	22.6	6.8
	100	30.71	0.6	6.7		100	0.19	4.1	8.2
DMSO/ THF	0	3.15	7.1	10.4	GVL/THF	0	3.15	7.1	10.4
	29.98	15.90	5.7	8.4		10.31	1.28	6.9	10.1
	64.93	24.60	3.2	6.5		19.98	1.29	6.7	9.8
	100	30.71	0.6	6.7		40.17	1.05	6.2	9.1
EtOH/ GVL	0	0.19	4.1	8.2		49.98	0.94	6.0	8.9
	20.11	1.37	3.4	6.5		60.01	0.73	5.6	8.6
	39.85	2.01	2.4	6.1		79.84	0.48	4.9	8.3
	60.06	2.03	1.3	7.0		89.96	0.37	4.5	8.2
	79.94	1.67	0.1	8.3		94.91	0.22	21.2	8.2
	100	0.92	1.0	9.8		100	0.19	4.1	8.2
GVL/DMSO	0	30.71	0.6	6.7	THF/MeOH	0	1.59	3.9	13.4
	30.50	22.38	1.7	6.9		40.15	3.09	24.3	8.6
	49.80	18.06	2.4	7.1		49.88	3.16	23.1	7.8
	69.80	13.75	3.1	7.5		59.81	3.41	3.5	7.5
	100	0.19	4.1	8.2		89.94	2.17	19.0	9.1

Table 29. Values of $R_{i,j}$ and $\Delta\delta_T$ for Organic-Organic Mixtures at Varying Mass Fractions of Organic 1 (w_{Org}). Data collected at $T = 293$ K and $P = 0.1$ MPa.[a]

[a]Standard uncertainties were $u(w_{Org}) = 0.002$, $u(T) = 0.3$ K, $u(P) = 0.1$ kPa and relative uncertainties were $u_r(w_{FDCA}) = 0.061$ (for $10^2 w_{FDCA} < 5$), 0.128 (for $10^2 w_{FDCA} > 5$).

Org 2	w_{DMSO}	w_{Org}	$10^2 w_{FDCA}$	$R_{i,j}$	Org 2	w_{DMSO}	w_{Org}	$10^2 w_{FDCA}$	$R_{i,j}$
GVL	0.05	0.46	1.58	25.1	SULF	0.40	0.40	10.9	7.1
	0.10	0.41	1.28	21.3		0.60	0.20	9.34	4.3
	0.19	0.41	2.09	14.6		0.50	0.30	9.53	4.5
	0.21	0.28	1.10	16.1	THF	0.05	0.45	1.66	24.4
	0.20	0.60	5.58	8.9		0.05	0.75	2.30	18.4
	0.31	0.20	1.30	12.5		0.10	0.10	0.28	23.3
	0.31	0.40	4.38	8.7		0.21	0.30	1.36	14.4
	0.30	0.50	7.38	5.9		0.20	0.40	2.83	12.9
	0.40	0.10	1.19	14.6		0.20	0.60	3.09	7.6
	0.39	0.12	1.10	10.7		0.30	0.40	5.24	7.7
	0.40	0.20	2.89	11.3		0.30	0.40	6.98	6.6
	0.40	0.20	3.26	9.1		0.30	0.50	16.4	5.5
	0.41	0.30	5.61	7.2		0.40	0.10	1.23	9.2
	0.40	0.40	7.88	5.9		0.40	0.20	3.18	7.6
	0.60	0.20	10.25	4.4		0.40	0.30	8.63	6.8
	0.50	0.30	9.89	4.5		0.40	0.30	6.00	6.0
SULF	0.05	0.45	0.59	25.6		0.40	0.40	13.7	4.7
	0.05	0.75	1.87	20.4		0.50	0.30	15.0	4.5
	0.10	0.11	0.23	24.6		0.59	0.27	20.7	4.2
	0.20	0.30	0.80	17.2		0.60	0.20	17.0	4.5
	0.20	0.41	1.42	14.6					
	0.20	0.60	4.42	10.3					
	0.30	0.40	2.93	9.0					
	0.30	0.50	6.42	6.2					
	0.40	0.10	0.89	12.0					
	0.40	0.21	1.83	8.9					
	0.39	0.31	4.50	7.0					

Table 30. Values of $R_{i,j}$ and FDCA Solubilized ($10^2 w_{FDCA}$) for Ternary H_2O, DMSO (w_{DMSO}), and Secondary Organic (w_{Org}) Mixtures at $T = 293$ K and $P = 0.1$ MPa.[a]

[a]Standard uncertainties were $u(w_{DMSO}, w_{Org}) = 0.002$, $u(T) = 0.3$ K, $u(P) = 0.1$ kPa and relative uncertainties were $u_r(w_{FDCA}) = 0.061$ (for $10^2 w_{FDCA} < 5$), 0.128 (for $10^2 w_{FDCA} > 5$).

APPENDIX B

HMF OXIDATION AND REACTION ANALYSIS PROCEDURE

Parr Reactor Reaction Procedure

1. Ensure proper PPE is worn (glasses and gloves).
2. Retrieve a weigh boat from the weigh supplies drawer.
3. Place the weigh boat on the OHAUS Discovery analytical balance, located in the fume hood in Cobleigh 301 B.
4. Use the Zerostat 3 Milty anti-static device to remove static from the weigh boat.
5. Tare the scale.
6. Go to the small fridge under the lab bench in Cobleigh 301A and retrieve the HMF bottle.
7. Bring the HMF to the fume hood in Cobleigh 301B.
8. Go to the beige shelving unit with sliding glass doors in Cobleigh 301B and retrieve the catalyst. (Typically either 5% Pt/C or MnO_2, both from Thermo Fisher Scientific)
9. Place the catalyst next to the HMF in the fume hood.
10. Open the scale door and weigh the required amount of catalyst into the weigh boat.
11. Place the catalyst in one corner of the weigh boat for easier transfer later.
12. Close the scale door and allow the mass reading to stabilize.
13. Record the catalyst mass in your lab notebook.
14. Return the catalyst container to storage.
15. Tare the scale again.
16. Using a clean scooper, weigh the required amount of HMF directly over the catalyst in the weigh boat.
17. Close the scale door and allow the weight to stabilize.
18. Record the HMF mass in your lab notebook.
19. Place the used scooper in the sink for cleaning.
20. Return the HMF bottle to the fridge.
21. Retrieve the 30 mL Parr reactor (usually in the drying rack).
22. Add a small stir bar (<1 cm) to the reactor.
23. Place the Parr reactor in the fume hood near the balance.

24. Open the balance door and carefully remove the weigh boat containing catalyst and HMF.
25. Remove static from the reactor if needed.
26. Carefully tip the contents of the weigh boat (catalyst and HMF) into the Parr reactor over the stir bar.
27. Set the empty weigh boat aside for rinsing.
28. 28. Get a clean ~20 mL beaker and place it on the analytical balance.
29. Tare the balance.
30. Locate the correct solvent for your reaction.
    - For organic solvents, check the yellow flammables cabinet.
    - If not there, look in the cabinet under the fume hood in 301B. A lot of blended solvents are stored there.
31. Bring the solvent to the fume hood.
32. Use the same dropper throughout the measurement process.
33. Carefully add slightly more than 10 g of solvent to the beaker.
34. Record the mass in your lab notebook.
35. DO NOT TARE THE SCALE.
36. Use the solvent to rinse the weigh boat, collecting any remaining catalyst or HMF into the Parr reactor.
37. Weigh the beaker again.
38. Subtract this final mass from the original to determine how much solvent was transferred.
39. Record the net solvent mass in your lab notebook.
40. Place the beaker in the sink for washing.
41. Dispose of the dropper and weigh boat appropriately (trash is fine).
42. Place the lid securely on the Parr reactor.
43. Attach the two clamshell/collar pieces with six bolts around the lid.
44. Hand-tighten the bolts.
45. Place the solid collar around the clamshell pieces and secure it using the side screw.

46. Use a 9/16" wrench to tighten the top bolts in a star pattern. (Think like changing a tire).
47. Turn the oxygen valve counterclockwise to begin pressurizing the reactor. Make sure that the pressure release valve on the Parr is CLOSED before you do this.
48. Verify the pressure matches between the Parr gauge and the (lefthand) oxygen tank gauge. The lefthand gauge on the green oxygen tank is the value the line is pressurized to, and by proxy the Parr. The righthand gauge is the tank pressure, which should be higher.
49. Once pressurized, close the oxygen valve on the reactor (turn clockwise).
50. Slowly depressurize the reactor by turning the pressure release valve counterclockwise. As a helpful tip, you can use a wrench for control and leverage.
51. Repeat steps 47–50 once more for a second purge.
52. Pressurize the reactor a third and final time to your desired reaction pressure.
53. Record the final reactor pressure in your lab notebook.
54. Walk to the computer in Cobleigh 301A (next to the door that leads to Ryan's lab) and open the EasyLog USB software.
55. Confirm the Omega USB temperature logger is plugged into a USB-A port.
56. Click the green arrow labeled "Set Up and Start USB Data Logger."
57. Enter a reaction name in the dialog box.
58. Set the logging interval to 10 seconds.
59. Set the temperature scale to degrees Celsius.
60. Set the thermocouple type to "K."
61. Click **Next**.
62. Set display to: "LCD on for 30 seconds after button press."
63. Set logger behavior to: "Logger stops when full."
64. Click **Next**.
65. Do not set any alarms. Click **Next** again.
66. Select "Immediate start" and click **Finish**.
67. Confirm the green checkmark and click **OK**.

68. Remove the USB logger from the computer.
69. Bring the logger to the fume hood.
70. Align the "+" and "–" prongs on the logger with the thermocouple prongs and plug them in. The thermocouple that plugs in is currently yellow (3/2025), but if you're using these instructions sometime in the future that may have changed.
71. Secure the USB logger to the wall using the Velcro so it is out of the way.
72. Insert both thermocouples prongs (the thin wire-like portions of the yellow USB thermocouple and the brown temperature controller thermocouple) into the probe port on the Parr reactor.
73. Place the Parr reactor into the heating jacket on the stir plate.
74. Align the bottom of the reactor with the marked circle (smiley face!) to ensure proper mixing.
75. Turn on the Omega CN7500 temperature controller (toggle switch on back).
    - The "|" symbol should be depressed; display should light up.
76. Turn on the stir plate and set stirring speed to 1000 RPM.
77. Use the laminated instructions (bottom-right corner of the fume hood) to program the controller. Alternatively, see below:

    1. **To set pattern:**

        1. Press and hold  for 3 seconds.
        2. Press  until "Ctrl" appears.
        3. Using arrows, select "Prog" and press  to set.
        4. Press  once — display will show "PAtn."
        5. Adjust program number with arrows.
        6. Press , set temp to ramp to with arrows, then press .
        7. Press , set time in hh:mm with arrows, then press  (in minute increments).
        8. Press , set temp at soak with arrows, then press .

9. Press , set time in hh:mm with arrows, then press .
10. Continue until the program is complete (leave unnecessary steps as zeroes).
11. Ensure “link” is set to “off.”
12. Press to exit.

2. To select pattern:

1. Press to see “r–S” and arrow to “stop,” then press .
2. Press until “Ptrn” appears, and select # with arrows, then press .
3. Press to see “r–S” and arrow to “run,” then press .
4. Press to exit.

3. To adjust display during program run:

1. Use up and down arrows, then press .
2. Options: Temperature set point (SP), Program step (X–XX), Remaining time for a given step (H:MM)

78. Start the program once entered.
79. Turn on the fume hood fan and turn off the hood light.
80. Record:
    - Reaction start time
    - Ramp-up end time
    - Reaction end time in your lab notebook.

<u>Reactor Effluent Analysis</u>

1. If you’re not wearing PPE (goggles, gloves), go put them on.
2. Once the reaction has completed, remove the Parr reactor from the heating jacket and return it to the stir plate to cool.

3. Use the house compressed air line in the fume hood to blow air across the base of the reactor and speed cooling.
    - You can clip the air hose in place to keep it directed at the reactor.
4. Handle the reactor carefully. It may be very hot.
5. Wait until the reactor has cooled below 30°C before opening or depressurizing.
6. While waiting, retrieve the Omega USB temperature logger and take it to the computer in Cobleigh 301A.
7. Plug it into a USB-A port, then in EasyLog USB software, click the red arrow icon labeled “Stop the USB Data Logger and Download Data.”
8. When prompted, click Yes to confirm.
9. In the pop-up with the stop sign icon, click OK.
10. Save the exported .txt file with an appropriate reaction name. Typically something like: 032725_2H_5Pt, as this indicates the date, HMF concentration, and catalyst type.
11. A graph of temperature over time will appear — you may close this window.
12. Open the saved text file from your recent files list or file explorer.
13. Copy and paste the data into the Reaction Temperature Data spreadsheet.
14. Name your Excel sheet tab with the reaction name.
15. If a template isn’t already available in another tab, manually record the following:
    - Start of temperature ramp-up (time)
    - End of temperature ramp-up (time)
    - End of reaction (time)
16. Highlight the ramp-up end and reaction end cells in yellow for easier reference.
17. Calculate the total reaction time, then average temperature using Excel’s ‘AVERAGE()’ formula
18. Record the total reaction time and average temperature in your lab notebook.
19. Meanwhile, begin collecting the necessary glassware for effluent analysis.
    - 250 mL Erlenmeyer flask

- Ceramic vacuum filter
- Two Whatman 44, 70 mm filter papers
- Two 100 mL volumetric flasks (for DI water)
- 50 mL beaker
- 10 mL pipette and pipette bulb
- 0.5-5 mL auto pipette (thumb push style)
- 100–1000 µL auto pipette

20. Turn on the fume hood fan and light if they are off.
21. Check and record the final reactor pressure from the Parr pressure gauge in your lab notebook.
22. Slowly depressurize the reactor by turning the pressure release valve counterclockwise.
    - Use a 9/16" wrench for control if needed.
23. Once fully depressurized, use the wrench to loosen the top bolts of the Parr collar.
24. Unscrew the side screw of the solid circular collar.
25. Remove both collar pieces.
26. Leave the Parr reactor resting in the fume hood, covered, until the filtration system setup is complete (Steps 27 – 30). IF you need to pull an unrinsed sample, do so now before proceeding to Step 27.
27. Set up your filtration system:
    - Attach the 250 mL Erlenmeyer flask to house vacuum via rubber tubing.
    - Insert the ceramic vacuum filter into the flask mouth.
28. Fold and cut the two 70 mm filter papers so they fit the ceramic filter snugly.
    - Stagger the folds to prevent catalyst getting through.
29. Fill both 100 mL volumetric flasks with DI water up to the neckline.
30. Using the 10 mL pipette and pipette bulb, measure 20 mL of dimethyl sulfoxide (DMSO) into the 50 mL beaker.
    - The DMSO is stored in the yellow ‘Flammables’ cabinet.

31. Bring the 20 mL DMSO and 5 mL auto pipette to the fume hood.
32. Use the DMSO to rinse the inside of the reactor, targeting:
    - Temperature probe
    - Reactor lid
    - Reactor walls
33. Use the auto pipette to siphon solvent stuck in the lid holes back into the reactor.
34. Once rinsing is complete, bring the reactor, remaining DMSO, and auto pipette to the benchtop filter setup.
35. First, pour one full 100 mL DI water flask through the filter to wet the filter papers.
36. Pour ~50 mL from the second water flask through the filter.
    - Save the remaining 50 mL for a final rinse later.
37. Use the auto pipette to begin moving reactor effluent through the filter into the Erlenmeyer flask.
38. Do not overfill the filter—this can cause catalyst to go through if it gets over the filter "walls".
39. After filtering the bulk of the effluent, remove the stir bar from the reactor. I typically just dump it into the vacuum filter to sit on top of the catalyst and get some extra rinsing.
40. Use remaining DMSO and DI water to rinse down the interior of the reactor.
    - End with a DI water rinse to ensure all soluble furans are flushed through.
40. Allow the vacuum to continue for several minutes after filtration finishes to dry the catalyst.
    - Use this time to start dishwashing or prep your next reaction.
41. Once the catalyst surface appears dry and no more filtrate is coming through, shut off the vacuum.
42. Disconnect the vacuum tubing from the Erlenmeyer flask.
43. Retrieve and rinse your stir bar.
44. Carefully remove and dispose of the used filter papers and catalyst.

45. If the catalyst contains precious metals, store it in a labeled Nalgene container on the shelf in Cobleigh 301A.

HPLC Sample Prep and Chromeleon 7 Setup

1. Once the reaction is diluted, retrieve an HPLC vial and cap from the supply on the lab bench in Cobleigh 301 B (or the extra storage in the cabinets in COB 301A).
2. Label the vial with:
    - Date
    - Your initials
    - Sample description (e.g., catalyst, solvent, temp)
3. Get a 3 mL plastic syringe from the same bench.
4. Attach a screw-on PTFE syringe filter (0.2 µm, Agilent).
5. Use a dropper to collect ~1.5 mL of reaction solution.
6. Transfer the solution into the syringe.
7. Use volumetric markings to ensure volume accuracy (do not exceed 1.5 mL or the vial will overflow and make a mess).
8. Filter the solution into the HPLC vial.
9. Cap the vial securely.
10. Dispose of the syringe and filter properly (trash is fine).
11. Take the vial to the HPLC desk.
12. Open the autosampler door.
13. Place the vial in an open slot and note the tray code/color.
14. Close the autosampler door.
15. On the HPLC computer, open Chromeleon 7.
16. Click Create → Sequence.
17. Select the Vanquish HPLC instrument and click Next.

18. Choose the vial position that matches your autosampler tray code on the visual display. You can literally click on the appropriate tray in the little picture.
19. In the method setup window, fill in:
    - Injection name pattern (e.g., 20250327_Pt/C_THF_90C_4h_JM_#r)
    - Number of vials
    - Injections per vial: 3
    - Start position: match tray code/color (e.g., R:C7)
    - Injection volume: 2.00 µL
20. Click Next.
21. Set method/reporting as follows:
    - Instrument method: CatAnalysis.instmeth
    - Channel: UV_1
22. Click Next.
23. Add sequence comments (date, reaction temp, catalyst, solvent, etc.).
24. Click Finish.
25. Save the sequence using the format YYYYMMDD.
26. In the main window, review the new sequence at the top.
27. Edit injection names by clicking in the "Name" column if needed.
28. Save any edits using the top-left Save button.
29. Navigate to the Instruments section in the interface. (Bottom left, above ‘Data’ and ‘eWorkflows’).
30. Select the ColumnComp tab along the top of the screen.
31. Under Temperature Control toggle the Temperature Control feature on (the light on the column compartment will turn green or start blinking green).
32. Select the UV detector tab along the top of the screen.
33. Under Commands, click the UV Lamp button to turn it on. The light on the UV detector will turn green or start blinking green.
34. Go to the Queue tab.

35. Confirm your sequence shows as “Pending.”
36. Click Ready Check to ensure the system is ready.
37. Confirm that enough mobile phase is available.
    - At 0.6 mL/min, each 1-hour run uses 36 mL × number of injections. Calculate appropriately. With 2000 mL of mobile phase, you can run a maximum of 55 injections in a single sequence.
38. If no issues are flagged, click Start to begin the injection sequence.
39. Approve any warnings (if applicable, always read the warning first). Sometimes Chromeleon will provide unnecessary warnings like ‘Pump Maintenance due in 97 days.’ You can ignore these. Report any major problems to Stephanie.

Data Collection Using Chromeleon 7 Software

1. Open Chromeleon 7 on the HPLC computer.
2. In the lower left corner, click on the Data tab.
3. On the left side of the screen, under the header labeled Data, you will see a list of directories.
4. Locate and click the directory that corresponds to the date your sequence was run.
5. After selecting the correct directory, a list of individual injections will appear.
    - Each injection is listed by its name and includes a small HPLC chromatogram preview.
6. Double-click on one of the previewed chromatograms to open the Chromatography Studio view.
7. In the top left corner of the Chromatography Studio window, look for a box labeled Presets.
    - This box usually displays two options: Results and Calibration & Processing Methods.
8. On the right edge of the Presets box, click the down arrow until you see Processing Method.

9. Double-click on Processing Method.
10. A window titled Choose a Processing Method Template will appear.
11. Select Basic Quantitative, then click Next in the bottom right corner of the window.
12. After applying the processing method, return to the Presets box.
13. Use the up arrow to select Results Method.
14. Once selected, your results will appear in a blue spreadsheet at the bottom of the Chromatography Studio window.
15. You can switch between different results by clicking on sample names under the Data Processing and Injections headers on the left side of the screen.
16. Review and record the desired peak area, retention time, or other values relevant to your analysis.

APPENDIX C

SUPPLEMENTAL MATERIALS FOR 'USING ARTIFICIAL NEURAL NETWORKS TO PREDICT 2,5-FURANDICARBOXYLIC ACID SOLUBILITY FOR SOLVENT SELECTION'

Additional Figures, Tables, and Equations

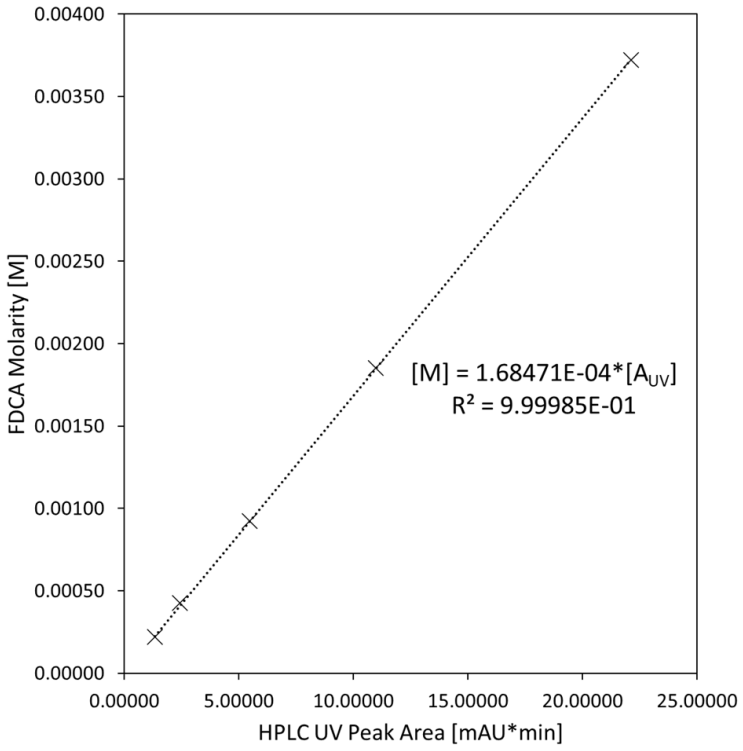

Figure 58. HPLC standard line and equation for FDCA analysis.

Compound	δ_D	δ_P	δ_H
FDCA	19.4	10.3	12.9
2-PrOH	15.8	6.1	16.4
Acetone	15.5	10.4	7
Cyclohexane	16.8	0	0.2
DMSO	18.4	16.4	10.2
DMAc	16.8	11.5	9.4
THF	16.8	5.7	8
ACN	15.3	18	6.1
MeOH	14.7	12.3	22.3
EtOH	15.8	8.8	19.4
SULF	17.8	17.4	8.7
GVL	16.8	16.5	6.7
GBL	18	16.6	7.4
H_2O	15.6	16	42

Table 31. HSP data ($MPa^{1/2}$) for pure compounds at T = 293 K as determined using the HSPiP software.[56]

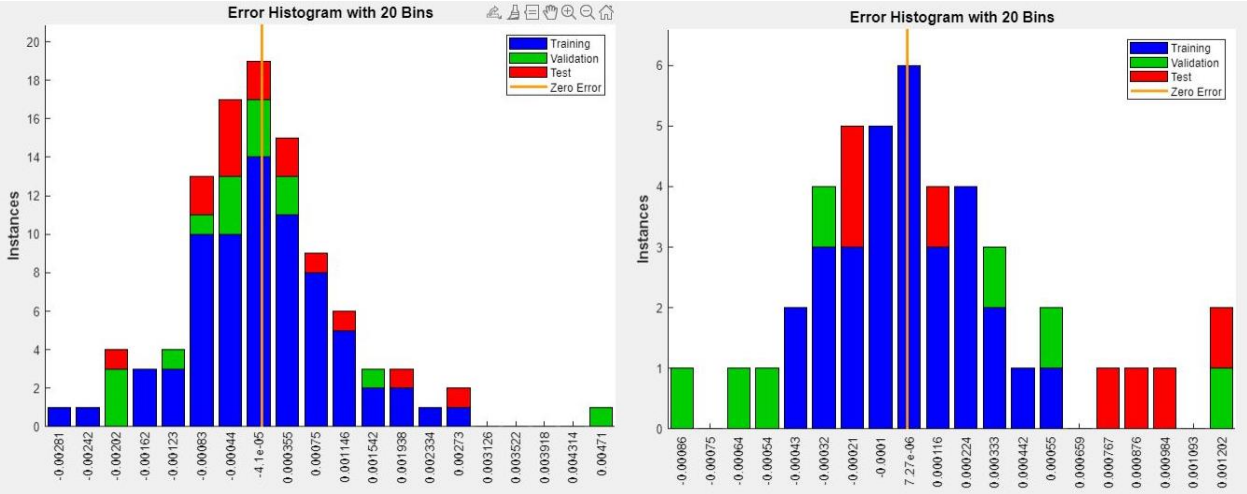

Figure 59. MATLAB generated plots for the assessment of error distribution across training data (blue), validation data (green), and test data (red) for the non-alcohol model (left) and the alcohol model (right).

$$AICc = AIC + \frac{2k(k+1)}{n-k-1} \qquad Eqn.\,25$$

$$AIC = n * \ln\left(\frac{SSE}{n}\right) + 2k \qquad Eqn.\,26$$

where n is the number of datapoints, SSE is the sum of squared errors, and k is the number of hidden nodes.

$$SSE = \sum_i (y_i - t_i)^2 \qquad Eqn.\,27$$

where y is the experimental value and t is the ANN-predicted target value across i samples.

$$MSE = \sum_i \frac{(y_i - t_i)^2}{n} \qquad Eqn.\,28$$

where n is the number of samples.

$$RMSE = \sqrt{MSE} \qquad Eqn.\,29$$

	Alcohol ANN	Non-alcohol ANN
Training Set (70%)		
R^2	0.999	0.998
SSE	4.1e-05	7.4e-05
RMSE	9.3e-04	1.0e-03
Validation Set (15%)		
R^2	0.998	0.996
SSE	1.6e-05	4.2e-05
RMSE	1.3e-03	1.7e-03
Test Set (15%)		
R^2	0.996	0.998
SSE	1.3e-05	2.1e-05
RMSE	1.1e-03	1.2e-03
All Data (100%)		
R^2	0.998	0.997
SSE	6.9e-05	1.4-04
RMSE	1.0e-03	1.2e-03
NRMSE	3.0e-04	1.1e-05
AICc	-578.7	-1266.6

Table 32. Statistical metrics for ANN models for alcohol and non-alcohol datasets.

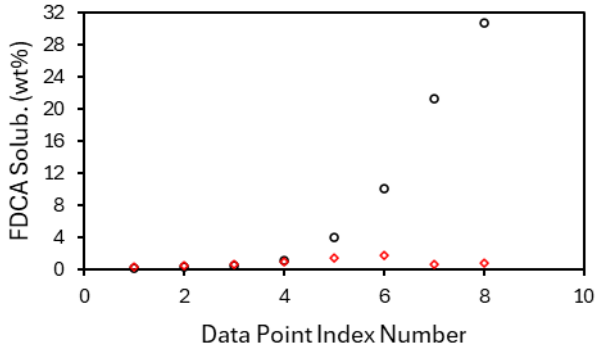

Figure 60. Experimental (○) and non-alcohol ANN predicted (◊) values of FDCA solubility in blends of water and DMSO, from pure water on the far left to pure DMSO on the far right.

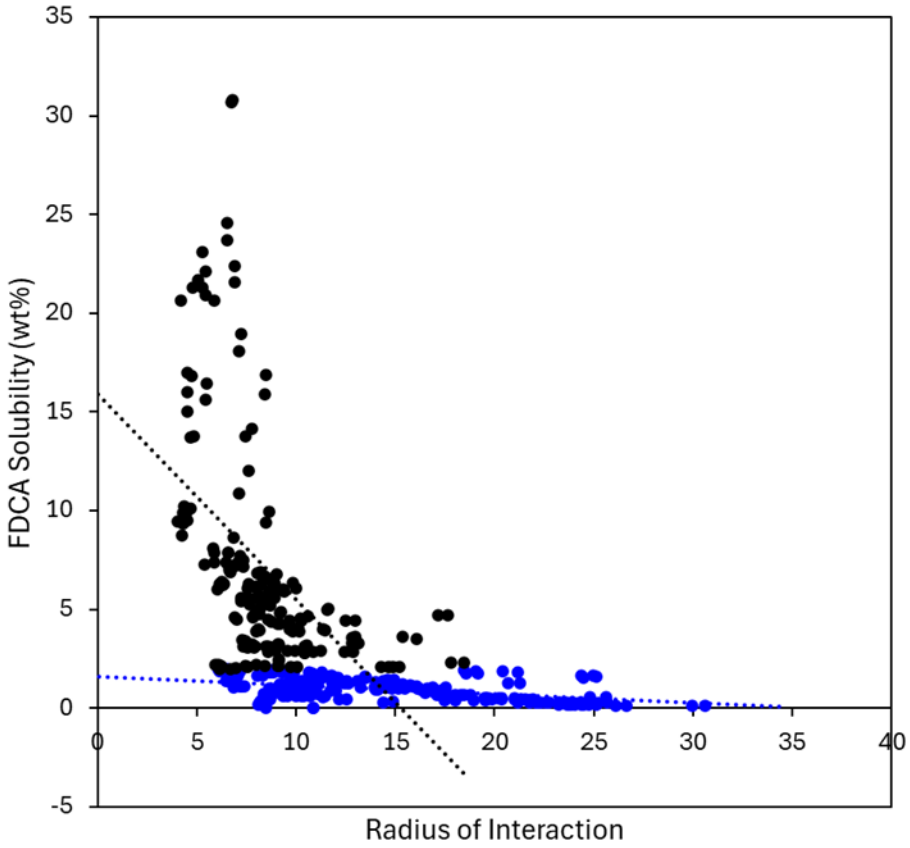

Figure 61. Visualization of the non-linear relationship between the Hansen $R_{i,j}$ parameter and FDCA solubility. Data represented with blue circles (●) has solubility below 2 wt% and is fairly linear, while data represented with black circles (●) has solubility above 2 wt% and is quite nonlinear.

Derivation 1: HSPs to Excess Enthalpy

Background

COSMO-RS calculates excess Gibbs free energy (G^E) from chemical potential values (μ) using:

$$\mu_i^{solv} = \mu_i^{pure} + RTln(\gamma_i x_i) \qquad Eqn. 30$$

where R is the gas constant, T is temperature, γ_i is the activity coefficient, and x_i is mole fraction. Excess enthalpy (H^E) is then calculated from this with the Gibbs-Helmholtz equation:

$$H^E = -RT^2 \frac{d\left(G^E/_{RT}\right)}{dT} \qquad Eqn.31$$

The software uses iterative numerical methods and mean screening charge density (σ) profiles to solve for μ_i^{solv} and γ_i.

Hansen solubility parameters dissolve the enthalpy of mixing (ΔH_{mix}) of a system or compound into the contributions of intermolecular forces: London dispersion forces (δ_D), polarity (δ_P), and hydrogen bond interactions (δ_H). The total HSP is defined as:

$$\delta_T = \sqrt{\delta_D^2 + \delta_P^2 + \delta_H^2} \qquad Eqn.32$$

and this is related to ΔH_{mix} by:

$$\Delta H_{mix} = \varphi_1 \varphi_2 V_m \left(\delta_{T,1} - \delta_{T,2}\right)^2 \qquad Eqn.33$$

where φ_i represents the volume fraction of a component and V_m is the molar volume of the mixture, calculated by:

$$V_m = \sum_i x_i V_{m,i} \qquad Eqn.34$$

HSPs are more fundamentally derived from the concept of Cohesive Energy Density (CED), related by:

$$CED = \delta_T^2 \qquad Eqn.35$$

and where another definition is also useful:

$$CED = \frac{\Delta H_{vap} - RT}{V_m} \qquad Eqn.36$$

Or, through rearranging and substitution (Eqn. 36):

$$\Delta H_{vap} = V_m \delta_T^2 + RT \qquad Eqn.37$$

Formal Derivation

Beginning with Eqn. 31:

$$H^E = -RT^2 \frac{d(G^E/RT)}{dT}$$

with a focus on the derivative term, which is solved by quotient rule:

$$\frac{d}{dT}\left(\frac{G^E}{RT}\right) = \frac{\left(\frac{dG^E}{dT} * RT\right) - \left(G^E * \frac{d(RT)}{dT}\right)}{(RT)^2} = \frac{\left(\frac{dG^E}{dT} * T\right) - (G^E)}{RT^2} = \frac{T\frac{dG^E}{dT} - G^E}{RT^2} \quad Eqn.\,38$$

We now return to G^E, defined as:

$$G^E = \sum_i x_i\left(\mu_i^{solv} - \mu_i^{ideal}\right) \quad Eqn.\,39$$

and substitute rearranged forms of Eqn. 30 or, for μ_i^{ideal}, Raoult's Law:

$$G^E = \sum_i x_i\left(-\mu_i^{pure} - RTlnx_i + \mu_i^{pure} + RTlnx_i\gamma_i\right) = \sum_i x_i RT\left(ln\frac{\gamma_i x_i}{x_i}\right)$$

$$G^E = \sum_i x_i RTln\gamma_i \quad Eqn.\,40$$

Having solved for one undefined term of Eqn. 38, we must now solve for the other:

$$\frac{d}{dT}(G^E) = \frac{d}{dT}\left[\sum_i x_i RTln\gamma_i\right] = \sum_i x_i \frac{d}{dT}(RT * ln\gamma_i)$$

by product rule:

$$\frac{dG^E}{dT} = \sum_i x_i\left(Rln\gamma_i + RT\frac{dln\gamma_i}{dT}\right) \quad Eqn.\,41$$

We can now substitute Eqns. 40 and 41 into Eqn. 38, and Eqn. 38 into Eqn. SM31:

$$H^E = -RT^2 \frac{d}{dT}\left(\frac{G^E}{RT}\right) = -RT^2\left[\frac{T\sum_i x_i\left(Rln\gamma_i + RT\frac{dln\gamma_i}{dT}\right) - \sum_i x_i RTln\gamma_i}{RT^2}\right]$$

$$= \sum_i -x_i RT ln\gamma_i - RT^2 \frac{dln\gamma_i}{dT} + x_i RT ln\gamma_i = -RT^2 \sum_i x_i \frac{dln\gamma_i}{dT} \qquad Eqn. 42$$

Now that H^E is in terms of γ_i, we can find a relationship to ΔH_{vap} and through it, connect back to HSPs and CED. We'll start with the Clausius-Clapeyron equation:

$$\frac{\Delta H_{vap,i}}{RT^2} = \frac{d(lnP_i^{sat})}{dT} \qquad Eqn. 43$$

Substitute a modified version of modified Raoult's Law into Eqn. 43:

$$P_i = \gamma_i x_i P_i^{sat} \qquad Eqn. 44$$

$$lnP_i = ln(\gamma_i x_i P_i^{sat}) = ln\gamma_i + lnx_i + lnP_i^{sat}$$

$$\frac{d}{dT} lnP_i = \frac{d}{dT} ln\gamma_i + \frac{d}{dT} lnx_i + \frac{d}{dT} lnP_i^{sat} = \frac{dln\gamma_i}{dT} + \frac{dlnP_i^{sat}}{dT}$$

$$\frac{dlnP_i^{sat}}{dT} = \frac{dlnP_i}{dT} - \frac{dln\gamma_i}{dT} \qquad Eqn. 45$$

Substitute Eqn. 45 into Eqn. 43:

$$\frac{\Delta H_{vap,i}}{RT^2} = -\frac{dln\gamma_i}{dT} + \frac{dlnP_i}{dT}$$

$$\frac{dln\gamma_i}{dT} = \frac{dlnP_i}{dT} - \frac{\Delta H_{vap,i}}{RT^2} \qquad Eqn. 46$$

Substitute Eqn. 46 into Eqn. 42:

$$H^E = -RT^2 \sum_i x_i \left(\frac{dlnP_i}{dT} - \frac{\Delta H_{vap,i}}{RT^2}\right)$$

Rearrange and distribute:

$$H^E = \sum_i x_i \Delta H_{vap,i} - RT^2 \frac{dlnP_i}{dT} \qquad Eqn.\,47$$

Finally, substitute Eqn. 37 into Eqn. 47:

$$H^E = \sum_i x_i (V_m \delta_T^2 + RT) - RT^2 \sum_i x_i \frac{dlnP_i}{dT} \qquad Eqn.\,48$$

Now, we apply a few assumptions to simplify Eqn. 48. First, we note that HSP values are only valid for a single, defined value of T. Therefore, the equation is only able to be applied in isothermal systems. Thus, Eqn. 48 becomes:

$$H^E = \sum_i x_i (V_m \delta_T^2 + RT) \qquad Eqn.\,49$$

Second, we recall the form of Eqn. 31 wherein H^E is typically negative. We add this negativity back into the equation, noting the shortcoming of this equation in its inability to describe positive values of H^E (an equal but opposite shortcoming of Hansen's Eqn. 33):

$$-H^E = V_m \sum_i^k x_i \delta_{T,i}^2 + kRT \qquad Eqn.\,50$$

where k is the total number of components.

Q.E.D.

<u>Test Case Demonstrating Eqn. 50</u>

A 50/50 w/w mixture of tetrahydrofuran (THF) and H_2O is equivalent to an 20/80 n/n mixture. Thus, define the following:

$$x_{H_2O} = 0.8\,;\; x_{THF} = 0.2\,;\; V_{m_{H2O}} = 0.018\left[{}^{L}/_{mol}\right];\; V_{m_{THF}} = 0.0819\left[{}^{L}/_{mol}\right]$$

and from Eqn. 34:

$$V_m = 0.03078 \left[{}^{L}/_{mol} \right]$$

Values for component HSPs are retrieved from the HSPiP Master Dataset and total HSPs are calculated using Eqn. 32.

Substituting all known values into Eqn. 50 and solving:

$$-H^E = \left(0.03078 \ {}^{L}/_{mol}\right) * \left[0.8\left(47.6\ MPa^{\frac{1}{2}}\right)^2 + 0.2\left(18.3\ MPa^{\frac{1}{2}}\right)^2\right] +$$

$$(2)\left(8314.5\ \frac{L{\cdot}MPa}{mol{\cdot}K}\right)(298.15\ K) = 62.82\ \frac{L{\cdot}MPa}{mol} * \frac{1\ m^3}{1000\ L} * \frac{10\ bar}{1\ MPa} = 0.6282\ \frac{m^3 bar}{mol}$$

$$H^E = \ -0.6282 \ {}^{J}/_{mol}$$

COSMO-RS predicts a value of $H^E = \ -0.6265 \ {}^{J}/_{mol}$.

APPENDIX D

SUPPLEMENTAL MATERIALS FOR 'NOVEL SOLVENT SYSTEMS FOR THE BASE-FREE OXIDATION OF 5-HYDROXYMETHYLFURFURAL TO 2,5-FURANDICARBOXYLIC ACID'

Additional Figures



Figure 62. Comparison of degradation products visually apparent in a pure water system (left) and a 50/50 sulfolane/water system (right). Reaction conditions: 90°C, 4h, 40 bar O_2, 1000 rpm stirring, 0.43698 g of 5% Pt/C catalyst, 10 wt% HMF concentration.

Solvent Degradation

Improved solubility and selectivity towards FDCA are significant to HMF oxidation reactions, but recyclability and management of a solvent system is also important.[26] To assess the robustness of each of the six studied solvent systems, 50/50 organic/water mixtures were subjected to reaction conditions without HMF present and assessed via HPLC-RI. The results, summarized in Figure 6, with no additional peaks appearing after 4 h at 363 K and 40 bar O_2 in the presence of the 5% Pt/C catalyst.

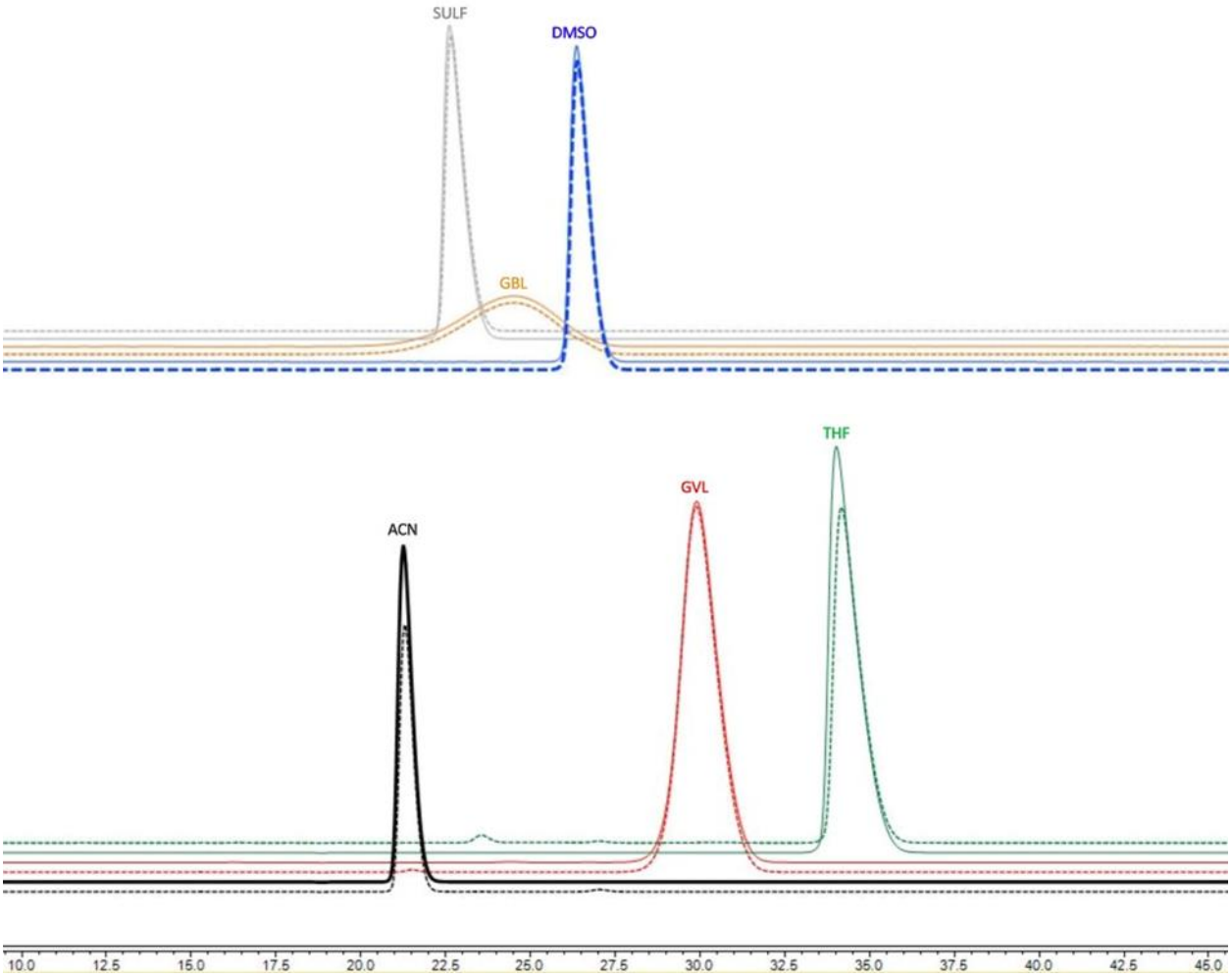

Figure 63. Synopsis of solvent degradation for DMSO (-), ACN (-), SULF (-), GBL (-), GVL (-), and THF (-). Treated solvent samples are designated with dashed lines. Reaction conditions for treated solvent samples: 90°C, 4h, 40 bar O_2, 1000 rpm stirring, 0.43698 g 5% Pt/C catalyst.

THF displayed a clear degradation peak at a retention time of 23.5 minutes, consistent with the expected time of a GBL peak (Figure 63, dashed green line). Prior literature has reported that THF can oxidize to GBL at temperatures as low as 363 K in the presence of suitable oxygen and catalyst.[162] Though the degradation peak is relatively small compared to the larger THF peak at 35 minutes, it does indicate the potential for degradation and side product

formation. ACN (dashed black line) and GVL (dashed red line) both showed similar small degradation peaks. For ACN, a small peak appeared at 27 minutes after treatment. This change indicates some small degradation, though the dominant solvent peak at 21 minutes remained relatively unchanged. These results align with prior literature, wherein ACN degradation occurred slowly and at much higher temperatures (>800 K) than those studied here.[208] The peak at 21 minutes in the treated GVL sample may have correlated to 4-hydroxyvaleric acid, with was observed by Jusner et al. to be the primary degradation product of GVL at temperatures near 373 K.[209]

Sulfolane, GBL, and DMSO exhibited the highest stability under the oxidative conditions studied (Figure 63; grey, orange, and blue lines, respectively). In the standard injections, solvent peaks were observed at 22.5, 24, and 26 minutes and these peaks did not change or shift significantly after treatment. The treated sulfolane peak was nearly indistinguishable from the standard injection, whereas slight differences were detectable in the DMSO and GBL peaks. Consistent with these observations, Zoghi et al. demonstrated that sulfolane degradation did not occur even at elevated temperatures (403 K) and oxygen pressure (>1 bar pure O_2) after extended time.[210] The high stability of each of these solvents under catalytic oxidative conditions reinforces the potential applicability of sulfolane/water mixtures for the conversion of biomass to FDCA. This was confirmed experimentally by conducting a sulfolane degradation assessment at 403 K with the same catalyst loading (5% Pt/C) for 4 h with 580 psi of O_2 (Figure 64). Only a single, small degradation peak was observed (Figure 64, blue dashed line) at a retention time of 27 minutes.

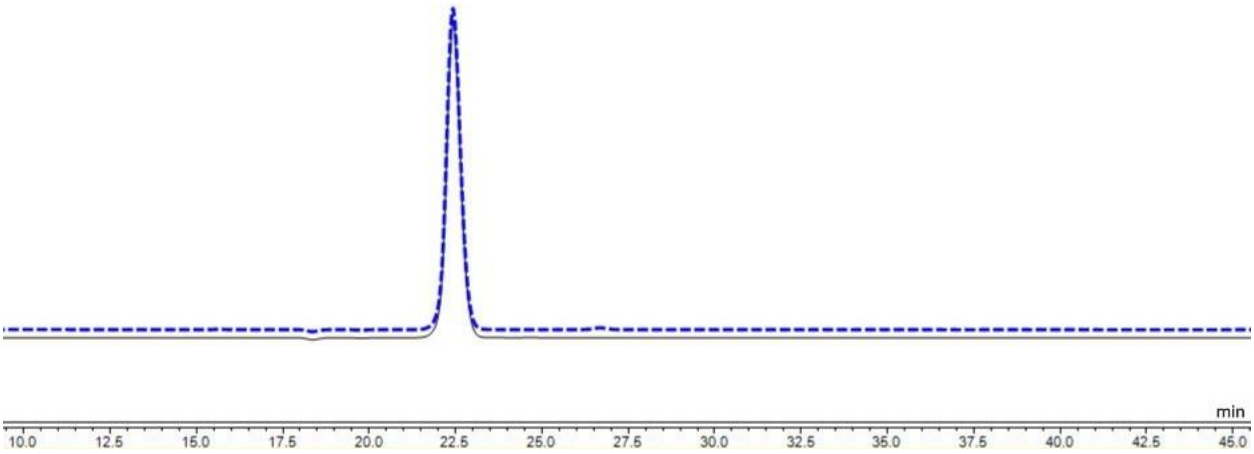

Figure 64. Degradation study on sulfolane at 403 K. The standard injection is shown as a solid black line (−) while the treated sample is shown as a dashed blue line (---).